Investigating the Bactericidal Mechanism of Anti-LPS Antibodies Against *Pseudomonas aeruginosa* Serotype O6

by

Gabrielle Richard

A Thesis
presented to
The University of Guelph

In partial fulfilment of requirements
for the degree of
Doctor of Philosophy
in
Environmental Science

Guelph, Ontario, Canada

© Gabrielle Richard, September, 2017

ABSTRACT

INVESTIGATING THE BACTERICIDAL MECHANISM OF ANTI-LPS ANTIBODIES AGAINST *PSEUDOMONAS AERUGINOSA* SEROTYPE O6

Gabrielle Richard
University of Guelph, 2017

Co-advisors:
Professor Emeritus J. Christopher Hall
Dr. C. Roger MacKenzie
Dr. Marc B. Habash

Our group previously demonstrated that the S20 antibody, and scFv and Fab fragments derived therefrom, exerts direct bactericidal activity towards *Pseudomonas aeruginosa* strain O6a, 6d. By binding to the LPS, and more specifically the O-specific antigen (OSA), the S20 antibody was observed to induce severe cell wall damage by a mechanism that remained elusive. It was initially proposed that the S20 was an abzyme that possessed a potent catalytic activity towards strain O6a, 6d. The main goal of this dissertation was to elucidate the unusual bactericidal mechanism of the S20 antibody. The first objective was to determine if this activity is unique and harboured within the S20 antibody sequence *per se*. We surveyed additional anti-LPS monoclonal antibodies (mAbs) that have been published and were made available to us from the laboratory of Dr. Joseph S. Lam (University of Guelph). Targeting the OSA of serotype O6 with mAb MF23-1 and its Fab fragment induced direct bactericidal activity against all wild-type O6 strains that have an OSA^+ phenotype. Since the S20 and MF23-1 antibodies share little sequence identity in their respective variable domains, one would not anticipate that their bactericidal activity be residing in their sequences *per se* as would be expected for a

catalytic antibody. Instead, we provide the evidence to show that these antibodies are exploiting a vulnerable target on the surface of *P. aeruginosa*, the OSA of serotype O6. The second objective of this thesis was to study the mechanism of the bactericidal antibodies. Based on our high-resolution AFM images, we propose that the mechanism of action of the two bactericidal antibodies involves the following steps: 1- LPS-binding step; 2- Micellization of the LPS-rich OM; 3- Appearance of membrane pits; 4- Loosening of the OM from the peptidoglycan layer; 5- Sloughing of the OM; 6- Membrane blebbing. Our work has established a novel mechanism by which antibodies can mediate direct antimicrobial immunity without the recruitment of phagocytes or the complement system.

ACKNOWLEDGMENTS

I foremost would like to thank my co-advisor, Professor Emeritus J. Christopher Hall, for encouraging me to pursue graduate studies in such an exciting field. My PhD project – studying how an antibody can directly kill a microorganism! – was truly interesting, and I was always honoured to have been given the opportunity to make advancements on this project. You have always looked out for the best interest of your students, and allowing me to take 'your project' at the National Research Council is just another example.

With as much gratitude, I sincerely thank Dr. C. Roger MacKenzie from the NRC for accepting to be my co-advisor, and for hosting me in his laboratory during the course of my PhD work. Thank you for your continual advice, guidance and care, and for making sure I always had opportunities available.

I would also like to thank Dr. Marc Habash for taking on the role as my Advisor when Dr. Chris Hall retired; your help with the final stages on my thesis was especially appreciated.

A special thanks to my other advisory committee members, Dr. Joseph Lam and Dr. James C. Richards for your feedback. Joe, thank you for providing me some of the anti-*P. aeruginosa* mAbs that your laboratory had developed. MAb MF23-1 was instrumental in my work. I sincerely thank you both for expediting the reviewing of my thesis, especially while retired.

To my many NRC colleagues – it was such a pleasure to work with all of you! Thank you for your support and for making the many years of my PhD so enjoyable. Many thanks to Henk van Faassen for training me on the Biacore 3000 and for guiding

me with the preparation of LPS liposomes. Thank you Than-Dung Nguyen for your various support over the years, especially for taking care of Èva in your retirement so that I could finish writing my thesis. Thanks to my dearest friends Jyothi Kumaran and Hiba Kandalaft for sharing your protein purification expertise, but more importantly your wonderful friendships. Thank you Kristin Kemmerich for your kind friendship and your continual encouragement to finish my thesis, knowing it was especially difficult to manage with a baby.

A special thanks to Dr. Maohi Chen for spending many hours training me so that I could use the atomic force microscope independently. Many thanks to Dr. Evgenii Vinogradov for preparing the O6a, 6d O-Ag fractions and sparing me to work with hydrofluoric acid! Thank you Perry Fleming for preparing a 24L culture of *P. aeruginosa*, and for providing various bacterial strains for my studies. I sincerely thank Dr. Stephen V. Evan and his lab (University of Victoria) for their attempts to crystallize the bactericidal antibodies.

Thank you to my parents, to my Lonsdale family, and to Elise and Roger Hollingworth, for your support over the years and for believing in me! To my parents – I can't wait to have more time to spend with you home in NB.

Finally, I am forever grateful to my husband Owen Lonsdale, who I met during my thesis, for his constant love, support and encouragement over the years. This final year has not been easy, with the arrival of our baby Èva and the start of a new career for me, all while trying to finish my thesis. Thank you for your incredible support when I thought it was impossible. I look forward for our new adventures as a family. However, your line "Trust me I'm a doctor" won't work on me anymore!

ACKNOWLEDGEMENTS ..... **iv**

TABLE OF CONTENTS ..... **vi**

LIST OF FIGURES ..... **ix**

LIST OF TABLES ..... **xiii**

LIST OF ABBREVIATIONS ..... **xiv**

CHAPTER 1: GENERAL OVERVIEW **1**

CHAPTER 2: INTRODUCTION **4**

2.1. *PSEUDOMONAS AERUGINOSA* **4**
2.1.1. General characteristics and occurrences 4
2.1.2. Cell envelope 6
2.1.3. Lipopolysaccharide 8
2.1.3.1. O-polysaccharide *10*
2.1.3.1.1. Structure of the OSA from the 20 IATS serotypes 11
2.1.3.1.2. O6 OSA 17
2.1.3.1.3. Common polysaccharide antigen, CPA 19
2.1.3.2. Core region *19*
2.1.3.3. Lipid A *23*

2.2. BASIC STRUCTURE AND CLASSIC EFFECTOR FUNCTIONS OF ANTIBODIES **25**

2.3. THE BACTERICIDAL S20 ANTIBODY **28**

CHAPTER 3: ANTIBODIES TARGETING THE O-SPECIFIC ANTIGEN (OSA) OF *PSEUDOMONAS AERUGINOSA* SEROTYPE O6 MEDIATE DIRECT BACTERICIDAL ACTIVITY. **33**

3.1. ABSTRACT **33**

3.2. INTRODUCTION **34**

3.3. MATERIALS AND METHODS **39**
3.3.1. Anti-LPS antibodies used in this study 39
3.3.1.1. Production of mAbs in hybridoma tissue culture *40*
3.3.1.2. Purification of mAbs *40*
3.3.1.3. Production of antibody fragments *41*
3.3.1.3.1. S20 scFv monomer and dimer 41
3.3.1.3.2. N1F10 scFv 43
3.3.1.3.3. 3B1 scFv 43
3.3.1.3.4. MF23-1 Fab 44
3.3.2. Bacterial strains and culture conditions 44

3.3.3. Bactericidal assays 45
3.3.4. Statistical analyses 46
3.3.5. Determining the MIC 46
3.3.6. LPS preparation 47
3.3.6.1. LPS extraction by the hot-phenol/water method 47
3.3.6.2. Hydrolysis of O-polysaccharide into O-Ag fractions 48
3.3.7. SDS-PAGE, silver-staining, and ELISA 49
3.3.8. Surface plasmon resonance (SPR) 49
3.3.8.1. Preparation of LPS liposomes for use in SPR analysis 50
3.3.8.2. Kinetic analysis using immobilized LPS liposomes 51
3.3.8.3. Kinetic analysis using O6a, 6d repeating units 52
3.3.9. Sequence analysis 54

3.4. RESULTS AND DISCUSSION 55
3.4.1. Purification of the S20 scFv monomer and dimer 55
3.4.2. Binding and bactericidal specificity of S20 57
3.4.3. Comparing the binding specificity of MF23-1 and S20 antibodies 63
3.4.4. Bactericidal specificity of MF23-1 65
3.4.5. SPR analysis 66
3.4.5.1. Binding of the S20 scFv to immobilized O6a, 6d LPS 66
3.4.5.2. Binding of the S20 and MF23-1 antibodies to O6a, 6d repeating units 71
3.4.6. Determining the MIC 77
3.4.6.1. S20 scFv 77
3.4.6.2. MF23-1 mAb 81
3.4.6.3. Correlation between the affinity and bactericidal potency 84
3.4.7. Sequence analysis of the variable domains of the bactericidal S20 and MF23-1 antibodies 84
3.4.8. Targeting the OSA of serotype O3 88
3.4.9. Targeting the highly conserved inner core region 91
3.4.10. Targeting the common polysaccharide antigen (CPA, A-band) 94
3.4.11. Targeting the OSA of *Salmonella* Typhimurium with 3B1 scFv 99

3.5. CONCLUSION 101

CHAPTER 4: ATOMIC FORCE MICROSCOPY REVEALS THAT THE ANTI-O-SPECIFIC-ANTIGEN (OSA) S20 AND MF23-1 ANTIBODIES MEDIATE THEIR BACTERICIDAL ACTION TOWARDS *P. AERUGINOSA* STRAIN O6A, 6D BY PERMEABILIZING THE OUTER MEMBRANE USING A DETERGENT-LIKE MECHANISM. 102

4.1. ABSTRACT 102

4.2. INTRODUCTION 103

4.3. MATERIALS AND METHODS 108
4.3.1. Preparation of bactericidal antibodies for AFM studies 108
4.3.2. Treatment of *P. aeruginosa* strain O6a, 6d cells for AFM studies 109
4.3.3. Atomic force microscopy 110

4.4. RESULTS 111
4.4.1. Untreated O6a, 6d cells 111
4.4.2. O6a, 6d cells treated with the bactericidal S20 and MF23-1 antibodies 113

4.5. DISCUSSION 133

CHAPTER 5: GENERAL CONCLUSIONS AND FUTURE DIRECTIONS 143

REFERENCES.....147

APPENDIX.....162

LIST OF FIGURES

Figure 1. The cell envelope of Gram-negative bacteria 8

Figure 2. LPS glycoforms on the surface of a single cell of *P. aeruginosa*. 9

Figure 3. Chemical structures of the O-specific antigen (OSA) repeating units of *Pseudomonas aeruginosa* IATS serotypes O1–O20 16

Figure 4. Structure of the OSA of various strains from *P. aeruginosa* serotype O6 18

Figure 5. Structures of core oligosaccharide. 22

Figure 6. Comparison of the lipid A structure from a laboratory *P. aeruginosa* strain, a clinical *P. aeruginosa* isolate, and an *E. coli*. 24

Figure 7. Basic structure of an immunoglobulin G (IgG). 26

Figure 8. Bactericidal activity of antibodies. 27

Figure 9. FE-SEM images of *P. aeruginosa* strain O6a, 6d treated with 6.7 µM S20 scFv 32

Figure 10. Purification of the S20 scFv. 56

Figure 11. ELISA showing the high specificity of the S20 scFv to *P. aeruginosa* strain O6a, 6d compared to the 20 IATS *P. aeruginosa* serotypes and PAO1. 58

Figure 12. Overlaid growth curves of the 20 IATS *P. aeruginosa* serotypes and PAO1 in the absence or presence of the S20 scFv. 59

Figure 13. Western immunoblot comparing the cross-reactivity of mAb MF23-1 to various OSA+ O6 strains versus the high specificity of S20 to strain O6a, 6d. 61

Figure 14. Bactericidal activity of S20 scFv, mAb MF23-1 and MF23-1 Fab against various O6 strains of *P. aeruginosa* 62

Figure 15. SDS-PAGE gel of various purified anti-LPS antibodies used in this study. . 64

Figure 16. Binding of the S20 scFv monomer and dimer to immobilized LPS from *P. aeruginosa* strain O6a, 6d. 69

Figure 17. SPR analysis of immobilized S20 scFv and mAb MF23-1 to O6a, 6d repeating unit oligosaccharides 74

Figure 18. SPR analysis confirming that the MF23-1 Fab fragment binds O6a, 6d repeating unit oligosaccharide 76

Figure 19. Concentration-dependent effect of S20 scFv monomer, S20 scFv dimer and MF23-1 mAb on the growth curves of *P. aeruginosa* strain O6a, 6d 79

Figure 20. Turbidity versus antibody concentration graph to determine the minimal inhibitory concentration 80

Figure 21. Concentration-dependent effect of mAb MF23-1 on the growth curve of various wild-type (OSA+) strains of *P. aeruginosa* serotype O6. 82

Figure 22. Turbidity versus mAb MF23-1 concentration graph to determine the minimal inhibitory concentration 83

Figure 23. Western immunoblot showing that commercial mAb ab84607 targets the OSA *P. aeruginosa* serotype O3..... 89

Figure 24. Bactericidal activity of mAb ab84607 against *P. aeruginosa* serotype O3 IATS (ATCC 33350). 90

Figure 25. Bactericidal assay using mAb 7-4 to target inner core LPS antibody various smooth and rough strains of *P. aeruginosa* serotype O5 and O6. 93

Figure 26. Purification of the anti-CPA antibodies, N1F10 IgM and its scFv 97

Figure 27. Bactericidal assay using the anti-CPA N1F10 antibodies against various strains of *P. aeruginosa*.. 98

Figure 28. AFM images showing an overview of the mechanism of action of the bactericidal mAb MF23-1 and S20 scFv against *P. aeruginosa* strain O6a, 6d..... 119

Figure 29. AFM image of an untreated *P. aeuginosa* strain O6a, 6d cell..... 120

Figure 30. Comparing natural outer membrane vesicles (OMVs) from a Gram-negative bacterium to the micelles released upon treatment of P. *aeruginosa* strain O6a, 6d with the S20 scFv. 121

Figure 31. AFM image of a *P. aeuginosa* strain O6a, 6d cell treated with mAb MF23-1 at 0.4× MIC_{50} (1 µM), illustrating the desorption of many irregularly-shaped micelles. 122

Figure 32. AFM image of a *P. aeuginosa s*train O6a, 6d cell, highlighting the appearance pits in the outer membrane..... 123

Figure 33. AFM image of a *P. aeuginosa* strain O6a, 6d cell treated with mAb MF23-1 at 0.4× MIC_{50} (1 µM). 124

Figure 34. AFM image of a *P. aeuginosa* strain O6a, 6d cell treated with mAb MF23-1 at 4 × MIC_{50} (10 µM), illustrating the process of OM fragments being released from the cell 125

Figure 35. AFM image of a *P. aeuginosa* strain O6a, 6d cell treated with the S20 scFv monomer at 22 × MIC_{50} (10 µM), illustrating the smooth topography of the LPS deficient surface 126

Figure 36. AFM image of a *P. aeuginosa* strain O6a, 6d cell treated with the S20 scFv monomer at 22 × MIC_{50} (10 µM), illustrating the release of aggregated vesicle-/micelle-like material from the outer membrane. 127

Figure 37. AFM image showing the desorption of vesicle-/micelle-like material from the membrane. 128

Figure 38. Side-view topography (3D) image comparing the rough surface of an untreated cell versus the smooth surface of an S20 scFv monomer treated cell. 129

Figure 39. Surface topography analysis 130

Figure 40. Enlargement of 3D surface patches (400 × 400 nm) of O6a, 6d cells treated with the S20 and MF23-1 antibodies. 131

Figure 41. Cross-sections of cells. **132**

Figure 42. Standard curve for SEC Superdex™ S75 and S200 16/60 column chromatography 162

APPENDIX FIGURES:

Figure 43. Mass spectroscopy analysis of the S20 scFv monomer. 163

Figure 44. Fluorescence micrographs showing the binding of FITC-labelled S20 scFv towards *P. aeruginosa* strain strain O6a, 6d 164

Figure 45. MSA of the VH and VL domains of the bactericidal S20 and MF23-1 and non-bactericidal mAbs 7-4, N1F10 and LPT3-1. 165

Figure 46. SPR sensogram showing the hydrolysis of immobilized *Shigella* LPS by tailspike protein 167

Figure 47. Crystal model of the S20 scFv, showing the long CDR1 of V_L protruding from paratope. 168

Figure 48. Purification and binding of mAb 7-4 169

Figure 49. Western immunoblot showing the reactivity of purified N1F10 IgM to various *P. aeruginosa* strains 170

Figure 50. Measurements of membrane pits. 171

Figure 51. AFM image of a *P. aeuginosa* strain O6a, 6d cell treated with mAb MF23-1 at 4× MIC_{50} (1 µM) 172

Figure 52. AFM image of a *P. aeuginosa* strain O6a, 6d cell treated with the S20 scFv monomer at 22 × MIC_{50} (10 µM), illustrating the smooth topography of the LPS deficient surface. 173

Figure 53. AFM image of a P. aeuginosa strain O6a, 6d cell treated with the S20 scFv monomer at 22 × MIC_{50} (10 µM), illustrating the smooth topography of the LPS deficient surface. 174

Figure 54. Surface area of 400 nm × 400 nm from untreated and S20 scFv-treated cells (10 µM) that were used to analyze the surface roughness 175

LIST OF TABLES

Table 1. Summary of anti-LPS antibodies used in this study. 39

Table 2. K_D and rate constants of the S20 scFv and MF23-1 antibodies to immobilized O6a, 6d LPS and to hydrolyzed O6a, 6d repeating unit oligosaccharides..... 70

Table 3. Multiple sequence alignment (MSA) of the CDRs from the variable domains of the bactericidal (S20 and MF23-1) and non-bactericidal (7-4, N1F10 and LPT3-1) antibodies.. 87

Table 4. The grand average of hydropathy (GRAVY) scores of the CDRs..... 166

LIST OF ABBREVIATIONS

.

Abbreviation	Definition
A-band	Common polysaccharide antigen (CPA) of *P. aeruginosa*
ADCC	Antibody-dependent cell-mediated cytotoxicity
AFM	Atomic force microscopy
ATCC	American type culture collection
B-band	O-specific antigen (OSA) of *P. aerugnisa*; O-antigen (O-Ag)
CDC	Complement-dependent cytotoxicity
CDR	Complementarity determining region
CFU	Colony forming unit
C_H	Constant domain of heavy chain
C_L	Constant domain of light chain
CPA	Common polysaccharide antigen; A-band
CV	Column volume
Da	Dalton
DMEM	Dulbecco's Modified Eagle's Medium
DMPC	1,2-Dimyristoyl-*sn*-glycero-3-phosphocholine
EDTA	Ethylenediaminetetracetic acid
ELISA	Enzyme-linked immunosorbent assay
Fab	Fragment antigen binding
Fc	Fragment crystallizable
FcR	Fc receptor

FR	Framework region
GalN	N-acetyl galactosamine
GalNAcAN3Ac	2-acetamido-3-O-acetyl-2-deoxygalacturonamide
GalNFoAN	2-formamido-2-deoxygalacturonamide
Glc	Glucose
Gm^R	Gentamicin-resistance
HBS-E	10 mM HEPES, pH 7.4, 150 mM NaCl, 3 mM EDTA
HBS-EP	10 mM HEPES, pH 7.4, 150 mM NaCl, 3 mM EDTA, 0.005% P-20
HBS-EP+	10 mM HEPES, pH 7.4, 150 mM NaCl, 3 mM EDTA, 0.005% surfactant P-20
HEPES	4-(2-hydroxyethyl)-1-piperazine-ethanesulfonic acid
IATS	International Antigenic Typing Scheme
IF	Immunofluorescence
Ig	Immunoglobulin
IgA	Immunoglobulin alpha (α)
IgD	Immunoglobulin delta (δ)
IgE	Immunoglobulin epsilon (ε)
IgG	Immunoglobulin gamma (γ)
IgM	Immunoglobulin mu (μ)
IMAC	Immobilized metal affinity chromatography
IMAC A	10 mM HEPES, 500 mM NaCl, pH 7.5
IMAC B	500 mM imidazole, 10 mM HEPES, 500 mM NaCl, pH 7.5

k_{on}	Association rate constant (M^{-1} s^{-1})
K_D	Equilibrium dissociation constant
kDa	Kilodalton
Kdo	3-deoxy-D-*manno*-octulosonic acid
k_{off}	Dissociation rate constant
L	Liter
LB	Luria-Bertani media / lysogeny broth (10 g/L tryptone, 5 g/L yeast extract, 10 g/L NaCl, pH 7.5)
LC_{50}	Lethal concentration that causes 50% killing; median lethal concentration
LPS	Lipopolysaccharide
M	Molar
mM	Millimolar (10^{-3} M)
µM	Micromolar (10^{-6} M)
nM	Nanomolar (10^{-9} M)
mAb	Monoclonal antibody
MIC	Minimal inhibitory concentration
MIC_{50}	MIC which causes a 50% reduction of cell turbidity
Mr	Molar mass
MW	Molecular weight
O-Ag	O-antigen
OSA	O-specific antigen of *P. aeruginosa*; B-band
o/n	Overnight; 12-16 h

OD	Optical density
OD_{600}	OD at 600 nm
O6a, 6d	*P. aeruginosa* strain O6a, 6d
OMVs	Outer membrane vesicles
PBS	Phosphate buffered saline (137 mM NaCl, 10 mM phosphate, 2.7 mM KCl, pH 7.4)
PBST	Phosphate buffered saline with 0.05% Tween 20
PLL	Poly-L-lysine
PMN	polymorphonuclear leukocytes
PVDF	Polyvinylidene fluoride
QuiNAc	2-acetamido-2,6-dideoxyglucose
Rha	Rhamnose
R_{max}	Maximum response defined as saturation (in surface plasmon resonance)
RT	Room temperature
RU	Response unit (in surface plasmon resonance)
SEC	Size exclusion chromatography
scFv	Single-chain variable fragment
SDS	Sodium dodecyl sulphate
SDS-PAGE	Sodium dodecyl sulphate polyacrylamide gel electrophoresis
SPR	Surface plasmon resonance
TSB	Tryptic soy broth
V_H	Variable region of heavy chain of a conventional antibody

V_L	Variable region of light chain of a conventional antibody
v/v	Volume/volume
w/v	Weight/volume
WB	Western blot
wt	Weight
Zeo	zeocin
3D	Three dimensional

CHAPTER 1: GENERAL OVERVIEW

In the classical view of immunology, antibodies typically do not directly destroy their target pathogens, but instead exert their protective function by activating other arms of the immune system [i.e., via other processes including complement system, opsonic phagocytosis, antibody-dependent cell-mediated cytotoxicity (ADCC)]. Paradoxically, some antibodies have been discovered to bypass this pillar of immunology by directly killing their target microorganisms (1-6). The antimicrobial mechanisms of these antibodies range from catalyzing the production of oxidative molecules (1-3), to interfering with biological functions (4), or directly damaging their target's membrane (5-10). In 2010, our group reported the first antibody that destroys its specific bacterium by targeting surface lipopolysaccharide (LPS). LPS, which is the most abundant component of the outer leaflet of the OM of Gram-negative bacteria, generally provides a protective barrier to the cell wall, and also plays an important role in the structural integrity of the OM. However, our group demonstrated that the S20 antibody and its antibody fragments (single-chain variable fragment, scFv; fragment antigen binding, Fab) directly kill *P. aeruginosa* strain O6a, 6d by targeting the O-specific antigen (OSA) of the LPS. Binding of the S20 antibody to the LPS induces severe cell wall perturbation in a mechanism that remained unknown at the time.

P. aeruginosa can cause life-threatening infections in immunocompromised individuals such as those suffering from AIDS, cancer, burn wounds and patients afflicted with the recessive genetic disease cystic fibrosis (CF) (11-13). Unfortunately, strains found in hospitals are becoming increasingly difficult to treat because they are becoming more resistant to nearly all antibiotics; in fact, *P. aeruginosa* accounts for 13% of all healthcare-associated infections (14).

There are currently no commercially available vaccines to prevent *P. aeruginosa* infections. Therefore, passive immunotherapy with monoclonal antibodies (mAbs), and especially bactericidal antibodies, could represent a potential strategy for the treatment of patients fighting *P. aeruginosa* infections.

The objective of Chapter 3 was to further characterize the S20 antibody, and determine if its bactericidal activity is unique and residing in its sequence *per se*, or if targeting the LPS of *P. aeruginosa* with antibodies is responsible for its bactericidal activity. To unravel if this activity is unique and harboured within the S20 antibody molecule, we surveyed additional anti-LPS monoclonal antibodies (mAbs) that have been published and were made available to us from the laboratory of Dr. Joseph Lam (University of Guelph). Our results indicated that targeting the highly conserved LPS inner-core and the common polysaccharide antigen (CPA) with specific antibodies did not affect the viability of various *P. aeruginosa* strains. However, targeting the OSA of serotype O6 with mAb MF23-1 and its Fab fragment mediated direct bactericidal activities towards all OSA+ O6 strains. Since the MF23-1 antibody has an entirely different sequence than the S20 antibody, especially in the complementarity determining regions (CDRs), these results suggested that the bactericidal activity does not reside in their antibody sequence *per se,* i.e., they are not catalytic in nature. Instead, these antibodies are exploiting a vulnerable target on *P. aeruginosa*: the O6 OSA.

The objective of Chapter 4 was to unravel the mechanism of the S20 and MF23-1 antibodies. Earlier studies by electron microscopy demonstrated that the S20 antibody induces severe cell wall damage; however, the precise manner in which it did so remained unknown (5). Since atomic force microscopy (AFM) has proven a useful tool to unravel the step-wise manner in which antimicrobial peptides disrupt the outer membrane of Gram-negatives (15, 16), we

chose to use it to study the membranolytic effects the S20 and MF23-1 antibodies on *P. aeruginosa* strain O6a, 6d. Based on our high-resolution AFM images, we propose that these bactericidal antibodies act in a detergent-like mechanism with the following sequence of events: 1- LPS-binding step; 2- Micellization of the LPS-rich OM; 3- Appearance of membrane pits; 4- Loosening of the OM from the peptidoglycan layer; 5- Sloughing of the OM; 6- Membrane blebbing.

CHAPTER 2: INTRODUCTION

2.1. PSEUDOMONAS AERUGINOSA

2.1.1. General characteristics and occurrences

P. aeruginosa, a member of the *Pseudomonadaceae* family, is the most commonly encountered rod-shaped Gram-negative bacterium that is not a member of the *Enterobacteriaceae* family. Because of its incredible metabolic diversity and its ability to adapt, *P. aeruginosa* is able to grow in most environments, including soil, water (lakes and rivers) and marshes, sewage, and hospitals (17, 18). In fact, it can even survive and multiply in deionized or distilled water (19-21), some disinfectant solutions (22) and the hostile environment of lungs. *P. aeruginosa* can exist in the planktonic form as a single-celled organism or as part of a surface-associated biofilm community. Its arsenal of virulence factors and metabolic diversity allows it to successfully infect humans, animals, and even plants (13).

Irrespective of previous exposure to antibiotics, most strains of *P. aeruginosa* are naturally resistant to a wide range of antibiotics, making it a dangerous and dreaded human pathogen (23). It owes its high resistance to antibiotics, in part, to the poor permeability of its outer membrane (OM) (24) in combination with the multidrug efflux pumps that expel drugs out of the cell (25). For example, compared to *Escherichia coli* (*E. coli*), the OM of *P. aeruginosa* is about 100-fold less permeable to small hydrophilic compounds, including the antibiotics cephacetrile and cephaloridine (24). Furthermore, clinical isolates can overproduce the amount of multidrug efflux pumps in their OM, thereby further increasing their resistance to antibiotics such as β-lactams (except imipenem), fluoroquinolones, tetracyclines, macrolides,

chloramphenicol, novobiocin, trimethoprim, and sulfamethoxazole (26-30). Other mechanisms which contribute to a multidrug-resistant phenotype include the production of enzymes (β-lactamases, aminoglycoside-modifying enzymes and 16S rRNA methylases), the loss of outer membrane porins (e.g., OprD) and target alteration (e.g., quinolone resistance-determining regions) (31).

Another major reason *P. aeruginosa* does so well is that it is able to adapt to the hostile environments of its host during the course of infection. Most notably, it can make alterations in its LPS expression and structure [e.g., loss of *O*-polysaccharide chains, addition of structural elements to lipid A; reviewed in (32, 33)], it can develop as a biofilm, and it can produce a protective extracellular exopolysaccharide matrix.

P. aeruginosa can cause life-threatening infections in immunocompromised individuals such as those suffering from AIDS, cancer, burn wounds and patients afflicted with the recessive genetic disease cystic fibrosis (CF) (11-13). In addition, *P. aeruginosa* accounts for 13% of all healthcare-associated infections (HAI) including pneumonia (13%), urinary tract infections (UTIs) (11%), surgical-site infections (6%), bloodstream infections (4%), and gastrointestinal infections (1%) (14, 34, 35) (http://www.cdc.gov/hai/organisms/pseudomonas.html). Many of these infections are a result of device-associated infections (i.e., ventilator-associated pneumonia, catheter-associated urinary tract infection, and central-catheter–associated bloodstream infection). Unfortunately, strains found in hospitals are becoming more difficult to treat because they are becoming more resistant to nearly all antibiotics including, aminoglycosides, cephalosporins, fluoroquinolones, and carbapenems (14). Doripenum (tradename DORIBAX™), a broad-spectrum β-lactam antibiotic agent belonging to the carbapenem group which was approved by the US FDA in 2007, is used to treat nosocomial pneumonia and is

especially potent against *P. aeruginosa* (14). Nevertheless, multidrug resistant *P. aeruginosa* strains have been given a threat level of serious in the Antibiotic Resistance (AR) Threat report by the Centers for Disease Control and Prevention (CDC).

Serotype O6, followed by serotype O11, is one of the most clinically prevalent *P. aeruginosa* serotypes (36-38). Interestingly, a mouse challenge assay demonstrated that, out of 16 IATS serotypes, the LPS from O6 was the most protective component in the *P. aeruginosa* Polyvalent Extract Vaccine (PEV, Wellcome Biotechnology) (39, 40). Unfortunately, this vaccine did not prove to be efficacious to children afflicted with CF, and its development has been ceased (41, 42). There is therefore a need to develop alternative therapies, including immunotherapy and immonoprophylaxis, for controlling *P. aeruginosa* infections.

2.1.2. Cell envelope

The cell envelope of Gram-negative bacteria is composed of an OM, an inner membrane (IM), and a thin peptidoglycan sheet that lies in the periplasmic space between the OM and IM (Figure 1). The IM, also called cytoplasmic membrane, is composed of a phospholipid bilayer. The OM is asymmetric: the inner leaflet is comprised of phospholipids and the outer leaflet is comprised mainly of LPS (~90%). LPS is a multifunctional molecule that provides structural integrity to the OM and acts as a permeable barrier to limit the passive diffusion of hydrophobic molecules into the cell wall. Moreover, the LPS is an important virulence factor contributing to the pathogenicity of Gram-negative pathogens, including *P. aeruginosa* (43-45). The peptidoglycan layer is composed of long carbohydrate polymers of alternating *N*-acetylglucosamine (NAG) and *N*-acetylmuramic acid (NAM) residues that are covalently cross-linked to one another by peptide interbridges (46). The peptidoglycan layer is rigid and protects

most cells. Peptidoglycan-associated outer membrane lipoproteins stabilize the envelope by forming various crosslinks (47). In *E. coli*, Braun's lipoprotein (Lpp) covalently links the peptidoglycan to the OM; the porin outer-membrane protein A (OmpA) interacts non-covalently with the peptidoglycan; and the Tol–Pal complex spans the envelope from the IM to the OM (48-52). The cell envelope of *P. aeruginosa* contains homologs to these *E. coli* lipoproteins: the OprF is an OmpA homolog, the OprL is a Pal homolog, and the OprI is a homolog of Lpp (53).

OM components, including LPS, lipids and proteins, are in constant lateral movement along the membrane, in what is known as the membrane fluid mosaic model first proposed by Singer and Nicolson (54). In addition to lateral movements, LPS can rotate along its long axis, and its *O*-polysaccharide chains can freely bend in different directions (55).

The lipidome of *P. aeruginosa* also differs from enteric bacteria. While phosphatidylcholine (PC) is the most abundant phospholipids found in the membrane of eukaryotes, the membrane of most bacteria (ca. 90%), including *E. coli* and *Salmonella*, do not contain PC. However, in addition to the typical prokaryotic phospholipids (phosphatidylethanolamine, phosphatidylglycerol, and cardiolipin), *P. aeruginosa* can synthesize PC as a minor membrane phospholipid if choline is available from the host or from complex growth medium (56).

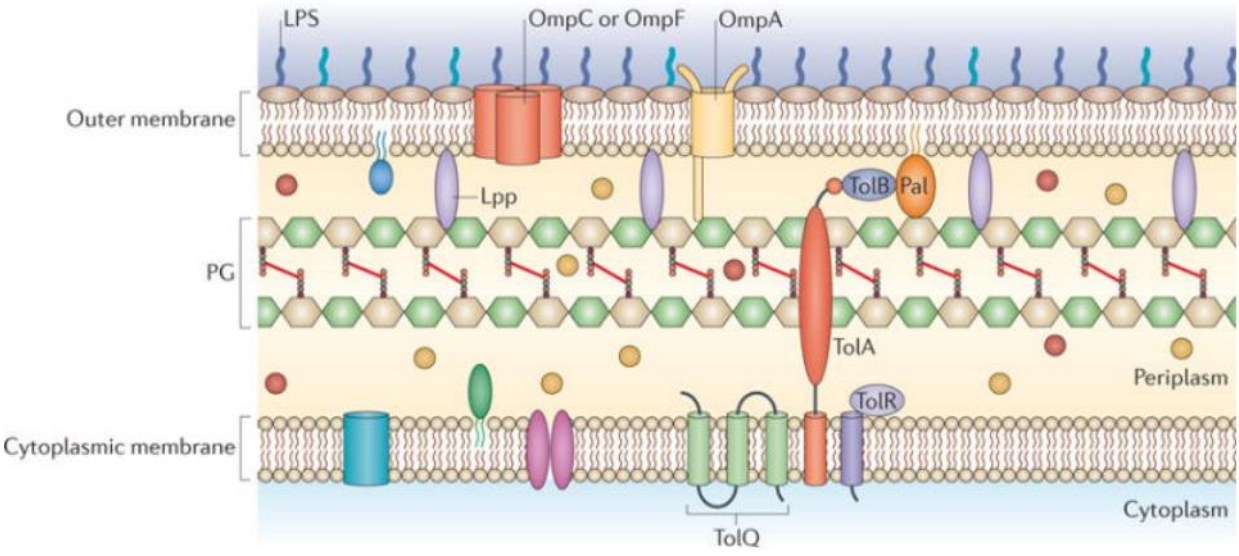

Figure 1. The cell envelope of Gram-negative (*E. coli*) cells. This figure was taken from Schwechheimer and Kuehn (47); permission to reuse the figure was granted by Nature Publishing Group.

2.1.3. Lipopolysaccharide

LPS, the most abundant component of the outer leaflet of the OM, is an important virulence factor contributing to the pathogenicity of *P. aeruginosa* (43). It is composed of three structurally distinct domains: 1) the lipid A (endotoxin), a highly acylated diglucosamine (di-GlcNAc) backbone that is embedded in the outer leaflet of the OM; 2) the oligosaccharide core region, which is composed of the highly conserved and unusual sugars, ketodeoxyoctonic acid (Kdo) and heptoses; and 3) an *O*-polysaccharide chain which extends about 30 – 40 nm away from the OM (55, 57, 58). The structure of the LPS from *P. aeruginosa* will be discussed below; however, the interested reader is advised to consult the comprehensive reviews by King *et al.* (59) and by Lam *et al.* (33). These reviews also include information regarding the biosynthesis of LPS which will not be discussed herein.

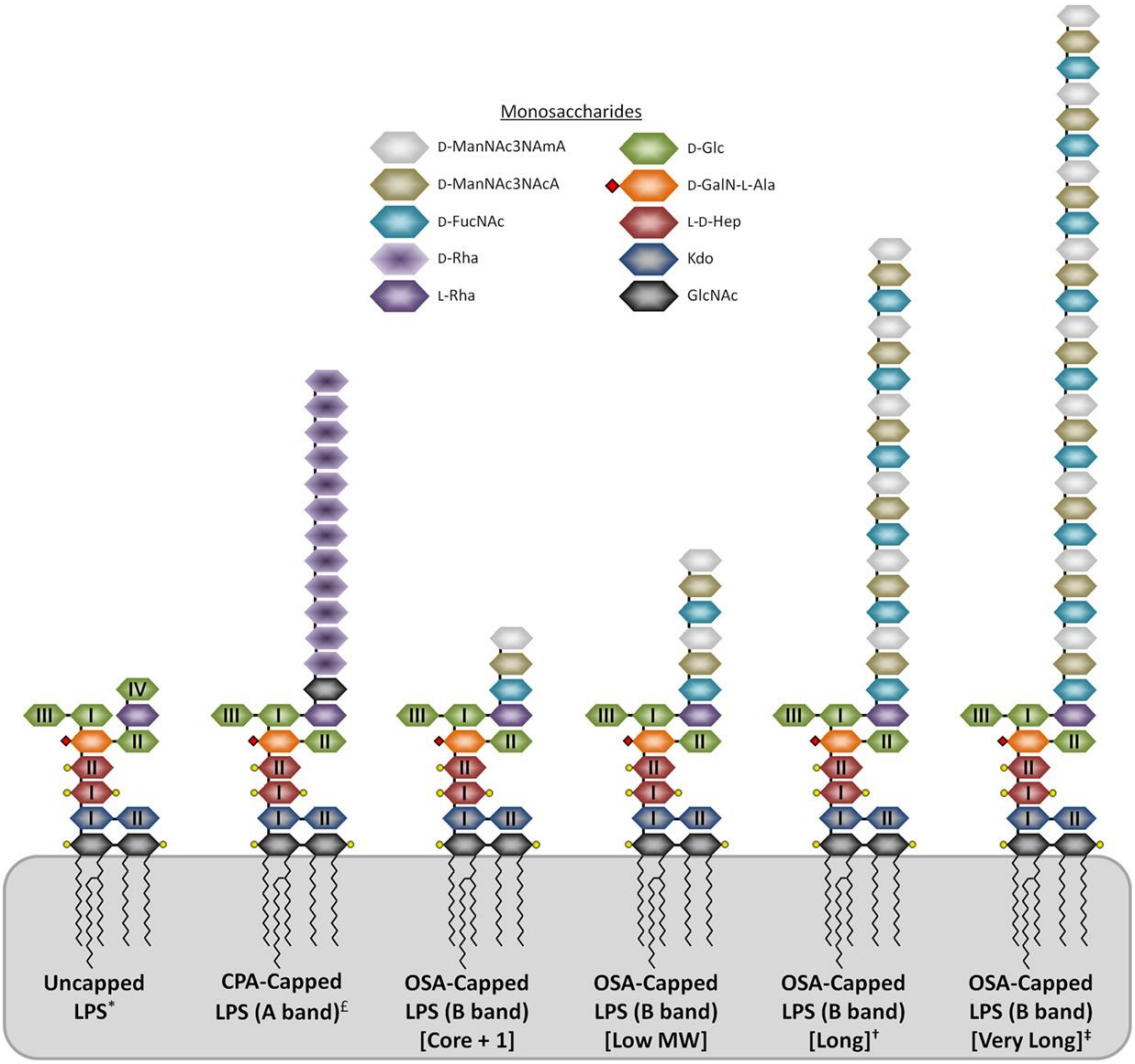

Figure 2. Diversity of LPS glycoforms on the surface of a single cell of *P. aeruginosa* (O-specific antigen of serotype O5 illustrated). This figure was taken from Lam *et al*. (33) with permission from the authors.

2.1.3.1. *O*-polysaccharide

Most planktonic (wild-type) strains of *P. aeruginosa* simultaneously produce two structurally distinct *O*-polysaccharides: the common polysaccharide antigen (CPA; formerly called A-band) and the O-Specific Antigen (OSA; formerly called as B-band) (60, 61). Like enteric bacteria, smooth strains of *P. aeruginosa* contain a heterogenous mixture of LPS glycoforms on a single cell; variability comes from the presence (smooth LPS) or absence (rough LPS) of anchored *O*-polysaccharide, the chain lengths of *O*-polysaccharides (1 – 50 repeating units), and the type of *O*-polysaccharide (OSA vs CPA) (Figure 2). Since the OSA [up to ca. 50 repeating units, (62)] can extend almost twice the length of the CPA [ca. 70 sugars = 23 repeating units (59)], it has been suggested that it masks the accessibility of anti-CPA antibodies to the shorter-chain CPA (60). In *P. aeruginosa*, the chain length of the OSA is regulated by two Wzz polysaccharide polymerases, namely Wzz_1 [modulates 12–16 repeats and 22–30 repeats; (62, 63)] and Wzz_2 [modulates 40–50 repeat length; (62)]. While the OSA is the predominant form of *O*-polysaccharide in wild-type strains and strains isolated from acute infections, its production, unlike that of CPA, is either reduced or completely abrogated as a result of chronic selective pressures in clinical isolates, especially those isolated from CF patients (60, 64). The loss of the OSA phenotype is generally caused by a permanent genetic modification (e.g. insertion of IS elements) within the OSA biosynthesis gene cluster as opposed to a reversible down-regulation (33, 65). While the driving force of this strong selective pressure is not completely understood, it is believed that it is a way *P. aeruginosa* evades the immune system since the OSA is very immunogenic.

2.1.3.1.1. **Structure of the OSA from the 20 IATS serotypes**

Within the species of *P. aeruginosa*, the chemical structure of the OSA can vary markedly from one isolate to another (66). Since the OSA is the surface antigen which elicits the strongest antibody response (43, 67), it forms the basis of serotyping *P. aeruginosa*. *P. aeruginosa* is classified into 20 major serotypes, O1 to O20, according to a comprehensive International Antigenic Typing Scheme (IATS) (68, 69). The chemical structures of all the OSAs from the 20 IATS type strains have been elucidated by Knirel and colleagues (70) and are presented as drawings in Figure 3 (71, 72). In addition to the IATS serotypes presented in Figure 3, Knirel and colleagues (70) comprehensively review the structures of subserotypes/subgroup along with their Lányi and Bergan O-serogroup (73) and Fisher immunotype (74) nomenclatures.

As illustrated, the OSAs are built of repeating units containing 2–5 sugars which are composed by various combinations of sugars and intersugar linkages (α or β) (66). Biologically rare, acidic and/or amino (75) sugars are found as a component of many of these OSAs. Some of the rare sugars include L-FucNAc (a component of the O4, O11 and O12 OSAs), di-*N*-acetylated mannuronic acid (D-ManNAc3NAcA, a component of the O5, O16, O18 and O20 OSAs), and a uronamide sugar GalNAcAN (a component of the O6 OSA) (33, 76-78). The presence of acidic sugars [e.g., mannuronic acid and L-guluronic acid derivatives, pseudaminic acid (Pse), 8-epilegionaminic acid (8eLeg), etc.], which are seldom found in other Gram-negative bacteria including *E. coli* (79), *Shigella* (80), or *Salmonella* species (81, 82), is characteristic to most *P. aeruginosa* serotypes. The result of acidic residues is an *O*-polysaccharide chain with a net-negative charge which contributes to the overall hydrophilic properties of the surface of *P. aeruginosa* (72, 83). This hydrophilic surface, in turn, has been demonstrated to play an important role in the adherence of OSA+ cells (OSA+/CPA+ and OSA+/CPA-) to surfaces such

as glass. With the exception of serotype O15 and O17, all serotypes possess either D-QuiNAc (2-acetamido-2-deoxy-D-quinovose), D-FucNAc (2-acetamido-2-deoxy-D-fucose) or a derivative of these at the reducing terminus of their repeating units (84).

Figure 3. Chemical structures of the O-specific antigen (OSA) repeating units of *P. aeruginosa* IATS serotypes O1–O20. Structures are clustered based on similarities in composition. –OH groups linked to the preceding (⧫) and succeeding (*) OSA repeating unit are indicated. Monosaccharides are coloured as followed: red, fucose (Fuc); navy blue, quinovose (Qui); purple, galactose (Gal); black, glucose (Glc); brown, rhamnose (Rha); amber, xylose (Xyl); teal, mannose (Man); grey, gulose (Gul); green, 8-epilegionaminic acid (8eLeg); cyan, pseudaminic acid (Pse); magenta, ribose (Rib). Chemical modifications: Ac, acetyl; Am, amidino; Fo, formyl; *R*Hb and *S*Hb, (*R*)- and (*S*)-3-hydroxybutanoyl, respectively. The stereochemistry of the sugars is denoted by L- and D-. This figure was taken from Islam and Lam (72) with permission from the authors.

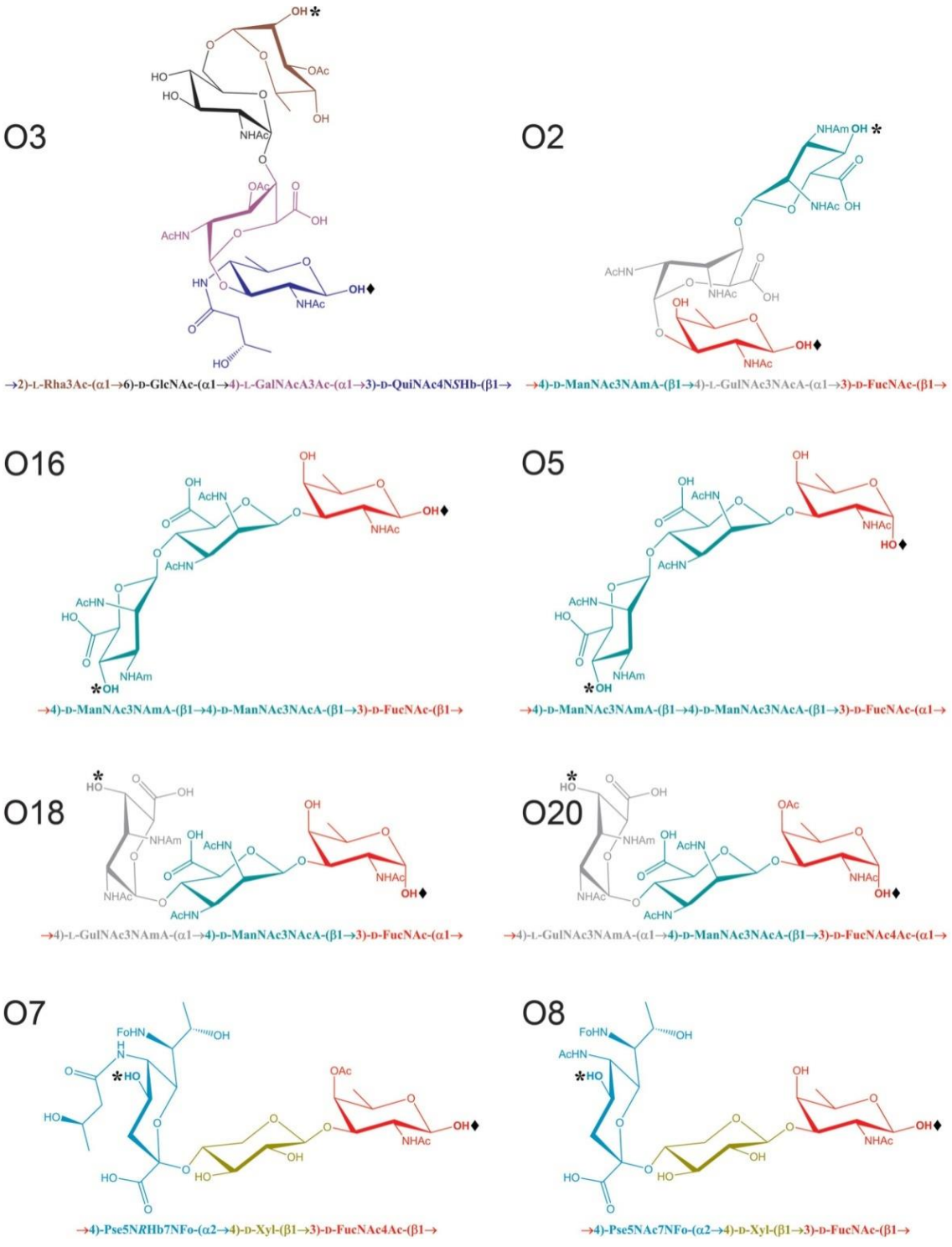

Figure 3. (continued).

O11

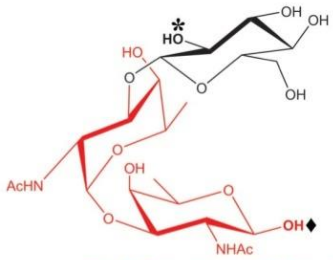

→2)-D-Glc-(β1→3)-L-FucNAc-(α1→3)-D-FucNAc-(β1→

O6

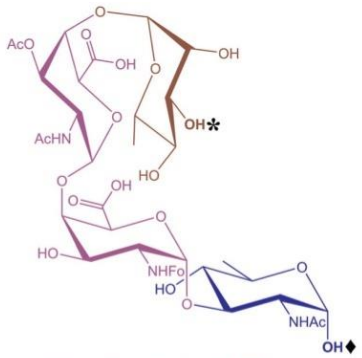

→3)-L-Rha-(α1→4)-D-GalNAcA3Ac-(α1→4)-D-GalNFoA-(α1→3)-D-QuiNAc-(α1→

O13

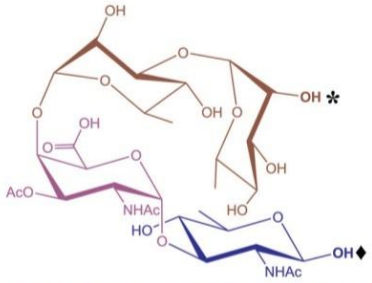

→2)-L-Rha-(α1→3)-L-Rha-(α1→4)-D-GalNAcA3Ac-(α1→3)-D-QuiNAc-(β1→

O14

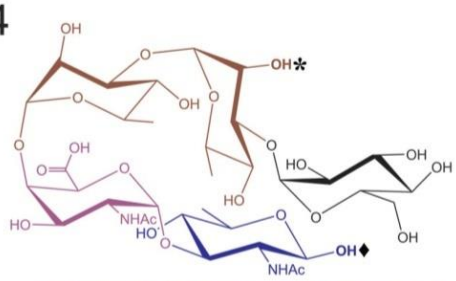

→2)-[D-Glc(α1→3)]-L-Rha-(α1→3)-L-Rha-(α1→4)-D-GalNAcA-(α1→3)-D-QuiNAc-(β1→

O10

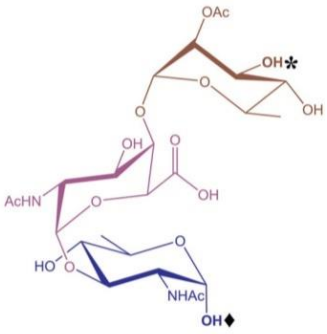

→3)-L-Rha2Ac-(α1→4)-L-GalNAcA-(α1→3)-D-QuiNAc-(α1→

O19

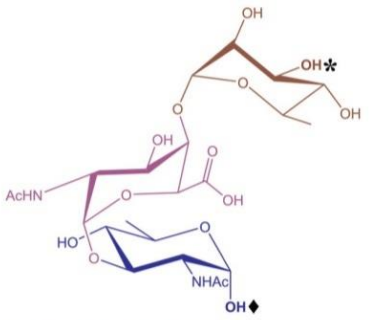

→3)-L-Rha-(α1→4)-L-GalNAcA-(α1→3)-D-QuiNAc-(α1→

O4

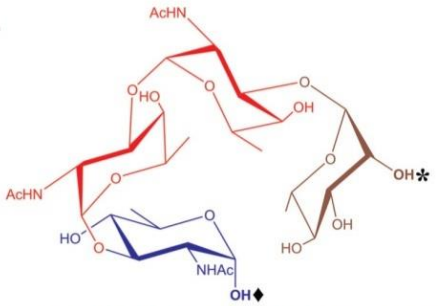

→2)-L-Rha-(α1→3)-L-FucNAc-(α1→3)-L-FucNAc-(α1→3)-D-QuiNAc-(α1→

O12

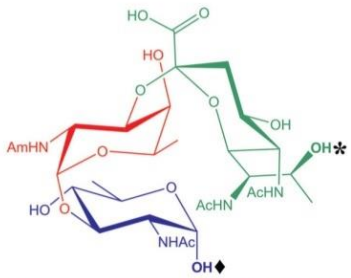

→8)-8eLeg5NAc7NAc-(α2→3)-L-FucNAm-(α1→3)-D-QuiNAc-(α1→

Figure 3. (continued).

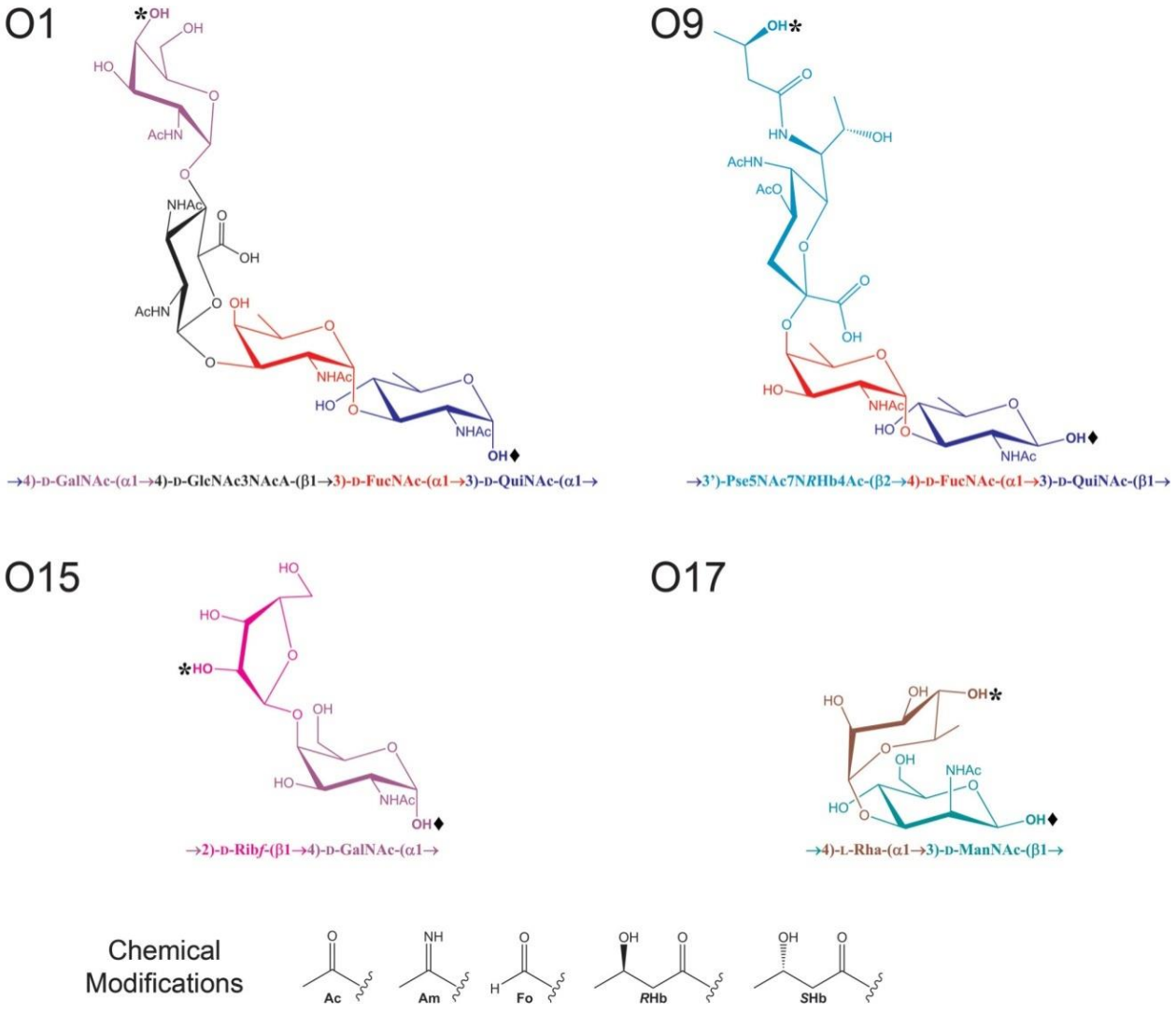

Figure 3. (continued).

2.1.3.1.2. **O6 OSA**

Since the work of this thesis centres around serotype O6, and in particular the O6a, 6d strain, we will take a closer look at the structure of the O6 OSA. Serotype O6 encompasses serologically related strains that possess fine structural variations away from the IATS O6 type strain. Before the implementation of the IATS serotyping scheme, *P. aeruginosa* strain O6a,6d was designated as Lányi O4a,d (85). Lányi serogoup O4 also included O4a,b and O4a,c. Since these were demonstrated to be serologically related to serotype O6 (Habs classification) and immunotype I (Fisher classification), these were united into serogroup O6 (73, 86). Strains O4a,b, O4a,c and O4a,d became O6a, O6a,b, O6a,c and O6a,d, respectively. Other serologically related O6 strains that have different nomenclature include PAK, Fisher 1 and Homma G.

The backbone of the O6 OSA is composed of a tetrasaccharide of L-rhamnose (L-Rha), 2-acetamido-2-deoxy-D-galacturonamide (D-GalNAcAN), 2-deoxy-2-formamido-D-galacturonic acid (D-GalNFoA), and 2-acetamido-2,6-dideoxy- D-glucose (D-QuiNAc) (70) (Figure 4). Both GalNA derived sugars can exist in a uronamide form, which is rare in nature (87). D-GalNAcAN always exists in the uronamide form, while that of D-GalNFoA is strain dependent. Other structural variations among O6 strains include 3-O-acetylation of the D-GalNAcAN sugar (D-GalNAc3OAcAN) (70), the degree of amidation of the D-GalNFoA sugar (D-GalNFoAN, i.e., the uronamide form) (88), the stereochemistry (α or β) between the D-QuiNAc and L-Rha linkage, and the site that D-QuiNAc attaches to L-Rha (at position 2 or 3) (84). The primary strain used for the work of this thesis is O6a, 6d; its D-GalNAcAN is 80% 3-O-acetylated (67), its D-GalNFoA sugar is 20% amidated (88), D-QuiNAc is attached to L-Rha at position 3 in a β configuration, a unique feature among elucidated O6 structures.

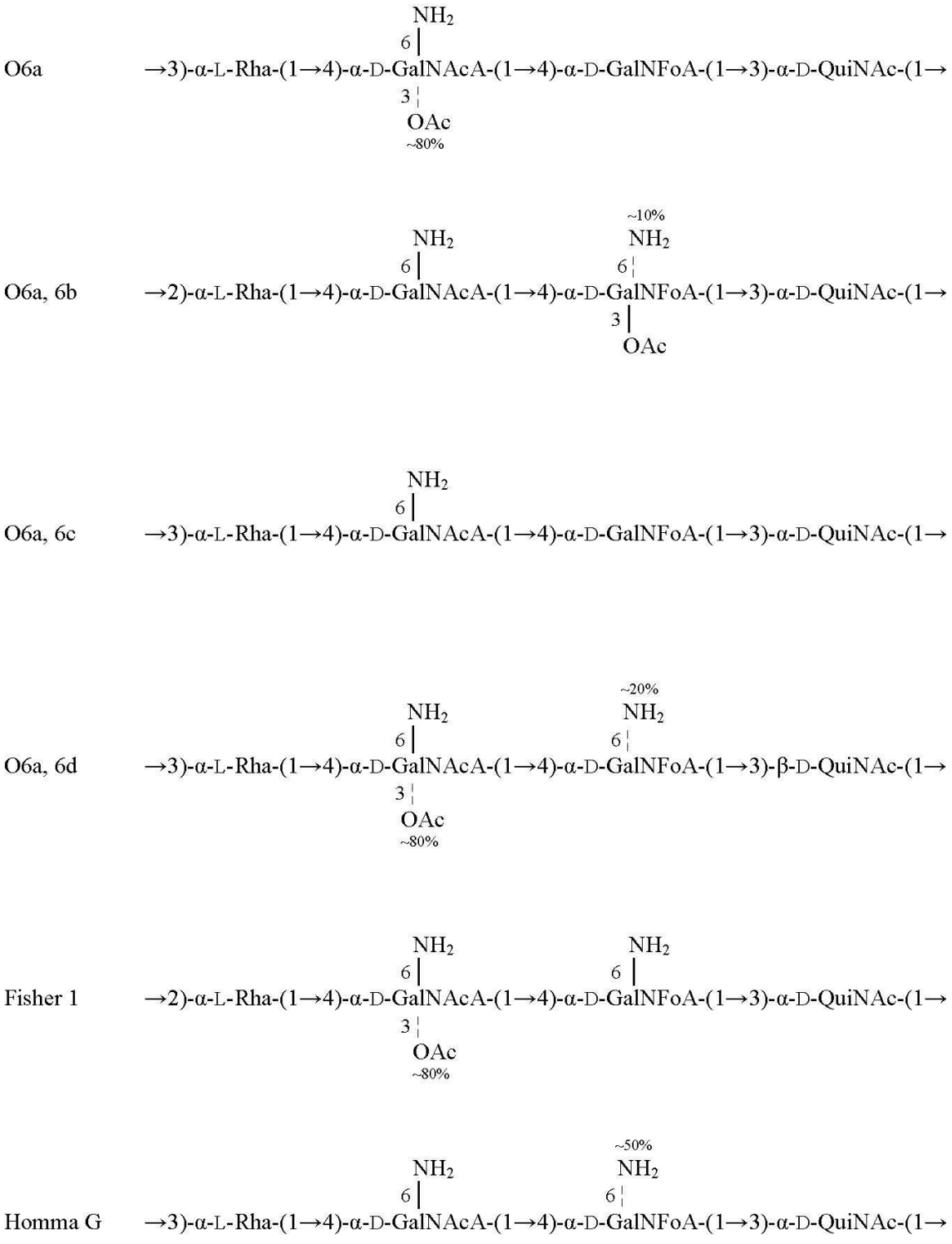

Figure 4. Structure of the OSA of various strains from *P. aeruginosa* serotype O6. Adapted from King *et al*. (59), Knirel *et al*. (70), Stanislavsky and Lam (67) and Vinogradov et al. (88). Note that strain O6a is also called O6 IATS, and Habs 6 and Fisher 1 are also called Immunotype 1.

2.1.3.1.3. **Common polysaccharide antigen, CPA**

The CPA is a neutrally charged, weakly immunogenic, homopolymer of D-rhamnose, a rare sugar only found in bacteria (32, 89-93). The CPA of *P. aeruginosa* is arranged in the following trisaccharide repeating unit: $[\rightarrow 3)$D-Rha$(\alpha 1 \rightarrow 3)$D-Rha$(\alpha 1 \rightarrow 2)$D-Rha$(\alpha 1 \rightarrow]_n$ (94-97). Other bacterial strains that express this same trisaccharide repeating unit in their *O*-polysaccharide include plant pathogens: *P. syringae* strains (92, 98, 99) and *Xanthomonas campestris* pv. *phaseoli* var. *fuscans* GSPB 271 (93). Moreover, this same repeating unit is present in at least two other hospital-acquired pathogens associated with lung infections in CF patients: *Burkholderia cepacia* (previously called *Pseudomonas cepacia)* (100) and *Stenotrophomonas maltophilia* (101-103). While the biological function of the CPA is not fully understood, it is thought that the CPA of *P. aeruginosa* plays a vital role in adherence of cells to human airway epithelial cells (104). In fact, the CPA, which confer hydrophobicity to the cell surface (83), is crucial for the development of biofilms which is important to establish long-term colonization in hosts (105).

The synthesis of the CPA is assembled via an ABC (ATP-binding cassette) transport system (106, 107); this pathway has been extensively reviewed and will not be covered herein (108).

2.1.3.2. Core region

The core regions of many strains, including reference strains from all 20 serotypes, of *P. aeruginosa* have been elucidated (71, 84, 109-114). The core oligosaccharide is composed of a highly conserved inner core region and a more variable outer core region (Figure 5) (71). The outer core is synthesized into two distinct glycoforms: an uncapped glycoform (also known as

glycoform 1) and capped glycoform (also known as glycoform 2) which differ in the position of a terminal L-rhamnose (L-Rha^{A} and L-Rha^{B}) residue (Figure 5) (59). For all serotypes of *P. aeruginosa*, the *O*-polysaccharide can only be attached to the outer core via position 3 of the L-Rha^{B} of the capped glycoform. The linkage of the CPA to outer core has not been structurally elucidated yet (107). Even for smooth OSA+/CPA+ strains, most LPS molecules of *P. aeruginosa* (ca. 92%) are uncapped (i.e., deficient in *O*-polysaccharide), which is much more than other Gram-negatives (61). While the capping with *O*-polysaccharide is not essential for the viability of *P. aeruginosa* (115), the complete inner core and possibly the first residue of the outer core (GalN) are required (97, 104, 110, 113).

The inner core of *P. aeruginosa* is highly conserved; in fact, the anti-inner core mAb 7-4, which was generated in Dr. Joseph Lam's laboratory (University of Guelph), is reactive towards the inner core of all 20 IATS *P. aeruginosa* serotypes and with that of other species of *Pseudomonas* (116). The inner core region is covalently linked to the lipid A moiety, and consists of sugars commonly found in the inner core, two residues of 3-deoxy-D-*manno*-oct-2-ulosonic acid (Kdo^{I} and Kdo^{II}) and two residues of L-*glycero*-D-*manno*-heptose (Hep^{I} and Hep^{II}). The Hep residues are substituted by various degrees of phosphorylation (P) and by a 7-O-carbomyl (Cm) group. Among all LPS core described, the inner core of *P. aeruginosa* is the most phosphorylated (59, 117). These phosphate groups along with the amino sugars on the OSA make the LPS of *P. aeruginosa* highly negatively charged. Core phosphate groups are essential for the survival of *P. aeruginosa* and also confer intrinsic drug resistance (117). Like other Gram-negatives, LPS molecules are cross-linked to one another via the ionic interactions formed between divalent cations (Mg^{2+} and Ca^{2+}) and the negatively charged phosphate (P) on the Hep residues, thereby forming a stable and highly ordered OM structure (118). While the

inner core of the OSA LPS is rich in phosphate groups, that of the CPA is substituted with the very unusual presence of sulfates (119).

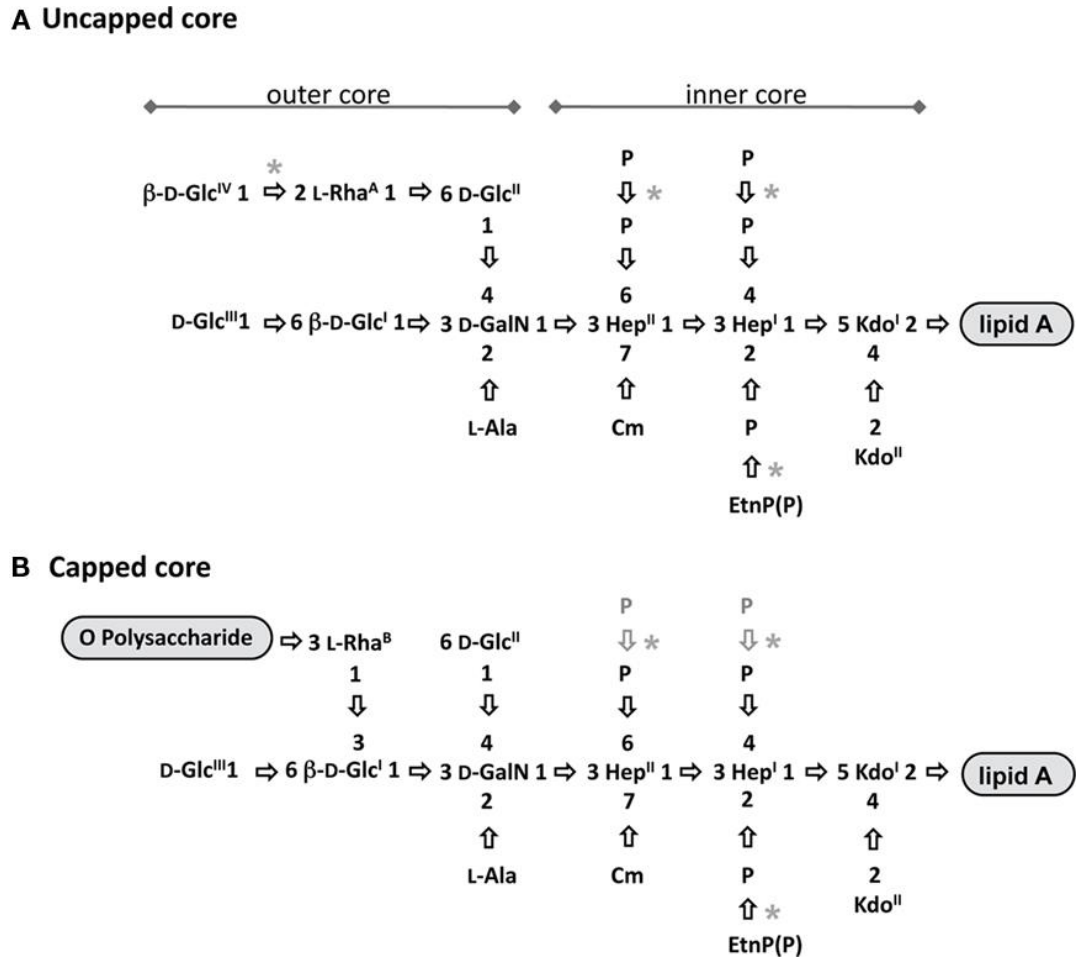

Figure 5. Structures of uncapped core oligosaccharide (A) and capped core oligosaccharide (B). Unless otherwise indicated, sugars have the *α* configuration. Asterisks indicate variable substitutions. For example, serotype O6 (immunotype I), which is the primary serotype used in this study, does not possess the Glc^{IV} residue in the uncapped core (84). Ala, alanine; Cm, carbamoyl; Etn, ethanolamine; GalN, 2-amino-2-deoxy-galactose (galactosamine); Glc, glucose; Hep, L-glycero-D-*manno*-heptose; Kdo, 3-deoxy-D-*manno*-oct-2-ulosonic acid; Rha, rhamnose. This figure taken from Lam *et al*. (33) with permission from the authors.

2.1.3.3. Lipid A

The lipid A consists of a doubly-phosphorylated diglucosamine (di-GlcNAc) backbone that carries several fatty acid chains that are embedded in the outer leaflet of the OM (Figure 6). Most laboratory strains of *P. aeruginosa* have five (75% of strains) or six (25% of strains; Figure 6A red acyl chain) acyl chains which are shorter than those from the lipid A of *E. coli* (Figure 6C) (59, 120). Clinical strains of *P. aeruginosa* adapt by altering the structure of their lipid A in various ways [Figure 6B, reviewed by King *et al*. (59) and Lam *et al*. (33)], for e.g. by the addition of acyl chains or the addition of 4-amino-4-deoxy-L-arabinose (L-Ara4N) on the phosphate groups (121-123). Some of these modifications are found when laboratory strains are grown under particular conditions (e.g., in the presence of polymyxin B or low Mg^{2+} concentration).

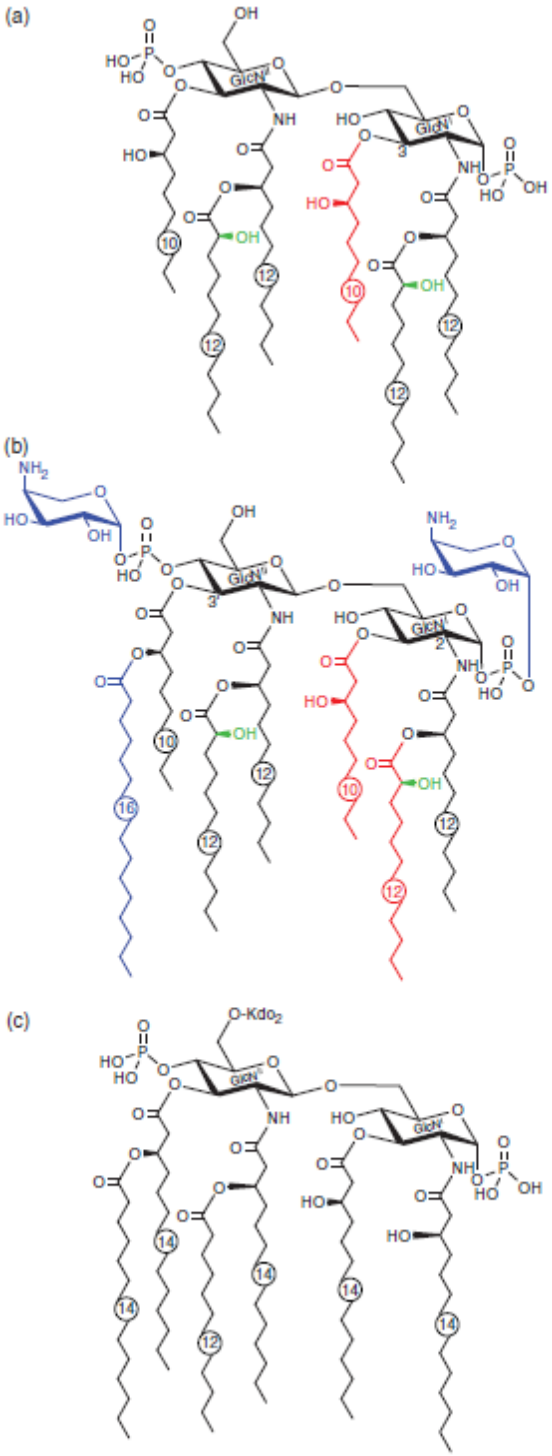

Figure 6. Comparison of the lipid A structure from (a) a laboratory *P. aeruginosa* strain, (b) a clinical *P. aeruginosa* isolate, and (c) an *E. coli*. Figure taken from King *et al*. (59); permission to reuse figure was granted by SAGE Publishing.

2.2. BASIC STRUCTURE AND CLASSIC EFFECTOR FUNCTIONS OF ANTIBODIES

Antibodies, also known as immunoglobulins (Ig), are heterodimeric glycoproteins which are naturally produced and secreted by mammalian plasma cells (B cells) as a defence mechanism towards foreign antigens. Among the five distinct classes of antibodies, i.e., IgA, IgD, IgE, IgG, and IgM, IgG is the most abundant class of antibody in serum and accounts for about 80% of the total serum antibodies (124). There are four subclasses of IgGs, known as IgG_1, IgG_2, IgG_3 and IgG_4 in humans, and IgG_1, IgG_{2a}, IgG_{2b} and IgG_3 in mice. While their specificity may differ extensively, the structure and composition of IgGs are highly conserved among vertebrate species. Whole IgG molecules are composed of two identical heavy (H) chains and two identical light (L) chains, which are joined together by disulfide bonds to form a tetrameric molecule of about 150 kDa (Figure 7). Heavy chains fold into three constant domains (C_H1, C_H2 and C_H3), and one variable domain (V_H) which is located at the amino terminus of the polypeptide. Light chains fold into two domains; a constant light domain (C_L) and a variable light domain (V_L). The antigen-binding site is mostly formed by the combination of three complementarity-determining regions (CDRs, denoted as CDR-H1, CDR-H2, CDR-H3, CDR-L1, CDR-L2 and CDR-L3) provided by both variable domains. Since these CDRs account for most of the variability and differences among antibodies they are also known as hypervariable regions. These CDR regions determine the antigen-binding specificity and affinity by forming a surface complementary to the structure of the epitope on an antigen. The CDRs are supported by a conserved Ig scaffold formed by the framework regions (FR; designated FR1, FR2, FR3 and FR4).

IgGs have two functionally separable regions: a Fab (fragment antigen binding) fragment for target recognition and a Fc (fragment crystallizable) region for triggering effector functions

and regulating *in vivo* half-life and biodistribution (Figure 7). The Fc region mediates immune effector functions, including complement-dependent cytotoxicity (CDC), opsonic phagocytosis of target cells, and antibody-dependent cell-mediated cytotoxicity (ADCC) (124). Through their interaction with Fc receptors (FcR) expressed on immune effector cells, antibodies act as opsonins to facilitate ingestion and destruction by phagocytic cells (macrophages and neutrophils) (Figure 8). The complement system includes a set of serum proteins and proteases that represent one arm of innate humoral immunity; their interactions with antibodies bridge the innate and adaptive immune systems (124). The interaction of antibodies on the surface of an extracellular pathogen (e.g., *P. aeruginosa*) recruits, via interaction with the Fc region, C1q complexes from the complement system (Figure 8). In turn, C1q:antibody complexes activate pathogen lysis through the formation of membrane attack complex (MAC) pores via the classical pathway of the complement system.

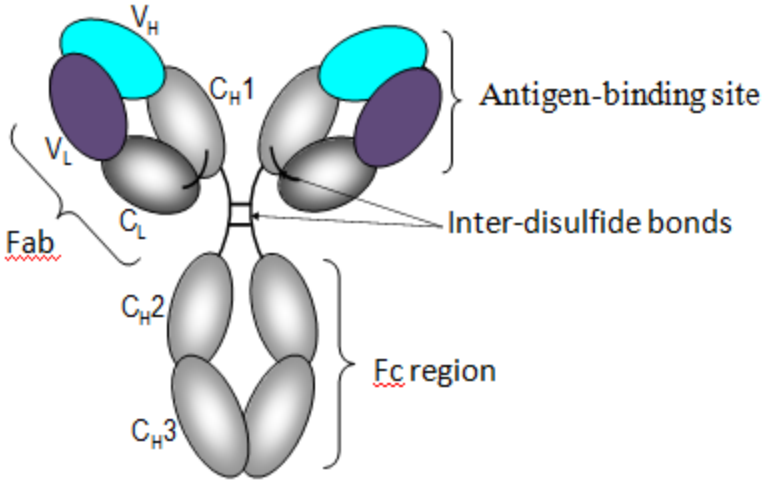

Figure 7. Basic structure of an immunoglobulin G (IgG).

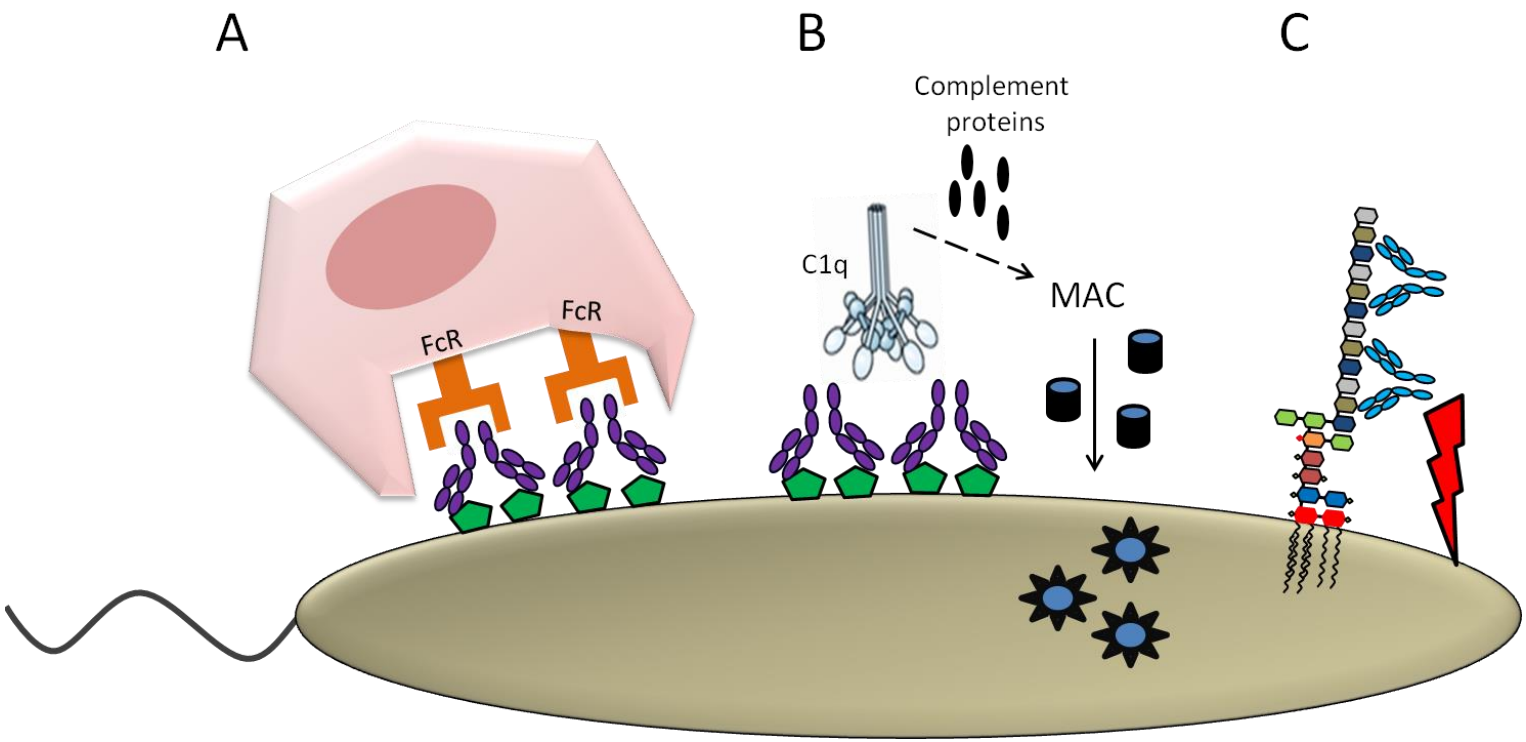

Figure 8. Bactericidal activity of antibodies. Pathogen-associated antibodies A) recruit macrophages and neutrophils via their interaction with Fc receptors (FcR), thereby facilitating opsonic phagocytosis, and B) recruit C1q complexes from the complement system, which in turn activate the classical pathway of the complement system. The complement cascade ultimately leads to the formation of membrane attack complexes (MAC) that insert in the pathogen's membrane, thereby leading to osmotic lysis. C) Some antibodies escape the traditional pillers of antimicrobial immunity, and have the capacity to directly kill their target pathogen without requiring MAC or cellular assistance. One such antibody is S20, an anti-*P. aeruginosa* strain O6a, 6d (5). By binding the LPS, and more specifically the OSA, the S20 antibody has been demonstrated to severely damage the OM of strain O6a, 6d in a mechanism that was unknown at the time (Figure 9). Chapter 4 of this thesis will elucidate the mechanism of the S20 antibody.

2.3. THE BACTERICIDAL S20 ANTIBODY

The parental S20 antibody, an IgG_2, was produced by Dr. J. Schreiber and colleagues in the early 2000s (125). To generate this antibody, mice transgenic for human heavy and light Igs [XenoMouse, Abgenix; (126)] were immunized, intraperitoneally, with 10^7 heat-killed *P. aeruginosa* strain O6a, 6d cells. Thereafter, hybridomas were generated by standard hybridoma technology, and supernatants were screened by ELISA for binding against immobilized high molecular weight (MW) LPS isolated from strain O6a, 6d. The S20 antibody was selected based on its binding strength towards the LPS of strain O6a, 6d. While Hemachandra *et al*. (125) performed an S20-mediated, complement-dependent opsonisation assay with human polymorphonuclear leukocytes (PMN), it appears that a control consisting of strain O6a, 6d cells in the presence on only the S20 antibody was not included. As such, the direct bactericidal activity of the S20 antibody was not observed by this group.

As a proof of concept, Dr. J. Christopher Hall's laboratory, who worked towards expressing potential therapeutic monoclonal antibodies (mAbs) *in planta*, selected to express a version of the S20 antibody in transgenic tobacco plants. The antigen-binding variable domains (V_H and V_L) of the S20 antibody were synthesized, using the published DNA-coding sequences (GenBank accession numbers AAK39434 and AAK39435, respectively), and fused to the constant-region sequences of gamma-1 and kappa-2, generating the S20 IgG_1 (127). Using an *in vitro* opsonophagocytosis assay with human PMN as a source of effector cells, the purified plant-produced S20 IgG_1 was demonstrated to be capable of recruiting immune system effector function with O6a, 6d cells. Thereafter, when Xuemei Xie, a PhD student of Dr. Hall, was performing an *in vitro* assay, she unexpectedly observed a significant reduction in bacterial cells

(>90%) counts from one of her control treatments, i.e., live O6a, 6d cells and purified S20 IgG_1 [called tobacco-expressed human IgG_1; te-hS20 in (5)]. After performing blind studies, she confirmed that the S20 antibody, diverges from the traditional immunological dogma, and elicits direct bactericidal activity towards *P. aeruginosa* strain O6a, 6d, independent of the complement system and phagocytosis (5, 128).

To demonstrate that the bactericidal activity is independent of the Fc region of the antibody and agglutination effects, Xie *et al*. (5) engineered two antibody fragments of the S20 IgG_1: a single-chain fragment variable (scFv) and a fragment antigen-binding (Fab). For the S20 scFv, the DNA coding sequences of the V_L and V_H domains were chemically synthesized and joined by a $(Gly4Ser)_3$ linker in the V_L-linker-V_H direction; at its C-terminal end, the construct carries the His6x- and c-Myc tags. The S20 scFv construct was cloned into a *Pichia pastoris* expression vector, pPICZαA vector (Invitrogen, Carlsbad, CA), which carries the methanol-inducible AOX promoter, an α-secretion signal, and zeocin-resistance. Following expression, the S20 scFv was purified by immobilized metal ion affinity chromatography (IMAC); however, since scFvs are prone to dimerization, it will undergo size exclusion chromatography (SEC) following IMAC in this current study. The Fab fragment was not used in this current work, therefore, the interested reader can refer to Xie *et al*. (5) for its cloning strategy.

Both the S20 scFv and Fab fragments retained bactericidal activity comparable to the parental IgG_1 [>90% reduction in colony forming units, (CFU)], thus proving that the activity is independent of the Fc region of the antibody. Moreover, since these antibody fragments are monomeric, agglutination of O6a, 6d cells is not a contributing factor to the bactericidal activity. The variable domains were thus presumed to be exclusively responsible for the bactericidal

action against *P. aeruginosa* strain O6a, 6d. Pre-incubation of the antibodies with purified O6a, 6d LPS completely abolished the bactericidal activity, indicating the requirement for the antibodies to bind to cell surface LPS. A live/dead staining experiment revealed that the S20 antibody increases the membrane permeability of O6a, 6d cells in a time-dependent manner. Corroborating this result, electron micrographs demonstrated that the S20 antibody severely disrupts the integrity of cell wall of strain O6a, 6d (Figure 9). Treatment with 6.7 μM of S20 scFv induced the formation of membrane blebs or vesicles, almost uniformly over the entire cell surface. Other morphological effects induced by the S20 antibody included increased surface roughness, indentation, vesiculation, possible leakage of cellular contents, and the release of the flagella.

Importantly, the S20 antibody and its fragments provided *in vivo* protection in a leukopenic mouse model of *P. aeruginosa* strain O6a, 6d infection. While the S20 antibody showed no effect towards *E. coli* TG1, *Streptococcus agalactiae*, and *P. aeruginosa* IATS O10, Xie *et al*. (5) reported that it displayed non-specific bactericidal activity towards PAO1 (serotype O5), albeit at lower levels (ca. 30 – 60%). It is possible that the S20 antibody exhibits very low binding affinity, which was not detected by ELISA, to the LPS of PAO1. The fact that S20 antibody had been demonstrated to kill a strain to which it does not bind warranted further investigation: perhaps the S20 antibody has broader bactericidal activity than thought. This will need to be addressed in order to make progress in understanding the bactericidal mechanism of the S20 antibody.

While the S20-mediated bactericidal mechanism remained elusive, Xie *et al*. (2010) hypothesized that this antibody was an abzyme that possesses both antigen binding activity and catalytic activity against strain O6a, 6d. Catalytic antibodies, which are also known as abzymes,

combine the specificity of antibodies with the catalytic powers of enzymes. Some catalytic antibodies have been shown to be able to catalyze formation of toxic by-products that directly damage target cells or antigens (1, 3, 129). For example, antibodies can produce toxic oxygen species, including hydrogen peroxide (H_2O_2), trioxidane (H_2O_3), and ozone (O_3), from singlet dioxygen ($1O_2$*) and water (2, 130-132). Xie *et al*. (5) did not, however, detect peroxidase, DNase, or proteinase activities from the S20 antibody. It was then proposed that perhaps the S20 antibody exerts its bactericidal activity by hydrolyzing the LPS of *P. aeruginosa* strain O6a, 6d. In fact, some antibodies from human milk and from the sera of patients with cancer and multiple sclerosis possess polysaccharide-hydrolyzing or lipase activities (133-136). The possibility of the S20 hydrolyzing the LPS of strain O6a, 6d will be addressed in Chapter 3. Another hypothesis proposed by Xie *et al*. (5) was that S20, through its V_H domain rich in basic residues (arginine and lysine), functionally mimicked the bactericidal action of cationic antimicrobial peptides (AMPs) (137-139).

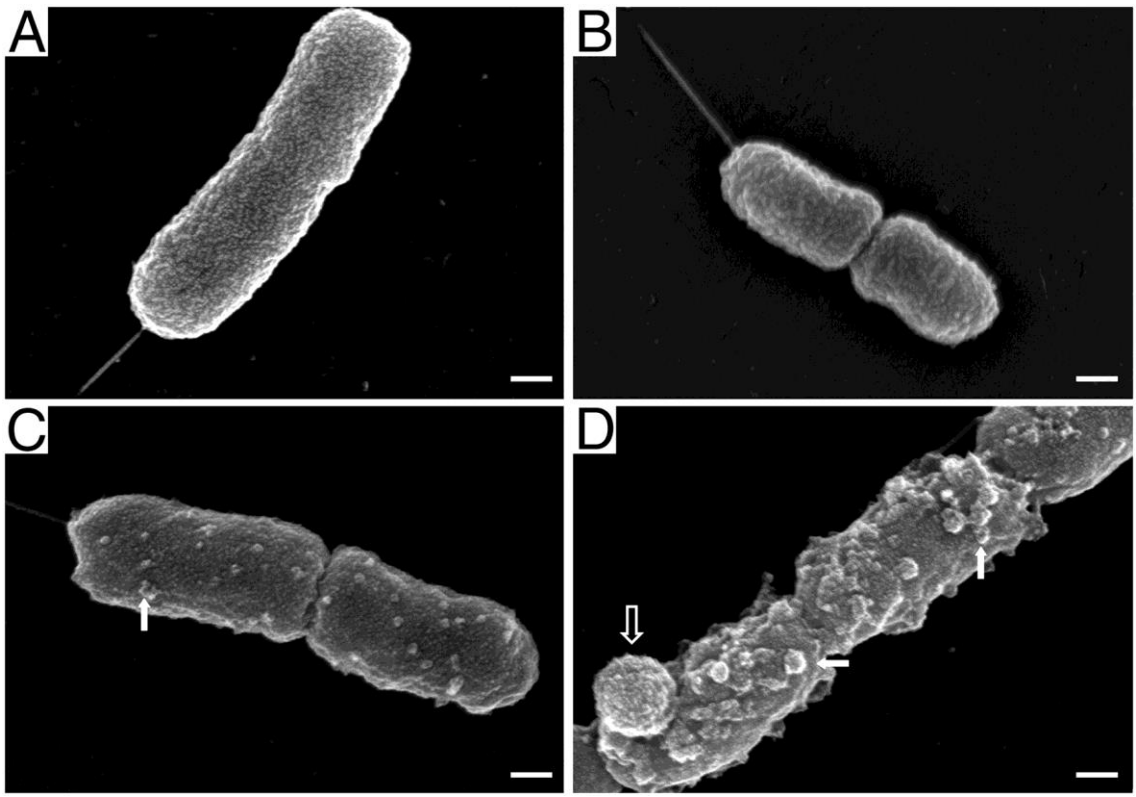

Figure 9. Field emission-scanning electron microscopy (FE-SEM) images of *P. aeruginosa* strain O6a, 6d. A and B, Untreated cells that were incubated in PBS without antibody at 37°C for 30 min and 6 h, respectively. C and D, Cells treated with 6.7 µM S20 scFv at 37°C for 30 min and 6 h, respectively. Treatment with the 20 scFv induced the formation of membrane blebs or vesicles (white arrows) and leakage of cellular content (black arrow). Magnification bars represent 600 nm. This figure was taken from Xie *et al*. (5); permission to reuse it was granted by The Journal of Immunology.

CHAPTER 3: ANTIBODIES TARGETING THE O-SPECIFIC ANTIGEN (OSA) OF *PSEUDOMONAS AERUGINOSA* SEROTYPE O6 MEDIATE DIRECT BACTERICIDAL ACTIVITY.

3.1. ABSTRACT

Our group previously demonstrated that the S20 antibody, and scFv and Fab fragments derived therefrom, exerts direct bactericidal activity towards *Pseudomonas aeruginosa* strain O6a, 6d. By binding to the LPS, and more specifically the O-specific antigen (OSA), the S20 antibody was observed to induce severe cell wall damage by a mechanism that remained elusive. It was initially proposed that the S20 was an abzyme that possessed a potent catalytic activity towards strain O6a, 6d. To unravel if this activity is unique and harboured within the S20 antibody molecule, we surveyed additional anti-LPS monoclonal antibodies (mAbs) that have been published and were made available to us from the laboratory of Dr. Joseph Lam (University of Guelph). MAb 7-4 that targets the highly conserved LPS inner-core and mAb N1F10 (and its scFv) specific for the common polysaccharide antigen did not affect the viability of various *P. aeruginosa* strains. However, by targeting the OSA of serotype O6 with mAb MF23-1 and its Fab fragment, direct bactericidal activity was immediately apparent against all wild type O6 strains that have an OSA^+ phenotype. It is worth noting that O6 is the most clinically prevalent *P. aeruginosa* serotype reported in numerous epidemiology studies to date. Our data established that there is a direct correlation between the affinity (K_D) of the antibodies (based on surface

plasmon resonance studies) and their bactericidal potency towards strain O6a, 6d, the order of most bactericidally active being: S20 scFv dimer [K_D (apparent) = 21 nM; MIC_{50} = 60 nM] > S20 scFv monomer [K_D = 560 nM; MIC_{50} = 450 nM] > mAb MF23-1 [K_D (monovalent) = 18 μM; MIC_{50} = 2.5 μM]. Since the S20 and MF23-1 antibodies share little sequence identity in their respective variable domains, one would not anticipate that their bactericidal activity be residing in their sequences *per se* as would be expected for a catalytic antibody. Instead, we provide the evidence to show that these antibodies are exploiting a vulnerable target on the surface of *P. aeruginosa*, the OSA of serotype O6. Thus targeting the *O*-polysaccharide, whose main role is to provide a protective shield to its bacterium, is a viable option to make *P. aeruginosa* vulnerable to bactericidal activities rendered by specific antibodies. The observation made in this work provides some insight into the strong-selective pressure on long-term clinical *P. aeruginosa* isolates to lose their OSA+ phenotype.

3.2. INTRODUCTION

Antibodies typically do not directly eliminate their target pathogens, but instead exert their protective function by activating other arms of the immune system [i.e., via other processes including complement dependent-cytotoxicity (CDC), opsonic phagocytosis, Ab-dependent cell-mediated cytotoxicity (ADCC)] which ultimately lead to destruction of the invading microbial organisms (124). Paradoxically, some antibodies have the capacity to directly kill their target bacterium independent of the complement system or immune effector cells (4, 5, 9, 140-142). The antimicrobial mechanisms of these antibodies range from catalyzing the production of oxidative molecules (1-3), to interfering with biological functions (4), or directly damaging their target's membrane (5-10).

In 2010, Xie *et al*. (5) reported that the S20 antibody (IgG_1), which is directed against LPS and more specifically the O-specific antigen (OSA) of *P. aeruginosa* strain O6a, 6d (Figure 4), mediates bactericidal activity independent of the complement system or phagocytes (5). The Fc region of this antibody is not required as the S20 scFv and Fab fragments retain comparable levels of bactericidal activity as the parental antibody: all were able to cause a reduction of *in vitro* O6a, 6d colony forming unit (CFU) counts by >90% within 30 min. Importantly, the S20 antibody and its fragments provided *in vivo* protection in a leukopenic mouse model of *P. aeruginosa* strain O6a, 6d infection. While no binding was detected towards the OSA of serotype O5, Xie *et al*. (5) reported that the S20 antibody exerts non-specific bactericidal activity towards PAO1 (serotype O5), albeit at lower levels (ca. 30–60%). A live/dead staining experiment revealed that the S20 antibody increases the membrane permeability of O6a, 6d cells in a time-dependent manner. Some of the cell wall damage induced by treatment of O6a, 6d with the S20 scFv, as observed by electron microscopy, includes increased surface roughness and indentation, release of flagella, and the formation of membrane blebs or vesicles, and leakage of cellular contents.

P. aeruginosa is a rod-shaped, motile, and Gram-negative bacterium widely found in the environment (17). It is an opportunistic pathogen (nosocomial pathogen) which causes disease in individuals with impaired host defences, such as those suffering from AIDS, cancer, burn wounds and patients afflicted with the recessive genetic disease cystic fibrosis (CF) (13). The cell wall of Gram-negative bacteria is composed of an asymmetric outer membrane (OM), an inner membrane (IM), and a thin peptidoglycan sheet that lies in the periplasmic space between the OM and IM. The most abundant component (~90%) of the outer leaflet of the OM is the LPS. LPS is a multifunctional molecule that provides structural integrity to the outer membrane

(OM) and acts as a permeable barrier to limit the passive diffusion of hydrophobic molecules (e.g., antibiotics, detergents) into the cell wall. LPS is composed of three structurally distinct domains: 1) the lipid A (endotoxin), a highly acylated diglucosamine (di-GlcNAc) backbone that is embedded in the outer leaflet of the OM; 2) the oligosaccharide core region, which is composed of the highly conserved and unusual sugars, ketodeoxyoctonic acid (KDO) and heptoses; and 3) an *O*-polysaccharide chain which extends about 30–40 nm away from the OM (55, 57, 58). Most planktonic strains of *P. aeruginosa* simultaneously produce two structurally distinct *O*-polysaccharides: the common polysaccharide antigen (CPA; formerly called A-band) and the O-Specific Antigen (OSA; formerly called B-band) (60, 61) (Figure 2). While the CPA is composed of a weakly immunogenic homopolymer of D-rhamnose [→ 3)D-Rha(α1 → 3)D-Rha(α1 → 2)D-Rha(α1 →]$_n$ (94-97), the OSA is a highly immunogenic heteropolymer of two to five distinct, and often unusual, sugars in the repeating units (66, 70, 71). Since the OSA is the surface antigen which elicits the strongest antibody response (43, 67), it forms the basis of serotyping *P. aeruginosa*. *P. aeruginosa* is classified into 20 major serotypes, O1 to O20, according to a comprehensive International Antigenic Typing Scheme (IATS) (68, 69). The chemical structures of all the OSA from the 20 IATS type strains have been elucidated by Knirel and colleagues (70), and were presented as chemical drawings by Islam and Lam (72) (Figure 3 of Chapter 2) (71). The chemical structures of various strains from serotype O6, the main serotype used in this study, have also been elucidated (Chapter 2, Figure 4). Like enteric bacteria, smooth strains of *P. aeruginosa* contain a heterogenous mixture of LPS molecules with different chain lengths of OSA (Figure 2). In *P. aeruginosa* the chain length of the OSA is regulated by two Wzz polysaccharide polymerases, namely Wzz_1 [modulates 12–16 repeats and 22–30 repeats; (62, 63)] and Wzz_2 [modulates 40–50 repeat length; (62)]. While the OSA is the

predominant form of LPS in wild-type strains and strains isolated from acute infections, its production, unlike that of CPA, appeared to be regulated as a result of adaptation due to pathogen host interactions; i.e., OSA is either reduced in amount or completely abrogated as a result of chronic selective pressures in clinical isolates, especially those isolated from CF patients (60, 64).

While the S20-mediated bactericidal mechanism remained elusive, Xie *et al*. (2010) hypothesized that this antibody is an abzyme that has co-evolved to possess both antigen binding and catalytic activity towards O6a, 6d. Catalytic activities including DNase, proteinase, and peroxidase were not detected from the S20 antibody. It was therefore proposed that perhaps the S20 antibody exerts its bactericidal activity by hydrolyzing the LPS of *P. aeruginosa* strain O6a, 6d, similar to the action of some bacteriophage tailspike proteins. In fact, some antibodies from human milk and from the sera of patients with cancer and multiple sclerosis possess polysaccharide-hydrolyzing or lipase activities (133-136). Another hypothesis proposed was that S20 functionally mimicked cationic antimicrobial peptides (AMPs).

Before commencing the laborious work of identifying the likely amino acids involved in the killing mechanism of the S20 antibody, we first needed to establish if this unusual activity truly resides in the antibody sequence *per se*, or if targeting the LPS of *P. aeruginosa* is responsible for its bactericidal activity. Thus, we decided to start by screening antibodies that target various epitopes in the LPS molecule of *P. aeruginosa* (Table 1). MAb MF23-1 (and its Fab fragment) was screened since it not only binds the O6a, 6d OSA (i.e., same antigen as S20) but also cross-reactively binds all O6 OSA (Figure 4) (143). A commercial anti-O3 mAb (ab84607) was screened to determine if targeting the OSA of another serotype, i.e., serotype O3, produces similar effects. Since the OSA of *P. aeruginosa* is highly variable among

strains/serotypes and since its expression tends to progressively diminish in clinical strains, we examined the effect of treating O6 strains with two mAbs that were specific against two conserved LPS antigens, namely the CPA and the inner core LPS, respectively. We also investigated whether targeting the *O*-polysaccharide of another Gram-negative bacterium would generate similar bactericidal effects as those observed towards *P. aeruginosa*. We chose to screen 3B1 scFv, an anti-*Salmonella* serogroup B *O*-polysaccharide antibody (144), because its parental mAb Se155-4 is a very well-characterized antibody with available X-ray crystal structure data (145, 146).

Here we report, for the first time, that mAb MF23-1 and its Fab fragment to target OSA (same antigen specificity as mAb S20) also mediate direct bactericidal activity towards wild type O6 strains. Since MF23-1 does not share significant level of sequence identity with S20, especially in the complementarity determining regions (CDRs), the bactericidal activity could not reside in the S20 and MF23-1 antibody sequences *per se*, i.e., they are not catalytic in nature. Instead, these antibodies are exploiting a vulnerable target on *P. aeruginosa*: the O6 OSA. This discovery further broadens the classical views of how antibodies mediate effective defence mechanisms to destroy invading gram-negative bacteria. Based on our initial findings, we decided to further characterize the S20 and MF23-1 antibodies, in terms of sequence, binding, minimal inhibitory concentration (MIC), before proceeding to studying their effects on the surface of *P. aeruginosa* by atomic force microscopy (Chapter 4).

3.3. MATERIALS AND METHODS

3.3.1. Anti-LPS antibodies used in this study

Table 1 provides a summary of the different mAbs and antibody fragments that were screened in this study.

Table 1. Summary of anti-LPS antibodies used in this study. Unless specified, these antibodies target the LPS of *P. aeruginosa*.

Antibody or fragment	Specificity	Expression system	Source	Reference
S20 scFv	O6a, 6d OSA	*Pichia pastoris*	Dr. J. Christopher Hall	(5)
MF23-1 (murine IgG3)	O6 OSA	Hybridoma	Dr. Joseph S. Lam	(143)
MF23-1 Fab	O6 OSA	Obtained by papain-digestion of MF23-1 mAb	This study	This study
7-4 (murine IgG2b)	Inner-core LPS	Hybridoma	Dr. Joseph S. Lam	(116)
N1F10 (murine IgM)	CPA	Hybridoma	Dr. Joseph S. Lam	(60)
N1F10 scFv	CPA	*Pichia pastoris*	This study	This study
***ab84607 (murine IgG3)**	O3 OSA	Hybridoma	Abcam	N/A
LPT3-1 (murine IgG2a)	Inner-core LPS of *Neisseria meningitidis*	Hybridoma	Dr. Andrew D. Cox	(147)
3B1 scFv (parental mAb: Se155-4)	O-Ag of *Salmonella* serogroup B	*Escherichia coli*	Dr. N. Martin Young	(148), (144)

* The Abcam anti-O3 mAb (ab84607) is no longer commercially available; however, its product datasheet can still be accessed on the Abcam website.

3.3.1.1. Production of mAbs in hybridoma tissue culture

The hybridoma culture medium was composed of Dulbecco's Modified Eagle Medium (DMEM, Sigma) supplemented with 10% (v/v) Gibco™ fetal bovine serum (FBS, ultralow IgG, < 5 μg mL-1, US origin) (Invitrogen), 1% (v/v) antibiotic-antimycotic (Invitrogen) and 20 mM L-glutamine (Invitrogen). Immediately following thawing (not completely thawed) in a 37°C water bath with swirling, the contents of a one vial of a hybridoma clone were transferred to 5 mL of culture medium and gently centrifuged at 300 rpm for 3 min to remove DMSO. The pelleted cells were gently resuspended in 5 mL of culture medium, transferred in a T25 tissue culture flask and incubated at 37°C in a CO_2 incubator. The hybridoma cell lines were split to obtain ca. 10^6 cells mL^{-1} (ca. 1:4, ca. every 2-3 days), and transferred to an appropriate tissue culture flask (T75 or T175). Since hybridoma cells secrete the mAb, the tissue culture supernatant was collected, filtered through a 0.22 μm PVDF membrane (Stericup filter unit, Millipore), and stored at 4°C until ready for purification.

3.3.1.2. Purification of mAbs

MAbs MF23-1 and LPT3-1 were purified from the hybridoma cell culture supernatant by standard protein G affinity chromatography followed by exchanging the buffer to PBS (pH 7.4) using a HiPrep Desalting 26/10 column (GE Healthcare). The purification of mAb 7-4 was more challenging as it precipitated immediately upon acidic elution from protein A/G columns, even before reaching the Eppendorf tube that contained the neutralization buffer, 1M Tris-HCl, pH 8.0. The addition of salts (0.15 M NaCl) to the elution buffer (0.1 M sodium citrate, 0.15 M NaCl, pH 3.6) and binding buffer (20 mM sodium phosphate, 0.15 M NaCl, pH 7.4) stabilized this antibody. MAb 7-4 was purified using a 5-mL protein A column (GE Healthcare) (Figure

48A), and was buffer exchanged to PBS (pH 7.4) using a HiPrep Desalting 26/10 column (GE Healthcare) (Figure 48B).

N1F10 IgM was purified using a 1 mL HiTrap IgM Purification HP column (GE Healthcare) and according to the manufacturer's instructions, and further polished by SEC using a HiLoad S200 16/60 (GE Healthcare).

Commencial ab84607 (anti-O3) was passed through a 5-mL HiTrap desalting column (GE Healthcare) to remove the sodium azide (0.09%) preservative before proceeding with the bactericidal assay.

All purified antibodies were prepared in PBS, pH 7.4, 0.22 µm filtered and stored at 4°C.

3.3.1.3. Production of antibody fragments

3.3.1.3.1. **S20 scFv monomer and dimer**

The S20 scFv, which was previously cloned in the pPICZα-A vector [Invitrogen; (5)], was expressed in *Pichia pastoris* strain X-33 (pPICZαA-scFv-S20) in a manner similar to that described in the EasySelect™ *Pichia* Expression Kit Manual (Cat. no. K1740-01, Invitrogen). This vector has an alpha factor secretion signal which directs extracellular expression. Briefly, a single colony of *Pichia pastoris* strain X-33 harbouring the pPICZαA-scFv-S20 was picked from a YPD (Yeast Extract Peptone Dextrose)/zeocin (100 µg mL^{-1}) agar plate and inoculated into 25 mL of BMGY (Buffered Glycerol-Complex Medium) with Zeocin (100 µg mL^{-1}). The starter culture was grown at 28°C, with shaking at 250 rpm, until the OD_{600} reached 2 to 6 (ca. 16-18 h). The large-scale culture was started by inoculating the 25-mL starter culture into 1 L of BMGY which was contained in a 4L baffled flask, and grown in the same manner as the starter culture. When the OD_{600} reached 2-6 (log-phase), the cells were harvested by centrifugation (3,000 rpm,

10 min, RT) and resuspended in 250 mL of the induction medium BMMY (Buffered Methanol-complex Medium) which contained 0.5% methanol (v/v). To increase the stability of the recombinant protein (i.e., scFv), the temperature was reduced to 24°C during the induction phase. Induction was done for a maximum of 3 days and was maintained by the addition of 0.5% methanol every 24 h. Once the expression was complete, the cells were removed by centrifugation (3,000 × *g*, 10 min, RT), and the supernatant was filtered through a 0.22 µm PVDF membrane (Stericup filter unit, Millipore).

The S20 scFv, which has a C-terminal His6-tag, was purified by standard immobilized metal affinity chromatography (IMAC) using a 5-mL HisTrap^{TM} HP nickel affinity column (GE Healthcare) on an ÄKTAxpress system (GE Healthcare). After loading the filtered supernatant, the column was washed with 3 column volumes (CVs) of IMAC A buffer (10 mM HEPES, 500 mM NaCl, pH 7.5) and eluted with IMAC B buffer (500 mM imidazole, 10 mM HEPES, 500 mM NaCl, pH 7.5) using 0–100% gradient elution over the course of 9 CVs (i.e., 45 mL). Fractions representing the S20 scFv were collected, pooled, and concentrated to a maximum of 5 mL with an Amicon ultra-15 centrifugal filter unit with a MWCO of 10 kDa. Size exclusion chromatography (SEC) on a S75 16/60 column (GE Healthcare) was used to separate the monomeric and dimeric forms of the scFv. Phosphate buffered saline (PBS), pH 7.4, was used as the elution buffer for SEC. The proteins were eluted (with PBS) from the column over the course of 1.5 CVs at a flow rate of 1 mL min^{-1}. Fractions representing the monomers or dimers were pooled, concentrated with a centrifugal filter unit as described previously, and then passed through a 0.22 µm filter membrane (Millipore, Nepean, ON). The purity of the S20 scFv monomer and dimer was assessed by standard reducing SDS-PAGE. Mass spectrometry (MS)

analysis determined that the molar mass (Mr) of the scFv S20 monomer is 29,635 Da (Figure 43).

3.3.1.3.2. **N1F10 scFv**

The V_L (GenBank: U25104.1) and the V_H (GenBank: U25107.1) sequences of N1F10 were joined by a $(Gly_4Ser)_3$ linker and terminated with c-Myc and 6xHis C-terminal tags (V_L-linker-V_H-C-Myc-His). The coding sequence of the scFv was commercially synthesized, optimizing for *P. pastoris* codon utilization using a proprietary method, and cloned into the *P. pastoris* expression vector, pD912-AKS, by DNA2.0 (California, USA). Like the pPICZα-A vector used for the S20 scFv, the pD912-AKS vector has the methanol-inducible AOX promoter, an α-secretion signal, and carries zeocin-resistance.

The pD912-AKS-N1F10-scFv plasmid obtained by DNA2.0 was propagated in *E. coli* TG1 to obtain larger quantities of plasmid. The plasmid was linearized with *Sac*I and then introduced into *P. pastoris* X-33 (Invitrogen) by electroporation, as described in the EasySelect™ Pichia Expression Kit Manual (Cat. no. K1740-01,Invitrogen). Transformants were screened on Yeast Extract Peptone Dextrose (YPD) plates containing Zeocin (100 µg mL^{-1}, Invitrogen). N1F10 scFv was expressed and purified in the same manner as described for the S20 scFv antibody. The N1F10 scFv was mostly in a monomeric form.

3.3.1.3.3. **3B1 scFv**

3B1 scFv was expressed in *E. coli* as previously described by Deng *et al*. (144) and Young *et al*. (148). Thereafter, it was purified by IMAC and SEC in the same manner as described for the S20 scFv antibody.

3.3.1.3.4. **MF23-1 Fab**

The intact mAb MF23-1 was digested to release the MF23-1 Fab fragment using a protocol similar to that as described by Parker *et al*. (149). The optimal papain-digestion reaction conditions were: papain concentration, 0.02 mg mL^{-1}; mAb MF23-1 concentration, 2 mg mL^{-1}; digestion time, 4 h; temperature, 37°C (data not shown).

3.3.2. Bacterial strains and culture conditions

The principal strain used in this study, *P. aeruginosa* strain O6a, 6d (170010 reference strain, CPA^+/OSA^+), was kindly provided by Dr. John R. Schreiber (Tufts University, Boston, MA, USA) (125). The complete set of International Antigenic Typing Scheme (IATS) *P. aeruginiosa* strains, including types O1 (ATCC 33348), O2 (ATCC33349), O3 (ATCC 33350), O4 (ATCC 33351), O5 (ATCC 33352), O6 (ATCC 33354), O7 (ATCC 33353), O8 (ATCC 33355), O9 (ATCC 33356), O10 (ATCC 33357), O11 (ATCC 33358), O12 (ATCC 33359), O13 (ATCC 33360), O14 (ATCC 33361), O15 (ATCC 33362), O16 (ATCC 33363), O17 (ATCC 33364), and serotypes O18-O20 [O1-O17: (68), O18-O20: (69)] were obtained from the American Type Culture Collection (ATCC). Fisher 1 (ATCC 27312, serotype O6, CPA^+/OSA^+), PAK [serotype O6, CPA^+/OSA^+, (150, 151)], PAK *wbpO* [serotype O6, CPA^+/OSA^-, gentamicin-resistant (Gm^R, 200 µg mL^{-1}) (152)], PAK *rmlC* [serotype O6, CPA^-/OSA^-, Gm^R (300 µg mL^{-1}) (153)] and PAO1 (serotype O5, CPA^+/OSA^+) were obtained from Dr. Joseph S. Lam (University of Guelph). PAO1 Δ*algC*::tet [serotype O5, CPA^-/OSA^-, deficient in alginate exopolysaccharide; $tetracycline^R$ (100 µg mL^{-1}) (154)] was kindly provided by Dr. Sven Müller-Loennies (Research Center Borstel, Germany). AK1012 [PAO1-derived, serotype O5, CPA^-/OSA^- (155)] and AK1401 [PAO1-derived, serotype O5, CPA^+/OSA^-, (156, 157)] were obtained

from the NRC. *Salmonella enterica* serovar Typhimurium was obtained from the ATCC (ATCC 19585).

Strains of *P. aeruginosa* and *Salmonella* were cultured in tryptic soy broth (TSB; Difco, Detroit, Michigan) and nutrient broth (NB), respectively. Antibiotics [e.g., gentamicin sulfate (Sigma), tetracycline (Sigma)] were only supplemented for the growth of resistant strains. Bacteria from a single colony were picked from an agar plate and grown overnight (o/n) at 37°C, 220 rpm. Subcultures were inoculated with a 1:50 dilution from the o/n culture into 5 mL broth and grown as previously described until optical density at 600 nm (OD_{600}) reached 0.5–0.7. Bacteria were harvested by centrifugation (3,000 rpm, 5 min, room temperature [RT]), washed three times with a 5 mL of PBS, and then diluted to obtain the desired OD_{600} or CFU mL^{-1} concentrations. For ELISA, bacteria were prepared as described, then heat-killed at 60°C for 1 h and stored at -20°C.

3.3.3. Bactericidal assays

wo types of bactericidal assays were conducted: one used agar plates and the other used microtitre plates. Generally, the antibodies were first screened using the microtitre plate method because of its high-throughput abilities and higher accuracy. For the microtitre plate method, antibodies (50 μL, prepared in PBS at the desired concentration) were added to the wells of a 96-well flat-bottomed polystyrene plate (Corning, Corning, NY) containing 50 μL of the bacterial culture (OD_{600} = 0.024; ca. 5×10^7 CFU mL^{-1}). The negative control contained sterile PBS instead of antibody. A non-specific antibody (e.g., mAb LPT3-1, anti-*N. meningitidis*) was generally tested at the same time. Media (50 μL) diluted with PBS (50 μL) served as control for background subtraction. Three wells (triplicates) were used for each treatment. Microtitre plates

were sealed with an adhesive film, and incubated at 37°C, 50 rpm, using the automated Infinite 200 PRO microplate reader (Tecan, Mannedorf, Switzerland). Bacterial growth was evaluated by measuring the OD_{600}, every 10 min, for ca. 16 h. The growth curves presented represent the average of three replicates. The bactericidal assay using the agar plate method was done as previously described by Xie *et al*. (5).

3.3.4. Statistical analyses

Statistical analyses for the bactericidal assays were performed using an Excel Data Analysis ToolPak add-inn program. All data are displayed as mean ± SE (standar error) and graphs were generated using GraphPad Prism 5. Comparision between groups were performed using a One-way Analysis of Variance (ANOVA) test, and probability values of less than 0.05 were considered significant.

3.3.5. Determining the MIC

The minimal inhibitory concentration, which causes a 50% reduction (MIC_{50}) of cell turbidity compared to control, was determined using the microtitre plate method described in subheading 3.3.3. Antibodies (S20 scFv monomer, S20 scFv dimer and mAb MF23-1) were serially diluted 2-fold, starting at 20 µM for the S20 scFv monomer and 10 µM for the S20 scFv dimer and mAb MF23-1. The prepared antibody dilutions were added, in triplicate, to wells containing *P. aeruginosa* cells (50 µL). The microtitre plates were incubated as described in subheading 3.3.3. The data generated from the bacterial growth curves were used to prepare a turbidity (%) versus antibody concentration (nM) (log-scale) graph. First, the control growth curve was examined, and the time and turbidity to reach the midpoint of the growth curve was

determined. At this same time point, the turbidities of the antibody-treated cells were determined. Percent turbidity was calculated as follows: (turbidity of antibody-treated cells/turbidity of the control cells) × 100. The data were plotted as turbidity (%) versus antibody concentration (log-scale). The MIC_{50} represents the interpolated antibody concentration that caused a 50% reduction in the turbidity.

3.3.6. LPS preparation

Two different methods were used for the isolation of LPS. LPS isolated using the proteinase K digestion method of Hitchcock and Brown (H-B) (158) was used for Western blot and ELISA analyses. LPS isolated using the hot-phenol/water method (159) was used for the preparation of LPS liposomes and O6a, 6d repeating unit (1-, 2-, 3- repeating units) oligosaccharides.

3.3.6.1. LPS extraction by the hot-phenol/water method

For LPS preparation, large-scale 24 L *P. aeruginosa* strain O6a, 6d fermenter cultures were grown in Brain Heart Infusion (BHI) broth (Difco) in a 30 L fermenter (newMBR, Zurich, Switzerland) at 37°C with dissolved oxygen controlled at 15% saturation. Cells were killed by the addition of phenol [2% (w/v) final concentration], harvested using a using a CEPA Z41 continuous centrifuge [yield, 485 g (wet paste)], and lyophilized. Cells were washed with organic solvents (ethanol, acetone, light petroleum ether) to remove lipids and other lipophilic components (160). LPS was extracted from the air-dried cellular material (33.5 g) by the hot-phenol/water method (159) and essentially as previously outlined by St. Michael *et al*. (161). The aqueous phase was extensively dialyzed against tap water until free of phenol (ca. 48 h); the

retentate was then freeze-dried to yield 6.92 g of crude LPS extract. The lyophilized LPS was dissolved in water to give a 1% solution and treated with DNase and RNase at 37 °C for 3 h, followed by proteinase K treatment at 37 °C for 3 h. Small peptides were removed by o/n dialysis against water. After freeze-drying, the retentate was dissolved in water to give a 2% solution and centrifuged at 8,000 × *g* for 10 min (yielding an '8K pellet' of 413 mg). The supernatant from this 8K centrifugation was ultracentrifuged at 100,000 × *g* for 5 h, yielding a pellet with purified LPS. The pellet was re-dissolved in water and lyophilized again to yield 920 mg of purified LPS.

3.3.6.2. Hydrolysis of *O*-polysaccharide into O-Ag fractions

O6a, 6d LPS (400 g) was heated with 1% acetic acid (100 mL, 100°C, 2 h), the lipid precipitate was removed by centrifuging, and the corresponding *O*-polysaccharide (100 mg) as well as oligosaccharide fractions were isolated from the supernates by gel-filtration on Sephadex G-50. The O6a, 6d *O*-polysaccharide (100 mg) was treated with anhydrous hydrogen fluoride (HF) (10 mL) for 30 min at 0°C and then poured into a plastic petri dish for evaporation in a strongly ventilated hood. HF evaporated instantly, the residue was dissolved in water and separated on a Biogel P6 column in pyridine-acetic acid buffer pH 4.5 (4 mL pyridine and 10 mL AcOH in 1 L of water) monitored with a refractive index detector. The main product was repeating unit tetrasaccharide (30 mg); dimer (8 mg) and trimer (3 mg) of repeating unit were also obtained. The products were analyzed by ESI-MS. The expected mass for 1 repeating unit was 811.7 (observed 812.7 m/z), and for 2 repeating units 1605.5 (observed 1607.7 m/z).

3.3.7. SDS-PAGE, silver-staining, and ELISA

The purity of the purified antibodies was confirmed by sodium dodecyl sulfate (SDS)-polyacrylamide gel electrophoresis (PAGE). Antibody samples were electrophoresed under reducing conditions on a pre-cast, stain-free 12% gel (Mini-PROTEAN TGX stain-free precast gels, Bio-Rad). Following electrophoresis, proteins in the gel were visualized using the Bio-Rad Gel Doc XR+ Imaging System (Bio-Rad, Hercules, CA, USA).

The LPS from various *P. aeruginosa* strains were isolated using the proteinase K digestion method of Hitchcock and Brown (H-B) (158), and used for Western immunoblots and silver staining. LPS samples (5 µL) were electrophoresed on a 12% pre-cast gel (Bio-Rad), and visualized by silver staining using the Bio-Rad Silver Stain Kit (Bio-Rad, Hercules, Ca, USA). Electrophoresed LPS samples from another gel were transferred onto a PVDF membrane for Western immunoblotting. Membranes were blocked with 4% skim milk in PBS, and incubated o/n with 10 µg of the desired mAb (S20, MF23-1, 5c7-4) in 15 mL of 4% skim milk in PBST. The membranes were washed 3× with PBST and probed with a rabbit anti-human IgG heavy and light chain-alkaline phosphatase conjugate (ThermoFisher) for the S20 IgG, or with a goat anti-mouse $F(ab')_2$-alkaline phosphatase conjugate (Jackson ImmunoResearch) for the murine mAbs, both diluted to 1:2,000. ELISAs were done as previously described by Xie *et al*. (5).

3.3.8. Surface plasmon resonance (SPR)

For the S20 scFv, two types of experimental designs were used for SPR analysis. The first one involved immobilizing O6a, 6d LPS liposomes and then flowing the S20 scFv as the analyte. In the second design, the antibodies (S20 scFv and MF23-1) were immobilized and the analytes were the O6a, 6d repeating units that were obtained by HF hydrolysis.

3.3.8.1. Preparation of LPS liposomes for use in SPR analysis

Since the S20 scFv can bind to numerous sites per LPS molecule (up to 50 repeating units/OSA chain), LPS immobilization on the surface of the SPR sensor chip was required for binding kinetics analysis. Liposomes displaying LPS can easily be captured onto the surface of an L1 biosensor chip (GE Healthcare). Liposomes with incorporated O6a, 6d LPS were prepared as follows. For each liposome preparation, 10 mg of lyophilized 1,2-dimyristoyl-*sn*-glycero-3-phosphocholine (DMPC; Catalog #P2663, Sigma-Aldrich, Oakville, Ontario, Canada) were hydrated in 1 mL of chloroform in scintillation vials. The lipids were placed on a heating block set to low-medium heat and dried under a nitrogen stream, followed by 1 h under vacuum (freeze-drying). One mL of purified LPS (from a 2 mg mL^{-1} solution in milli-Q water) or PBS (for LPS-free negative control liposomes) was added to the freeze dried DMPC lipid and incubated for 2 h at 37°C with shaking. Thereafter, the lipid:LPS solutions were sonicated 2-3 times in a water bath for 30 sec at 37 °C until a homogeneous solution was obtained. Liposomes were left to anneal for at least 16 h and in some case for as long as 48 h at 4 °C. The liposomes were then washed twice with 5 mL of SPR HBS-E running buffer (HBS-E: 10 mM HEPES pH 7.4 containing 150 mM NaCl, 3 mM EDTA) and collected by ultracentrifugation for 1 h at 50,000 rpm. The final liposome pellets were resuspended in 0.5 mL of HBS-E running buffer and stored at 4°C until used for SPR analysis. Negative control liposomes with incorporated LPS from *Shigella flexneri* serotype Y were prepared, using the same protocol, by a colleague, Henk van Faassen (NRC-HHT, Antibody Engineering group).

3.3.8.2. Kinetic analysis using immobilized LPS liposomes

Immediately prior to SPR analysis, monomeric and dimeric S20 scFv were separated by gel filtration (Figure 10). The affinity and rate constants for their interaction with immobilized O6a, 6d LPS were determined by surface plasmon resonance (SPR) using a Biacore 3000 biosensor instrument (GE Healthcare). LPSs were incorporated into liposomes as described in subheading 3.3.8.1. An L1 sensor chip (GE Healthcare) was used to immobilize the liposomes as described by the manufacturer, with minor modifications. Prior to capturing the liposomes, the surface of the L1 sensor chip was cleaned with three injections of 10 µL of 20 mM 3-[(3-Cholamidopropyl)dimethylammonio]-1-propanesulfonate hydrate (CHAPS hydrate, Sigma), a detergent, at a flow rate of 20 µL min^{-1}. LPS-free liposomes were immobilized on the reference flow cell 1 (FC-1), $LPS_{O6a, 6d}$ liposomes on FC-2 and $LPS_{Shigella}$ liposomes on FC-3. Approximately 3,000 resonance units (RUs) of liposomes were captured on the surfaces at a low flow rate of 5 µL min^{-1}. Thereafter, the surface was stabilized by flowing HBS-E running buffer [10 mM HEPES, pH 7.4, 150 mM NaCl, 3 mM EDTA, (GE Healthcare)] for 30 min at a high flow rate of 100 µL min^{-1} followed by two short injections of 5 µL of 10 mM NaOH at a flow rate of 50 µL min^{-1} to remove loosely bound liposomes. Non-specific sites were blocked by injecting 10 µL of 0.1 mg ml^{-1} of bovine serum albumin (BSA) followed by 5 µL of 10 mM NaOH to complete the preparation of the surface. Binding experiments were done in HBS-E running buffer at RT at a flow rate of 20 µL min^{-1}. The S20 scFv monomer was injected at concentrations ranging from 100 nM–1 µM (100, 150, 200, 250, 300, 400, 400, 500, 700 and 1,000 nM) for 300 s and allowed to dissociate from the surface for 1,200 s. Prior to each antibody injection, a buffer blank was injected under the same conditions and was thereafter subtracted from the following injection to correct for baseline drift. Since the S20 scFv dimer is

a bivalent molecule, only one concentration of 1 µM (i.e., 1,000 nM) was injected over the surface. The surface was not regenerated between the S20 scFv monomer injections in the same experiment; however, a new surface was prepared between experiments or after injecting one concentration of the S20 scFv dimer. Before preparing a fresh surface, the immobilized liposomes were stripped from the surface of the sensor chip by injecting three short pulses of 0.5% SDS and three short pulses of 50 mM NaOH:isopropanol (2:3 v/v) at a high flow rate of 100 µL min^{-1}. Fresh surfaces were prepared as described earlier, i.e., commencing with cleaning of the surface with CHAPS. Liposomes that were recaptured on the same surface were found to be stable and reproducible between experiments. A non-specific antibody fragment (single-domain PKF1, 200 nM, provided by a colleague) served as a negative antibody control. The rate and affinity constants were determined by locally fitting the data set with a one-to-one interaction model using BIAevaluation 4.1 software (GE Healthcare).

3.3.8.3. Kinetic analysis using O6a, 6d repeating units

As described in subheading 3.3.6.2, the *O*-polysaccharide from LPS purified from *P. aeruginosa* strain O6a, 6d was hydrolyzed into different lengths of 1, 2 and 3 repeating units. The affinities of the S20 and MF23-1 antibodies towards these three O6a, 6d repeating units (analytes) were measured by SPR using a Biacore T200 instrument (GE Healthcare). This instrument provides good quality sensorgrams for the binding analysis of low MW analytes because of low background noise. The S20 scFv (3,139 RUs; FC-2; pH 5.0) and the mAb MF23-1 (7,218 RUs; FC-3; pH 4.0) were immobilized using standard amine coupling onto a research grade CM5 sensor chip (Biacore) in 10 mM sodium acetate buffer (GE Healthcare) at the indicated pHs. The reference FC-1 was blocked with ethanolamine and a non-specific mAb

7-4 (inner-core specific) (7,228 RUs; pH 4.5) was immobilized onto FC-4. The SPR running buffer used was HBS-EP+ [10 mM HEPES, pH 7.4, 150 mM NaCl, 3 mM EDTA, 0.005% surfactant P-20 (GE Healthcare)]. The O6a, 6d repeating units were diluted in HBS-EP+ running buffer and passed over the coated sensor chip. For the S20 scFv, the 2 repeating unit and 3 repeating unit oligosaccharides were injected at concentrations ranging from 0.3–30 μM (0.3, 0.5, 1, 2, 3, 5, 5 and 10 μM) and 0.05–5 μM (0.05, 0.1, 0.3, 0.7, 1, 2 and 5 μM), respectively. Since the MF23-1 antibody showed low affinity towards these oligosaccharides, they were injected at higher concentrations with the 2 repeating unit and 3 repeating unit oligosaccharides at concentrations ranging from 1–500 μM (1, 3, 5, 10, 10, 25, 50, 100, and 500 μM) and 0.5–100 μM (0.5, 1, 3, 5, 5, 10, 25, 75 and 100 μM), respectively. For both antibodies, as high as 1 mM of the 1 repeating unit oligosaccharide was injected but no binding was detected. All experiments were conducted at RT at a flow rate of 40 μL min^{-1}, and the surfaces were not regenerated. For the S20 antibody, the contact time was 240 s (4 min) and the dissociation time was 1,200 s (20 min). The rate and affinity constants of the S20 scFv towards the O6a, 6d oligosaccharides were determined by global fitting the data set with a one-to-one interaction model. As the MF23-1 antibody showed very rapid rate constants towards the O6a, 6d repeating units, the contact time was decreased to 30 s and the dissociation time was decreased to 30 s. Since the rate constants (k_{on} and k_{off}) of the MF23-1 towards the O6a, 6d oligosaccharides were too fast for kinetic analysis using the 1:1 binding model, the K_D values were determined by fitting equilibrium data to a steady state affinity model. The responses (RU) at 5 s after the injection over a window of 5 s were used for data analysis. All the analyses were performed using the Biacore T200 Evaluation Software Version 1.0 (GE Healthcare).

On a later date, SPR analysis was used to confirm the functionality the MF23-1 Fab fragment which was prepared by digesting the parental MF23-1 mAb with the enzyme papain. The MF23-1 Fab fragment (3,511 RUs; FC2; pH 4.0) and mAb MF23-1 (5,440 RUs; FC-3; pH 4.0) were immobilized on a CM5 sensor chip as previously described. Only the O6a, 6d oligosaccharide with 3 repeating units was used for this screen. The same conditions, as were previously described for the MF23-1 mAb, were used.

3.3.9. Sequence analysis

Using the IMGT numbering system (162), the sequences of the variable heavy (V_H) and variable light (V_L) domains of the S20 and MF23-1 antibodies were aligned with each other and with selected non-bactericidal LPS binding antibodies, namely mAb 7-4, N1F10, and LPT3-1. Not only were the identities of the amino acids from the CDRs compared but also their physicochemical properties. IMGT has standardized the classification of the 20 amino acids into 11 classes based on the physicochemical properties of their side chains, including hydropathy (hydrophobic, neutral, hydrophilic), volume (from very small to very large), chemical characteristics (aliphatic, aromatic, sulfur, hydroxyl, basic, acidic and amide), hydrogen donor or acceptor atoms, and polarity (163). The following IMGT website was used for this analysis: http://www.imgt.org/IMGTeducation/Aide-memoire/_UK/aminoacids/IMGTclasses.html.

In addition, the sequences of the six CDRs of both bactericidal antibodies were searched against an antimicrobial peptide database [APD database; http://aps.unmc.edu/AP/main.php; (164-166)] and against the NCBI protein database.

The grand average of hydropathy (GRAVY) values of all CDR loops were calculated to determine if the bactericidal antibodies possess particularly hydrophobic CDRs. These were

calculated by summing the hydropathy values of individual amino acids (of the CDR) divided by the number of amino acids (i.e., CDR length) according to the Kyte-Doolittle scale (167) (see, http://www.imgt.org/IMGTeducation/Aide-memoire/_UK/aminoacids/IMGTclasses.html). Alternatively, GRAVY values can be easily computed using the ProtParam tool on the ExPaSy bioinformatic website (http://web.expasy.org/protparam/).

3.4. RESULTS AND DISCUSSION

3.4.1. Purification of the S20 scFv monomer and dimer

Since the publication of Xie *et al*. (5), we have determined that the S20 scFv is prone to dimerization, a dynamic process common for scFvs (168-171). Therefore, the IMAC-purified S20 scFv (Figure 10A) was subjected to gel filtration using a Superdex^{TM} 75 column (GE Healthcare), which gives good resolution for biomolecules in the Mr range of ~3–70 kDa (Figure 10B). The two prominent peaks, Peak #3 (ca. 35%) and Peak #4 (ca. 50%), represent the S20 scFv dimer [apparent MW (MWapp) of 70.3 kDa] and S20 scFv monomer (MWapp of 30.8 kDa), respectively (Figure 10B and D), while the smaller peaks that eluted earlier (Peak #1 and Peak #2) represent larger aggregates present in the sample. The MWapp of each peak was calculated from the equation of the standard line (**Figure 42**) ($Log_{10}MW = -0.0329Ve + 6.723$) and by using their respective eluted volume (Ve). The MWapp of the S20 scFv monomer is in very good agreement to the MW (29.6 kDa) determined by mass spectrometry (Figure 43). Following SEC, a reducing SDS-PAGE gel showed that the S20 scFv monomer and dimer, the later which dissociated under reducing condition, were of high purity (Figure 10C).

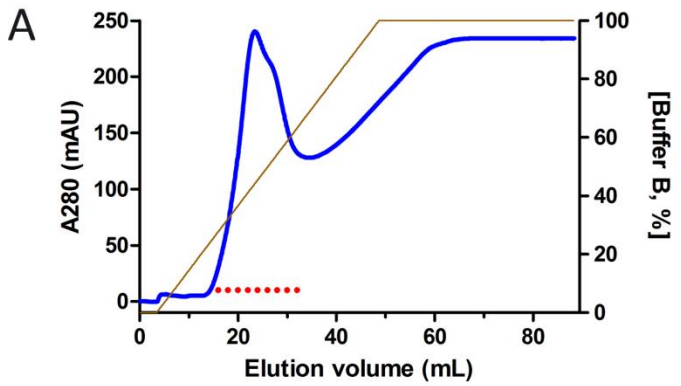

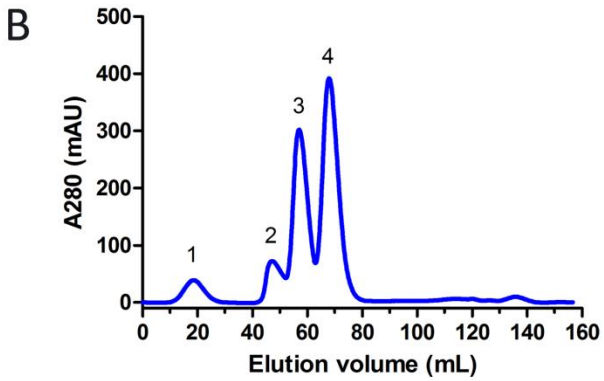

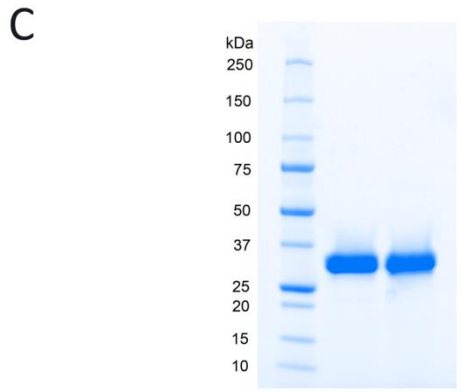

D

Peaks	Ve (mL)	MWapp (KDa)	Protein form	Area/Peak area (%)
1	38.6*	>>149**	Large aggregates	6.2
2	47.2	~149**	Aggregates	8.7
3	57.0	70.3	Dimer	34.4
4	67.9	30.8	Monomer	48.5

*Eluted in the void volume.
**Superdex 75 16/60 prep grade gives good resolution for biomolecules with Mr ranging from 3 – 70 kDa. Therefore, it is difficult to accurately determine the MWapp of of aggregates >70 kDa.

Figure 10. Purification of the S20 scFv. A) IMAC chromatogram, B) S75 16/60 chromatogram. The equation of the standard line (Figure 42B, Appendix) ($Log_{10}MW = -0.0329Ve + 6.723$) was used to calculate the apparent MW (MWapp) of the eluted peaks. C) Reducing 12% SDS-PAGE gel. Legend: Lane 1: Precision Plus Protein™ Unstained standards (12 µL), Lane 2: S20 monomer (6 µg), Lane 3: S20 dimer (6 µg). D) Summary table providing the elution volume (Ve, mL), the apparent MW (MWapp), the protein form and the area (% of total area) of the respective peak.

3.4.2. Binding and bactericidal specificity of S20

In addition to the O6a, 6d strain of *P. aeruginosa*, Xie *et al*. (5) reported that the S20 antibody displays non-specific bactericidal activity towards PAO1 (serotype O5), albeit at lower levels (ca. 30–60% killing towards PAO1 versus ca. >90 % towards O6a, 6d). The fact that the S20 antibody had been demonstrated to kill a strain to which it has little or no binding warranted further investigation, i.e., S20 may have broader bactericidal activity than previously thought. Therefore, to further understand the relationship between the binding and bactericidal specificities of S20, the S20 scFv was screened for binding (Figure 11) and bactericidal (Figure 12) activities against all the 20 IATS serotypes of *P. aeruginosa*. Although the specificity of S20 has previously been published by Hemachandra *et al*. (125), they only provided binding data for a few strains, namely O6a, 6d, PAO1, IATS O11, IATS O16, and the 170003 reference strain. Our ELISA results confirm that the S20 antibody is highly specific for *P. aeruginosa* strain O6a, 6d and has negligible binding towards any of the 20 IATS serotypes and PAO1 (serotype O5). Furthermore, a Western immunoblot showed that S20 does not cross-react, even with low levels of binding, with other O6 strains with which it shares high structural similarities with their O-antigen (Figure 13B). Moreover, images obtained by immunofluorescence (IF) microscopy clearly illustrate that the S20 scFv-FITC uniformly targets the surface of *P. aeruginosa* strain O6a, 6d cells, and no binding was detected towards PAO1 (Figure 44).

The bactericidal assays, using both the highly sensitive microtitre (Figure 12) and agar (data not shown) plate methods, showed that the S20 scFv does not exhibit any bactericidal activity towards PAO1, as previously reported. Furthermore, it has no bactericidal activity

towards any of the other closely related OSA+ O6 (Figure 14) strains or any of the 20 IATS *P. aeruginosa* serotypes (Figure 12).

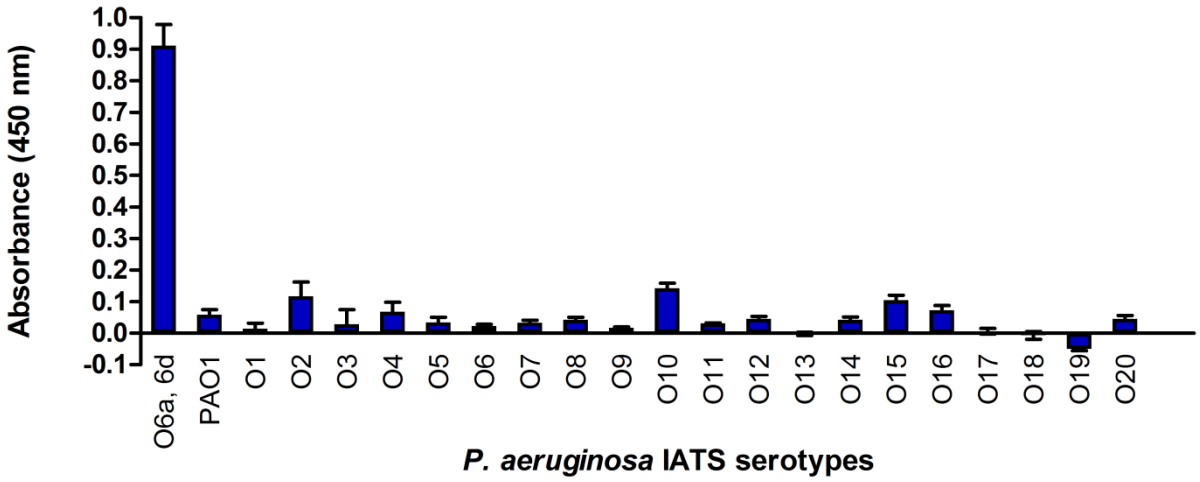

Figure 11. ELISA showing the high specificity of the S20 scFv to *P. aeruginosa* strain O6a, 6d compared to the 20 IATS *P. aeruginosa* serotypes and PAO1. These binding results correlate with the bactericidal activity results (Figure 12), i.e., S20 only exhibits bactericidal activity towards the strain to which it binds. Data represent means of three replicates ± SE.

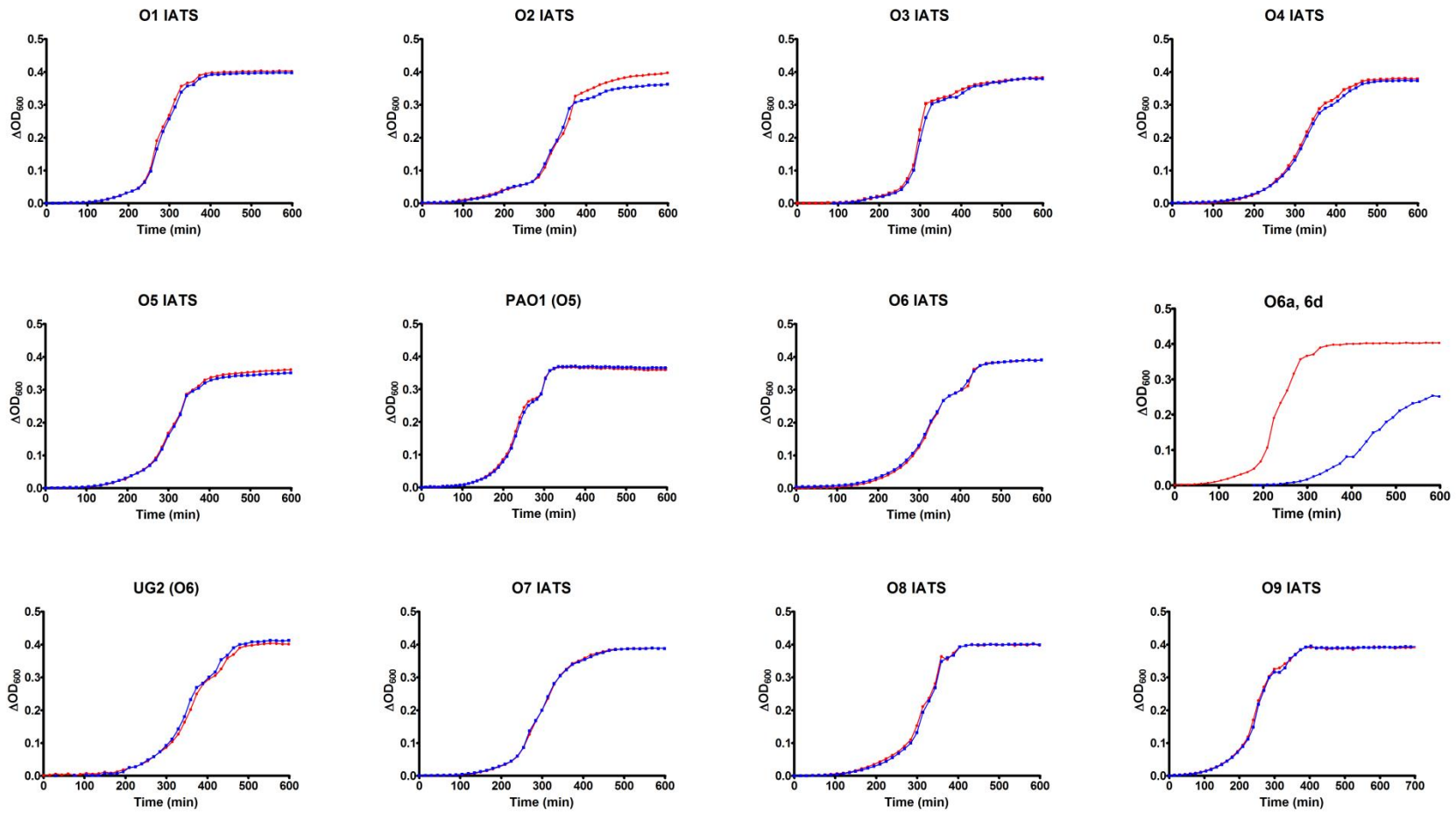

Figure 12. Overlaid growth curves of the 20 IATS *P. aeruginosa* serotypes and PAO1 in the absence (red curves) or presence (blue curve) of the S20 scFv (10 µM, pre-SEC purified). Aside from the positive control, i.e., *P. aeruginosa* strain O6a, 6d, the S20 scFv did not affect the growth of any of the 20 IATS serotypes.

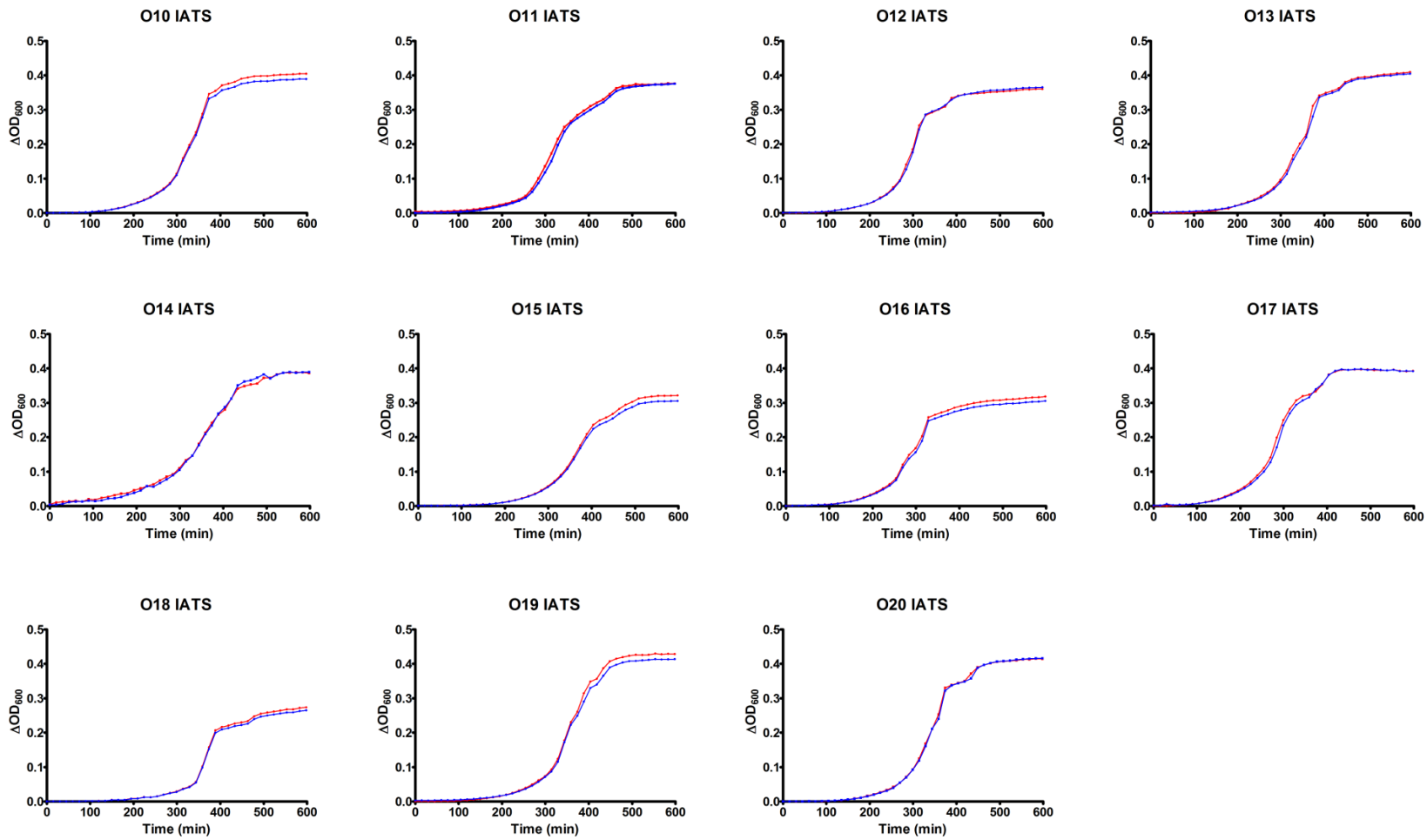

Figure 12. (continued).

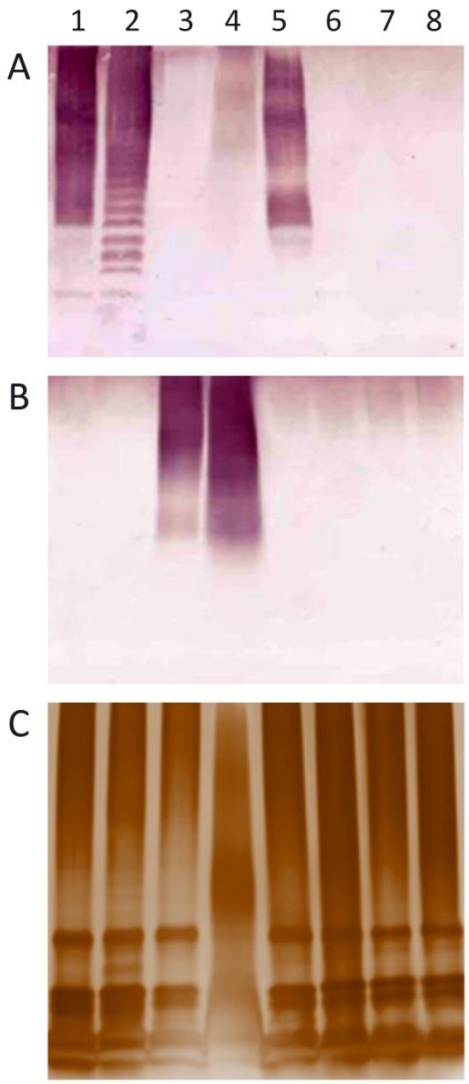

Figure 13. Western immunoblot showing (A) the cross-reactivity of mAb MF23-1 to various OSA+ O6 strains versus (B) the high specificity of S20 to strain O6a, 6d. The silver stain of the LPS preparations is provided in (C). Lane 1: O6 IATS; Lane 2: Fisher 1; Lane 3: O6a, 6d; Lane 4: O6a, 6d, 10 µg purified LPS; Lane 5: PAK (A^+B^+, wild-type); Lane 6: PAK *wbpO* (A^+B^-); Lane 7: PAK *rmlC* (A^-B^-); Lane 8: PAO1 (serotype O5). All the LPS samples, except for that of Lane 4, were prepared according to the Hitchcock and Brown preparation method (158). The O6a, 6d LPS loaded into Lane 4 was purified following the phenol-hot-water method (see Materials and Methods for more details). Similarly as observed by Makin and Beveridge (83), the banding pattern of low molecular masses of the OSA are more distinct (Figure 13A, Lane 2) while that of high molecular masses of OSA are poorly resolved and appear as a smear.

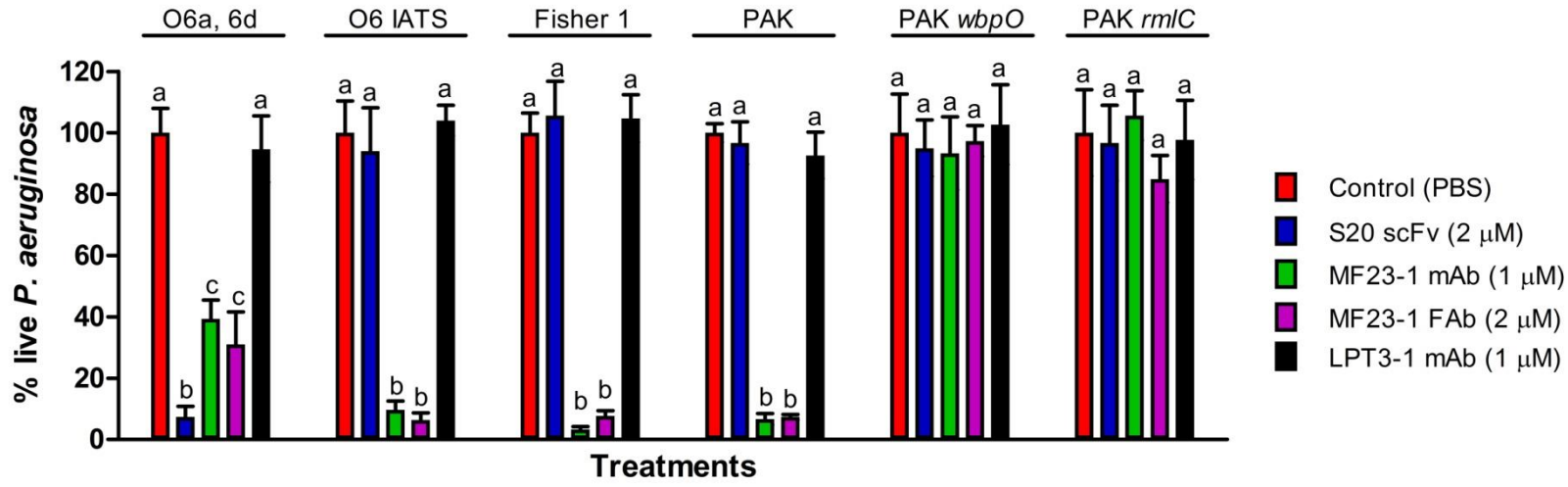

Figure 14. Bactericidal activity of S20 scFv, mAb MF23-1 and MF23-1 Fab against various O6 strains of *P. aeruginosa*. The bactericidal activity was determined by counting CFUs on agar plates following 30 min incubation of the bacteria (ca. 1×10^7 CFU mL^{-1}) with the antibodies at 37°C. Untreated bacteria (PBS) and bacteria treated with the non-specific LPT3-1 antibody served as controls. Data represent means of three replicates ± SE. The different letters a-c indicate statistical differences among treatments ($p<0.05$).

3.4.3. Comparing the binding specificity of MF23-1 and S20 antibodies

MAb MF23-1 was purified by standard protein G chromatography, and its purity and identity were confirmed by SDS-PAGE gel (Figure 15, Lane 6) and by WBs (data not shown). The high specificity of S20 towards O6a, 6d (Figure 13B) versus the broader reactivity of mAb MF23-1 towards various OSA^+ O6 strains (Figure 13A) were compared by WBs. As illustrated, mAb MF23-1 showed strong reactivities to most OSA+ O6 strains, including O6 IATS, Fisher 1 and PAK wild type (Figure 13A). However, no reactivity was detected to the Hitchcock and Brown LPS preparation (H-B) prep (158) of O6a, 6d (Lane 3), and very low reactivity was detected when as much as 10 µg of O6a, 6d LPS, purified using the hot-phenol/water method, was loaded (Lane 4). This low reactivity to O6a, 6d is not surprising since SPR analysis revealed that mAb MF23-1 has a k_{off} that is too rapid for kinetic analysis (see Figure 17 below), and therefore is expected to easily be washed the Western membrane. It should be noted, however, that better reactivity of mAb MF23-1 to purified O6a, 6d LPS has been detected when less stringent conditions (i.e., less membrane washing, more Ab) were applied (data not shown). Contrary to mAb MF23-1, the S20 antibody had very strong reactivity towards O6a, 6d but showed no detectable reactivities to any other OSA^+ O6 strains tested (Figure 13B). These results, along with those presented in the ELISA data in Figure 11, demonstrate how specific the S20 antibody is for the OSA of O6a, 6d.

The O-Ag repeating unit of serotype O6 is composed of four sugars: D-QuiNAc, two sugars related to 2-amino-2-deoxy-D-galacturonic acid (D-GalNA), and L-Rha (59, 70) (Figure 4). Strains of this serotype differ in their O-antigen structures by their degree of D-GalNA amidation (88), by the presence/absence of 3-*O*-acetylation of GalNAcAN(3OAc), and by the

linkages between their repeating units (α versus β and/or 1→2 versus 1→3) (70). Based on the current structural data available, the only unique structural difference of O6a, 6d compared to the other O6 strains is the β-linkage between the D-QuiNAc and L-Rha residues of O6a, 6d (the other strains have an α-linkage). Therefore, the exquisite specificity of the S20 antibody is likely in part due to interaction with this β-linkage. Likewise, mAb MF23-1 may have a strong, but less restrictive, preference for the α-linkage between the D-QuiNAc and L-Rha residues. Furthermore, MF23-1 does not appear to be restrictive for amiditation of GalNA since it is able to bind both Fisher 1 (100% amidated) and O6a (O6 IATS) (0% amidated). To gain more structural insight into the high specificity of S20 compared to the broader specificity of MF23-1, X-ray co-crystallization studies with either the S20 scFv and MF23-1 Fab using the hydrolyzed O6a, 6d repeating units were attempted by Dr. Stephen Evans' laboratory, University of Victoria; unfortunately, these experiments were not successful.

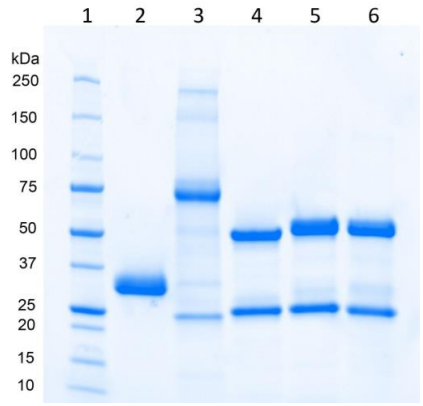

Figure 15. Reducing 12% SDS-PAGE gel of various purified anti-LPS antibodies used in this study. Legend - Lane 1: Precision Plus Protein™ Unstained standards (12 µL); Lane 2: N1F10 scFv monomer (5 µg); Lane 3: N1F10 IgM (7.5 µg); Lane 4: mAb LPT3-1 (7.5 µg); Lane 5: mAb 7-4 mAb (7.5 µg); Lane 6: mAb MF23-1 (7.5 µg).

3.4.4. Bactericidal specificity of MF23-1

As revealed in the bactericidal assay, mAb MF23-1 and its Fab fragment significantly decreased the viability of OSA+ O6 strains, including O6 IATS, PAK, Fisher 1 and O6a, 6d, independent of phagocytosis and CDC (Figure 14). No effects were observed to O6 strains deficient in OSA, namely PAK *wbpO* (OSA-/CPA+) and PAK *rmlC* (OSA-/CPA-), which represent ideal negative controls. LPT3-1, a mAb specific for *N. meningitidis* inner core LPS epitope, did not produce any effects on the growth curves of any of the strains tested. When incubated for 30 min with the MF23-1 antibodies, the viability of Fisher 1, O6 IATS and PAK were all reduced below 90% CFU mL^{-1} compared to the control (PBS). These levels of bactericidal activity are comparable to those produced by S20 and its fragments (i.e., as IgG, Fab and scFv) towards its specific strain of O6a, 6d, as previously published (5) and also illustrated in Figure 14. Although the MF23-1 and its Fab fragment significantly reduced the viability of O6a, 6d by about 60%, they were significantly less efficacious towards this strain compared to the other OSA+ O6 strains tested. In addition, the S20 antibody was significantly more bactericidal to O6a, 6d compared to the MF23-1 antibodies. As discussed previously, S20 has almost a 20-fold higher affinity (K_D) for the O6a, 6d O-antigen compared to the MF23-1 (Table 2), thereby providing further evidence that the affinity of the anti-OSA antibody is important contributor to the levels of bactericidal activity. The monovalent MF23-1 Fab fragment, which lacks the Fc-region, produced the same bactericidal effect as its parental antibody. These results are in agreement with the previously published data regarding the S20 antibody and its fragments (Fab and scFv) (5), i.e., these bactericidal antibodies exert their bactericidal activity as intact IgG

molecules or as antibody fragments (e.g., scFv, Fab). These results support the observation that their bactericidal effect is not mediated through the Fc-region nor is bivalency a pre-requisite.

In summary, targeting the same antigen as the S20 antibody, i.e., the O6a, 6d OSA, with a different antibody, i.e., MF23-1, also mediates targeted cell death, indicating that the bactericidal activity previously observed to O6a, 6d is not a unique property of the S20 antibody.

3.4.5. SPR analysis

3.4.5.1. Binding of the S20 scFv to immobilized O6a, 6d LPS

The affinities of the S20 scFv monomer and S20 scFv dimer against immobilized O6a, 6d LPS liposomes were measured by surface plasmon resonance (SPR) using a Biacore 3000. The overall shapes of the sensorgrams confirm monovalent and bivalent binding of the monomer and dimer, respectively (Figure 16). Their rate and affinity constants, which are provided in Table 2 were determined by locally fitting (i.e., separate fitting of individual sensorgram data at different antibody concentrations) the data set (black lines) with a simple one-to-one interaction model (red lines). Overall, the data collected for the S20 scFv monomer is in good agreement with the model. There is, however, some discrepancy at the tail-end of the dissociation curve that shows that some of the antibody remains bound to the immobilized surface, especially when higher antibody concentrations are injected. Although the S20 scFv was subjected to gel filtration (Figure 10B) prior to SPR analysis, this could be a result of trace amount of the S20 scFv dimer. The good fit of the dimer data to a one-to-one model indicates that the binding is homogeneous – i.e., all bivalent (2:2).

The analysis revealed that the affinity (K_D value of 5.6×10^{-7} M, i.e., 0.56 μM) of the S20 scFv monomer towards the O6a, 6d LPS is higher than that generally observed for carbohydrate-

protein interactions (K_D of 10^{-3} to 10^{-5} M) (172). Compared to the S20 scFv monomer, the functional affinity of the S20 scFv dimer was approximately 30-fold higher (K_D value of 2.1 x 10^{-8}, i.e., 21 nM), as a result of the effect of avidity. This lower K_D is largely a result of the much slower dissociation rate constant (k_{off}) of the dimer (1.2×10^{-4} s^{-1}) compared to monomer (2.9×10^{-3} s^{-1}), while their association rate constants (k_{on}) are similar. There was no binding of S20 to both the non-specific *Shigella* LPS and antibody fragment (single-domain PK1) (data not shown).

Since the S20 scFv monomer and dimer have similar association rate constants (k_{on}) (5.2 × and 5.9×10^3 M^{-1} s^{-1}, respectively), they should bind the OSA in the O6a, 6d membrane at similar rates. Thus, one should expect similar local concentrations for both these antibody formats near the surface of O6a, 6d. However, once in a bound state, the S20 scFv dimer dissociates very slowly from the OSA: 87% remains bound to the OSA after the SPR surface has been washed with running buffer for 20 min during the dissociation phase (Figure 16B, calculation not shown). Since the S20 scFv dimer is ca. 8-fold more bactericidally potent compared to the monomer (subheading 3.3.5, Figure 20), its much slower dissociation rate constant likely plays an important role in its activity. This tight LPS binding contrasts with the action of cationic AMPs. Although LPS is also the first site of interaction with cationic AMPs, they are then thought to target a second site and directly integrate into and disrupt the membrane. If our bactericidal antibodies directly inserted into the membrane, then one would expect the format with the faster k_{off}, i.e., the S20 scFv monomer, to be more available to then target the membrane. Thus, we propose that our bactericidal antibodies do not have a second site of action/interaction like AMPs.

In addition to kinetics data, SPR analysis revealed that the S20 scFv monomer and dimer do not hydrolyze the immobilized LPS of O6a, 6d. If the S20 antibodies were able to hydrolyze the *O*-polysaccharide chain, a decrease in resonance units from the immobilized baseline levels would have been detected upon, or soon after, antibody injection. Instead, injection of the S20 antibodies resulted in classic sensorgram curves (Figure 16, Appendix Figure 46B). As a comparison, we provide the unusual sensorgram curve that resulted from the hydrolysis of immobilized *Shigella flexneri* serogroup Y LPS by the bacteriophage tailspike Sf6 (Appendix Figure 46A). Sf6 is known to interact and cleave the O-antigen of *S. flexneri* serogroup X and Y by endorhamnosidase activity (endo-1, 3-α-l-rhamnosidase) (173, 174). When recombinant wild-type Sf6 tailspike protein was injected over a surface with immobilized *Shigella* LPS, an immediate decrease in resonance units, below the immobilized baseline levels, was seen, indicating the release of immobilized components from the prepared surface. Meanwhile, mutants of Sf6 (single-mutant residue positions: 366, 399; double-mutant residue positions: 366/399) showed lower levels of LPS hydrolysis. Thus, these results support the idea that the bactericidal mechanism of action of the S20 antibody is not a result of LPS hydrolysis.

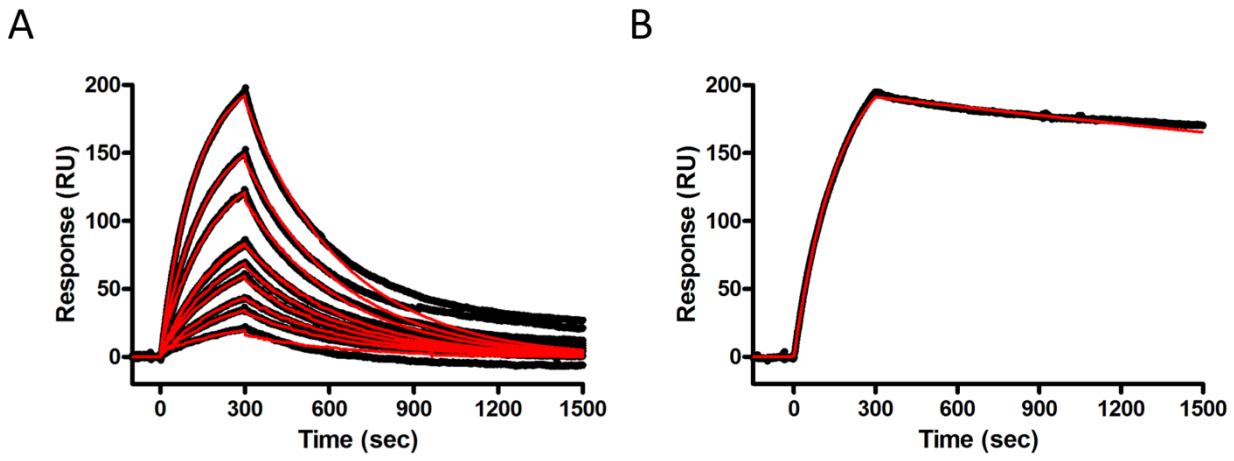

Figure 16. Binding of the S20 scFv A) monomer and B) dimer to immobilized LPS from *P. aeruginosa* strain O6a, 6d. The monomeric and dimeric fractions of S20 scFv were obtained by gel filtration (SEC 75 16/60; Figure 10B) immediately prior to the SPR analysis. The S20 scFv monomer was injected at concentrations ranging from 100 nM–1 µM (100, 150, 200, 250, 300, 400, 400, 500, 700 and 1,000 nM) (A) while only one concentration of the bivalent S20 scFv dimer (1,000 nM) was injected (B). The antibodies were injected over the surface for 300 sec and allowed to dissociate for 1200 sec. The data collected (black lines) were locally fitted to a 1:1 interaction model (red lines). The k_{on}, k_{off} and K_D are presented in Table 2. The SPR experiments were done using the Biacore 3000 biosensor instrument (GE Healthcare).

Table 2. Summary of the equilibrium dissociation constant (K_D) and rate constants (k_{off} and k_{on}) of the S20 scFv and MF23-1 antibodies to immobilized O6a, 6d LPS and to hydrolyzed O6a, 6d repeating unit oligosaccharides. The sensorgrams for immobilized LPS are presented in Figure 16, those towards the repeating units are presented in Figure 17 and Figure 18. No binding was detected to the 1 repeating unit oligossacharide for both the S20 scFv and MF23-1 antibodies. The Chi^2 value is a measure of the average deviation of the data from the fitted curve, where lower values indicate a better fit.

	Immobilized LPS	**2 repeating unit**	**3 repeating unit**
S20 scFv monomer	$K_D = 5.6 \times 10^{-7}$ M $k_{off} = 2.9 \times 10^{-3}$ s^{-1} $k_{on} = 5.2 \times 10^{3}$ M^{-1} s^{-1} $Chi^2 = 2.53$	$K_D = 4.7 \times 10^{-6}$ M $k_{off} = 5.1 \times 10^{-3}$ s^{-1} $k_{on} = 1.1 \times 10^{3}$ M^{-1} s^{-1} $Chi^2 = 0.256$	$K_D = 1.1 \times 10^{-6}$ M $k_{off} = 4.7 \times 10^{-3}$ s^{-1} $k_{on} = 4.4 \times 10^{3}$ M^{-1} s^{-1} $Chi^2 = 0.602$
S20 scFv dimer	$K_D = 2.1 \times 10^{-8}$ M $k_{off} = 1.2 \times 10^{-4}$ s^{-1} $k_{on} = 5.9 \times 10^{3}$ M^{-1} s^{-1} $Chi^2 = 2.04$	ND	ND
MF23-1 mAb	ND	$K_D = 8.8 \times 10^{-5}$ M $Chi^2 = 0.533$	$K_D = 1.8 \times 10^{-5}$ $Chi^2 = 0.964$
MF23-1 Fab	ND	ND	$K_D = 2.7 \times 10^{-5}$ $Chi^2 = 0.746$

ND: Not determined

3.4.5.2. Binding of the S20 and MF23-1 antibodies to O6a, 6d repeating units

The *O*-polysaccharide from the LPS of *P. aeruginosa* strain O6a, 6d was hydrolyzed into different lengths of 1, 2 and 3 repeating units. The affinities of these three O6a, 6d oligosaccharides for immobilized S20 scFv and mAb MF23-1 were measured by SPR using a Biacore T200 (Figure 17). Neither antibody bound the O6a, 6d oligosaccharide with a length of 1 repeating unit (negative sensorgram not shown); however, both S20 and MF23-1 antibodies bound, with different affinities, to the O6a, 6d oligosaccharides with lengths of 2 and 3 repeating units. The overlaid sensorgrams of the S20 antibody binding to the 2 and 3 repeating unit are provided in Figure 17A and B, respectively. As illustrated, the data collected (black lines) fit well to a simple one-to-one interaction model (red lines) with local fitting, and their rate and affinity constants are provided in Table 2. The analysis revealed that the S20 scFv has about 4-fold greater affinity to the 3 repeating unit oligosaccharide (K_D = 1.1 μM) compared to the 2 repeating unit oligosaccharide (K_D = 4.7 μM). The higher affinity to the 3 versus 2 repeating unit oligosaccharide is due to a faster association rate constant (k_{on} 4.4 $\times 10^3$ M^{-1} versus 1.1 $\times 10^3$ M^{-1}, respectively); their dissociation rate constants (k_{off}) were similar. The higher affinity to the 3 repeating unit versus 2 repeating unit is likely explained by additional interactions with the larger ligand; nonetheless its affinity is still about 2-fold lower than for the non-hydrolysed LPS (K_D = 0.6 μM, Figure 16, Table 2), indicating that the S20 epitope may span more than 3 repeating units.

The overlaid sensorgrams of mAb MF23-1 binding the 2 and 3 repeating unit oligosaccharides are provided in Figure 17C and D, respectively. Since the association and dissociation phases of antigen binding to the MF23-1 antibody were too rapid for kinetic analysis

using a 1:1 binding model, the K_Ds were determined by steady state affinity (Figure 17E and F). These K_Ds are reliable since the highest concentrations of the oligosaccharides used were above the K_Ds values and since the K_D values are outside the linear range of the steady state binding curves. Like the S20 scFv, mAb MF23-1 exerts its strongest affinity to the O6a, 6d oligosaccharides with 3 (K_D = 18 μM) versus 2 repeating units (K_D = 88 μM). However, compared to the S20 scFv, the MF23-1 antibody has about a 20-fold weaker affinity to these O6a, 6d oligosaccharides. This is not that surprising since the S20 antibody was generated to be specific for the O6a, 6d strain while the MF23-1 antibody was generated to be cross-reactive to various strains of serotype O6. Although kinetic analyses were not done with LPS from other O6 strains, it is expected that mAb MF23-1 has a much greater affinity to the O6 strains that showed strong reactivities by WB, including O6 IATS, Fisher 1 and PAK (Figure 13).

The binding functionality of the MF23-1 Fab fragment, which was prepared by digesting mAb MF23-1 with papain, was confirmed by SPR (Figure 18). Its affinity (K_D = 27 μM) towards the 3 repeating unit was comparable to that of its parental intact IgG.

Figure 17. SPR analysis of immobilized S20 scFv and mAb MF23-1 to O6a, 6d repeating unit oligosaccharides. Both antibodies did not show any binding activity to the 1-repeating unit of O6a, 6d oligosaccharide (negative sensorgram not shown). For the immobilized S20 scFv, the (A) 2-repeating unit and (B) 3-repeating unit oligosaccharides were injected over the surfaces for 240 sec (4 min), and allowed to dissociate for 1200 sec. The data collected (black lines) fit well to a 1:1 interaction model, with local fitting (red lines). The k_{on}, k_{off} and K_D are presented in Table 2. For the immobilized mAb MF23-1, the (C) 2-repeating unit and (C) 3-repeating unit oligosaccharides were injected over the surfaces for 30 sec, and allowed to dissociate for 30 sec. Since the rate constants (k_{on} and k_{off}) were too rapid for kinetic analysis using a 1:1 interaction model, the K_D were determined by steady state affinity. The responses (RU) at 5 sec after the injection over a window of 5 sec in (C) and (D) were used to generate the steady state graph for (E) and (F), respectively. All the analyses were done using the Biacore T200 Evaluation Software Version 1.0 (GE Healthcare).

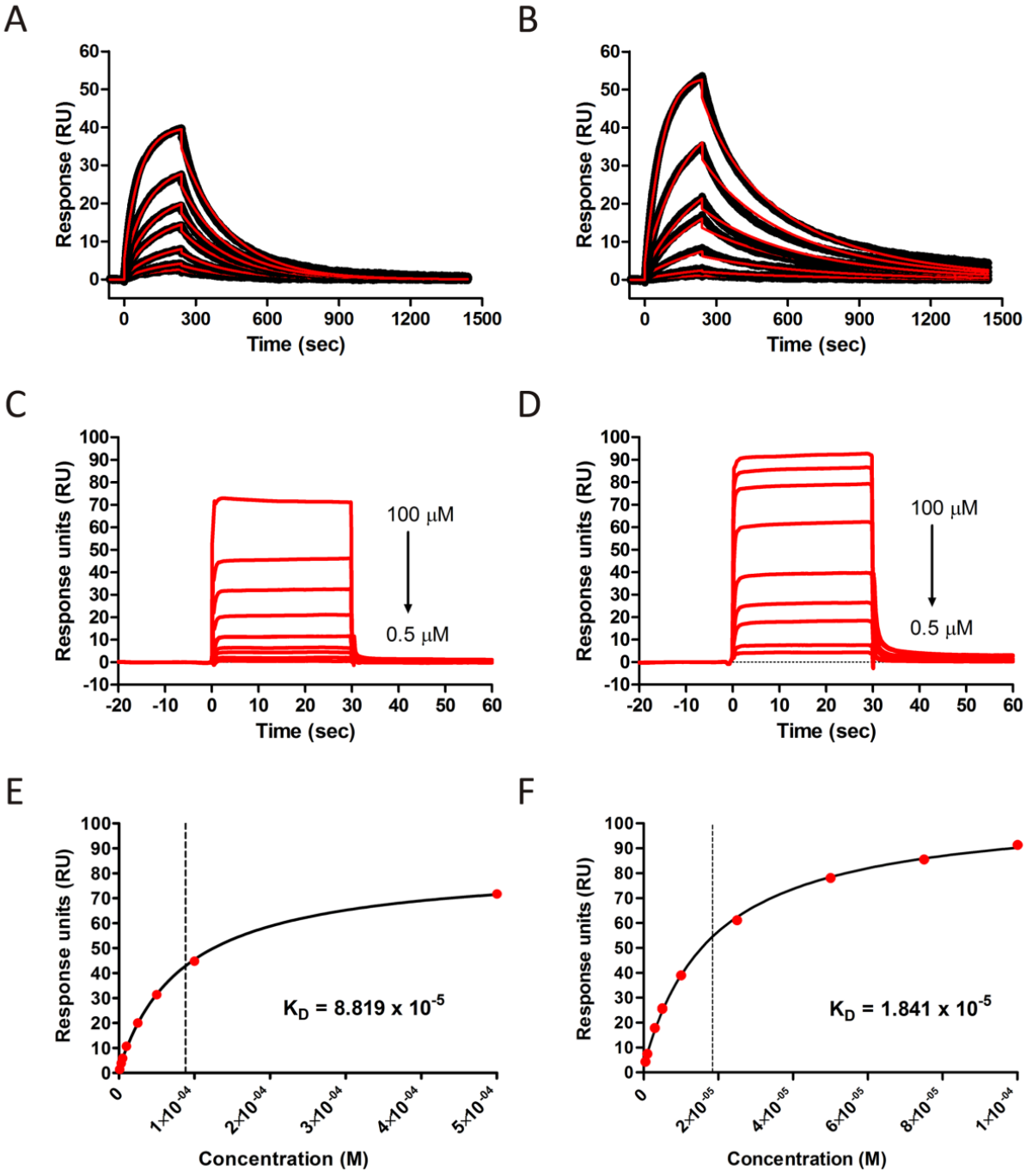
A
B
C
D
E
F
Response (RU)
Time (sec)
Response units (RU)
100 µM
0.5 µM
Concentration (M)
K_D = 8.819 x 10^{-5}
K_D = 1.841 x 10^{-5}

Figure 17.

Figure 18. SPR analysis confirming that papain-prepared MF23-1 Fab fragment functionally binds the O6a, 6d oligosaccharide with an affinity similar to its parental mAb. The O6a, 6d unit of 3 repeating units was injected over immobilized (A) mAb MF23-1 (B) MF23-1 Fab for 30 sec, and allowed to dissociate for 30 sec. Since the association and dissociation phases were too rapid for kinetic analysis using a 1:1 interaction model, the K_D were determined by steady state affinity. The responses (RU) were calculated at position 5 sec after the injection over a window of 5 sec in (A) and (C), and used to generate the steady state graph for (B) and (D), respectively. All the analyses were done using the Biacore T200 Evaluation Software Version 1.0 (GE Healthcare).

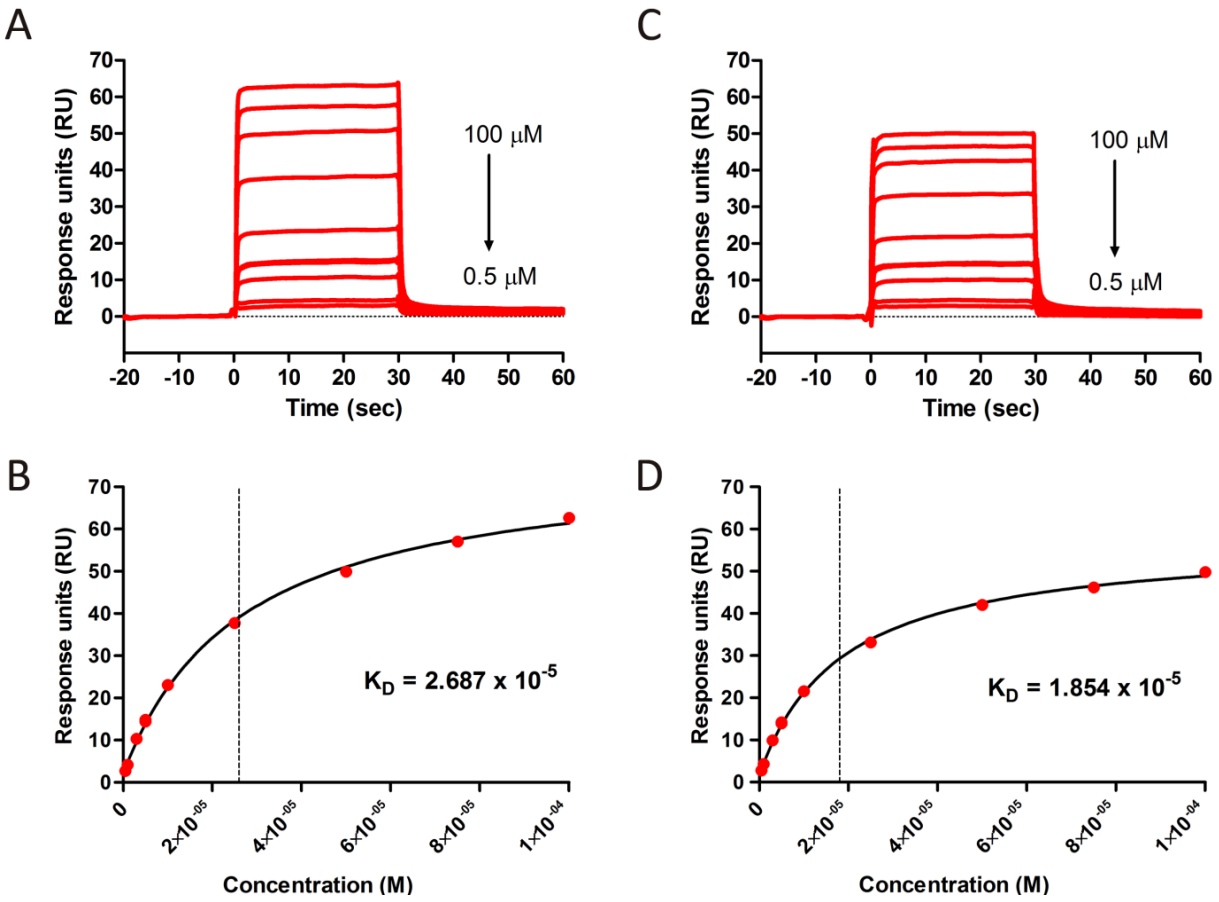
A
C
B
D
Response units (RU)
Time (sec)
100 μM
0.5 μM
Concentration (M)
K_D = 2.687 x 10^{-5}
K_D = 1.854 x 10^{-5}

Figure 18.

3.4.6. Determining the MIC

3.4.6.1. S20 scFv

Since Xie *et al*. (5) did not separate the S20 scFv by gel filtration, their experiments with the S20 scFv contained a heterogeneous mixture of monomer, dimer and some contaminating aggregates. Therefore, after we determined that the S20 was prone to dimerization (Figure 10), it was unknown if the bactericidal activity observed in the previous assays was exhibited by only one or all of these S20 scFv formats. A clear understanding of this could help us make some progress in understanding the bactericidal mechanism of action of the S20 antibody. For example, if the bactericidal activity is only exhibited by the S20 scFv dimer, then perhaps dimerization or cross-linking of surface LPS molecules is an important step in the bactericidal mechanism.

The bactericidal assay revealed that both the monomeric and dimeric forms of the S20 scFv mediate direct bactericidal activity towards *P. aeruginosa* strain O6a, 6d (Figure 19A and B). These results have also been confirmed using the agar plate method (data not shown). Overall, the S20 scFv dimer was more efficacious at reducing the growth and viability of O6a, 6d compared to the same concentrations of the monomer. The lowest concentrations to produce a difference on the growth of O6a, 6d over the entire growth curves were 78.1 nM and 10 nM for the monomer and dimer, respectively. Although the effects generated were mostly concentration-dependent, concentrations higher than 1.25 µM (highest concentration shown) did not further reduce the turbidity. Likewise, the effects of the S20 monomer appeared to plateau at about 10 µM.

The differences in the efficacy of the S20 monomer and dimer are more clearly illustrated in the turbidity (%) versus antibody concentration (nM) (log-scale) graph (Figure 20A). By interpolating, this graph revealed that the S20 scFv monomer and dimer have MIC_{50} of 450 nM and 60 nM, respectively. Thus, the S20 scFv dimer is ca. 8-fold more bactericidally potent than the monomer (Figure 20B).

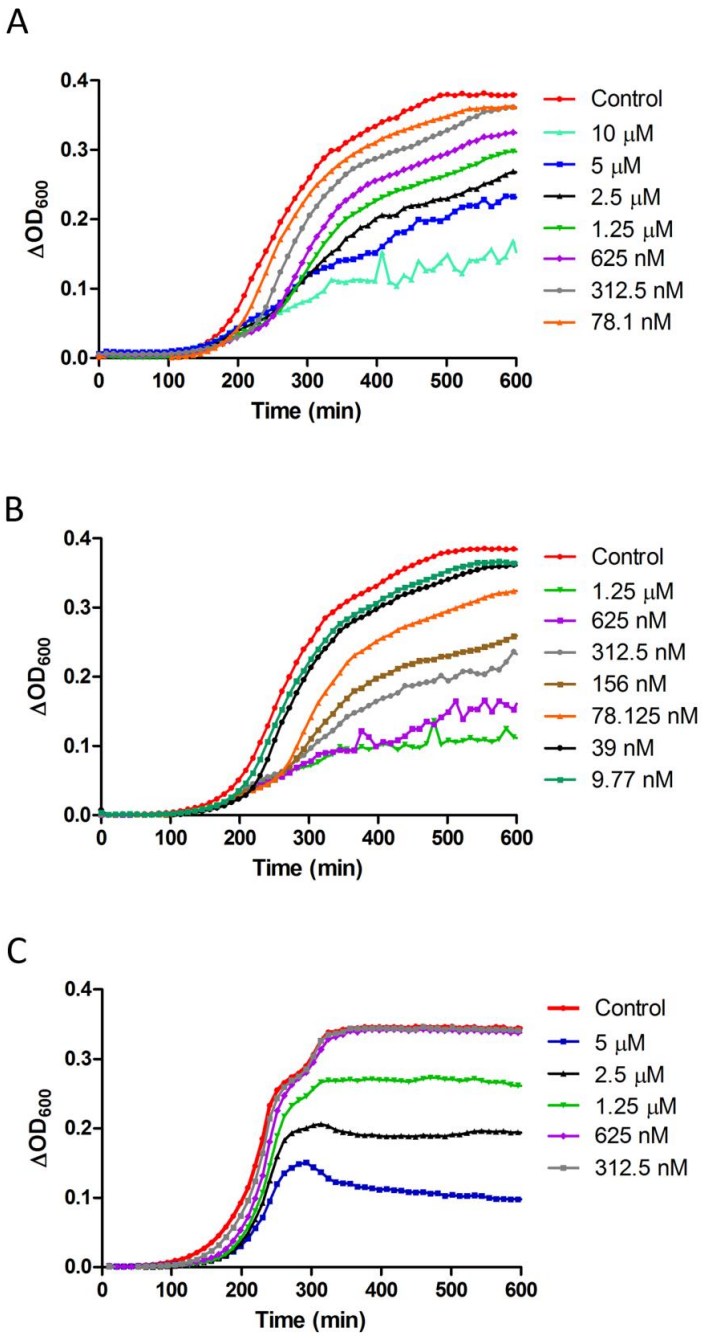

Figure 19. Concentration-dependent effect of A) S20 scFv monomer, B) S20 scFv dimer and C) MF23-1 mAb on the growth of *P. aeruginosa* strain O6a, 6d, at 37°C, 50 rpm, over 10 h. The curves represent the average of three replicates; for improved clarity, error bars (SE) have been omitted. This microtitre assays were conducted in the automated Infinite 200 PRO microplate incubator/reader (Tecan, Mannedorf, Switzerland).

A

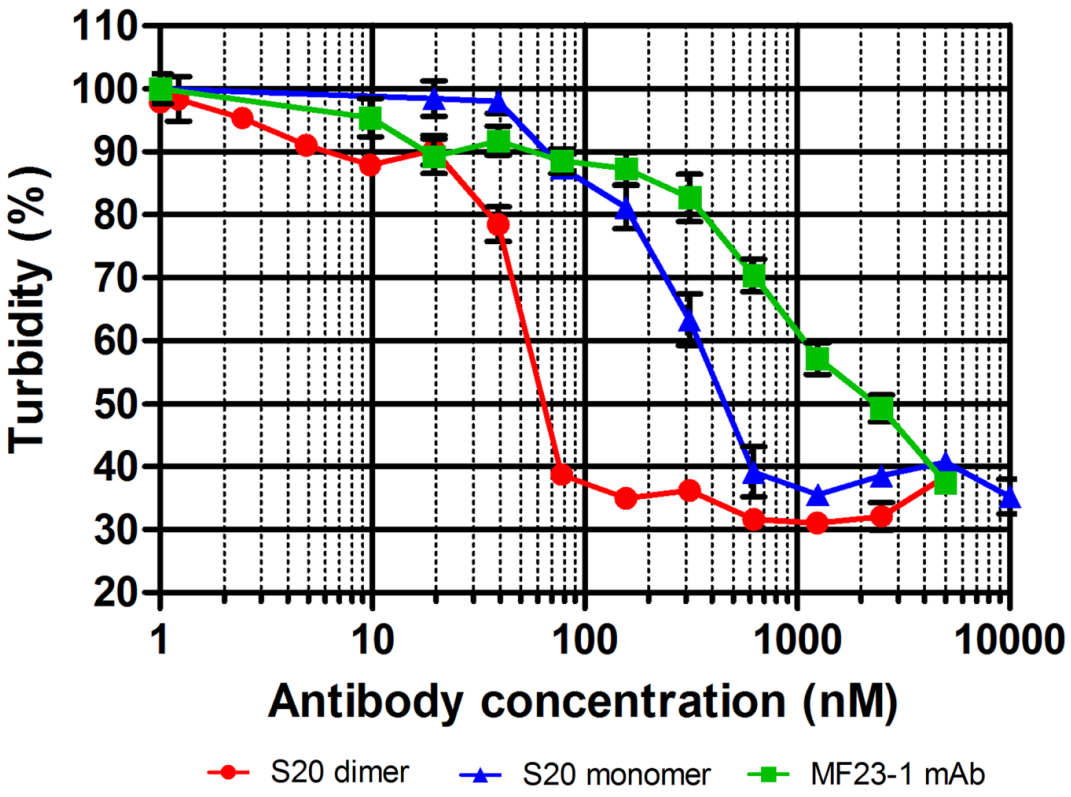

B

	MIC_{50} (nM)	K_D (M)	k_{ON} (M^{-1} s^{-1})	K_{OFF} (s^{-1})
S20 scFv dimer	60	2.1×10^{-8}	5.9×10^{3}	1.2×10^{-4}
S20 scFv monomer	450	5.6×10^{-7}	5.2×10^{3}	2.9×10^{-3}
MF23-1 mAb	2500	*1.8×10^{-5}	NA	NA

*K_D of the monovalent Fab fragment of MF23-1 towards 3-repeating units of O-Ag of O6a, 6d as determined by steady state affinity.

Figure 20. A) The data from the O6a, 6d growth curves generated in Figure 19 were used to prepare a turbidity (%) versus antibody concentration (nM) (log-scale) graph. The minimal inhibitory concentration which causes a 50% reduction (MIC_{50}) of cell turbidity was interpolated for each antibody. B) Relationship between the MIC_{50} of the antibodies and their affinities towards *P. aeruginosa* strain O6a, 6d.

3.4.6.2. MF23-1 mAb

As was observed with the S20 scFv monomer and dimer (Figure 19A and B), mAb MF23-1 showed bactericidal activity in a concentration-dependent manner towards its target strains, namely O6 IATS, PAK, O6a, 6d and Fisher 1 (Figure 21A–D). As revealed by the turbidity (%) versus the Ab concentrations graph (Figure 22), MF23-1 exhibits varying degrees of bactericidal efficacy to these strains. The MIC_{50} were calculated as 40, 200, 230 and 2500 nM for Fisher 1, PAK, O6 IATS and O6a, 6d, respectively. Thus, Fisher 1 is much more sensitive (62.5-fold) to mAb MF23-1 than O6a, 6d.

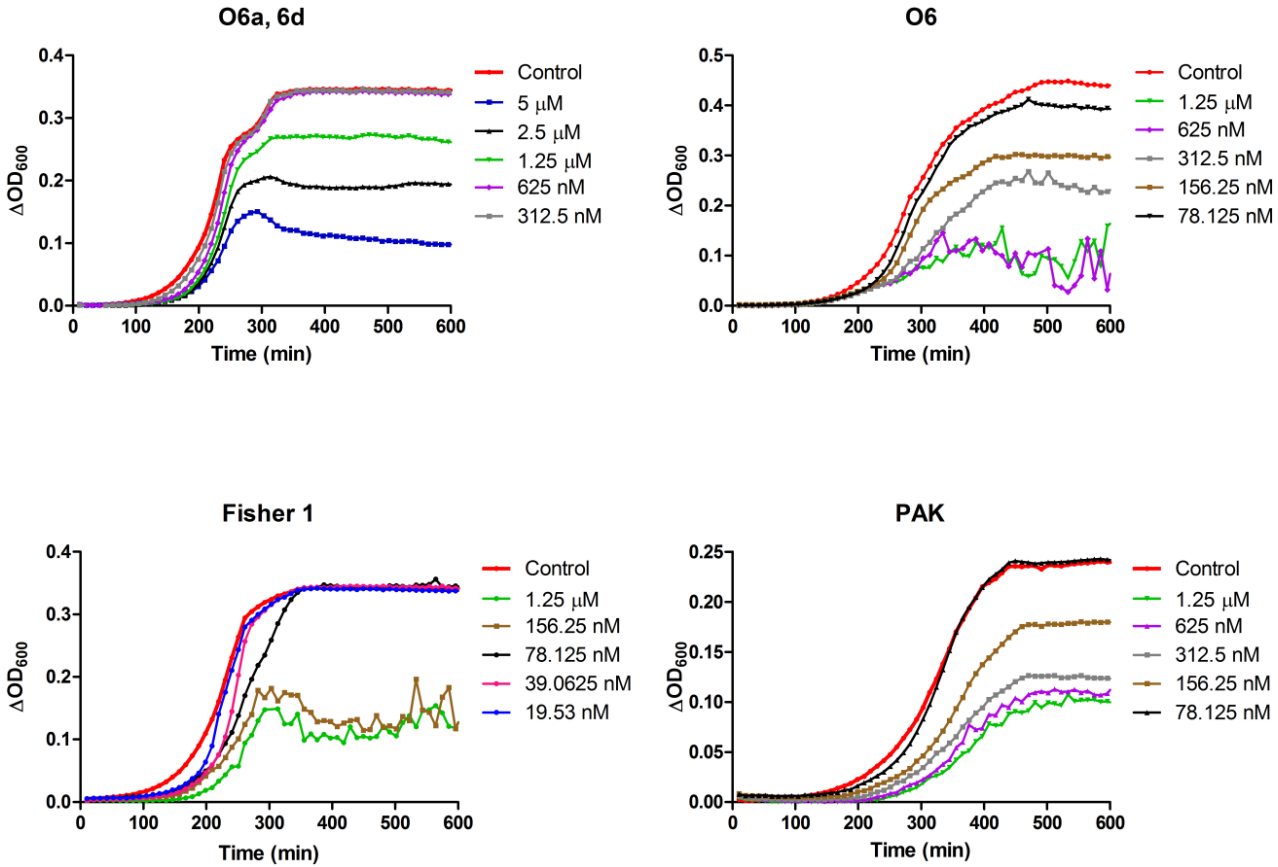

Figure 21. The concentration-dependent effect of mAb MF23-1 on the growth curve of various wild-type (OSA+) strains of *P. aeruginosa* serotype O6 grown at 37°C, 50 rpm, over 10 h. The curves represent the average of three replicates; for improved clarity, the bars (SE) have been omitted. This microtitre assays were conducted in the automated Infinite 200 PRO microplate incubator/reader (Tecan, Mannedorf, Switzerland). Note that the data presented for O6a, 6d in this figure is the same as presented in Figure 19.

A

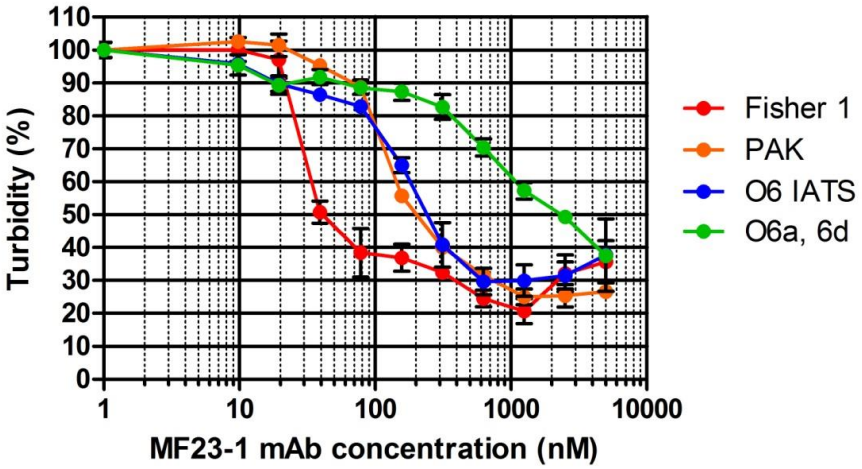

B

Strain	MIC_{50} (nM)
Fisher 1	40
PAK	200
O6 IATS	230
O6a, 6d	2500

Figure 22. A) The data from the growth curves generated in Figure 21 were used to prepare a turbidity (%) versus mAb MF23-1 concentration (nM) (log-scale) graph. B) The minimal inhibitory concentration that causes a 50% reduction (MIC_{50}) of cell turbidity was interpolated for each antibody.

3.4.6.3. Correlation between the affinity and bactericidal potency

Our data established that there is a direct correlation between the affinity (K_D) of the antibodies and their bactericidal potency (MIC_{50}) towards O6a, 6d. In order of most bactericidally active, the antibodies and their fragments are: S20 scFv dimer [K_D (apparent) = 21 nM; MIC_{50} = 60 nM] > S20 scFv monomer [K_D = 560 nM; MIC_{50} = 450 nM] > mAb MF23-1 [K_D (monovalent) = 18 µM; MIC_{50} = 2.5 µM] (Figure 16, Figure 20). Based on these results, we expect that the affinity of MF23-1 towards the other strains to follow the MIC_{50} trend we experimentally determined: Fisher 1 (MIC_{50} = 40 nM) > PAK (MIC_{50} = 200 nM) ≈ O6 IATS (MIC_{50} = 230 nM) >> O6a, 6d (MIC_{50} = 2500 nM) (Figure 22).

3.4.7. Sequence analysis of the variable domains of the bactericidal S20 and MF23-1 antibodies

Since the S20 and MF23-1 antibodies bind to structurally similar antigens, and are both bactericidal, it was hypothesized that they should share significant similarities in their CDRs. If they are catalytic antibodies they would likely share key amino acid residues involved in the killing mechanism. In fact, it has been demonstrated that catalytic antibodies directed against the same haptenic transition-state analog (chloramphenicol phosphonate) share significant sequence identity to each other, while non-catalytic antibodies directed at the same hapten share little identity to each other (175).

Our sequence alignment revealed that the CDR sequences of the S20 and MF23-1 antibodies are strikingly different from each other in terms of their lengths, their amino acid composition, and the physicochemical properties of their amino acids (Table 3: alignment of

CDR sequences; Appendix Figure 45: alignment of the complete variable domain sequences). In fact, although these antibodies essentially bind the same or very closely related O6 O-antigens (Figure 4, Figure 13), their CDR sequences are not more closely related to each other than to the non-specific/non-bactericidal antibodies, namely mAbs 7-4 (anti-LPS inner core of *P. aeruginosa*), N1F10 (anti-CPA) and LPT3-1 (anti-LPS inner core of *N. meningitidis*).

The CDR-H3, which is the most variable loop and known to play a key role in antigen recognition, differed considerably among the antibodies presented in Table 3. That of the S20 antibody is very long (12 residues) and is especially rich in basic [two arginines (R), one histidine (H)] and acidic [two aspartic acids (D)] residues, while that of the MF23-1 is short (7 residues) and devoid of charged residues. Basic residues [R, lysine (K), H] are located in the CDR-H2 of MF23-1. Presumably, these basic residues are involved in ionic interaction with the acidic sugars of the O6 OSA (Figure 3, Figure 4).

A NCBI protein blast search (data not shown) revealed that the S20 CDR-H1 and CDR-H2 share 100% identity with several anti-polysaccharide antibodies including, several anti-pneumococcal [e.g., GenBank accession numbers AAM46657.1, ABG38429] and several anti-RhD [e.g., GenBank accession numbers ABE97346.1, (176); CAA78220.1, (177)] antibodies. Furthermore, as previously reported, the human antibody response to bacterial polysaccharides, including that of *P. aeruginosa* (125) and *Streptococcus pneumoniae* (178-180), preferentially uses the VH3 gene family. In fact, the response to *S. pneumoniae* polysaccharides is restricted to the use of the VH3-33 and JH4 segments, the same used by the S20 antibody (180).

No hits were found when the six individual CDRs of the bactericidal S20 and MF23-1 antibodies were searched against the antimicrobial APD database [http://aps.unmc.edu/AP/; (164-166)] (data not shown). Moreover, it is not anticipated that the bactericidal antibodies

could integrate directly in the outer membrane of *P. aeruginosa*, in a mechanism similar to the barrel-stave or carpet-like models of AMPs, since GRAVY scores revealed that the CDRs are not particularly hydrophobic in nature (Table 4).

In summary, nothing was revealed within the variable sequences of the bactericidal antibodies that would be expected to confer antimicrobial activity. Together with our SPR data, we provide the evidence to show that these antibodies are exploiting a vulnerable target on the surface of *P. aeruginosa*, the OSA of serotype O6.

Table 3. Multiple sequence alignment (MSA) of the CDRs from the variable heavy and variable light domains of the bactericidal (S20 and MF23-1) and non-bactericidal (7-4, N1F10 and LPT3-1) antibodies. The MSA of the complete variable domain sequences, with IMGT numbering, is provided in Figure 45 of the Appendix. The dots represent no amino acid residue at a position, according to IMGT numbering system.

Antibody	CDR-H1	CDR-H2	CDR-H3	CDR-L1	CDR-L2	CDR-L3
S20	GFTF....SSYG	IWYD..GSNK	ARDPHY.TRGFDY	QSLLHS.DGMTY	EV.......S	MQNIQ....LPWT
MF23-1	GFTF....SDAW	IRSKANNHAT	TAGG......FAY	QEI......SGY	AA.......S	LQYAS....YPLT
5c7-4	GFKI....KDTY	IDPA..NGHT	ARRT.....GPAY	SSVS.....SSY	ST.......S	HQYHR....SPFT
N1F10	DYTF....SSYW	ILPG..IQST	ARRYYGSSYGFDY	QNI......NVW	KA.......S	QQGQS....YPLT
LPT3-1	GFTF....RRFG	IGGG..SSTI	TRDETG..SWFAY	SSV.......RY	DT.......S	QQWNG...YPPLT

3.4.8. Targeting the OSA of serotype O3

To determine if serotype O6 is particularly susceptible to anti-OSA antibodies, we investigated whether targeting a non-O6 OSA with antibodies would elicit similar bactericidal activity. We chose to target the OSA of serotype O3, another clinically prevalent serotype with the then commercially available mAb ab84607 (Abcam), a murine IgG_3. Since the antigen specificity of mAb ab84607 was not provided by the manufacturer, we first confirmed its binding to the OSA of serotype O3 IATS by WB (Figure 23A). As illustrated, mAb ab84607 reacted, in a smear-like way, which is characteristic of the reactivities anti-LPS antibodies, to cell lysate from serotype O3 that was digested with proteinase K (Lane 2), confirming its binding to the OSA of this serotype. As revealed by the bactericidal assay (Figure 24), the mAb ab84607 reduced the viability of serotype O3 by ca. 60%, and thus exerts direct bactericidal activity independent of phagocytes and the CDC. However, it was statistically less efficacious in inducing killing towards its specific strain compared to mAb MF23-1 which induced > 90% cell death to O6 IATS. Unfortunately, Abcam discontinued this commercial mAb ab84607 during our studies and, since our supply was limited, we were not able to further investigate this antibody.

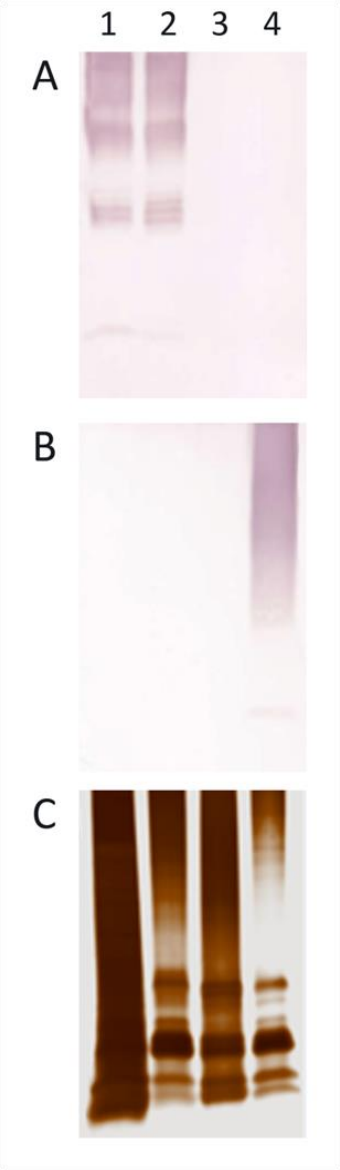

Figure 23. Commercial mAb ab84607 targets the OSA serotype O3 IATS (ATCC 33350). Lane 1: H-B cell lysis of serotype O3, no proteinase K; Lane 2: H-B cell lysis of serotype O3, with proteinase K treatment; Lane 3: H-B cell lysis of serotype O5 with proteinase K treatment; Lane 4: H-B cell lysis of serotype O6 with proteinase K treatment. Western immunoblot A was probed with mAb ab84607, as primary antibody, and goat anti-mouse $F(ab')_2$-alkaline phosphatase conjugate , as secondary antibody, and B was probed with mAb MF23-1, as the primary antibody, and with the same secondary antibody, and served as positive control. C shows the silver stain corresponding to the WBs. MAb ab84607 is specific for the O3 OSA since it reacts with proteinase-K digests in a smear like manner, which is characteristic of the probing with anti-OSA antibodies.

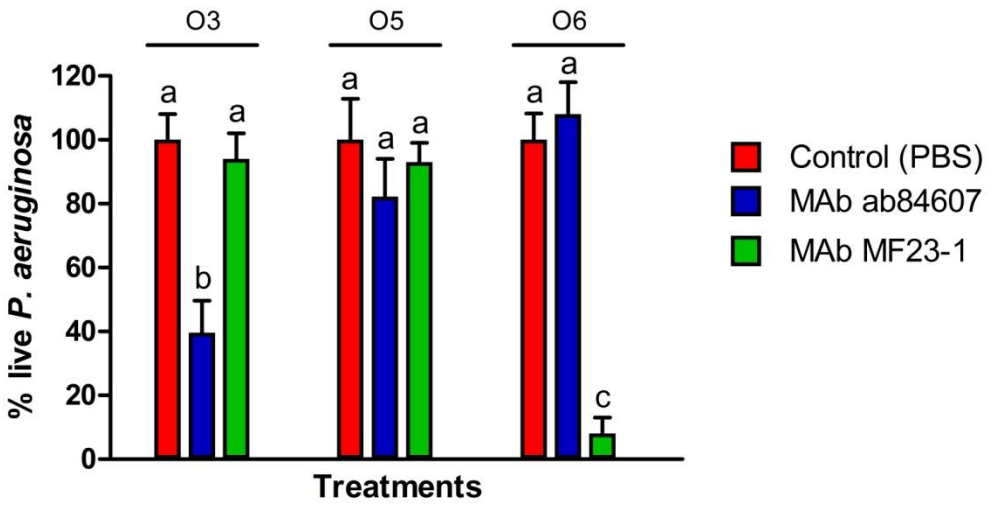

Figure 24. Bactericidal activity of mAb ab84607 against *P. aeruginosa* serotype O3 IATS (ATCC 33350). The bactericidal activity was determined by counting CFUs on agar plates following 30 min incubation of the bacteria (ca. 1×10^7 CFU mL^{-1}) with the antibodies at 37°C. Untreated bacteria (PBS) and non-specific serotype O5 and O6 served as negative controls. Treatment with mAb MF23-1 served as a positive control to serotype O6. Data represent means of three replicates ± SE. The different letters a-c indicate statistical differences among treatments ($p<0.05$), as analyzed by One-Way ANOVA.

3.4.9. Targeting the highly conserved inner core region

To further our understanding of the bactericidal mechanism of the anti-OSA antibodies, and in the hope of uncovering common LPS antigens that can be targeted to produce similar bactericidal effects towards all clinical strains, we decided to determine if targeting another LPS substructure would result in similar bactericidal activities. We investigated whether targeting a conserved LPS substructure would result in direct bactericidal activity similar to that observed when targeting the OSA with antibodies. Although the outer core LPS region is relatively accessible and well conserved between *P. aeruginosa* serotypes, some clinical isolates mutate to have a truncated deep rough form. Therefore, we chose to target the inner core region since it is both strictly conserved among all *P. aeruginosa* serotypes and is always wholly present in clinical strains. If successful, this region could represent an attractive target for therapeutic applications. Furthermore, knowing if cell viability is affected by antibody binding to the core region will further our understanding of the bactericidal mechanism of these antibodies.

MAb 7-4 (murine IgG2b), which has previously been shown to bind to the inner core region of LPS of all serotypes of *P. aeruginosa* by WB (116), was chosen for this experiment. Although the specificity of mAb 7-4 has previously been published, we confirmed its binding towards some of the strains before proceeding with this study (Figure 48, Appendix).

MAb 7-4 was screened for bactericidal activity against several strains with smooth CPA+/OSA+ (O6a, 6d; PAK; PAO1), CPA+/OSA- (PAK *wbpO*, add AK1401) and rough CPA-/OSA- (PAK *rmlC*; PAO1 ΔalgC::tet, AK1012) phenotypes. The rationale behind screening against rough strains was two-fold. First, we thought the long *O*-polysaccharide chains of the LPS would perhaps hinder the accessibility of mAb 7-4 to its target, i.e., the LPS inner core,

thereby not being able to produce its potential bactericidal effect. In fact, some rough strains (e.g., AK1012) have been shown by ELISA to have stronger binding reactivities with mAb 7-4 (116). Secondly, being able to target rough strains is attractive in terms of therapeutic application since long-term clinical strains have a tendency to become rough over time.

As illustrated in Figure 25, mAb 7-4 produced no statistical differences on the viability of any of the strains with smooth CPA+/OSA+ (O6a, 6d; PAK; PAO1), CPA+/OSA- (PAK *wbpO*, add AK1401) or rough CPA-/OSA- (PAK *rmlC*; PAO1 Δ*alg*C::tet, AK1012) phenotypes. The only treatments which produced statistical differences ($p<0.05$) on the viability of the cells were the positive control mAb MF23-1 towards O6a, 6d (33% viability, $p = 0.001964$) and O6 IATS (9% viability, $p = 0.000588$). Although the affinity of mAb 7-4 towards its inner core epitope has not been determined, we expect, based on WB reactivities, it to be much better than MF23-1 towards O6a, 6d ($K_D \approx 20$ μM). Thus, if mAb 7-4 has bactericidal activity, we would expect to be able to detect it at the tested concentration of 8 μM since this concentration is considerably higher than any of the MIC_{50} values determined for the anti-OSA antibodies (MIC_{50} range = 40–2500 nM; Figure 20, Figure 22). Therefore, we are confident that, unlike targeting the OSA, targeting the inner-core region with antibodies does not affect the integrity and viability of the cells.

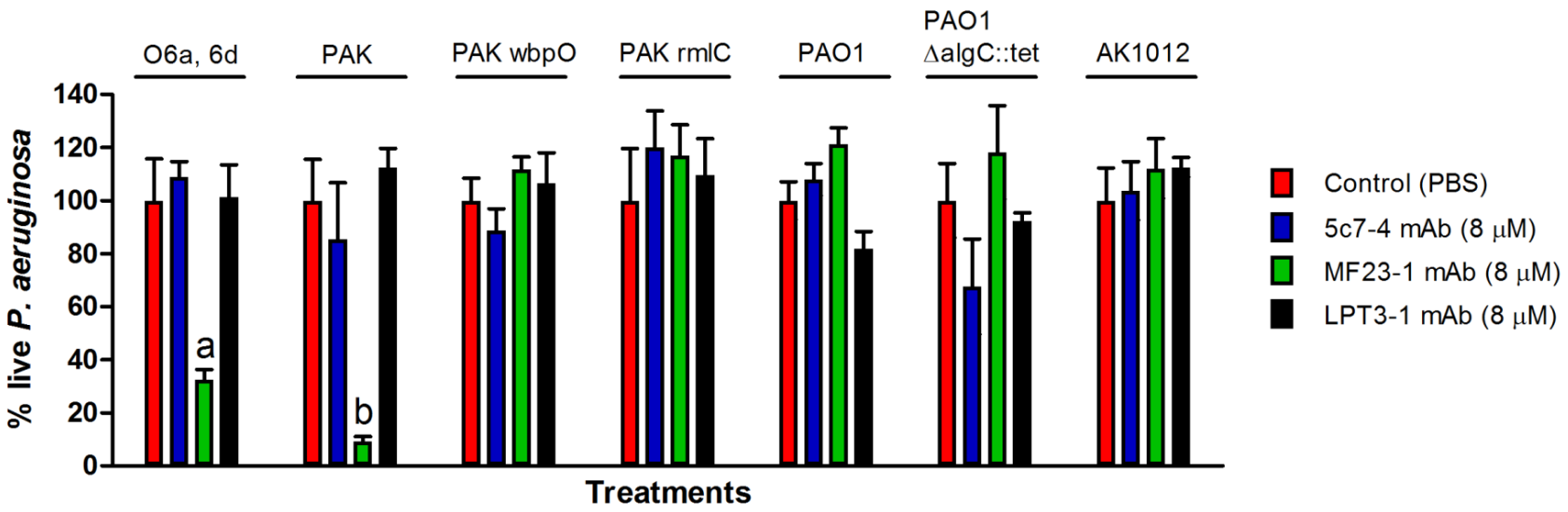

Figure 25. MAb 7-4, an anti-inner core LPS antibody, does not show bactericidal activity towards various smooth and rough strains of *P. aeruginosa* serotype O5 and O6 when tested at a high concentration of 8 µM. The bactericidal activity was determined by counting CFUs on agar plates following 30 min incubation of the bacteria (ca. 1×10^7 CFU mL^{-1}) with the antibodies at 37°C. Untreated bacteria (PBS) and bacteria treated with the non-specific LPT3-1 antibody served as controls. Treatment with mAb MF23-1 served as a positive control towards serotype O6. Data represent means of three replicates ± SE. The different letters a-c indicate statistical differences among treatments ($p<0.05$), as analyzed by One-Way ANOVA.

3.4.10. Targeting the common polysaccharide antigen (CPA, A-band)

Since *P. aeruginosa* cells are susceptible to antibodies binding their OSA (B-band LPS), we investigated whether targeting the CPA would produce similar bactericidal effects. We chose to target the CPA with N1F10 IgM (106) and our engineered N1F10 scFv. Following their purification (Figure 26), WBs confirmed the binding of the N1F10 IgM to various CPA+/OSA+ and CPA+/OSA- strains (Appendix Figure 49). No reactivity was detected when the N1F10 scFv was used in a WB, but low levels of binding were detected by ELISA (data not shown). This is not surprising since its affinity is likely very low because its parental Ig is an IgM.

To determine if targeting the CPA with antibodies affects the viability of *P. aeruginosa* cells, we screened the anti-CPA N1F10 IgM and its scFv against wild-type CPA+/OSA+ and CPA+/OSA- strains from serotype O6 and O5. On the surface of wild-type OSA+/CPA+ strains, the OSA [up to ca. 50 repeating units, (62)] extends almost twice the length of the CPA [ca. 70 sugars = 23 repeating units (59)]; therefore, it has been suggested that it masks the accessibility the N1F10 IgM to the shorter-chains of CPA (60). Because the N1F10 scFv has a much lower molar mass (ca. 30 kDa compared to ca. 960 kDa for the IgM) and is monovalent, one could expect it to have greater accessibility to the CPA of wild-type strains. The predominant form of LPS on wild-type strains is OSA; however, in the absence of OSA expression (CPA+/OSA-), the density of CPA increases (119). Therefore, if the anti-CPA antibodies mediate bactericidal activity, one would expect CPA+/OSA- strains to be more sensitive.

Our bacterical assay demonstrated that the N1F10 IgM and its scFv had no effect on the viability of CPA+/OSA+ (PAK, PAO1) and CPA+/OSA- (PAK *wbp*O, AK1401) strains (Figure

27). As high as 25 μM N1F10 scFv was tested against PAK *wbp*O, and no effects were observed (data not shown).

It remains perplexing why targeting the OSA, but not the CPA, is so critical to the viability of *P. aeruginosa*. However, these two types of LPSs do contain several structural differences. Their *O*-polysaccharides differ in their charge (OSA: negatively charged; CPA: neutral), their sugar compositions (OSA: rich in amino sugars and low in rhamnose; CPA: rich in rhamnose and low in amino sugars), and, in many cases, their chain lengths (CPA chains ≤ 23 sugars; OSA chains ≤ 50 repeating units). It is possible that targeting the very long chains of the OSA with antibodies, as opposed to the shorter CPA chains, exerts some sort of mechanical strain which either destabilizes the anchored LPS molecules or distorts the packaging of LPS molecules.

While the structure of the repeating units of the CPA polysaccharide has been elucidated as [→3)-α-D-Rha-(1→2)-α-D-Rha-(1→3)-α-D-Rha-(1→]$_n$ (94, 96, 97), its complete core-lipid structure has not been fully elucidated. It is presumed, however, that the OSA and CPA polysaccharides are linked, via the 3 position of L-Rha in the core oligosaccharide, to a similar lipid A–core region structure (181) (Figure 5). Nevertheless, it is not clear if there are any modifications or additional sugars on the distal terminus of the CPA (107). There does appear to be some structural difference in the lipid A of the CPA since it does not react with an anti-lipid A antibody that cross-reactively binds to the lipid A from the OSA LPS of *P. aeruginosa* and that of *E. coli* (119). Another difference is that the OSA LPS is rich in phosphate groups, while that of the CPA is deficient in phosphates but contains the very unusual presence of sulfates (119). Perhaps the sulfate groups offer some added stability to the CPA LPS in the OM of *P.*

aeruginosa. Until the structure of the CPA is fully elucidated, it will be difficult to understand why the OSA is so vulnerable to antibodies binding.

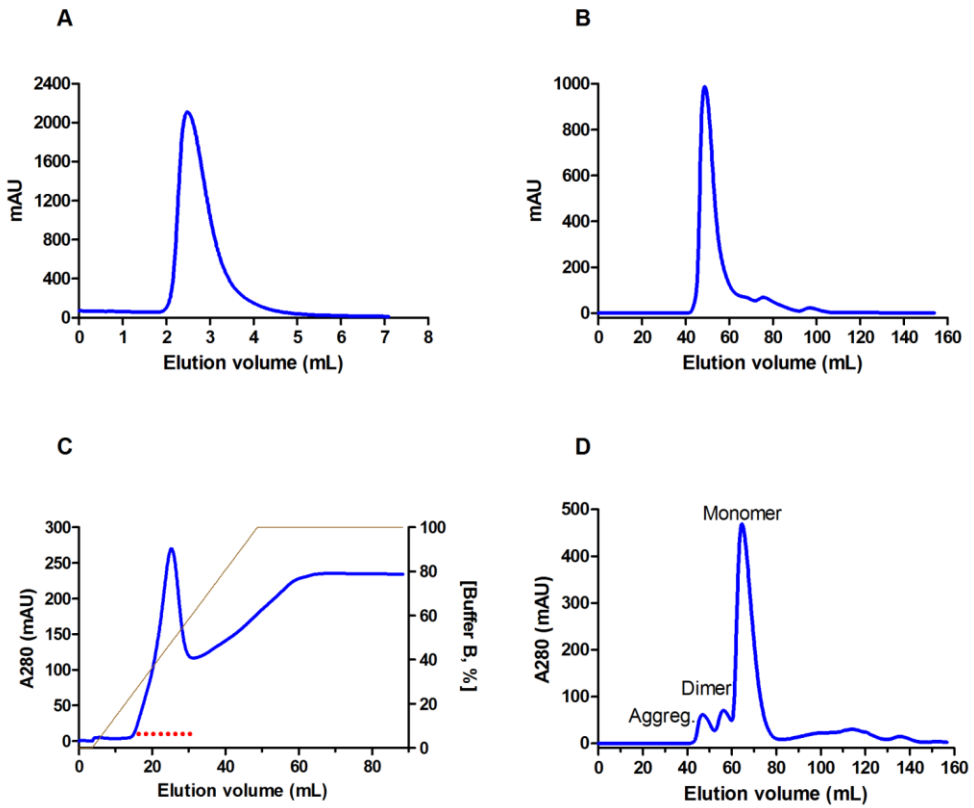

Figure 26. Purification of the anti-CPA antibodies, N1F10 IgM and its scFv. A. N1F10 IgM was purified from the hybridoma culture supernatant using a 1 mL HiTrap IgM Purification HP column (GE Healthcare). B. The eluted IgM peak recovered from A was polished by using SEC Superdex™ S200 16/60 (GE Healthcare). The equation of the standard line (Appendix Figure 42) ($Log_{10}MW = -0.04Ve + 7.973$) was used to calculate the apparent MW (MWapp) of the eluted peaks. The prominent peak (Ve = 48.8 mL) corresponds to the IgM (1050 kDa). C. IMAC chromatogram of N1F10 scFv. D. S75 16/60 chromatogram of N1F10 scFv, showing that the N1F10 scFv is less prone to dimerization than the S20 scFv (Figure 10, B and D). The equation of the standard line (Figure 42) ($Log_{10}MW = -0.0329Ve + 6.723$) was used to calculate the apparent MW (MWapp) of the eluted peaks.

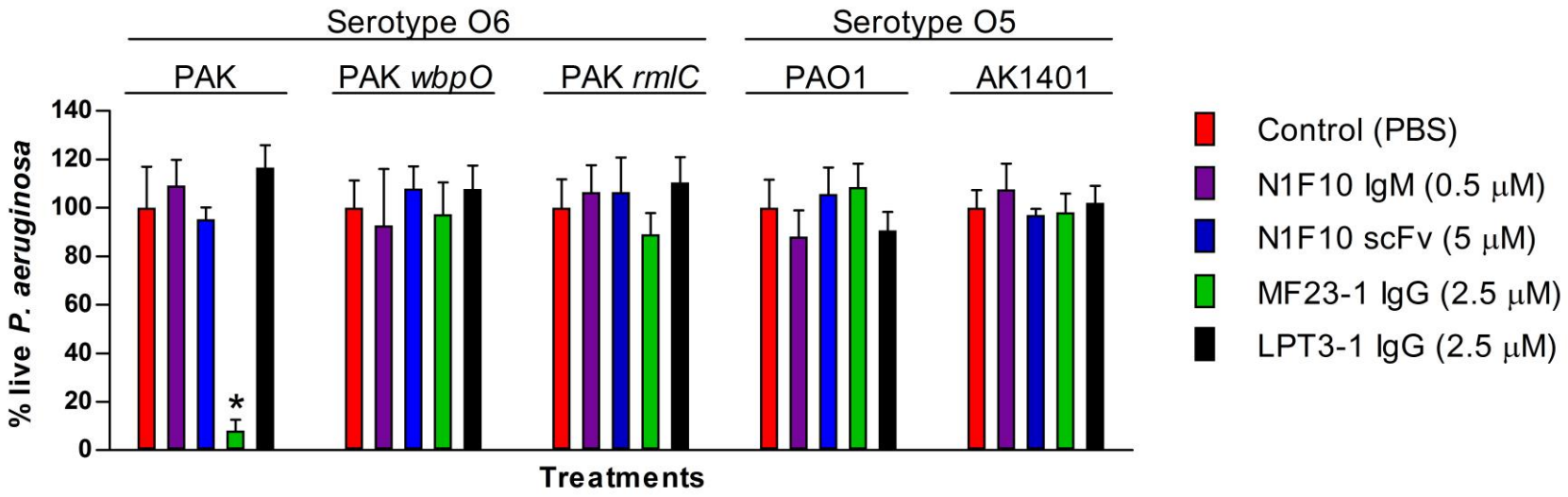

Figure 27. MAb N1F10 (IgM), an anti-CPA antibody, and its scFv do not show bactericidal activity towards various strains of *P. aeruginosa*, namely PAK (OSA^+/CPA^+; serotype O6), PAK *wbpO* (OSA^-/CPA^+; serotype O6), PAK *rmlC* (OSA^-/CPA^-; serotype O6), PAO1 (OSA^+/CPA^+; serotype O5), and AK1401 (OSA^-/CPA^+; serotype O5). The bactericidal activity was determined by counting CFUs on agar plates following 30 min incubation of the bacteria (ca. 1×10^7 CFU mL^{-1}) with the antibodies at 37°C. Untreated bacteria (PBS) and bacteria treated with the non-specific LPT3-1 antibody served as controls. Treatment with mAb MF23-1 served as a positive control towards serotype O6; the asterisk indicates a statistical difference for this treatment ($P<0.0001$), as analyzed by One-Way ANOVA. Data represent means of three replicates ± SE.

3.4.11. Targeting the OSA of *Salmonella* Typhimurium with 3B1 scFv

We investigated whether targeting the *O*-polysaccharide of another gram-negative bacterium would generate similar bactericidal effects as those observed towards *P. aeruginosa*. We chose to screen the 3B1 scFv, an anti-*Salmonella* serogroup B *O*-polysaccharide antibody (144, 148), because its parental mAb Se155-4 is very well-characterized antibody with available X-ray crystal structure data (145, 146). Our bactericidal assay showed that the viability of *S. enterica* serovar Typhimurium (ATCC 19585) (*S.* Typhimurium) was not affected by the 3B1 scFv (data not shown).

It is unclear why targeting the O-Ag affects the viability of *P. aeruginosa* but not that of *Salmonella*, and presumably most gram-negatives. Since the stability and integrity of membranes are often defined by the composition of their lipids, the discrepancy between *P. aeruginosa* and other gram-negatives may lie in their different lipid A structures (Figure 6) or lipidome. In essence, the lipid A from laboratory strains of *P. aeruginosa* have fewer and shorter acyl chains compared to that of many gram-negatives, including *E. coli*, *Salmonella* and *N. meningitidis* (59). Clinical strains of *P. aeruginosa* adapt by altering the structure of their lipid A in various ways [Figure 6, see reviews by King *et al*. (59) and Lam *et al*. (33)], for e.g., by the addition of acyl chains or the addition of 4-amino-4-deoxy-L-arabinose (L-Ara4N) on the phosphate groups (121-123). In fact, the addition of L-Ara4N is inducible in the presence of polymyxin B. Presumably, the structure of the lipid A of the O6 serotype strains used in this work resembles that of typical laboratory strains (Figure 6a). To gain an appreciation of the role of the composition of the lipid A, it would be of interest to test mAb MF23-1 against clinical isolates from serotype O6 (OSA+) known to have altered their lipid A.

The lipidome of *P. aeruginosa* also differs from enteric bacteria. While phosphatidylcholine (PC) is the most abundant phospholipid found in the membrane of eukaryotes, the membrane of most bacteria (ca. 90%), including *E. coli* and *Salmonella*, do not contain PC. However, in addition to the typical prokaryotic phospholipids (phosphatidylethanolamine, phosphatidylglycerol, and cardiolipin), *P. aeruginosa* can synthesize phosphatidylcholine (PC) as a minor membrane phospholipid if choline is available from the host or from complex growth medium (56). By growing *P. aeruginosa* in media with and without choline, it would be experimentally easy to determine if PC has an effect on the membrane stability when treated with the bactericidal antibodies. Further studies are warranted to investigate the role of PC and other membrane lipids in the bactericidal mechanism of our anti-OSA antibodies.

3.5. CONCLUSION

In 2010, our group reported that an antibody called S20 causes cell death by damaging the cell wall and increasing membrane permeability to its target *P. aeruginosa* strain O6a, 6d, independently of immune effector cells or the complement system (5). At the time, it was hypothesized that the S20 antibody was unique in that it possessed a potent catalytic activity against *P. aeruginosa* strain O6a, 6d. This hypothesis was disproved by the fact that a second antibody with an entirely unique amino acid sequence, i.e., mAb MF23-1, also exerts direct bactericidal activity towards O6 OSA+ strains. Instead, we now propose that these antibodies are exploiting a vulnerable target on the surface of *P. aeruginosa*: the OSA of serotype O6.

The OSA is the predominant form of LPS in wild-type strains and strains isolated from acute infections. However, its production, unlike that of CPA, appears to be regulated as a result of adaptation due to pathogen host interactions; i.e., OSA is either reduced in amount or completely abrogated as a result of chronic selective pressures in clinical isolates, especially those isolated from CF patients (60, 64). Thus, our findings that anti-OSA antibodies induce direct antimicrobial activity provide a better understanding of the particularly strong selective pressure *P. aeruginosa* face to evade the host's immune system.

CHAPTER 4: ATOMIC FORCE MICROSCOPY REVEALS THAT THE ANTI-O-SPECIFIC-ANTIGEN (OSA) S20 AND MF23-1 ANTIBODIES MEDIATE THEIR BACTERICIDAL ACTION TOWARDS *P. AERUGINOSA* STRAIN O6A, 6D BY PERMEABILIZING THE OUTER MEMBRANE USING A DETERGENT-LIKE MECHANISM.

4.1. ABSTRACT

The effects of the bactericidal anti-O-specific antigen (OSA) S20 and MF23-1 antibodies on the membrane of *P. aeruginosa* strain O6a, 6d were studied using atomic force microscopy (AFM). To elucidate the sequence of events involved in their mechanism of action, O6a, 6d cells were treated with a range of antibody concentrations, as multiples of the minimum inhibition concentration causing 50% growth inhibition (MIC_{50}), including 0.4 ×, 4 ×, 22 ×, and 167 × MIC_{50}. AFM revealed that the membranolytic effects caused by the antibodies used are apparently initiated by micellization of the LPS-rich outer membrane (OM), an early event that is also initiated by the action of other membrane-active compounds, including some cationic antimicrobial peptides and membrane-permeabilizers such as EDTA. Thereafter, larger patches of LPS/OM were observed to be released from the membrane, resulting in the formation of irregularly-shaped pits (ca. 15-35 nm deep) on the surface. After undergoing sufficient damage, the OM were found to be compromised and shedding of OM from the cell could be observed. Since *O*-polysaccharide chains account for the surface roughness of untreated cells, the resulting OM-/LPS-free, antibody-treated, bacterial cells generally have a much smoother topography compared to untreated cells. Moreover, as revealed by AFM phase imaging, the underlying

surface, which is exposed upon the sloughing of the OM, is composed of a stiffer material than the OM of untreated cells, and is presumably the cross-linked peptidoglycan. Since the overall morphology of the bacterial cells did not seem to be affected, both bactericidal antibodies, S20 and MF23-1, do not appear to interfere with the integrity of the cell wall structures due to the murine layer called peptidoglycan nor disrupting the organization of the inner membrane. AFM proved to be a valuable tool to elucidate the unusual bactericidal mechanism of these antibodies. In summary, we propose that the mechanism of action of the two bactericidal antibodies involves the following steps: 1- LPS-binding step; 2- Micellization of the LPS-rich OM; 3- Appearance of membrane pits; 4- Loosening of the OM from the peptidoglycan layer; 5- Sloughing of the OM; 6- Membrane blebbing.

4.2. INTRODUCTION

Antibodies typically do not directly eliminate their target pathogens, but instead exert their protective function by activating other arms of the immune system [i.e., complement system, opsonic phagocytosis, Ab-dependent cell-mediated cytotoxicity (ADCC)] which ultimately leads to pathogen destruction (124). Paradoxically, a handful of known antibodies combine the functions of target recognition and destruction. Bactericidal antibodies cause direct damage to their target pathogen through a variety of mechanisms (5, 9, 140, 141). Some execute their bactericidal activities by interfering with vital biological functions. For example, five monoclonal antibodies (IgMs) directed against the iron-regulated outer membrane proteins (IROMPs) of the nosocomial pathogen *Acinetobacter baumannii* block iron uptake in the absence of complement and phagocytosis (4). Other antibodies exert their bactericidal activities by severely damaging the structural integrity of the cell membrane. Numerous antibodies

display direct bactericidal activity towards the spirochete *Borrelia* by targeting and damaging one of two outer membrane proteins, variable major proteins (Vmps) or outer surface lipoprotein B (OspB) (6-10, 182-184). The bactericidal mAbs H4825 (IgG_{2a}) and CB515 (IgM) target Vmps of the spirochete responsible for relapsing fever (6, 8, 141, 184). H6831 (IgG_1) and CB2 (IgG_1) target the OspB of *Borrelia burgdorferi*, the causative agent of Lyme disease (7, 8, 184). Targeting either Vmps or OspBs could lead to the destruction of the outer membrane (OM) of the target spirochete (6-10). To the best of our knowledge, a more thoroughly studied bactericidal antibody is CB2. Some of the early effects resulting from the binding of mAb CB2 and H6831 to their target include conformational changes and/or proteolysis of OspB followed by the formation of unstable membrane projections and vesicles (9, 185, 186). These membrane vesicles are formed between unstable "lipid raft-like" microdomains composed of cholesterol and cholesterol-glycolipids, which are not usually present in bacteria but are in *B. burgdorferi* (10). When these unstable membrane projections/vesicles are released, they create fissures (not to be confused with pores) of 2.8–4.4 nm in the OM and lead to subsequent osmotic lysis of *B. burgdorferi* (9). The presence of cholesterol is thought to make *B. burgdorferi* particularly susceptible to the bactericidal activity of CB2 (9). The Fc region of these anti-*Borrelia* antibodies is not required for bactericidal activity, as engineered antibody fragments retain parental antibody function (7, 141, 184). While some antibodies possess antimicrobial, antifungal or antitumor activities in the complementarity determining regions (CDRs) of their variable domains (187), the CDRs of CB2 do not share sequence identity with known antimicrobial peptides (AMPs). Nevertheless, LaRocca *et al*. (9) suggested that CB2 may permeabilize the OM of *B. burgdorferi* using a mechanism similar to the 'carpet' model of action proposed for many AMPs (137-139, 188). In this model, peptides are first attracted to the

membrane via electrostatic interaction with the lipopolysaccharide (LPS), and coat the membrane in a carpet-like manner. When a threshold concentration is reached, the peptides cause LPS micellization which results in transient "cracks" in the OM, eventually leading to cell death.

Our group reported a bacterial surface antigen that is the target for antibody binding and the antigen-antibody interaction induces cell death. The target is the LPS of *Pseudomonas aeruginosa* serotype O6, the most clinically prevalent serotype (5) (Chapter 3). *P. aeruginosa* is a rod-shaped motile Gram-negative bacterium widely found in the environment (17). It is an opportunistic pathogen (nosocomial pathogen) which causes disease in individuals with impaired host defences, such as those suffering from AIDS, cancer, burn wounds and patients afflicted with the recessive genetic disease cystic fibrosis (CF) (13). The cell wall of Gram-negative bacteria is composed of an asymmetric outer membrane (OM), an inner membrane (IM), and a thin peptidoglycan sheet that lays in the periplasmic space between the OM and IM. The most abundant component (~90%) of the outer leaflet of the OM is LPS. LPS is a multifunctional molecule that provides structural integrity to the outer membrane (OM) and acts as a permeable barrier to limit the passive diffusion of hydrophobic molecules (e.g., antibiotics, detergents) into the cell wall. LPS is composed of three structurally distinct domains: 1) the lipid A (endotoxin), a highly acylated diglucosamine (di-GlcNAc) backbone that is embedded in the outer leaflet of the OM; 2) the oligosaccharide core region, which is composed of the highly conserved and unusual sugars, ketodeoxyoctonic acid (Kdo) and heptoses; and 3) an *O*-polysaccharide chain which extends about 30–40 nm away from the OM (55, 57, 58). Most planktonic strains of *P. aeruginosa* simultaneously produce two structurally distinct *O*-polysaccharides: the common polysaccharide antigen (CPA; formerly called A-band) and the O-Specific Antigen (OSA;

formerly called B-band) (60, 61) (Figure 2). While the CPA is composed of a weakly immunogenic homopolymer of D-rhamnose [→ 3)D-Rha(α1 → 3)D-Rha(α1 → 2)D-Rha(α1 →]$_n$ (94-97), the OSA is a highly immunogenic heteropolymer of two to five distinct, and often unusual, sugars in the repeating units (66, 70, 71). Like enteric bacteria, smooth strains of *P. aeruginosa* contain a heterogenous mixture of LPS molecules with different chain lengths of OSA (Figure 2). In *P. aeruginosa* the chain length of the OSA is regulated by two Wzz polysaccharide polymerases, namely Wzz_1 [modulates 12–16 repeats and 22–30 repeats; (62, 63)] and Wzz_2 [modulates 40–50 repeat length; (62)]. While the OSA is the predominant form of LPS in wild-type strains and strains isolated from acute infections, its production, unlike that of CPA, appeared to be regulated as a result of adaptation due to pathogen host interactions; i.e., OSA is either reduced in amount or completely abrogated as a result of chronic selective pressures in clinical isolates, especially those isolated from CF patients (60, 64).

In 2010, our group reported that an antibody called S20 causes cell death by damaging the cell wall and increasing membrane permeability to its target *P. aeruginosa* strain O6a, 6d, independently of immune effector cells or the complement system (5). Since this antibody binds exclusively to the OSA of *P. aeruginosa* strain O6a, 6d, it is not bactericidal towards any other strains/serotypes of *P. aeruginosa* (Chapter 3). Like the anti-*Borrelia* bactericidal antibodies (9), the Fc region of this antibody is not required for its bactericidal activity (5) (Chapter 3). The S20 antibody was initially thought to have its antimicrobial properties associated with the sequence in the CDR regions; however, we recently discovered that targeting the same LPS epitope with an entirely different antibody, mAb MF23-1, not only destroys *P. aeruginosa* strain O6a, 6d but also all OSA+ O6 strains to which it cross-reacts. Since the S20 and MF23-1 antibodies share little sequence identity in their variable domains, and especially in their CDRs (Table 3), their

bactericidal activity does not appear to reside in their sequence *per se*. Instead, these antibodies are apparently exploiting a vulnerable target on the surface of *P. aeruginosa*, the OSA of serotype O6.

Binding of a certain antibody to the OSA is presumed to be the first step in the bactericidal mechanism of our antibodies. We recently established a direct correlation between the affinity, and more specifically, the dissociation rate constant of the antibody and its bactericidal potency towards O6a, 6d. Some of the cell wall damage induced from exposure to the S20 scFv, include increased surface roughness and indentation, release of flagella, and the formation of membrane blebs or vesicles (5). In this study, we were interested to further define the events that result in these observed morphological changes.

Atomic force microscopy (AFM) is a valuable tool with which to study changes in the surface of the bacterial envelope. In addition to simplicity in sample preparation and the option to use live, non-fixed, bacterial cells, one of the greatest advantages of AFM is the ability to capture the real surface roughness of the bacterial envelope on a three-dimensional surface (189). For example, while other types of microscopy show Gram-negative bacteria as having a relatively smooth surface, AFM is able to capture their real surface micro-roughness as they generally express LPS molecules with varying lengths of *O*-polysaccharide chains (33, 190). Another distinctive feature of AFM is that different channels (types of images) are simultaneously acquired, including height (and derived 3D), phase, and amplitude. Amplitude images emphasize edges, while phase images offer contrast in material composition (e.g., elastic/rigid properties). Using AFM, Li *et al*. (15, 16) were able to eloquently unravel the stepwise manner in which the sushi peptide 3 (S3), an AMP derived from the horseshoe crab clotting factor C and known to interact with LPS, disrupts the outer membrane of *E. coli* and *P.*

aeruginosa. Their studies showed that S3 initiates the formation of LPS-S3 micelle complexes, which are released from the OM in a detergent-like manner.

In this study, we used AFM to investigate the stepwise manner in which our anti-O6 antibodies exert morphological changes on the cell wall of *P. aeruginosa* strain O6a, 6d. Our nanometer-scale AFM images captured unprecedented details of the surface of *P. aeruginosa* and revealed, for the first time, that our anti-OSA antibodies act as detergent-like membrane permeabilizers. Their membranolytic effects are initiated through induction of the desorption of large numbers of micelles from the OM, followed by the loosening and sloughing of large areas of the OM from the cell surface, thereby exposing the underlying peptidoglycan. This AFM study helps to shed light on the bactericidal mechanism of these antibodies.

4.3. MATERIALS AND METHODS

4.3.1. Preparation of bactericidal antibodies for AFM studies

The antibodies (mAb MF23-1, anti-O6; S20 scFv monomer and dimer, anti-O6a, 6d) used in this study were purified as previously described (Chapter 3). Stock aliquots, which are prepared in PBS, were diluted to the desired concentration in 0.1 mM sodium phosphate buffer, pH 7.4, just before the AFM experiments.

In a previous bactericidal assay with *P. aeruginosa* strain O6a, 6d, it was determined that the MIC_{50} of mAb MF23-1 (apparent $K_D = 1.8 \times 10^{-5}$ M), S20 scFv monomer ($K_D = 5.6 \times 10^{-7}$ M) and S20 scFv dimer ($K_D = 2.1 \times 10^{-8}$ M) were 2.5 µM, 450 nM and 60 nM, respectively (Figure 20). To capture the sequence of events in the bactericidal mechanism, O6a, 6d cells were treated with the putative bactericidal antibodies as follows: 1 µM mAb MF23-1 (0.4 ×

MIC_{50}), 10 µM mAb MF23-1 (4 × MIC_{50}), 10 µM S20 scFv monomer (22 × MIC_{50}), and 10 µM S20 scFv dimer (167 × MIC_{50}).

4.3.2. Treatment of *P. aeruginosa* strain O6a, 6d cells for AFM studies

A single colony of *P. aeruginosa* from a TSB agar plate was used to inoculate 5 mL of TSB broth, grown for ca. 16 h at 37 °C, 220 rpm. To obtain healthy cells for the experiment, a sub-culture was prepared by inoculating 50 mL of fresh TSB with a 1:250 dilution (i.e., 200 µL) of the starter culture, and grown as previously described until cells reached log-phase (OD_{600} = 0.3-0.4). Cultures were centrifuged at 2,000 rpm for 5 min, and pelleted cells were washed 4 × 25 mL with decreasing concentrations of sodium phosphate buffer (5, 1, 0.5 and 0.1 mM sodium phosphate buffer, pH 7.4) to prevent osmolytic shock. The OD_{600} of the cells was adjusted to ca. (6.4×10^8) CFU/ mL (OD_{600} = 0.4) in 0.1 mM sodium phosphate buffer, pH 7.4. Cells (50 µL) were treated with antibody (50 µL; final concentrations: 1 and 10 µM MF23-1 mAb; 10 µM S20 scFv monomer; 10 µM S20 scFv dimer, diluted in 0.1 mM sodium phosphate buffer, pH 7.4) or 0.1 mM sodium phosphate buffer (50 µL; negative control) in an Eppendorf microcentrifuge for 30 min at 37 °C while shaking (220 rpm). After incubation, antibody-treated and untreated bacterial suspensions (25 µL) were deposited and gently spread onto poly-L-Lysine (PLL) glass slides (Sigma), and allowed to immobilize for ca. 5-10 min. Non-adherent bacteria were removed by rinsing the PLL surface with ca. 3 mL of 0.1 mM sodium phosphate buffer. Slides were air-dried in a desiccator without vacuum for ca. 16 hours before proceeding to AFM imaging.

4.3.3. Atomic force microscopy

AFM images were recorded using a JPK NanoWizard®II BioAFM instrument (JPK Instruments, Berlin, Germany). Bacteria were mechanically probed with a NSC15/AlBS cantilever [spring constant (*k*) 40 N/m, tip radius ca. 10 nm; MikroMasch, CA] in intermittent contact mode (tapping mode; AC), in air, using a resonance frequency of ca. 350 kHz and a scan rate of 0.3-0.4 Hz. After scanning a large area (generally 500 × 500 µm), 6 individual cells per treatment were randomly selected and scanned (< 5 × 5 µm) to obtain higher resolution images. Height, phase, and amplitude images were simultaneously collected. Height images were used to generate high resolution topography/three-dimensional (3D) images, amplitude images emphasize sample edges, and phase images contrast differences in the material composition using a relative softness / hardness scale, where soft (adherent, elastic) surfaces are depicted as bright/white regions and hard (stiff, rigid) surfaces are depicted as darker regions. Image processing was done with the JPK Data Processing Software (JPK Instruments, Berlin, Germany). Images provided are representative of the respective samples.

The surface roughness of untreated and 22 × MIC_{50} (10 µM S20 scFv monomer) treated *P. aeruginosa* strain O6a, 6d cells were compared. Surface areas of 400 × 400 nm^2 were randomly selected from height images of five untreated and five treated cells (Appendix Figure 54). To account for cell curvature, the selected areas were flattened using a second order polynomial fit from the AFM JPK Data Processing software. The flattened image was then analyzed by measuring the average roughness (Ra), the root-mean-square roughness (Rq), and the peak-to-valley roughness (Rt). Comparison of statistical significance was made within the types of roughness parameters using a t-test from an Excel Data Analysis ToolPak add-inn program, and probability values of less than 0.05 were considered significant.

4.4. RESULTS

By using AFM, we were able to determine that the bactericidal S20 and MF23-1 antibodies act as detergent-like membrane permeabilizers. An overview of the step-wise model in which these antibodies disrupt the membrane of *P. aeruginosa* strain O6a, 6d is depicted in Figure 28. To offer more detailed contrast, some of the cells provided in Figure 28 are also illustrated along with their height, amplitude, and phase images (Figure 29, Figure 31, Figure 33, Figure 34, Figure 35, Figure 36). Enlargements, cross-sections, and different 3D views are also provided to highlight pertinent relevant details (Figure 32, Figure 37, Figure 38, Figure 40, Figure 41).

4.4.1. Untreated O6a, 6d cells

AFM images showed that the overall appearance of the prepared, untreated cells had good structural integrity with well-defined and intact cell wall and periphery (Figure 28A, Figure 29). Cross-sections of the bacterial cells in 3D images show that untreated cells possessed a uniformly shaped half-cylindrical surface curvature, measuring heights of 155–180 nm and widths of 1.2 μm (see representative cross-section on Figure 41A, D). The half-cylindrical shape in cross-sections, as opposed to fully cylindrical shape, is most likely an artifact due to the flattening of cells on the slides during the drying process. Since the cells were harvested from the exponential growth phase, many cells scanned were undergoing cell division, as evidenced from the transverse septum located at the middle of parent cell, and thus had lengths varying from 2.3–4.7 μm (measurements not shown). Most untreated cells possessed a single flagellum at one pole (unipolar, monotrichous). This is characteristic of *P. aeruginosa* WT strains and the flagellum organelle allows *P. aeruginosa* to be motile in a liquid culture. However, cells

possessing two polar flagella were also observed (data not shown). Multiflagellation has been reported as a characteristic of swarmer cells (191-194), i.e., cells that migrate to the periphery of colonies on solid surfaces, including those of *P. aeruginosa* (191). To the best of our knowledge, multiflagellation has not been documented for *P. aeruginosa* cultures grown in liquid media, as is the case here.

As is more evident from the topography images, AFM revealed that untreated cells possess a rough surface topography over their entire surface (Figure 28A and E, Figure 29B, Figure 30B, Figure 40A, Figure 38A, Figure 39). This micro-roughness is especially evident from the side-view of the untreated cells displayed in Figure 38A and from the enlargement of a 400 × 400 nm surface area from this same cell in Figure 40A. The micro-roughness observed on untreated cells is believed to be attributed to the varying lengths of *O*-polysaccharides, corroborating other studies examining Gram-negative bacteria by AFM (33, 190).

Untreated O6a, 6d cells contrasted very well under phase imaging. Phase imaging uses a relative softness/hardness scale, where soft (adherent, elastic) surfaces are depicted with a brighter colour and hard (stiff, rigid) surfaces are depicted with a darker colour. As revealed by the phase images, the surfaces of untreated O6a, 6d cells are predominantly bright with some interspersed dark speckles (Figure 29D). Thus, overall, the surfaces of untreated O6a, 6d cells are soft with some patchy rigid areas. Flagella, which contrasted especially well under this imaging channel, were detected to have soft surfaces.

Natural outer membrane vesicles (nOMVs), which are known to be naturally released from the surface of virtually all Gram-negative bacteria (55, 195-197) including *P. aeruginosa* (55, 195, 196, 198), were observed blebbing off and surrounding some untreated O6a, 6d cells by AFM (Figure 30A). When compared side by side, these nOMVs look very similar to those

observed by Beveridge *et al*. (55) from a thin section (transmission electron microscope) of an unidentified gram-negative bacteria isolated from a freshwater biofilm (Figure 30A). The diameter of individual nOMVs from Figure 30B ranged from 51–127 nm (average 72 nm; measurements not shown). This is in close agreement to the diameter range of 50–250 nm (55) and 21–232 nm (average 88 nm) (105) previously published for an OSA+/CPA+ PAO1 strain.

4.4.2. O6a, 6d cells treated with the bactericidal S20 and MF23-1 antibodies

The effects of the monomeric and dimeric forms of the S20 scFv and the MF23-1 mAb on the cell surface of *P. aeruginosa* O6a, 6d were examined. As expected and illustrated in Figure 28 (C, D, F-H), treatment with the weakest affinity antibody, mAb MF23-1 (1 µM: 0.4 × MIC_{50}; 10 µM: 4 × MIC_{50}) induced earlier events, treatment with the intermediate affinity antibody, S20 scFv monomer (10 µM: 22 × MIC_{50}) induced intermediate effects, and treatment with the highest affinity antibody, S20 scFv dimer (10 µM: 167 × MIC_{50}), severely damaged the surface of O6a, 6d cells (Figure 28).

To capture early membranolytic effects, O6a, 6d cells were treated with a low concentration (1 µM) of the weaker affinity antibody, namely mAb MF23-1, which represents ca. 0.4 × MIC_{50}. All the cells from this treatment were surrounded by large amounts of irregular-shaped micelles (Figure 28B, Figure 31, Figure 32 and Figure 33) which appear morphologically different from nOMVs released by untreated cells (Figure 30). The released micelles and membrane component appear sticky since some aggregate or clump together in undefined shapes (Figure 32A and B). Overall, the surfaces of these MF23-1-treated cells have comparable micro-roughness as untreated O6a, 6d cells; however, some have patchy areas with 15–30 nm deep pits (Figure 32, Figure 40B, Appendix Figure 50. Phase images from this treatment revealed the presence of a

rigid material (i.e., displayed in dark colour), especially at one apex and some of the periphery/edge of these cells (Figure 31D, Figure 33D). Another effect that was observed was early loss of the flagellum, presumably because the integrity of the outer membrane had already been sufficiently disturbed. The cell displayed in Figure 33 has a long fissure of ca. 475 nm (measurement not shown) at one apex: perhaps this is the apex where the machinery of the flagellum was once anchored, and its release created a prominent fissure which allowed the release of periplasmic content.

When cells were treated with a higher concentration of mAb MF23-1 (10 μM; ca. 4 × MIC_{50}), only a few micelle-like structures of about 50-60 nm width and height of ca. 10-15 nm (measurements not shown) were concentrated near the periphery of the cell(s) (Figure 34, Appendix Figure 51). The release of the micelles is therefore thought to be one of the earliest membranolytic events, where large amounts are released early, or at low MIC_{50}, with fewer micelles being released in later stages of the membranolytic process. In addition, topography images showed that this treatment produced cells with corrugated surfaces (Figure 28C, Figure 34, Figure 40C). However, as illustrated in the enlargement of a 400 × 400 nm surface patch in Figure 40C, which was obtained from the cell displayed in Figure 28C and Figure 34, these corrugations have a relatively smooth topography in terms of the micro-roughness observed on the surface of untreated cells (Figure 40A). Phase imaging detected two surface materials with different properties. A lighter coloured layer, i.e., softer/more adhesive material, is being released from the cell surface, thereby revealing an underlying darker coloured layer (Figure 34D, Appendix Figure 51). Thus, a layer with soft properties, which overlays a more rigid one, is released when cells are treated with ≥10 μM of mAb MF23-1. Moreover, the deposition to the bottom right and left of the cell in Figure 34 is of the same (soft/adhesive) elastic properties and

attached to the outermost layer (lighter colour) of the cell. The outermost, softer layer represents the OM while the underlying, more rigid one represents the peptidoglycan. Thus, the deposition of soft material at the bottom right of the cell is likely OM membrane material that is in the process of being released from the surface of this cell (as opposed to cellular leakage). The process of sloughing off OM fragments seems to have been initiated at one apex or the periphery of this cell. A cross-section of this cell (Figure 41B and E) showed that its height at 220 nm is higher than that of the untreated cells (150–175 nm). Since the cell appears to be in the process of losing its OM, this layer might have lost its physical anchorage to the underlying peptidoglycan layer, and therefore have a greater height. This loosely anchored OM could also explain why its surface has a corrugated topography.

The surfaces of O6a, 6d cells treated with 10 μM (22 × MIC_{50}) of S20 scFv monomer (Figure 28D, Figure 35, Figure 36, Appendix Figure 52 and Figure 53) were statistically smoother than that of untreated cells (Figure 39). The 3D side-views provided in Figure 38B and the 400 by 400 nm surface patch enlargements illustrated in Figure 40D clearly demonstrate that S20 scFv-treated cells are mostly deficient in the surface micro-roughness observed on untreated cells (Figure 40A, Figure 38A). The micro-roughness observed on untreated cells is attributed by the varying lengths of *O*-polysaccharides. The fact that the S20 scFv-treated cells have smoother surfaces suggests that they have lost some surface LPS molecules. Interestingly, the phase images of the cells treated with the S20 scFv monomer (Figure 35, Figure 36) show that their surfaces, unlike that of untreated cells and MF23-1-treated cells, are almost completely devoid of the soft, i.e., light coloured, material, corresponding to the OM. In other words, while the cell treated with mAb MF23-1 in Figure 34 was captured in the process of sloughing its OM, cells treated with the S20 scFv monomer (Figure 28D, Figure 35, Figure 36) have already

completely lost their OM. As revealed by the cross-section in Figure 41C and 13F, treatment with the S20 scFv monomer produced no noticeable effects on the widths and heights of cells from this treatment, suggesting that the peptidoglycan layer is intact and that there has been no cytoplasmic leakage.

While the cell illustrated in Figure 36 and Figure 37 appears to have an overall smoother surface (micro-roughness) compared to untreated cells, it does contain small 'pimple-like protrusions' on its surface. In fact, as highlighted in Figure 37, the image of this bacterial cell appeared to have been captured in the active process of releasing vesicle-like particles from its membrane. S20 scFv treated bacterial cells, (depicted in Figure 36), is also surrounded by many small micelle-/vesicle-like particles. When individually isolated, i.e., not touching others or in aggregate clusters, these vesicles measured an average of 92 nm (measurements not shown) and also formed large aggregates of more than 400 nm (Figure 37; measurement not shown). Since these aggregated vesicle-like particles formed following treatment with a monovalent antibody, i.e., S20 scFv monomer, they are not a result of agglutination. Moreover, such large vesicle-like aggregates were not characteristic of nOMVs released from untreated cells (Figure 30).

The bactericidal mechanism progressed faster following treatment with the highest affinity binder, the S20 scFv dimer (10 μM; 167 × MIC_{50}). The cells illustrated in Figure 28, G and H exhibit severe membrane damage with the formation of extensive membrane blebs. While only one of the daughter cells-to-be in Figure 28G contains membrane blebs, other cells did have membrane blebs on both daughter-cells-to-be (Figure 28H). Interestingly, the surface of the daughter cell-to-be that does not contain membrane bleb from Figure 28G is, like that of the S20 scFv monomer-treated cell, smoother, in terms of micro-roughness, compared to that of untreated cells. Early signs of membrane bleb formations were also observed in a few cells

scanned from the mAb MF23-1 and S20 scFv monomer treatments (Figure 28F, not all data shown).

Figure 28. Topography (3D) AFM images showing an overview of the sequence of events involved in the mechanism of action of the bactericidal mAb MF23-1 and S20 scFv towards *P. aeruginosa* strain O6a, 6d when treated at 37°C for 30 minutes. A) Untreated cells possess a fully intact cell wall and no visible malformations were observed. Since this strain has varying lengths of *O*-polysaccharide chains (Figure 13), AFM reveals that its surface is rough over the entire cell. B) Micellization and formation of pits – treatment of cells with low MIC_{50}s (0.4 × MIC_{50}; 1 µM MF23-1 mAb) results in the release of large amount of micelles, presumably LPS-antibody complexes, and the release of irregular-shaped membrane components and loss of flagellum. The desorption of LPS-micelles and membrane components likely contributes to the appearance of patchy, irregular-shaped pits (see Figure 32). C) Loosening and sloughing of the OM layer – after sufficient membrane damage, likely at one of the apex, treatment with 4 × MIC_{50} (10 µM MF23-1 mAb) loosens the OM from the rest of the surface, as evidenced by the corrugated topography (see Figure 40C) and higher cell height values (see Figure 41, B&E). The deposition at the bottom right of the cell, which is attached to the OM, shows that the OM layer starts sloughing off from the rest of the cell in quite large sections. D) OM-/LPS- free cell – treatment with 22 × MIC_{50} (10 µM S20 scFv monomer) results in the complete loss of the rough OM-/LPS- layer, thereby exposing the topographically smoother peptidoglycan layer. These findings are corroborated with phase images (Figure 35D, Figure 36D) which detect, as expected, the cross-linked peptidoglycan layer as a harder material than the OM. F-H) Membrane bleb formation – early signs of membrane blebs protruding from the surface were observed in a couple cells scanned from the treatment with the S20 scFv monomer (F). Membrane blebs continued to form over the entire surface when treated at 167 × MIC_{50} (10 µM S20 scFv dimer). E) Untreated cell captured in the process of releasing natural OMVs (nOMVs) from the OM. The micelles, vesicles and membrane components released upon treatment with the bactericidal antibodies morphologically differ from these nOMVs.

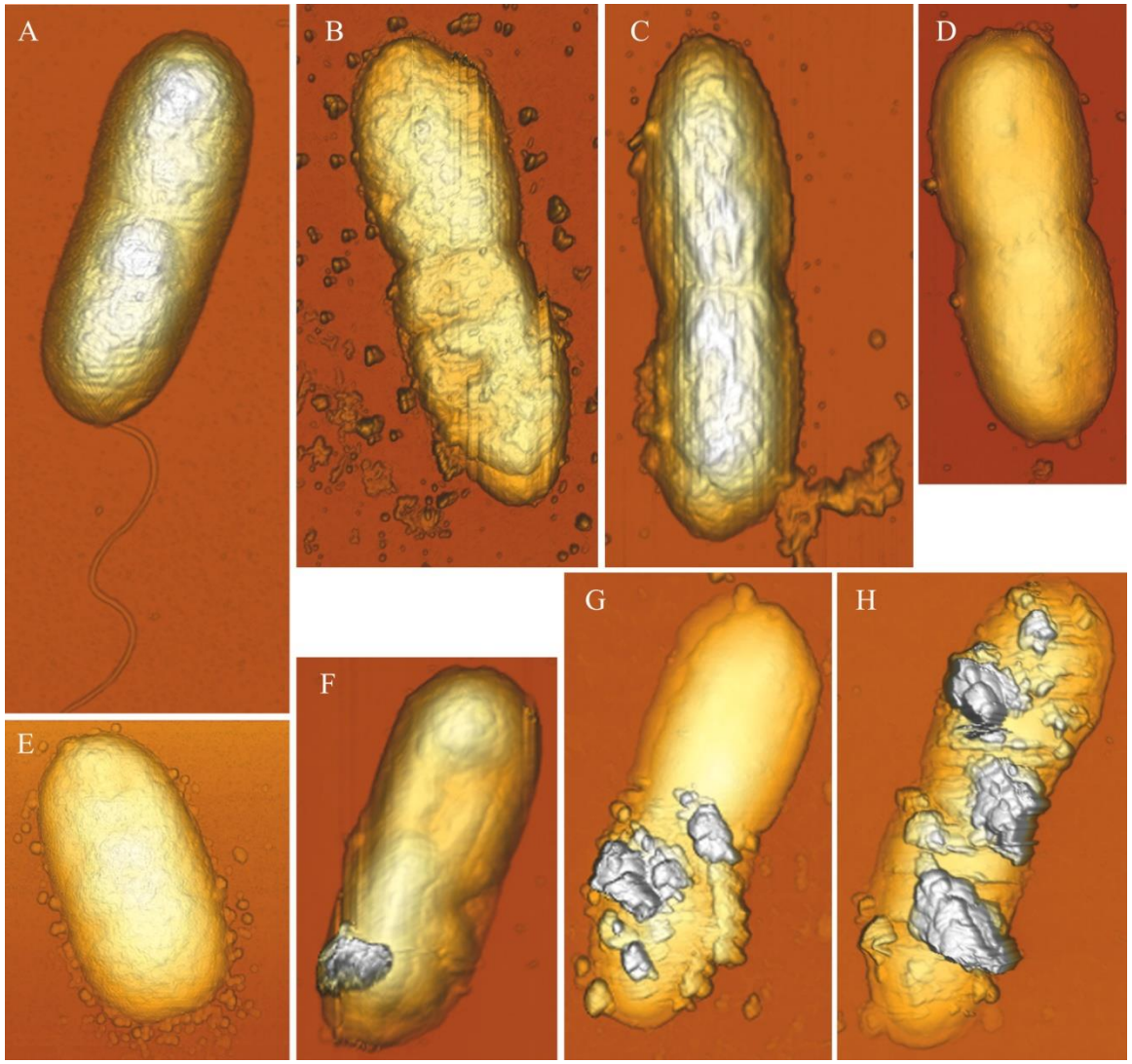

Figure 28.

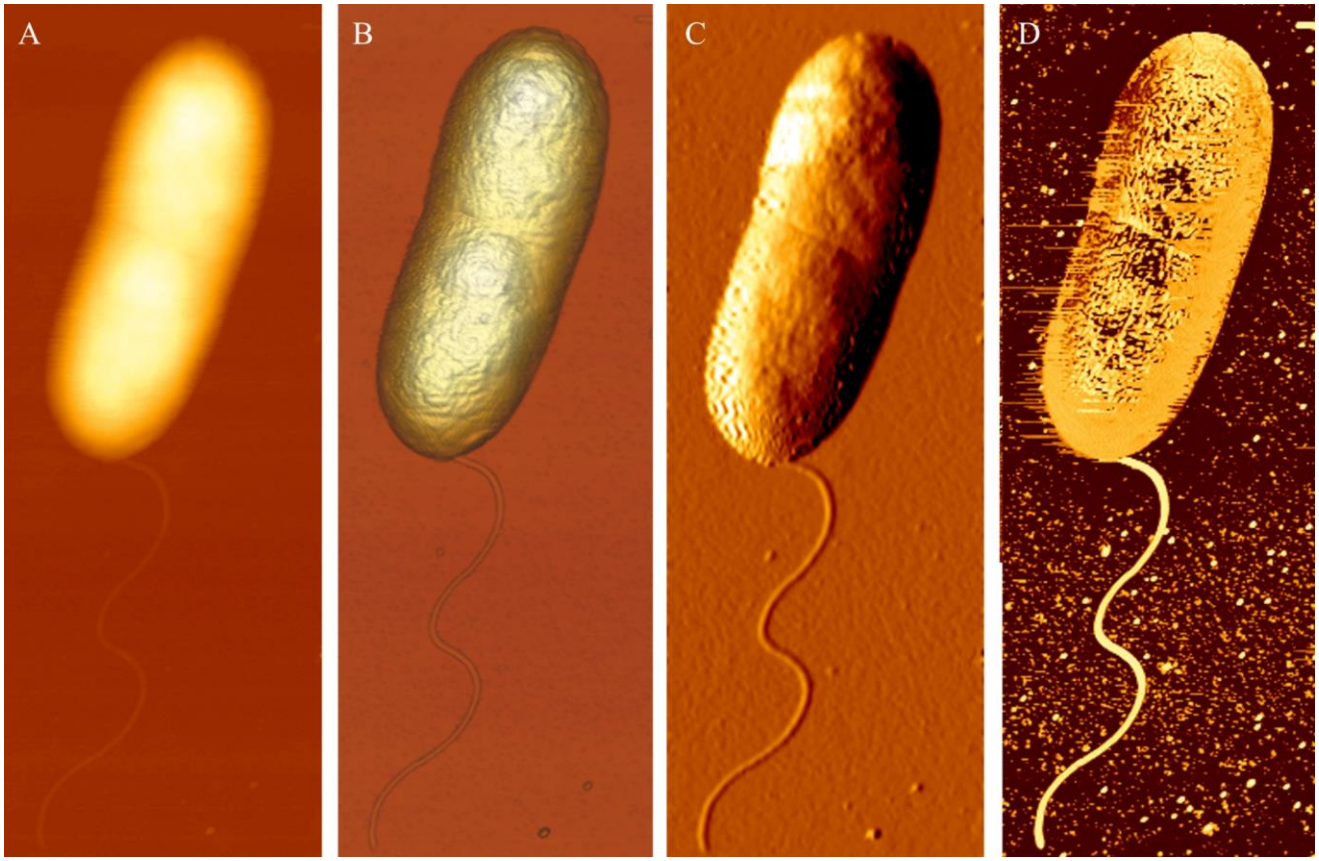

Figure 29. (A) Height image, (B) topography (3D), (C) amplitude image and (D) phase image of an untreated *P. aeuginosa* strain O6a, 6d cell, showing a fully intact cell wall and a polar flagellum. No visible malformations were observed. The 3D image revealed a micro-roughness over the entire surface of this smooth strain (OSA+/CPA+) which is attributed by the varying lengths of its *O*-polysaccharide chains, mostly OSA chains (Figure 13). Phase imaging use a softness/hardness scale where soft (adherent, elastic) surfaces are depicted as bright/white regions and hard (stiff, rigid) surfaces are depicted as darker regions. The phase image revealed that the OM is mostly composed of a soft (adherent, elastic) material. The cell was scanned in air using the intermittent contact mode (tapping mode; AC).

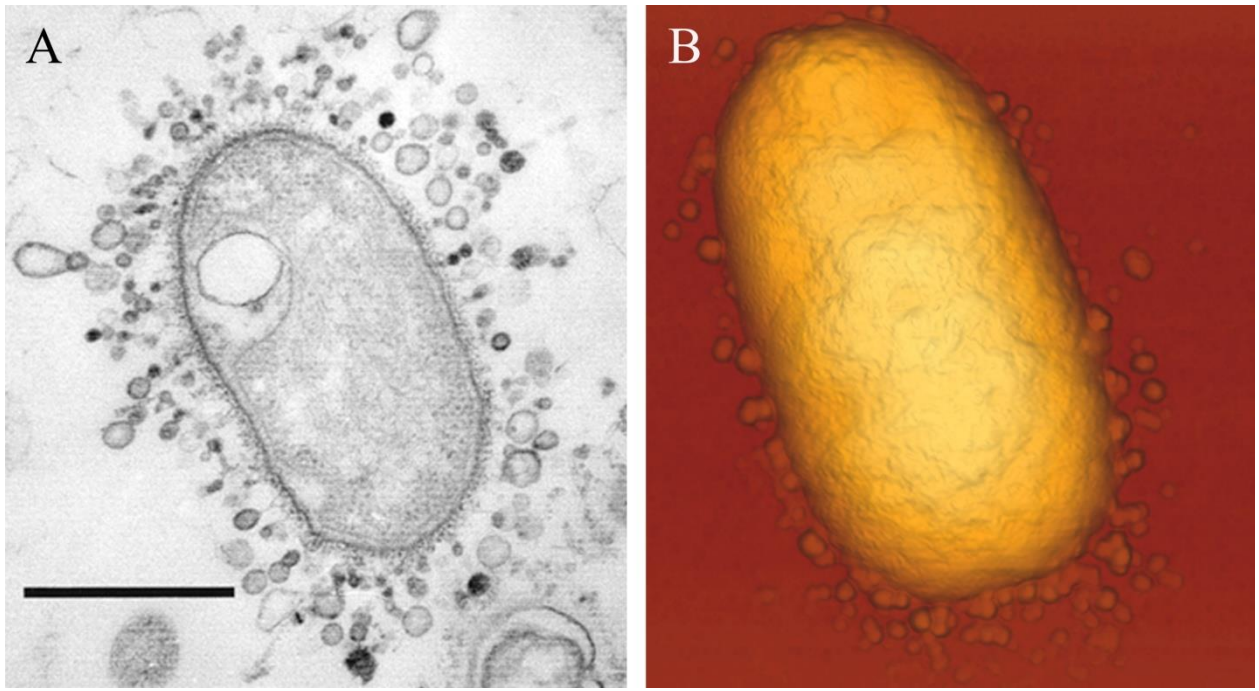

Figure 30. Natural outer membrane vesicles (OMVs) blebbing off an A) unidentified gram-negative bacteria isolated from a freshwater biofilm and viewed by thin section electron microscopy [taken from (55)], and an B) untreated *P. aeruginosa* strain O6a, 6d cell scanned by AFM and illustrated with a (3D) topography image (derived from height image). Note that the slide with the cell shown in Figure 30B was allowed to air-dry for 45 min, as opposed to 5 min, before washing.

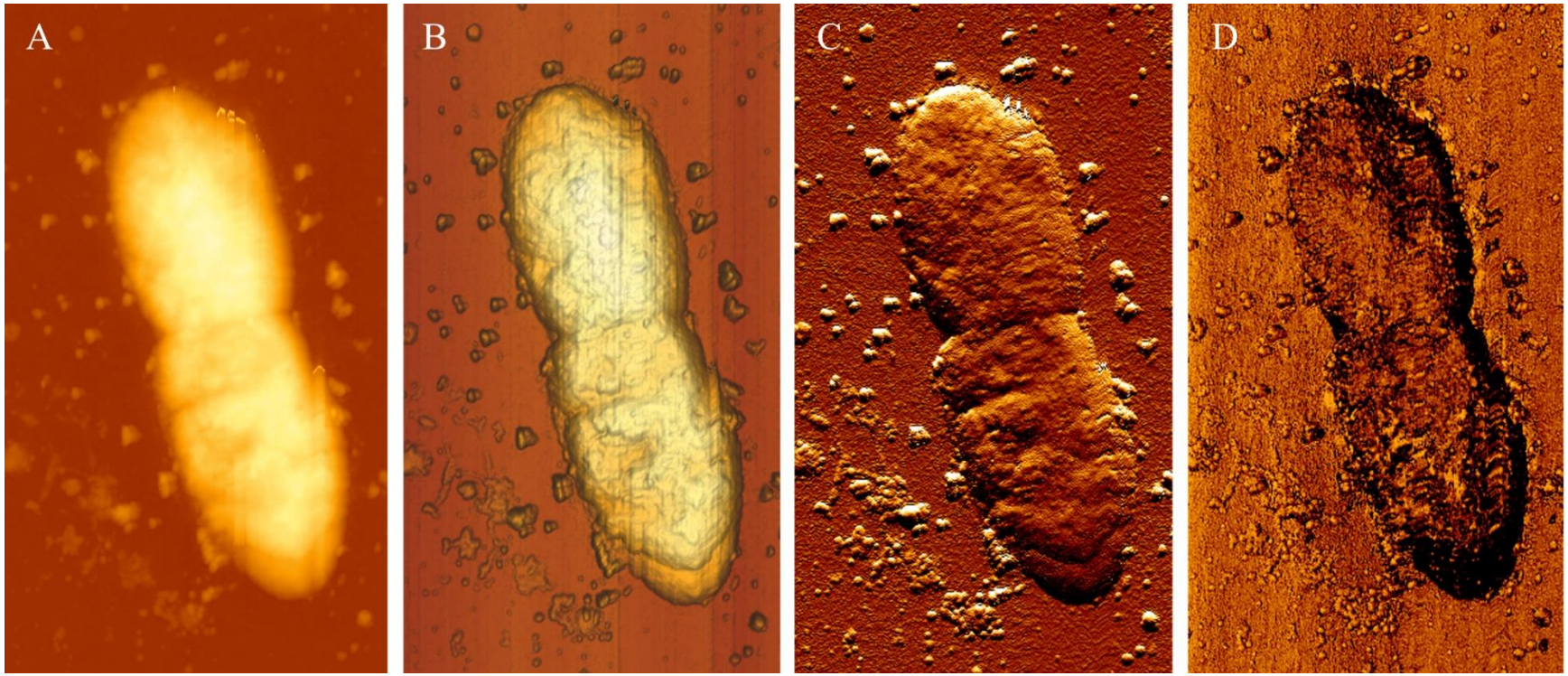

Figure 31. (A) Height image, (B) topography (3D), (C) amplitude image and (D) phase image of a *P. aeuginosa* strain O6a, 6d cell treated with mAb MF23-1 at 0.4× MIC_{50} (1 µM). Many irregularly-shaped micelles and clumpy membrane components were released from the membrane, creating some patchy areas with 15 – 30 nm deep pits (see Figure 32 and Appendix Figure 50). Phase imaging use a softness / hardness scale where soft (adherent, elastic) surfaces are depicted as bright/white regions and hard (stiff, rigid) surfaces are depicted as darker regions. The phase image revealed the presence of a rigid material, especially at the bottom apex, at the right periphery of the cell, and some regions with lower topography (e.g., bottom of pits). This rigid material is likely the underlying peptidoglycan layer that is beginning to be uncovered. The flagellum is absent from this cell. The cell was scanned in air using the intermittent contact mode (tapping mode; AC).

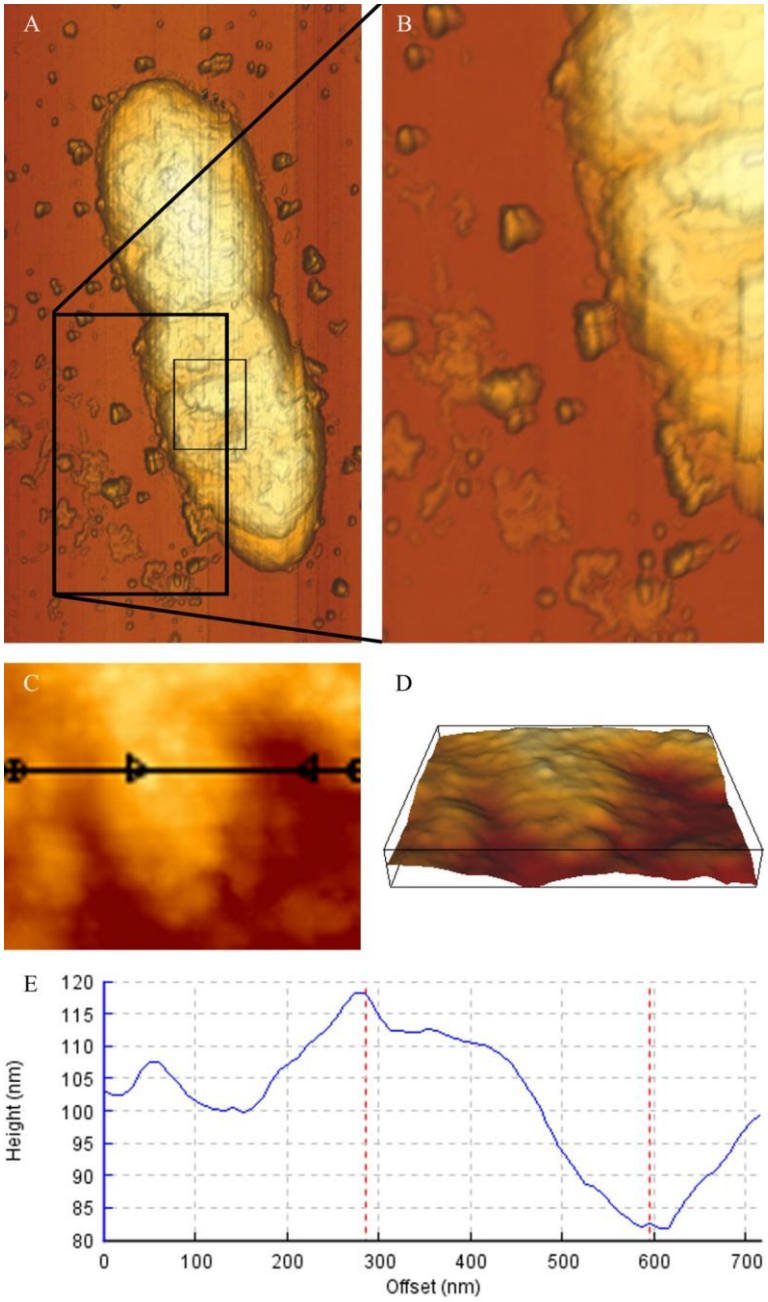

Figure 32. (A) Topography (3D) image of a *P. aeuginosa* strain O6a, 6d cell (same cell as illustrated in Figure 31) treated with mAb MF23-1 at 0.4 × MIC_{50} (1 µM). (B) Enlargement highlighting desorption of many clumpy, irregular-shaped micelles and membrane components from the cell. Their desorption eventually leads to the appearance of 15 – 35 nm deep pits in the membrane (C-E) (See Figure 50). Height (C) and derived 3D (D) images, which were obtained by zooming into the smaller boxed area from (A), illustrate an area that was particularly affected by the appearance of pits. Cross-section (E) of the black line from (C), measuring pits with up to ca. 35 nm depths.

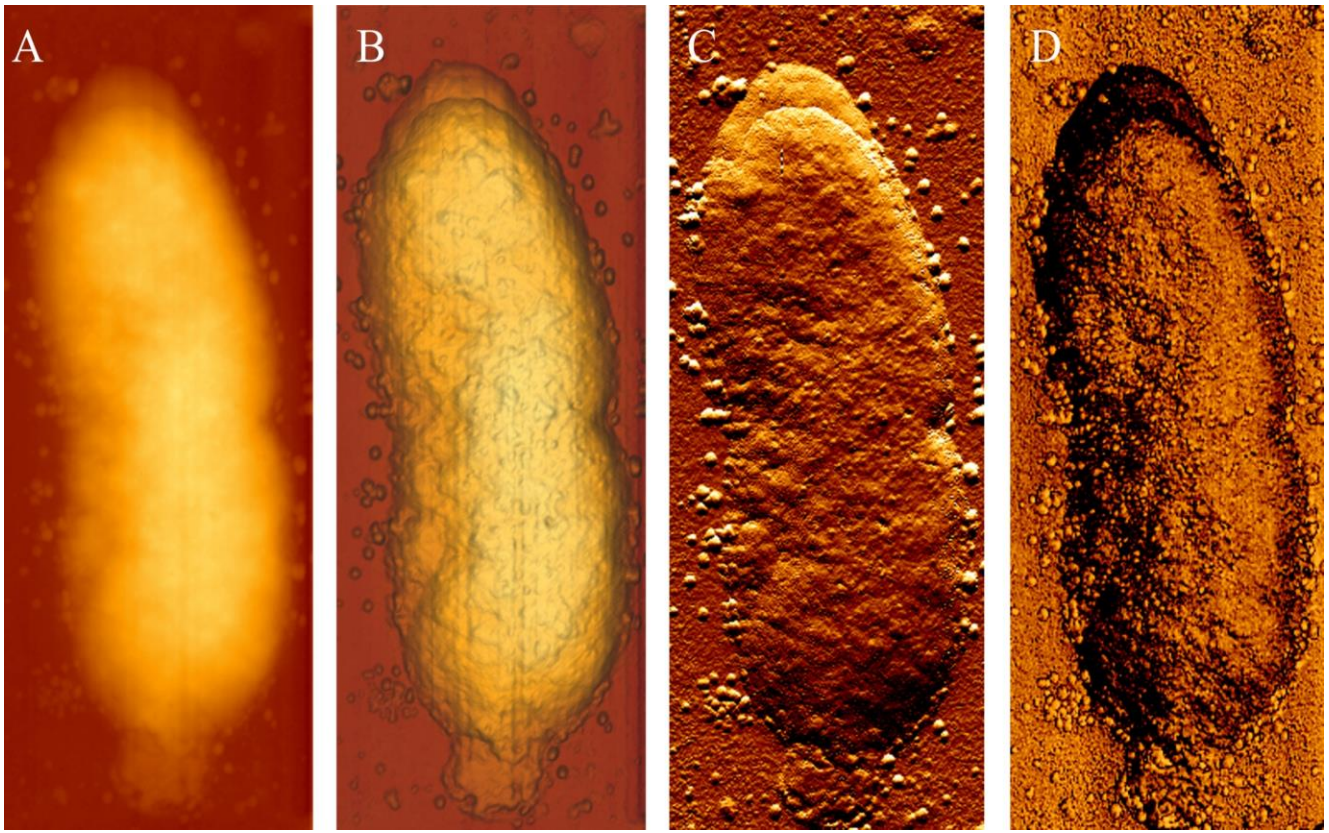

Figure 33. (A) Height image, (B) topography (3D), (C) amplitude image and (D) phase image of a *P. aeuginosa* strain O6a, 6d cell treated with mAb MF23-1 at 0.4× MIC_{50} (1 µM). Many micelles were released from the membrane. Phase imaging use a softness / hardness scale where soft (adherent, elastic) surfaces are depicted as bright/white regions and hard (stiff, rigid) surfaces are depicted as darker regions. The phase image revealed the presence of rigid material, especially at the top apex. This rigid material is likely the underlaying peptidoglycan layer that is beginning to be uncovered. A long fissure of ca. 475 nm (measurement not shown) was created at the bottom apex of this cell, perhaps where the flagellum machinery was once anchored. The material below this fissure is likely periplasmic content. The cell was scanned in air using the intermittent contact mode (tapping mode; AC).

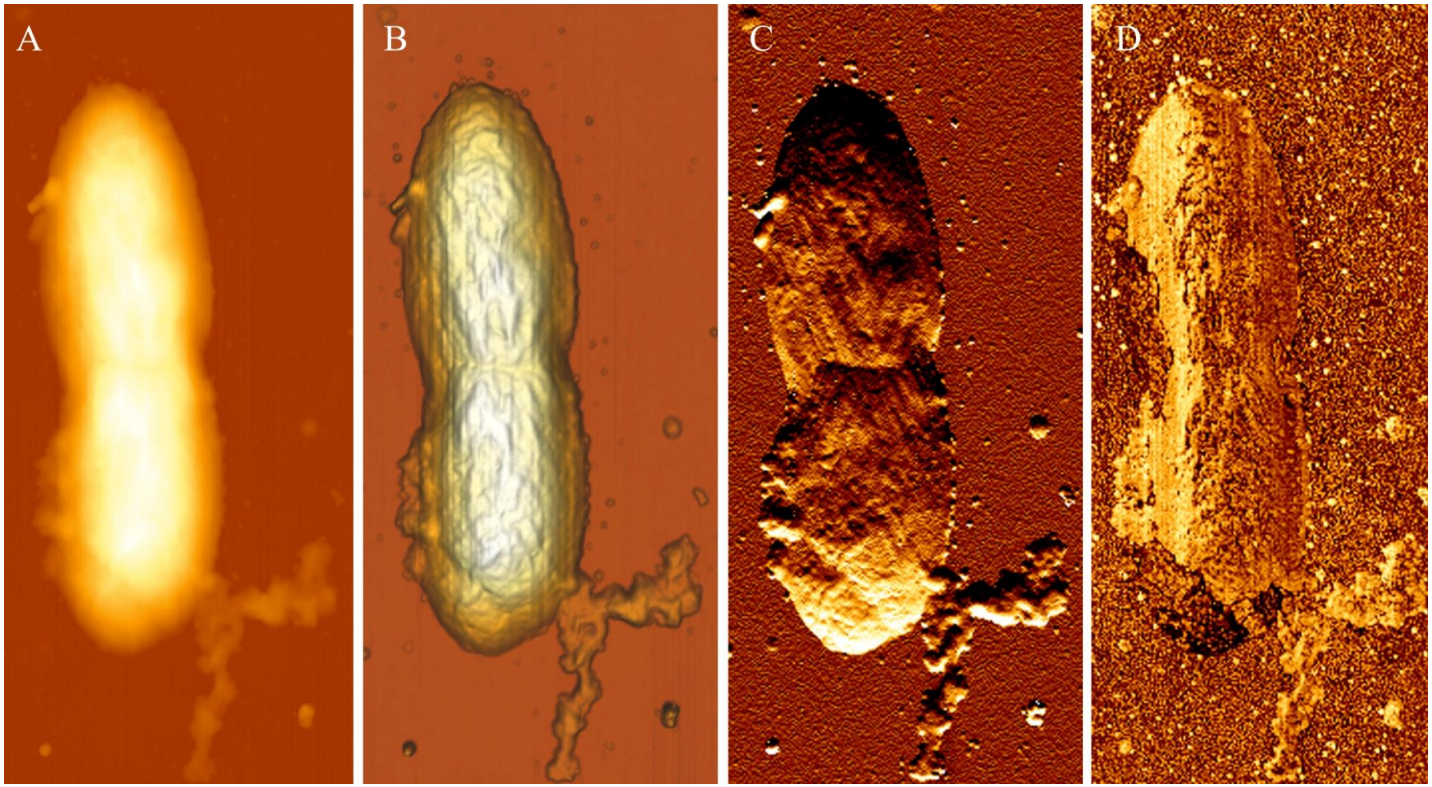

Figure 34. A) Height image, (B) topography (3D), (C) amplitude image and (D) phase image of a *P. aeuginosa* strain O6a, 6d cell treated with mAb MF23-1 at 4 × MIC_{50} (10 µM). Phase imaging use a softness / hardness scale where soft (adherent, elastic) surfaces are depicted as bright/white regions and hard (stiff, rigid) surfaces are depicted as darker regions. The phase image reveals that the OM (soft/adhesive material depicted in brighter colour) is in the process of sloughing from this cell, thereby exposing the underlaying peptidoglycan (rigid material depicted in darker colour) at the bottom left side of this cell. The deposition at the bottom right of this cell appears to be sloughed OM material since it is still attached to and of the same elastic properties (soft/adhesive) as the OM layer that remains on the cell. Some micelle-like structures are found concentrated near the periphery of this cell; however, much less than the treatment at 1 µM. The 3D image shows that the surface is corrugated (see enlargement on Figure 40C), presumably because the OM layer is now loosely anchored to the rest of the cell. The cell was scanned in air using the intermittent contact mode (tapping mode; AC).

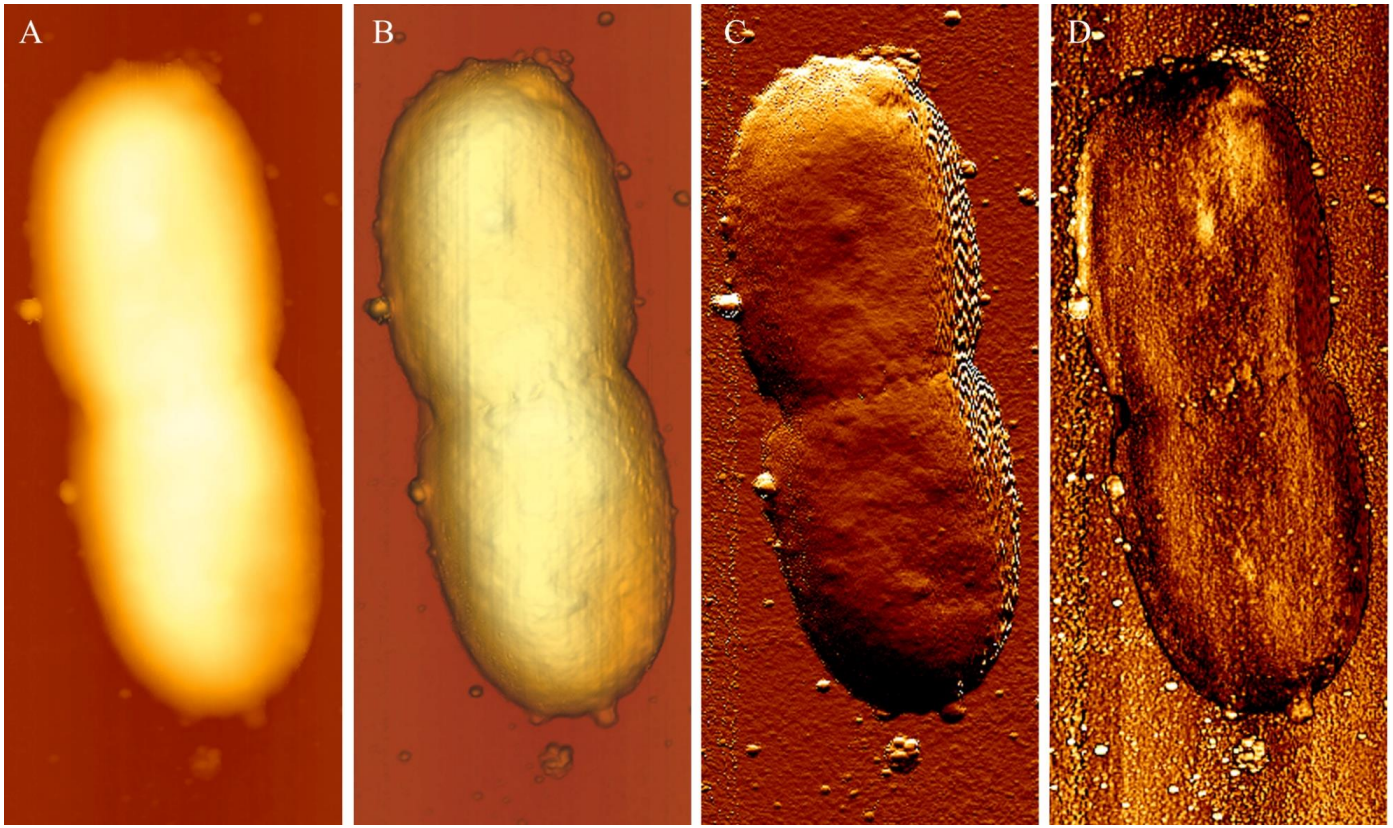

Figure 35. A) Height image, (B) topography (3D), (C) amplitude image and (D) phase image of a *P. aeuginosa* strain O6a, 6d cell treated with the S20 scFv monomer at 22 × MIC_{50} (10 µM). Phase imaging use a softness / hardness scale where soft (adherent, elastic) surfaces are depicted as bright/white regions and hard (stiff, rigid) surfaces are depicted as darker regions. The phase image reveals that the surface of this cell is composed of a rigid material, presumably the cross-linked peptidoglycan layer. The 3D image revealed that the surface of this cell is much smoother than that of untreated cells (see side view Figure 38B). Since the varying lengths of the *O*-polyssacharide chains largely accounts for the roughness observed on untreated cells, this suggest that the LPS/OM has been removed from this cell, corroborating with the phase image findings. The cell was scanned in air using the intermittent contact mode (tapping mode; AC).

Figure 36. A) Height image, (B) topography (3D), (C) amplitude image and (D) phase image of a *P. aeuginosa* strain O6a, 6d cell treated with the S20 scFv monomer at 22 × MIC_{50} (10 µM). Overall, the surface of this cell is smoother than that of untreated cells (3D). The membrane was captured in the process of releasing aggregated vesicle-/micelle-like material (see Figure 37), while several small micelle-like particles surround the cells. The phase image shows that the content being released is of a soft/adhesive material. The cell was scanned in air using the intermittent contact mode (tapping mode; AC).

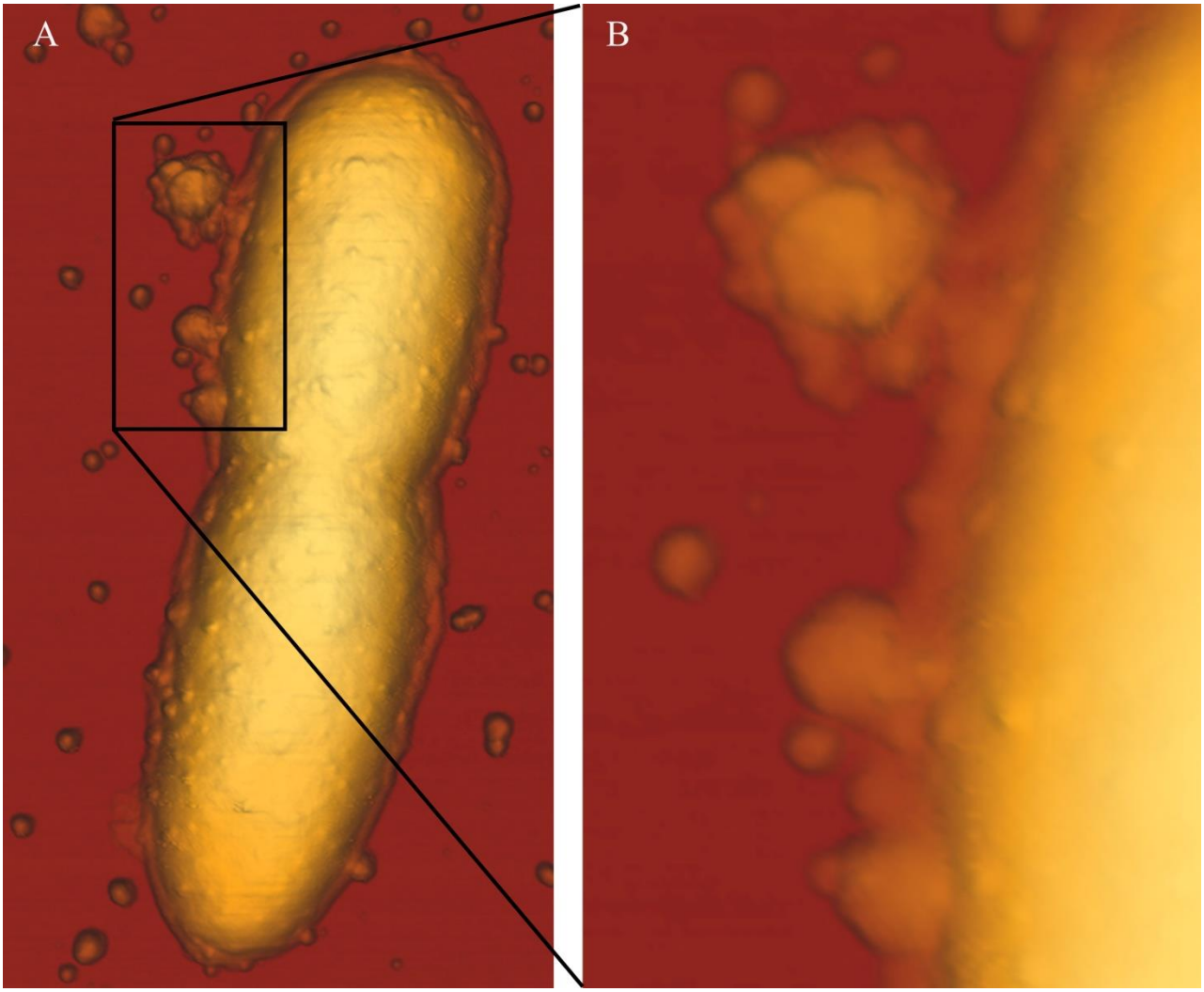

Figure 37. A) Topography (3D) image of the cell from Figure 36. B) Enlargement showing desorption of vesicle-/micelle-like material from the membrane. Some of the vesicle-/micelle tend to aggregate in clumps.

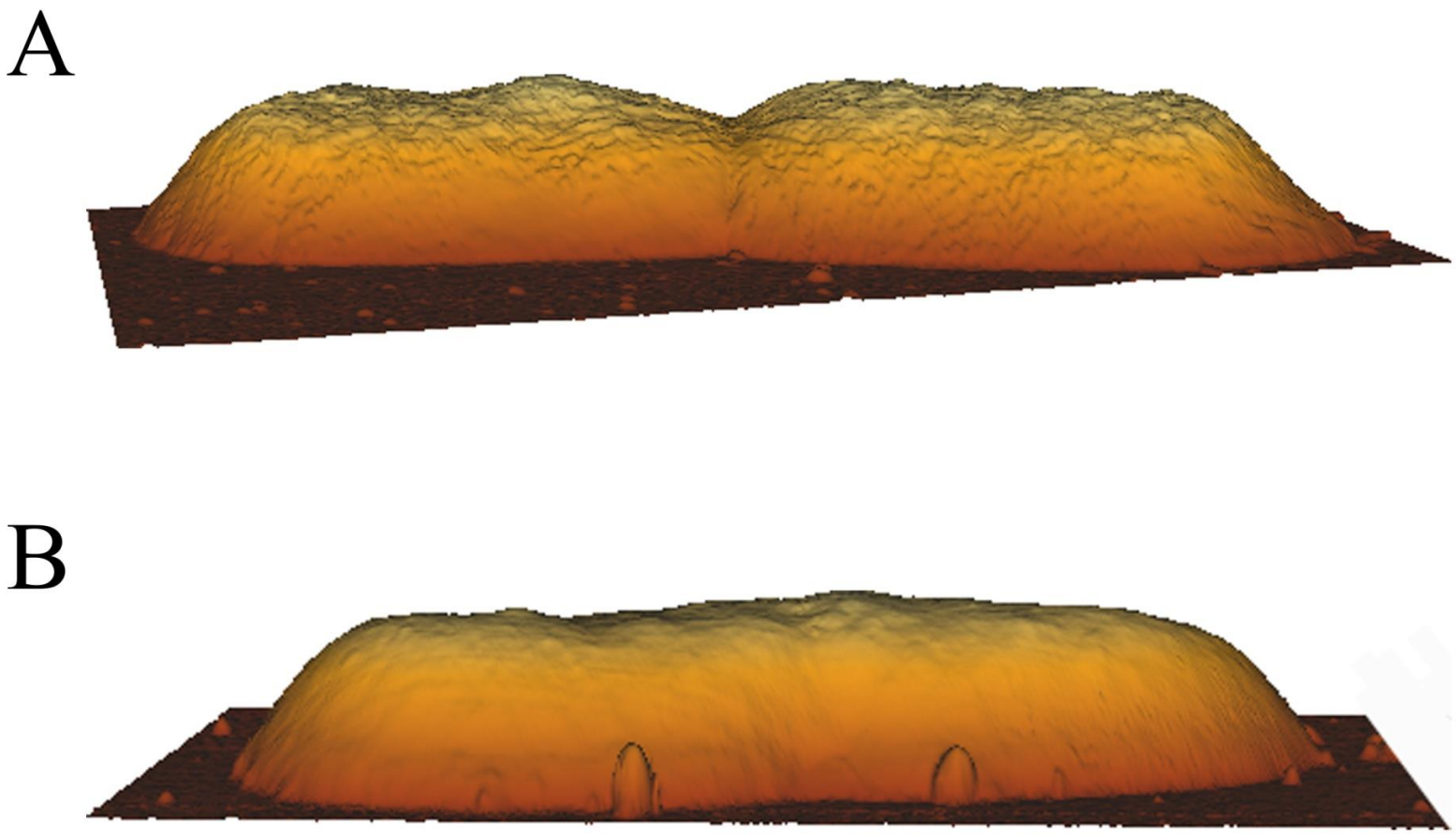

Figure 38. Side-view topography (3D) image comparing A) the rough surface of an untreated cell that possess varying lengths of *O*-polysaccharides (cell from Figure 29) to that of B) the smooth surface of an S20 scFv monomer treated cell that is deficient in OM/LPS (cell from Figure 35).

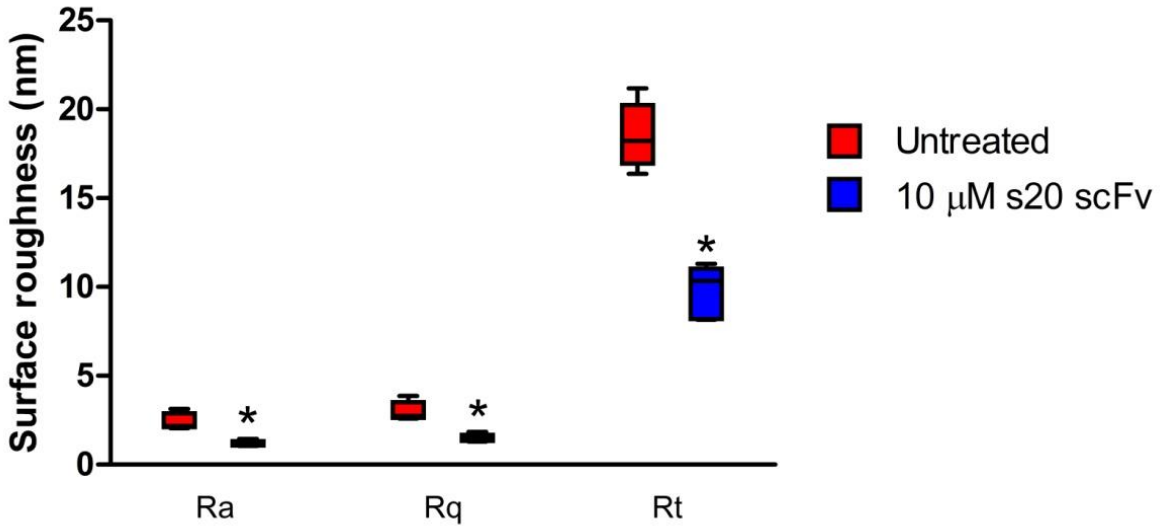

Figure 39. Surface topography analysis. The surface roughness of untreated and 22 × MIC_{50} (10 μM S20 scFv monomer) treated *P. aeruginosa* strain O6a, 6d cells were compared. Surface areas of 400 × 400 nm^2 were randomly selected from height images of untreated and treated cells (Figure 54). To account for cell curvature, the selected areas were flattened using a second order polynomial fit. The flattened image was then analyzed by measuring the average roughness (Ra), the root-mean-square roughness (Rq), and the peak-to-valley roughness (Rt). Comparision of statistical significance was made within the types of roughness parameters using a t-test ($p<0.05$). The data are presented as box-and-whisker plots where the bottom and top whiskers represent the minimum and maximum data points, respectively; the bottom and top of the box represents the 25th percentile and 75th percentile, respectively; the line in the box represents the median. Treated cells were significantly smoother for all three surface topography parameters (Ra, $p = 0.00194$; Rq, $p = 0.00278$; Rt, $p = 0.00075$).

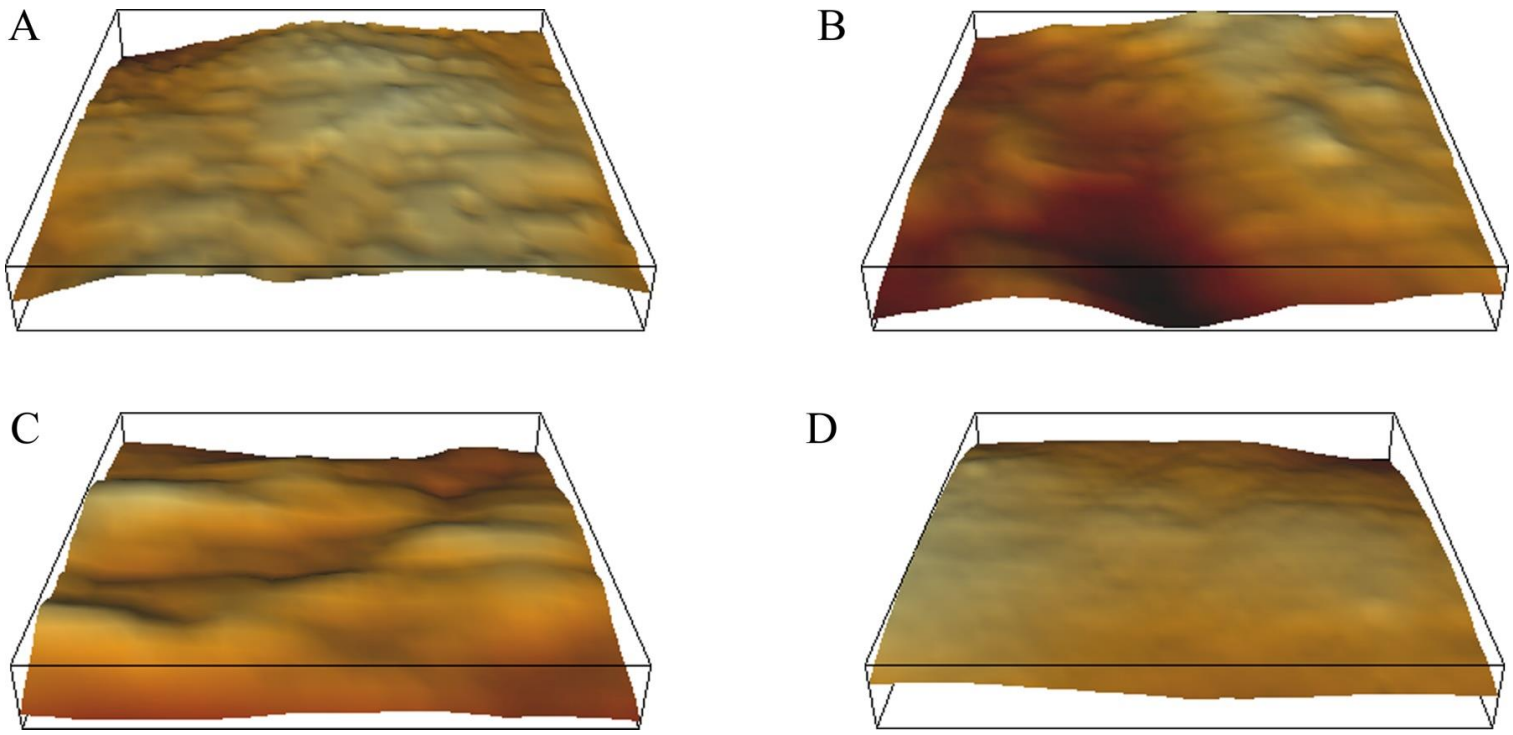

Figure 40. Enlargement of 3D surface patches (400 × 400 nm) of O6a, 6d cells treated with the mAb MF23-1 and S20 bactericidal antibodies. A) Rough surface topography attributed by the *O*-polysaccharide chains on an untreated cell. B) The release of a large amount of micelles and OM components (1 µM mAb MF23-1 treatment) eventually creates patchy areas with irregular shaped pits. The bottoms of these pits have a smoother topography than the crest of the pits. C) After sufficient membrane damage (10 µM mAb MF23-1 treatment), the OM loosens from the rest of the cell, thereby showing a corrugated topography. D) Surface of an OM-/LPS-free cell (10 µM S20 scFv treatment), showing the smoother topography of the peptidoglycan layer.

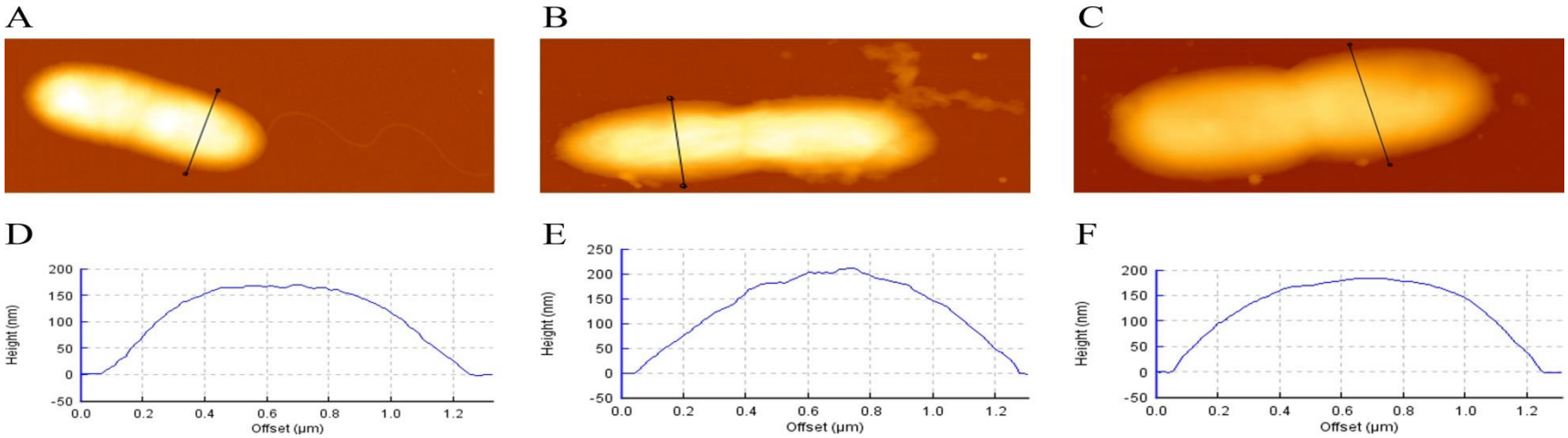

Figure 41. Cross-sections (D-F) of height images (A-C, respectively) providing a quantitative measure of the bacterial cell dimensions. An untreated O6a, 6d cell (A) showing a uniformly shaped surface curvature (D) with a height of 165 nm (range for untreated cells, 155–180 nm), a width of 1.2 µm and a length of 3.2 µM (dividing cell, measurement not shown). An O6a, 6d cell (B, same cell as provided Figure 34) treated with mAb MF23-1 (10 µM, 4 × MIC_{50}) possesses a surface curvature (E) that is relatively close to that of untreated cells. However, its height measures 215 nm which is slightly higher than untreated cells. The OM, which has a corrugated topography (Figure 40C) and is in the process of sloughing, is believed to be loosely anchored to the underlying peptidoglycan, possibly explaining the slightly more elevated height. An O6a, 6d cell (C, same cell as provided Figure 35) treated with the S20 scFv monomer (10 µM, 4 × MIC_{50}) possesses a surface curvature (F) and measurements (height: 180 nm; width: 1.2 µm) that is very comparable to that of untreated cells. The fact that the MF23-1 and the S20 scFv antibodies did not flatten the cells indicates that little or negligible loss of cytoplasmic content occurred, suggesting that the peptidoglycan and inner membrane remain intact.

4.5. DISCUSSION

The data presented in this study revealed intricate details of the mechanism of action of our bactericidal S20 and MF23-1 antibodies. To capture the sequence of events in which our antibodies disrupt the membrane of *P. aeruginosa* strain O6a, 6d, cells were treated with three antibodies, or formats, that exhibit different affinities, and hence different MIC_{50} (Figure 20), towards strain O6a, 6d: mAb MF23-1 (1 and 10 µM; 0.4 × and 4 × MIC_{50}, respectively), S20 scFv monomer (10 µM; 22 × MIC_{50}) and S20 scFv dimer (10 µM; 167 × MIC_{50}). Treatment with an antibody concentration as multiples of the established MIC_{50} correlated well with the progression of events involved in the mechanism of action of these antibodies, whereby the lowest MIC_{50} captured earlier membranolytic effects, treatment with an intermediate MIC_{50} captured intermediate effects and finally treatment with the highest MIC_{50} captured the most advanced/progressed membrane damage (Figure 28).

Micellization was found to be an early membranolytic effect induced by the antibodies, as cells treated with the lowest MIC_{50} released a large amount of micelle-like structures (Figure 28B, Figure 31, Figure 32, Figure 33). Most of these micelles were irregularly-shaped, clumpy, and morphologically different from natural OMVs (nOMVs) released from untreated cells (Figure 30). One could speculate that these micelle-like structures are monolayered, deficient in periplasmic content, and predominantly composed of components from the outer leaflet of the OM, including LPS. nOMVs, which are spherically-shaped bilayered membranous structures of ca. 20 to 250 nm in diameter naturally released from most gram-negatives, contain OM proteins, phospholipids, OSA (formerly called B-band LPS and periplasmic content within their lumen (55, 105) (Figure 30). The target of our antibodies, the OSA, as opposed to CPA (formerly

called A-band LPS) is an important constituent of nOMVs. In fact, during nOMV biogenesis, B-band LPS somehow laterally pools into small, localized regions on the outer leaflet of the OM where the eventual nOMV will form (198). It is possible that the binding of our antibodies to the OSA somehow interferes with lateral B-band LPS diffusion during biogenesis of nOMVs. Even the antibiotic gentamicin, which exhibits its bactericidal action by inhibiting bacterial protein synthesis through the targeting ribosomal 30S subunits (i.e., not even a membrane target), affects the formation of nOMVs (198). Thus, the effect of our bactericidal antibodies on the biogenesis and composition of OMVs warrants further investigation.

Micelle-/vesicle-like structures were also observed surrounding and sloughing from the O6a, 6d membrane following treatment at a range of multiples of the MIC_{50} concentration (Figure 34, Figure 35, Figure 36, Figure 37). However, since fewer micelles were observed with treatment at higher fold of MIC_{50}, it is believed that the micelle desorption step had mostly occurred prior to these cells being dried on the AFM slides. In addition, what appears as aggregated membrane components were also desorbed from cells treated with lower (Figure 31, Figure 32) and higher (Figure 36, Figure 37) MIC_{50} (with both MF23-1 and S20 scFv). Interestingly, several cationic AMPs, which are known to initially interact with LPS, also induce the formation of micelles as an early event in their antimicrobial mechanism of action (15, 16, 199-201). Many of the studies that have observed micellization as an early effect have hypothesized that AMPs disrupt the integrity of membranes using a carpet-like, which is a detergent-like, mechanism. Although our bactericidal antibodies are not likely to insert into the OM directly, they do ultimately share some of the membranotylic effects (i.e., micellization) induced by AMPs.

While it is counterintuitive, smooth strains, which by definition have smooth colony morphology and display *O*-polysaccharides, have been observed by AFM to possess rougher surface topography compared to rough strains, which by definition have rough colony morphology and are deficient in *O*-polysaccharides (33, 190, 202). It has been proposed that the varying lengths of *O*-polysaccharide chains, which can be composed of up to 50 O-antigen repeating units in *P. aeruginosa* (62), account for the rougher surface topography of smooth strains (190). The fact that AFM is able to capture the real topography of a sample represents an added benefit over other types of microscopy. In addition, AFM can even be used to measure the lengths of *O*-polysaccharide chains of a single cell. For example, the lengths of the *O*-polysaccharide chains of a wild-type *P. aeruginosa* smooth strain PA103 (serotype O11) were measured by AFM and shown to vary greatly from 90–280 nm, while that of its rough mutant (Wzy::GM mutant) only varied from ca. 20–70 nm (203). Overall, the *O*-polysaccharide chains extend ca. 30–40 nm above the OM of gram-negatives (55, 57, 58). Corroborating these findings, our high-resolution 3D AFM images showed that the surfaces of untreated O6a, 6d cells, a smooth strain with varying lengths of *O*-polysaccharides (Figure 13), also has a rough topography at nanometer resolution (Figure 28 A and E, Figure 29B, Figure 30B, Figure 40A, Figure 38A). This surface micro-roughness is especially evident from the side-view of the untreated cells displayed in Figure 38A and from the enlargement of a 400 x 400 nm surface area from this same cell in Figure 40A. Since AFM captures surface topography with higher resolution compared to other microscopy techniques, this surface roughness was not as evident in our earlier study using SEM and TE-SEM (5).

One of the most revealing observations which helped us make progress on understanding the mechanism of our bactericidal antibodies was the smoothening of the surface topography of

O6a, 6d cells when treated with 22 × MIC_{50} (10 μM S20 scFv monomer). As illustrated in Figure 28D, Figure 35, and Figure 36 (and Appendix Figure 52 and Figure 53) the surface topography of these cells was remarkably smoother than that of untreated cells and cells treated with the lower 0.4 × and 4 × MIC_{50} (1 and 10 μM of mAb MF23-1, respectively). The smoothening of the O6a, 6d surface is especially evident in the 3D side-view provided in Figure 38B and the 400 by 400 nm surface patch enlargement illustrated in Figure 40D. Moreover, statistical analysis of surface roughness revealed that cells treated with 22 × MIC_{50} (10 μM S20 scFv monomer) were statistically smoother than untreated cells (Figure 39). Since the rough surface topography is thought to be attributed by the varying chain lengths of *O*-polysaccharides, our results suggest that the bactericidal antibodies have induced desorption of surface LPS and perhaps the complete loss of the OM layer on these cells. While cells treated with lower MIC_{50}s have surface micro-roughness comparable to untreated cells, they also acquired some localized areas with 15 – 35 nm deep pits (Figure 32 and Appendix Figure 50). The formation of membrane pits is also induced by membrane permeabilizers and some cationic AMPs. EDTA, which is well known to permeabilize the OM of Gram-negatives, has been shown by AFM to release patches of LPS, thereby creating large irregularly-shaped pits that expose the underlying peptidoglycan layer of *E. coli* [(204) cited in (205)] (190), and *Pseudomonas* sp. (205). The cationic AMP epsilon-poly-L-lysine (ε-PL) also releases LPS in a patchy or pit-like manner from the OM of *E. coli* (200). Amro *et al*. (190) suggested that the observed smoother bottom of the pits created on the membrane of *E. coli* cells upon EDTA treatment are devoid of LPS molecules whereas the outside, i.e., more elevated and rougher topography, contain LPS. Our results are in agreement with Amro's findings in that the bottoms of the pits have a much smoother topography than the outside of the pits. Moreover, AFM phase images have corroborated these

findings by showing that LPS-deficient pits expose the underlying rigid peptidoglycan layer [(204) cited (205)].

Also in agreement with the effects induced by our bactericidal antibodies at higher concentration, Meincken *et al*. (199) observed that treatment of *E. coli* cells with >LC_{50} Mag 2a caused a significant decrease in surface micro-roughness, which was attributed to loss of outer membrane components, including LPS, by vesiculation. Thus, the fact that O6a, 6d cells treated with 22 × MIC_{50} (10 µM S20 scFv monomer) are almost entirely devoid of the rough surface topography observed on untreated cells strongly suggests that they have either lost their LPS/OM layer, or have lost some heterogeneity in their OSA chain lengths. However, as revealed by our earlier SPR experiment (Figure 46, Figure 16) and discussed in subheading 3.4.5.1, the S20 scFv does not hydrolyze the OSA of O6a, 6d. Therefore, the smoothing of the surface is not attributed to a reduction in the variability of the chain lengths of the OSA of O6a, 6d. Rather, we believe that the loss of surface micro-roughness is a result of the release of LPS-antibody micelles and OM components.

Our findings that the O6a, 6d surface topography becomes smooth and presumably deficient in LPS, correlated with our phase images which revealed that the surface stiffness changes upon treatment with our bactericidal antibodies. While the surfaces of untreated O6a, 6d cells are mostly composed of a soft/adhesive material (Figure 29D), phase imaging revealed that the surfaces of O6a, 6d cells treated with 22 × MIC_{50} (10 µM S20 scFv monomer) mostly consists of a rigid material (Figure 35D, Figure 36D). The soft material that is abundant on the surfaces of untreated cells is presumably the OM layer while the rigid material that is exposed upon treatment with our bactericidal antibodies is presumably the rigid cross-linked peptidoglycan layer. In fact, the peptidoglycan layer of an untreated Gram-positive bacterium

(*Propionibacterium acnes*), which is its outer most layer, is detected as a rigid (i.e., dark coloured) material in AFM (206). Meanwhile, the outermost layer of untreated Gram-negative bacteria mostly consists of a soft/adhesive material. Some of the cells treated with 4 × MIC_{50} (mAb MF23-1, 10 μM) captured the process of the loosening and release of the OM layer from the underlying rigid peptidoglycan layer (Figure 34, Figure 41 B and E). The OM appears to start peeling off from at least one apical end and periphery of the cell as evidenced by the appearance of the rigid material, i.e., peptidoglycan layer, in these areas (Figure 34D). Furthermore, the deposition to the right of the cell in Figure 34 appears to be sloughing of the OM layer since it is of the same material composition and is still anchored to the overlaying soft layer, i.e., the OM, on the cell. Taken together, it appears that the disruption of the OM is initiated by micellization and after sufficient membrane damage, likely near an apical end, the OM loosens and is released as larger intact patches instead of micelles. Similar to our phase imaging results, others have also observed changes in surface stiffness of cells treated with membrane permeabilizers [(204) cited (205)] and cationic AMPs (199, 200). For example, phase images showed that ε-PL, which releases the LPS layer from *E. coli* cells through the formation of vesicles/micelles, exposed patchy areas of rigid cellular surfaces (200). In another study, Meincken *et al.* (199) observed that the OM of *E. coli* cells separated from the inner membrane upon treatment with a >LC_{50} of the cationic AMP magainin 2a (Mag 2a), and that the exposed outer surface mostly consisted of a rigid material which they presumed was the peptidoglycan layer. In fact, the Mag 2a-treated *E. coli* cells with exposed peptidoglycan also had a very smooth surface topography which if thought to be attributed to the loss of OM components, including LPS, by vesiculation. Thus, like our current study, Mag 2a induced both the loss of surface roughness, resulting from loss of OM components, including LPS, through vesiculation,

and the appearance of rigid peptidoglycan layer. These authors suggest that the mechanism of action of Mag 2a likely follows the carpet-like model where the integration of the peptide in the outer membrane causes membrane permeabilization by micellization (137).

Several observations suggest that our bactericidal antibodies do not affect the structural integrity of the peptidoglycan layer nor the inner membrane (IM) of *P. aeruginosa* strain O6a, 6d. As O6a, 6d treated cells maintained their rod-shape morphology, which is governed by the cross-linked peptidoglycan layer, and did not undergo severe morphological changes indicates that the integrity of the peptidoglycan is not compromised. Furthermore, cross-sections of 3D images showed that treated cells preserved their cylindrical shape and that their height and width were comparable to that of untreated cells (Figure 41), indicating that the cytoplasmic contents were unaffected. Had the antibodies disrupted the IM, the cells would have flattened as a result of the release of cytoplasmic content. Similar results were obtained with EDTA-treated *E. coli* cells, where the height and width of the treated cells remained unchanged even after the LPS was released from the surface (190). In comparison, the AFM study by Braga and Ricci (189) revealed that targeting the peptidoglycan layer of *E. coli* with a beta-lactam antibiotic (cefodizime) resulted in flattened cells deficient of their cell wall, i.e., peptidoglycan layer, and which had lost most of their cytoplasmic content. Since the effects of our antibodies are very different from those produced by beta-lactams, it seems unlikely that our antibodies would affect the integrity of the peptidoglycan layer.

Interaction with the LPS, and more specifically the OSA, is likely the very first step in the mechanism of action of these bactericidal antibodies. Since the S20 scFv monomer and dimer have similar association rate constants (k_{on}) (5.2 × and 5.9 × 10^3 M^{-1} s^{-1}, respectively), they should bind the OSA in the O6a, 6d membrane at similar rates. Thus, one should expect similar

local concentrations for both these antibody formats near the surface of O6a, 6d. However, once in a bound state, the dimer dissociates very slowly from the OSA. Since treatment with the S20 scFv dimer progresses through the sequence of events at a faster rate compared to the monomer, its much slower dissociation rate constant (k_{off}) likely plays an important role in its bactericidal potency by promoting a quicker and more pronounced membrane disruption. This tight LPS binding contrasts with the action of cationic AMPs. Although LPS is also the first site of interaction with cationic AMPs, they are then thought to target a second site and directly integrate into and disrupt the membrane. If our bactericidal antibodies directly inserted into the membrane, then one would expect the format with the faster k_{off}, i.e., the S20 scFv monomer, to be more available to then target the membrane. Thus, we propose that our bactericidal antibodies do not have a second site of action/interaction like AMPs. The binding of antibodies to the OSA seems sufficient to disrupt the integrity of the membrane via the desorption of membrane micelles and other membrane components. Moreover, as discussed in Chapter 3, targeting the core region with mAb 7-4 did not affect the viability of various smooth and rough mutants of *P. aeruginosa*. Therefore, targeting the O6 OSA is either interfering with a functional role of the OSA in terms of viability or is perhaps adding a mechanical strain on the LPS that is transmitted to the OM. Since *P. aeruginosa* can survive without its OSA, then perhaps the latter explanation is more plausible. Further studies are required to understand why *P. aeruginosa* is particularly vulnerable to antibodies binding its OSA.

In summary, AFM proved to be a useful tool to help us unravel the bactericidal mechanism of action of the S20 and MF23-1 antibodies towards *P. aeruginosa* strain O6a, 6d. Many of the membranolytic effects observed by AFM, including the smoothing of the surface topography, the release of large amounts of micelles and OM components, and the uncovering of

the rigid peptidoglycan layer, were not captured by our previous SEM and TE-SEM study (5). Moreover, many of the effects induced by the S20 and MF23-1 antibodies paralleled some of the effects induced by other membrane-active compounds, including EDTA and several cationic AMPs which are thought to disrupt membranes according to the detergent-like/carpet-like mechanism (16, 199, 200) (Figures 19 and 20). As discussed in Chapter 3, the sequences of our bactericidal antibodies do not share identity with AMP sequences. However, the commonality between them lies in the fact that their very first site of interaction on the cell envelope is LPS, albeit on different epitopes. Thus, similar to the action of AMPs, it appears that our bactericidal antibodies are exploiting a sensitive target on the cell envelope of *P. aeruginosa* serotype O6. While LPS is known to act as a barrier that protects the membrane of Gram-negative bacteria and is an important virulence factor, it is ironic that targeting it with anti-LPS antibodies, independently of other components of the immune system (ADCC and CDC), makes *P. aeruginosa* serotype O6 vulnerable to targeted killing.

We propose that the sequence of events involved in the bactericidal mechanism of the S20 and MF23-1 antibodies is as follows:

1- **LPS-binding step**, where a slower dissociation rate constant (k_d) correlates with an accelerated progression through the membranolytic events and *vice versa*;
2- **Micellization** of the LPS-rich outer membrane initiates membrane disruption in a detergent-like manner;
3- **Appearance of membrane pits** upon the release of micelles and OM components**;**
4- **Loosening of the OM** from the peptidoglycan layer;
5- **Sloughing of the OM**, thereby uncovering the smoother, more rigid peptidoglycan layer;

6- Membrane blebbing.

It would be of interest to further investigate if targeting the OSA of all the 20 serotypes with antibodies also induces direct bactericidal activity. While passive immunotherapy with anti-O6 (OSA) antibodies could be beneficial for the treatment of acute *P. aeruginosa* serotype O6 infections, most chronic *P. aerugniosa* infections would unfortunately not respond since most clinical strains stop producing the OSA. Nevertheless, our findings provide a better understanding of the strong selective pressures on long-term clinical isolates of *P. aeruginosa* to stop producing *O*-polysaccharides.

CHAPTER 5: GENERAL CONCLUSIONS AND FUTURE DIRECTIONS

The main goal of this thesis was to investigate the complement- and phagocyte-independent bactericidal activity of the S20 antibody against *P. aeruginosa* strain O6a, 6d (5). It was initially hypothesized that S20 was a unique abzyme that exerted a potent catalytic activity (e.g., LPS hydrolysis, hydrogen peroxide production) against strain O6a, 6d. The intended direction of the project was to identify the likely amino acids of S20 involved in the killing mechanism. However, before commencing laborious molecular work, we questioned our hypothesis: is this activity truly unique and inherent in the S20 antibody? In this thesis, we demonstrated that a second antibody called mAb MF23-1, which was provided to us from the laboratory of Dr. Joseph Lam (University of Guelph) (143), also exerts direct bactericidal activity towards O6 OSA+ strains. The fact that the S20 and MF23-1 antibodies share little sequence identity, especially in their CDRs, indirectly established that these antibodies are not catalytic in nature. Instead, their interaction with the OSA induces cell death, in an affinity-dependent manner. Using AFM, we established that the S20 and MF23-1 antibodies mediate their bactericidal activity by permeabilizing the OM using a detergent-like mechanism similar to the action of cationic AMPs. We propose that the mechanism of action of the two bactericidal antibodies involves the following steps: 1- LPS-binding step; 2- Micellization of the LPS-rich OM; 3- Appearance of membrane pits; 4- Loosening of the OM from the peptidoglycan layer; 5- Sloughing of the OM; 6- Membrane blebbing. In the immunology context, our work established a novel mechanism by which antibodies can mediate direct antimicrobial immunity without the recruitment of phagocytes or the complement system (Figure 8).

Future experiments should focus on determining why the integrity of the OM of *P. aeruginosa* is compromised by the binding of anti-OSA antibodies. Since the stability and integrity of membranes are often defined by the composition of their lipids, the discrepancy between *P. aeruginosa* and other Gram-negatives may reside in their different lipid A structures or lipidome. In essence, the lipid A from laboratory strains of *P. aeruginosa* have fewer and shorter acyl chains compared to that of many Gram-negatives, including *E. coli, Salmonella* and *N. meningitidis* (Figure 6) (33, 59). Presumably, the structure of the lipid A of the O6 strains used in this work resembles that of a typical *P. aeruginosa* laboratory strains (Figure 6a). It is possible that the lipid A of *P. aeruginosa* is not as stably anchored in the OM compared to other Gram-negatives. The binding of many antibody molecules, on the OSA, especially very long chains (up to 50 repeating units), may somehow disorganize the packaging of LPS domains, thereby leading to micellization, in a detergent-like manner, of the OM.

In *P. aeruginosa*, the length of the OSA chain is regulated by two Wzz proteins, namely Wzz1 [modulates 12–16 repeats and 22–30 repeats; (62, 63)] and Wzz2 [modulates 40–50 repeat length; (62)]. Apparently, shorter chains of OSA, i.e., those conferred by Wzz1, are more virulent than the very long chains of OSA, i.e., those conferred by Wzz2 (207). It would be of interest to determine if the chain length of the OSA is a contributing factor to the bactericidal activity. For example, perhaps the bactericidal antibodies (e.g., S20 and MF23-1) only exert bactericidal activities when the cells display very long chains of OSA. One could test mAb MF23-1 against Wzz1 and Wzz2 knock-out mutants of O6 strains, similar to those created for PAO1 (serotype O5) by Dr. Joseph Lam's laboratory (62, 63).

The lipidome of *P. aeruginosa* also differs from that of enteric bacteria. While phosphatidylcholine (PC) is the most abundant phospholipids found in the membrane of

eukaryotes, the membrane of most bacteria (ca. 90%), including *E. coli* and *Salmonella*, do not contain PC. However, in addition to the typical prokaryotic phospholipids (phosphatidylethanolamine, phosphatidylglycerol, and cardiolipin), *P. aeruginosa* can synthesize phosphatidylcholine (PC) as a minor membrane phospholipid if choline is available from the host or from complex growth medium (56). By growing *P. aeruginosa* in media with and without choline, it would be experimentally straightforward to determine if PC has an effect on the membrane stability when treated with the bactericidal antibodies.

Similar to *P. aeruginosa*, the spirochete *Borrelia burgdorferi*, the agent of Lyme disease, also produces PC (208). Targeting the OM protein OspB of *B. burgdorferi* with antibodies [CB2 (IgG1) and H6831 (IgG1)] leads to the destruction of its OM (7-10, 184). It is not known if there is a relationship between the presence of PC and the bactericidal effect of the anti-*Borrelia* antibodies. However, in addition to PC, the membrane of *Borrelia* contains cholesterol lipids which form lipid rafts that are required for the bactericidal activity of the anti-OspB antibodies (10). While the membrane of *P. aeruginosa* does not contain cholesterol, this example nevertheless demonstrates that the bacterial lipodome can affect the stability of its membrane when surface antigens are targeted with bactericidal antibodies. Further studies are warranted to investigate the role of PC and other membrane lipids in the bactericidal mechanism of our anti-OSA antibodies.

The OSA is the predominant form of LPS in wild-type strains and strains isolated from acute infections. However, its production, unlike that of CPA, appears to be regulated as a result of adaptation due to pathogen host interactions; i.e., OSA is either reduced in amount or completely abrogated as a result of chronic selective pressures in clinical isolates, especially those isolated from CF patients (60, 64). Thus, our findings that anti-OSA antibodies induce

direct antimicrobial activity provide a better understanding of the particularly strong selective pressure *P. aeruginosa* face to evade the host's immune system.

In the immunology context, our work established a novel mechanism by which antibodies can mediate direct antimicrobial immunity without the recruitment of phagocytes or the complement system (Figure 8). The S20 and MF23-1 antibodies are the only described anti-LPS antibodies known to induce the permeabilization of the OM of Gram-negative bacteria. Since the S20 antibody exclusively binds to *P. aeruginosa* strain O6a, 6d, it would be of low therapeutic value. However, mAb MF23-1, which cross-reactively binds to all wild-type OSA+ O6 strains, could represent an attractive reagent for passive immunotherapy, since O6 is the most clinically prevalent *P. aeruginosa* serotype reported in numerous epidemiology studies to date (39-41).

REFERENCES:

1. Wentworth, P., J. E. McDunn, A. D. Wentworth, C. Takeuchi, J. Nieva, T. Jones, C. Bautista, J. M. Ruedi, A. Gutierrez, and K. D. Janda. 2002. Evidence for antibody-catalyzed ozone formation in bacterial killing and inflammation. *Science* 298:2195-2199.
2. Wentworth, P., L. H. Jones, A. D. Wentworth, X. Zhu, N. A. Larsen, I. A. Wilson, X. Xu, W. A. Goddard, K. D. Janda, and A. Eschenmoser. 2001. Antibody catalysis of the oxidation of water. *Science* 293:1806-1811.
3. Wentworth, A. D., L. H. Jones, P. Wentworth, K. D. Janda, and R. A. Lerner. 2000. Antibodies have the intrinsic capacity to destroy antigens. *Proceedings of the National Academy of Sciences* 97:10930-10935.
4. Goel, V. K., and A. Kapil. 2001. Monoclonal antibodies against the iron regulated outer membrane proteins of *Acinetobacter baumannii* are bactericidal. *BMC microbiology* 1:1.
5. Xie, X., M. D. McLean, and J. C. Hall. 2010. Antibody-dependent cell-mediated cytotoxicity-and complement-dependent cytotoxicity-independent bactericidal activity of an IgG against *Pseudomonas aeruginosa* O6ad. *The Journal of Immunology* 184:3725-3733.
6. Connolly, S. E., D. G. Thanassi, and J. L. Benach. 2004. Generation of a complement-independent bactericidal IgM against a relapsing fever *Borrelia*. *The Journal of Immunology* 172:1191-1197.
7. Coleman, J. L., R. C. Rogers, and J. L. Benach. 1992. Selection of an escape variant of *Borrelia burgdorferi* by use of bactericidal monoclonal antibodies to OspB. *Infection and immunity* 60:3098-3104.
8. Šadžiene, A., M. Jonsson, S. Bergström, R. K. Bright, R. C. Kennedy, and A. G. Barbour. 1994. A bactericidal antibody to *Borrelia burgdorferi* is directed against a variable region of the OspB protein. *Infection and immunity* 62:2037-2045.
9. LaRocca, T. J., D. J. Holthausen, C. Hsieh, C. Renken, C. A. Mannella, and J. L. Benach. 2009. The bactericidal effect of a complement-independent antibody is osmolytic and specific to *Borrelia*. *Proceedings of the National Academy of Sciences* 106:10752-10757.
10. LaRocca, T. J., J. T. Crowley, B. J. Cusack, P. Pathak, J. Benach, E. London, J. C. Garcia-Monco, and J. L. Benach. 2010. Cholesterol lipids of *Borrelia burgdorferi* form lipid rafts and are required for the bactericidal activity of a complement-independent antibody. *Cell host & microbe* 8:331-342.
11. Taneja, N., R. Emmanuel, P. S. Chari, and M. Sharma. 2004. A prospective study of hospital-acquired infections in burn patients at a tertiary care referral centre in North India. *Burns* 30:665-669.
12. Govan, J. R., and V. Deretic. 1996. Microbial pathogenesis in cystic fibrosis: mucoid *Pseudomonas aeruginosa* and *Burkholderia cepacia*. *Microbiological reviews* 60:539-574.
13. Lyczak, J. B., C. L. Cannon, and G. B. Pier. 2000. Establishment of *Pseudomonas aeruginosa* infection: lessons from a versatile opportunist. *Microbes and Infection* 2:1051-1060.
14. CDC, A. Z. 2013. Antibiotic resistance threats in the United States, 2013.

15. Li, A., P. Y. Lee, B. Ho, J. L. Ding, and C. T. Lim. 2007. Atomic force microscopy study of the antimicrobial action of Sushi peptides on Gram negative bacteria. *Biochimica et Biophysica Acta (BBA)-Biomembranes* 1768:411-418.
16. Li, A., B. Ho, J. L. Ding, and C. T. Lim. 2010. Use of atomic force microscopy as a tool to understand the action of antimicrobial peptides on bacteria. In *Antimicrobial Peptides: Methods and Protocols*. A. Giuliani, and C. A. Rinaldi, eds. Humana Press, Totowa, NJ. 235-247.
17. Green, S. K., M. N. Schroth, J. J. Cho, S. D. Kominos, and V. B. Vitanza-Jack. 1974. Agricultural plants and soil as a reservoir for *Pseudomonas aeruginosa*. *Applied Microbiology* 28:987-991.
18. Lambert, P. A. 2002. Mechanisms of antibiotic resistance in *Pseudomonas aeruginosa*. *Journal of the Royal Society of Medicine* 95:22.
19. van der Kooij, D., J. P. Oranje, and W. A. Hijnen. 1982. Growth of *Pseudomonas aeruginosa* in tap water in relation to utilization of substrates at concentrations of a few micrograms per liter. *Applied and Environmental Microbiology* 44:1086-1095.
20. Botzenhart, K., and R. Kufferath. 1976. [On the growth of various *Enterobacteriaceae*, *Pseudomonas aeruginosa* and *Alkaligenes* spec. in distilled water, de-ionized water, tap water, and mineral salt solution (author's transl)]. *Zentralblatt fur Bakteriologie, Parasitenkunde, Infektionskrankheiten und Hygiene. Erste Abteilung Originale. Reihe B: Hygiene, praventive Medizin* 163:470-485.
21. Warburton, D. W., B. Bowen, and A. Konkle. 1994. The survival and recovery of *Pseudomonas aeruginosa* and its effect upon salmonellae in water: methodology to test bottled water in Canada. *Canadian Journal of Microbiology* 40:987-992.
22. Morita, Y., T. Murata, T. Mima, S. Shiota, T. Kuroda, T. Mizushima, N. Gotoh, T. Nishino, and T. Tsuchiya. 2003. Induction of mexCD-oprJ operon for a multidrug efflux pump by disinfectants in wild-type *Pseudomonas aeruginosa* PAO1. *Journal of Antimicrobial Chemotherapy* 51:991-994.
23. Hancock, R. E. W. 1998. Resistance mechanisms in *Pseudomonas aeruginosa* and other nonfermentative gram-negative bacteria. *Clinical Infectious Diseases* 27:S93-S99.
24. Yoshimura, F., and H. Nikaido. 1982. Permeability of *Pseudomonas aeruginosa* outer membrane to hydrophilic solutes. *Journal of Bacteriology* 152:636-642.
25. Poole, K. 2004. Efflux-mediated multiresistance in Gram-negative bacteria. *Clinical Microbiology and Infection* 10:12-26.
26. Köhler, T., M. Kok, M. Michea-Hamzehpour, P. Plesiat, N. Gotoh, T. Nishino, L. K. Curty, and J.-C. Pechere. 1996. Multidrug efflux in intrinsic resistance to trimethoprim and sulfamethoxazole in *Pseudomonas aeruginosa*. *Antimicrobial Agents and Chemotherapy* 40:2288-2290.
27. Li, X.-Z., H. Nikaido, and K. Poole. 1995. Role of mexA-mexB-oprM in antibiotic efflux in *Pseudomonas aeruginosa*. *Antimicrobial Agents and Chemotherapy* 39:1948-1953.
28. Okamoto, K., N. Gotoh, and T. Nishino. 2001. *Pseudomonas aeruginosa* reveals high intrinsic resistance to penem antibiotics: penem resistance mechanisms and their interplay. *Antimicrobial Agents and Chemotherapy* 45:1964-1971.
29. Zhao, Q., X.-Z. Li, A. Mistry, R. Srikumar, L. Zhang, O. Lomovskaya, and K. Poole. 1998. Influence of the TonB energy-coupling protein on efflux-mediated multidrug

resistance in *Pseudomonas aeruginosa*. *Antimicrobial Agents and Chemotherapy* 42:2225-2231.
30. Ziha-Zarifi, I., C. Llanes, T. Köhler, J.-C. Pechere, and P. Plesiat. 1999. *In vivo* emergence of multidrug-resistant mutants of *Pseudomonas aeruginosa* overexpressing the active efflux system MexA-MexB-OprM. *Antimicrobial Agents and Chemotherapy* 43:287-291.
31. Hirsch, E. B., and V. H. Tam. 2010. Impact of multidrug-resistant *Pseudomonas aeruginosa* infection on patient outcomes. *Expert Review of Pharmacoeconomics & Outcomes Research* 10:441-451.
32. King, J. D., K. K. H. Poon, N. A. Webb, E. M. Anderson, D. J. McNally, J.-R. Brisson, P. Messner, R. M. Garavito, and J. S. Lam. 2009. The structural basis for catalytic function of GMD and RMD, two closely related enzymes from the GDP-d-rhamnose biosynthesis pathway. *FEBS Journal* 276:2686-2700.
33. Lam, J. S., V. L. Taylor, S. T. Islam, Y. Hao, and D. Kocíncová. 2011. Genetic and functional diversity of *Pseudomonas aeruginosa* lipopolysaccharide. *Frontiers in Microbiology*. 2:118.
34. Magill, S. S., J. R. Edwards, W. Bamberg, Z. G. Beldavs, G. Dumyati, M. A. Kainer, R. Lynfield, M. Maloney, L. McAllister-Hollod, and J. Nadle. 2014. Multistate point-prevalence survey of health care–associated infections. *New England Journal of Medicine* 370:1198-1208.
35. Cardo, D., T. Horan, M. Andrus, M. Dembinski, J. Edwards, G. Peavy, J. Tolson, and D. Wagner. 2004. National Nosocomial Infections Surveillance (NNIS) system report, data summary from January 1992 through June 2004, issued October 2004. *American Journal of Infection Control* 32:470-485.
36. Bert, F., N. Lambert-Zechovsky, and A. C. Seymour. 1996. Comparitive distribution of resistance patterns and serotypes in *Pseudomonas aeruginosa* isolates from intensive care units and other wards. *Journal of Antimicrobial Chemotherapy* 37:809-813.
37. Pirnay, J.-P., D. De Vos, C. Cochez, F. Bilocq, A. Vanderkelen, M. Zizi, B. Ghysels, and P. Cornelis. 2002. *Pseudomonas aeruginosa* displays an epidemic population structure. *Environmental Microbiology* 4:898-911.
38. Pirnay, J.-P., D. De Vos, C. Cochez, F. Bilocq, J. Pirson, M. Struelens, L. Duinslaeger, P. Cornelis, M. Zizi, and A. Vanderkelen. 2003. Molecular epidemiology of *Pseudomonas aeruginosa* colonization in a burn unit: persistence of a multidrug-resistant clone and a silver sulfadiazine-resistant clone. *Journal of Clinical Microbiology* 41:1192-1202.
39. MacIntyre, S., R. Lucken, and P. Owen. 1986. Smooth lipopolysaccharide is the major protective antigen for mice in the surface extract from IATS serotype 6 contributing to the polyvalent Pseudomonas aeruginosa vaccine PEV. *Infection and Immunity* 52:76-84.
40. Miler, J. M., J. F. Spilsbury, R. J. Jones, E. A. Roe, and E. J. L. Lowbury. 1977. A new polyvalent *Pseudomonas* vaccine. *Journal of medical microbiology* 10:19-27.
41. Döring, G., and G. B. Pier. 2008. Vaccines and immunotherapy against *Pseudomonas aeruginosa*. *Vaccine* 26:1011-1024.
42. Langford, D. T., and J. Hiller. 1984. Prospective, controlled study of a polyvalent pseudomonas vaccine in cystic fibrosis--three year results. *Archives of Disease in Childhood* 59:1131-1134.

43. Pier, G. B. 2007. *Pseudomonas aeruginosa* lipopolysaccharide: a major virulence factor, initiator of inflammation and target for effective immunity. *International Journal of Medical Microbiology* 297:277-295.
44. Cryz, S. J., T. L. Pitt, E. Fürer, and R. Germanier. 1984. Role of lipopolysaccharide in virulence of *Pseudomonas aeruginosa*. *Infection and immunity* 44:508-513.
45. Tang, H. B., E. DiMango, R. Bryan, M. Gambello, B. H. Iglewski, J. B. Goldberg, and A. Prince. 1996. Contribution of specific *Pseudomonas aeruginosa* virulence factors to pathogenesis of pneumonia in a neonatal mouse model of infection. *Infection and Immunity* 64:37-43.
46. Prescott, L. M., J. P. Harley, and D. A. Klein. 2005. Microbiology. 5th. *McGrawJHill Higher Education*.
47. Schwechheimer, C., and M. J. Kuehn. 2015. Outer-membrane vesicles from Gram-negative bacteria: biogenesis and functions. *Nature reviews microbiology* 13:605-619.
48. Braun, V., and H. Wolff. 1975. Attachment of lipoprotein to murein (peptidoglycan) of *Escherichia coli* in the presence and absence of penicillin FL 1060. *Journal of Bacteriology* 123:888-897.
49. Braun, V. 1975. Covalent lipoprotein from the outer membrane of *Escherichia coli*. *Biochimica et Biophysica Acta (BBA)-Reviews on Biomembranes* 415:335-377.
50. Yamagata, H., K. Nakamura, and M. Inouye. 1981. Comparison of the lipoprotein gene among the Enterobacteriaceae. DNA sequence of *Erwinia amylovora* lipoprotein gene. *Journal of Biological Chemistry* 256:2194-2198.
51. Cascales, E., A. Bernadac, M. Gavioli, J.-C. Lazzaroni, and R. Lloubes. 2002. Pal lipoprotein of *Escherichia coli* plays a major role in outer membrane integrity. *Journal of Bacteriology* 184:754-759.
52. Wang, Y. 2002. The function of OmpA in *Escherichia coli*. *Biochemical and Biophysical Research Communications* 292:396-401.
53. Hancock, R. E. W., R. Siehnel, and N. Martin. 1990. Outer membrane proteins of *Pseudomonas*. *Molecular Microbiology* 4:1069-1075.
54. Singer, S. J., and G. L. Nicolson. 1972. The fluid mosaic model of the structure of cell membranes. *Science* 175:720-731.
55. Beveridge, T. J. 1999. Structures of gram-negative cell walls and their derived membrane vesicles. *Journal of Bacteriology* 181:4725-4733.
56. Wilderman, P. J., A. I. Vasil, W. E. Martin, R. C. Murphy, and M. L. Vasil. 2002. *Pseudomonas aeruginosa* synthesizes phosphatidylcholine by use of the phosphatidylcholine synthase pathway. *Journal of Bacteriology* 184:4792-4799.
57. Lu, Q., J. Wang, A. Faghihnejad, H. Zeng, and Y. Liu. 2011. Understanding the molecular interactions of lipopolysaccharides during *E. coli* initial adhesion with a surface forces apparatus. *Soft Matter* 7:9366-9379.
58. Beveridge, T. J., and L. L. Graham. 1991. Surface layers of bacteria. *Microbiological Reviews* 55:684-705.
59. King, J. D., D. Kocíncová, E. L. Westman, and J. S. Lam. 2009. Review: lipopolysaccharide biosynthesis in *Pseudomonas aeruginosa*. *Innate Immunity* 15:261-312.
60. Lam, M. Y., E. J. McGroarty, A. M. Kropinski, L. A. MacDonald, S. S. Pedersen, N. Høiby, and J. S. Lam. 1989. Occurrence of a common lipopolysaccharide antigen in

standard and clinical strains of *Pseudomonas aeruginosa*. *Journal of Clinical Microbiology* 27:962-967.
61. Rivera, M., L. E. Bryan, R. E. Hancock, and E. J. McGroarty. 1988. Heterogeneity of lipopolysaccharides from *Pseudomonas aeruginosa*: analysis of lipopolysaccharide chain length. *Journal of Bacteriology* 170:512-521.
62. Daniels, C., C. Griffiths, B. Cowles, and J. S. Lam. 2002. *Pseudomonas aeruginosa* O-antigen chain length is determined before ligation to lipid A core. *Environmental Microbiology* 4:883-897.
63. Burrows, L. L., D. Chow, and J. S. Lam. 1997. *Pseudomonas aeruginosa* B-band O-antigen chain length is modulated by Wzz (Ro1). *Journal of Bacteriology* 179:1482-1489.
64. Hancock, R. E., L. M. Mutharia, L. Chan, R. P. Darveau, D. P. Speert, and G. B. Pier. 1983. *Pseudomonas aeruginosa* isolates from patients with cystic fibrosis: a class of serum-sensitive, nontypable strains deficient in lipopolysaccharide O side chains. *Infection and Immunity* 42:170-177.
65. Raymond, C. K., E. H. Sims, A. Kas, D. H. Spencer, T. V. Kutyavin, R. G. Ivey, Y. Zhou, R. Kaul, J. B. Clendenning, and M. V. Olson. 2002. Genetic variation at the O-antigen biosynthetic locus in *Pseudomonas aeruginosa*. *Journal of Bacteriology* 184:3614-3622.
66. Knirel, Y., E. V. Vinogradov, N. A. Kocharova, N. A. Paramonov, N. K. Kochetkov, B. A. Dmitriev, E. S. Stanislavsky, and B. Lanyi. 1988. The structure of O-specific polysaccharides and serological classification of *Pseudomonas aeruginosa* (a review). *Acta Microbiologica Hungarica* 35:3-24.
67. Stanislavsky, E. S., and J. S. Lam. 1997. *Pseudomonas aeruginosa* antigens as potential vaccines. *FEMS Microbiology Reviews* 21:243-277.
68. Liu, P. V., H. Matsumoto, H. Kusama, and T. O. M. Bergan. 1983. Survey of heat-stable major somatic antigens of *Pseudomonas aeruginosa*. *International Journal of Systematic Bacteriology* 33:256-264.
69. Liu, P. V., and S. Wang. 1990. Three new major somatic antigens of *Pseudomonas aeruginosa*. *Journal of Clinical Microbiology* 28:922-925.
70. Knirel, Y. A., O. V. Bystrova, N. A. Kocharova, U. Zähringer, and G. B. Pier. 2006. Review: conserved and variable structural features in the lipopolysaccharide of Pseudomonas aeruginosa. *Journal of Endotoxin Research* 12:324-336.
71. Bystrova, O. V., Y. A. Knirel, B. Lindner, N. A. Kocharova, A. N. Kondakova, U. Zähringer, and G. B. Pier. 2006. Structures of the core oligosaccharide and O-units in the R-and SR-type lipopolysaccharides of reference strains of *Pseudomonas aeruginosa* O-serogroups. *FEMS Immunology & Medical Microbiology* 46:85-99.
72. Islam, S. T., and J. S. Lam. 2014. Synthesis of bacterial polysaccharides via the Wzx/Wzy-dependent pathway. *Canadian Journal of Microbiology* 60:697-716.
73. Lányi, B., and T. Bergan. 1978. Chapter IV Serological Characterization of *Pseudomonas aeruginosa*. *Methods in Microbiology* 10:93-168.
74. Fisher, M. W., H. B. Devlin, and F. J. Gnabasik. 1969. New immunotype schema for *Pseudomonas aeruginosa* based on protective antigens. *Journal of Bacteriology* 98:835-836.

75. Wilkinson, S. G. 1983. Composition and structure of lipopolysaccharides from *Pseudomonas aeruginosa*. *Reviews of Infectious Diseases* 5:S941-S949.
76. Kneidinger, B., K. O'Riordan, J. Li, J.-R. Brisson, J. C. Lee, and J. S. Lam. 2003. Three highly conserved proteins catalyze the conversion of UDP-N-acetyl-d-glucosamine to precursors for the biosynthesis of O antigen in *Pseudomonas aeruginosa* O11 and capsule in *Staphylococcus aureus* Type 5. *Journal of Biological Chemistry* 278:3615-3627.
77. Westman, E. L., A. Preston, R. A. Field, and J. S. Lam. 2008. Biosynthesis of a rare di-N-acetylated sugar in the lipopolysaccharides of both *Pseudomonas aeruginosa* and *Bordetella pertussis* occurs via an identical scheme despite different gene clusters. *Journal of Bacteriology* 190:6060-6069.
78. King, J. D., E. Vinogradov, V. Tran, and J. S. Lam. 2010. Biosynthesis of uronamide sugars in *Pseudomonas aeruginosa* O6 and *Escherichia coli* O121 O antigens. *Environmental Microbiology* 12:1531-1544.
79. Stenutz, R., A. Weintraub, and G. Widmalm. 2006. The structures of *Escherichia coli* O-polysaccharide antigens. *FEMS Microbiology Reviews* 30:382-403.
80. Liu, B., Y. A. Knirel, L. Feng, A. V. Perepelov, S. y. N. Senchenkova, Q. Wang, P. R. Reeves, and L. Wang. 2008. Structure and genetics of *Shigella* O antigens. *FEMS Microbiology Reviews* 32:627-653.
81. Liu, B., Y. A. Knirel, L. Feng, A. V. Perepelov, S. y. N. Senchenkova, P. R. Reeves, and L. Wang. 2014. Structural diversity in *Salmonella* O antigens and its genetic basis. *FEMS Microbiology Reviews* 38:56-89.
82. Reeves, P. R., M. M. Cunneen, B. Liu, and L. Wang. 2013. Genetics and evolution of the *Salmonella* galactose-initiated set of O antigens. *PLoS One* 8:e69306.
83. Makin, S. A., and T. J. Beveridge. 1996. The influence of A-band and B-band lipopolysaccharide on the surface characteristics and adhesion of *Pseudomonas aeruginosa* to surfaces. *Microbiology* 142:299-307.
84. Bystrova, O. V., A. S. Shashkov, N. A. Kocharova, Y. A. Knirel, B. Lindner, U. Zähringer, and G. B. Pier. 2002. Structural studies on the core and the O-polysaccharide repeating unit of *Pseudomonas aeruginosa* immunotype 1 lipopolysaccharide. *European Journal of Biochemistry* 269:2194-2203.
85. Lányi, B. 1966/1967. Serological properties of *Pseudomonas aeruginosa*. I. Group-specific somatic antigens. *Acta microbiologica Academiae Scientiarum Hungaricae* 13:295.
86. Knirel, Y. A., E. V. Vinogradov, A. S. Shashkov, B. A. Dmitriev, N. K. Kochetkov, E. S. Stanislavsky, and G. M. Mashilova. 1985. Somatic antigens of *Pseudomonas aeruginosa*. The structure of the O-specific polysaccharide chains of lipopolysaccharides of *P. aeruginosa* serogroup O4 (Lányi) and related serotype O6 (Habs) and immunotype 1 (Fisher). *European Journal of Biochemistry/FEBS* 150:541.
87. Knirel, Y. A., A. S. Shashkov, B. A. Dmitriev, and N. K. Kochetkov. 1984. Structural studies of the *Pseudomonas aeruginosa* immunotype 1 antigen, containing the new sugar constituents 2-acetamido-2-deoxy-D-galacturonamide and 2-deoxy-2-formamido-D-galacturonic acid. *Carbohydrate Research* 133:C12-C14.
88. Vinogradov, E. V., Y. A. Knirel, A. S. Shashkov, and N. K. Kochetkov. 1987. Determination of the degree of amidation of 2-deoxy-2-formamido-d-galacturonic acid in

O-specific polysaccharides of *Pseudomonas aeruginosa* O4 and related strains. *Carbohydrate Research* 170:C1-C4.
89. Kocharova, N. A., Y. A. Knirel, G. Widmalm, P.-E. Jansson, and A. P. Moran. 2000. Structure of an atypical O-antigen polysaccharide of *Helicobacter pylori* containing a novel monosaccharide 3-C-methyl-D-mannose. *Biochemistry* 39:4755-4760.
90. Senchenkova, S. y. N., A. S. Shashkov, Y. A. Knirel, J. J. McGovern, and A. P. Moran. 1996. The O-specific polysaccharide chain of *Campylobacter fetus* serotype B lipopolysaccharide is a d-rhamnan terminated with 3-O-methyl-d-rhamnose (d-acofriose). *European Journal of Biochemistry* 239:434-438.
91. Molinaro, A., A. Silipo, R. Lanzetta, M.-A. Newman, J. M. Dow, and M. Parrilli. 2003. Structural elucidation of the O-chain of the lipopolysaccharide from *Xanthomonas campestris* strain 8004. *Carbohydrate Research* 338:277-281.
92. Ovod, V., K. Rudolph, Y. Knirel, and K. Krohn. 1996. Immunochemical characterization of O polysaccharides composing the alpha-D-rhamnose backbone of lipopolysaccharide of *Pseudomonas syringae* and classification of bacteria into serogroups O1 and O2 with monoclonal antibodies. *Journal of Bacteriology* 178:6459-6465.
93. Senchenkova, S. y. N., X. Huang, P. Laux, Y. A. Knirel, A. S. Shashkov, and K. Rudolph. 2002. Structures of the O-polysaccharide chains of the lipopolysaccharides of *Xanthomonas campestris* pv. phaseoli var. fuscans GSPB 271 and *X. campestris* pv. malvacearum GSPB 1386 and GSPB 2388. *Carbohydrate Research* 337:1723-1728.
94. Arsenault, T. L., D. W. Hughes, D. B. MacLean, W. A. Szarek, A. M. B. Kropinski, and J. S. Lam. 1991. Structural studies on the polysaccharide portion of 'A-band' lipopolysaccharide from a mutant (AK1401) of *Pseudomonas aeruginosa* strain PAO1. *Canadian Journal of Chemistry* 69:1273-1280.
95. Yokota, S., S. Kaya, Y. Araki, E. Ito, T. Kawamura, and S. Sawada. 1990. Occurrence of D-rhamnan as the common antigen reactive against monoclonal antibody E87 in *Pseudomonas aeruginosa* IFO 3080 and other strains. *Journal of Bacteriology* 172:6162-6164.
96. Yokota, S.-i., S. Kaya, S. Sawada, T. Kawamura, Y. Araki, and E. Ito. 1987. Characterization of a polysaccharide component of lipopolysaccharide from *Pseudomonas aeruginosa* IID 1008 (ATCC 27584) as D-rhamnan. *European Journal of Biochemistry* 167:203-209.
97. Choudhury, B., R. W. Carlson, and J. B. Goldberg. 2005. The structure of the lipopolysaccharide from a galU mutant of *Pseudomonas aeruginosa* serogroup-O11. *Carbohydrate Research* 340:2761-2772.
98. Vinogradov, E. V., A. S. Shashkov, Y. A. Knirel, G. M. Zdorovenko, L. P. Solyanik, and R. I. Gvozdyak. 1991. Somatic antigens of pseudomonads: structure of the O-specific polysaccharide chain of Pseudomonas syringae pv. syringae (cerasi) 435 lipopolysaccharide. *Carbohydrate Research* 212:295-299.
99. Smith, A. R. W., S. E. Zamze, S. M. Munro, K. J. Carter, and R. C. Hignett. 1985. Structure of the sidechain of lipopolysaccharide from *Pseudomonas syringae* pv. *morsprunorum* C28. *European Journal of Biochemistry* 149:73-78.
100. Cérantola, S., and H. Montrozier. 1997. Structural elucidation of two polysaccharides present in the lipopolysaccharide of a clinical isolate of *Burkholderia cepacia*. *European Journal of Biochemistry* 246:360-366.

101. Winn, A. M., and S. G. Wilkinson. 1998. The O7 antigen of *Stenotrophomonas maltophilia* is a linear D-rhamnan with a trisaccharide repeating unit that is also present in polymers from some *Pseudomonas* and *Burkholderia* species. *FEMS Microbiology Letters* 166:57-61.
102. Dalbøge, C. S., C. R. Hansen, T. Pressler, N. Høiby, and H. K. Johansen. 2011. Chronic pulmonary infection with Stenotrophomonas maltophilia and lung function in patients with cystic fibrosis. *Journal of Cystic Fibrosis* 10:318-325.
103. Waters, V. J., M. I. Gómez, G. Soong, S. Amin, R. K. Ernst, and A. Prince. 2007. Immunostimulatory properties of the emerging pathogen *Stenotrophomonas maltophilia*. *Infection and Immunity* 75:1698-1703.
104. Matewish, J. M. 2004. The functional role of lipopolysaccharide in the cell envelope and surface proteins of *Pseudomonas aeruginosa*. In *University of Guelph. Department of, Microbiology*. University of Guelph.
105. Murphy, K., A. J. Park, Y. Hao, D. Brewer, J. S. Lam, and C. M. Khursigara. 2014. Influence of O polysaccharides on biofilm development and outer membrane vesicle biogenesis in *Pseudomonas aeruginosa* PAO1. *Journal of Bacteriology* 196:1306-1317.
106. Rocchetta, H. L., and J. S. Lam. 1997. Identification and functional characterization of an ABC transport system involved in polysaccharide export of A-band lipopolysaccharide in *Pseudomonas aeruginosa*. *Journal of Bacteriology* 179:4713-4724.
107. Hao, Y., J. D. King, S. Huszczynski, D. Kocíncová, and J. S. Lam. 2013. Five new genes are important for common polysaccharide antigen biosynthesis in *Pseudomonas aeruginosa*. *MBio* 4:e00631-00612.
108. Greenfield, L. K., and C. Whitfield. 2012. Synthesis of lipopolysaccharide O-antigens by ABC transporter-dependent pathways. *Carbohydrate Research* 356:12-24.
109. Masoud, H., I. Sadovskaya, T. de Kievit, E. Altman, J. C. Richards, and J. S. Lam. 1995. Structural elucidation of the lipopolysaccharide core region of the O-chain-deficient mutant strain A28 from *Pseudomonas aeruginosa* serotype 06 (International Antigenic Typing Scheme). *Journal of Bacteriology* 177:6718-6726.
110. Sadovskaya, I., J.-R. Brisson, J. S. Lam, J. C. Richards, and E. Altman. 1998. Structural elucidation of the lipopolysaccharide core regions of the wild-type strain PAO1 and O-chain-deficient mutant strains AK1401 and AK1012 from *Pseudomonas aeruginosa* serotype O5. *The FEBS Journal* 255:673-684.
111. Sadovskaya, I., J.-R. Brisson, P. Thibault, J. C. Richards, J. S. Lam, and E. Altman. 2000. Structural characterization of the outer core and the O-chain linkage region of lipopolysaccharide from *Pseudomonas aeruginosa* serotype O5. *The FEBS Journal* 267:1640-1650.
112. Bystrova, O. V., B. Lindner, H. Moll, N. A. Kocharova, Y. A. Knirel, U. ZÃ¤hringer, and G. B. Pier. 2003. Structure of the lipopolysaccharide of *Pseudomonas aeruginosa* O-12 with a randomly O-acetylated core region. *Carbohydrate Research* 338:1895-1905.
113. Kooistra, O., G. Bedoux, L. Brecker, B. Lindner, P. S. Carballo, D. Haras, and U. Zähringer. 2003. Structure of a highly phosphorylated lipopolysaccharide core in the ΔalgC mutants derived from *Pseudomonas aeruginosa* wild-type strains PAO1 (serogroup O5) and PAC1R (serogroup O3). *Carbohydrate Research* 338:2667-2677.

114. Bystrova, O. V., B. Lindner, H. Moll, N. A. Kocharova, Y. A. Knirel, U. Zahringer, and G. B. Pier. 2004. Full structure of the lipopolysaccharide of *Pseudomonas aeruginosa* immunotype 5. *Biochemistry (Moscow)* 69:170-175.
115. Kintz, E., and J. B. Goldberg. 2008. Regulation of lipopolysaccharide O antigen expression in *Pseudomonas aeruginosa*. *Future Microbiology* 3:191-203.
116. de Kievit, T. R., and J. S. Lam. 1994. Monoclonal antibodies that distinguish inner core, outer core, and lipid A regions of *Pseudomonas aeruginosa* lipopolysaccharide. *Journal of Bacteriology* 176:7129-7139.
117. Walsh, A. G., M. J. Matewish, L. L. Burrows, M. A. Monteiro, M. B. Perry, and J. S. Lam. 2000. Lipopolysaccharide core phosphates are required for viability and intrinsic drug resistance in *Pseudomonas aeruginosa*. *Molecular Microbiology* 35:718-727.
118. Schnaitman, C. A., and J. D. Klena. 1993. Genetics of lipopolysaccharide biosynthesis in enteric bacteria. *Microbiological Reviews* 57:655-682.
119. Rivera, M., and E. J. McGroarty. 1989. Analysis of a common-antigen lipopolysaccharide from *Pseudomonas aeruginosa*. *Journal of Bacteriology* 171:2244-2248.
120. Kulshin, V. A., U. Zähringer, B. Lindner, K.-E. Jäger, B. A. Dmitriev, and E. T. Rietschel. 1991. Structural characterization of the lipid A component of *Pseudomonas aeruginosa* wild-type and rough mutant lipopolysaccharides. *The FEBS Journal* 198:697-704.
121. Ernst, R. K., S. M. Moskowitz, J. C. Emerson, G. M. Kraig, K. N. Adams, M. D. Harvey, B. Ramsey, D. P. Speert, J. L. Burns, and S. I. Miller. 2007. Unique lipid A modifications in Pseudomonas aeruginosa isolated from the airways of patients with cystic fibrosis. *The Journal of Infectious Diseases* 196:1088-1092.
122. Bhat, R., A. Marx, C. Galanos, and R. S. Conrad. 1990. Structural studies of lipid A from *Pseudomonas aeruginosa* PAO1: occurrence of 4-amino-4-deoxyarabinose. *Journal of Bacteriology* 172:6631-6636.
123. Moskowitz, S. M., R. K. Ernst, and S. I. Miller. 2004. PmrAB, a two-component regulatory system of *Pseudomonas aeruginosa* that modulates resistance to cationic antimicrobial peptides and addition of aminoarabinose to lipid A. *Journal of Bacteriology* 186:575-579.
124. Kindt, T. J., R. A. Goldsby, B. A. Osborne, and J. Kuby. 2007. *Kuby immunology*. W.H. Freeman, New York.
125. Hemachandra, S., K. Kamboj, J. Copfer, G. Pier, L. L. Green, and J. R. Schreiber. 2001. Human monoclonal antibodies against *Pseudomonas aeruginosa* lipopolysaccharide derived from transgenic mice containing megabase human immunoglobulin loci are opsonic and protective against fatal *Pseudomonas* sepsis. *Infection and Immunity* 69:2223-2229.
126. Mendez, M. J., L. L. Green, J. R. F. Corvalan, X.-C. Jia, C. E. Maynard-Currie, X.-d. Yang, M. L. Gallo, D. M. Louie, D. V. Lee, and K. L. Erickson. 1997. Functional transplant of megabase human immunoglobulin loci recapitulates human antibody response in mice. *Nature Genetics* 15:146-156.
127. McLean, M. D., K. C. Almquist, Y. Niu, R. Kimmel, Z. Lai, J. R. Schreiber, and J. C. Hall. 2007. A human anti-*Pseudomonas aeruginosa* serotype O6ad immunoglobulin G1

expressed in transgenic tobacco is capable of recruiting immune system effector function in vitro. *Antimicrobial Agents and Chemotherapy* 51:3322-3328.
128. Xie, X. 2009. Bactericidal activity and improvement of therapeutic potency of recombinant antibody fragments. In *Dept. of Environmental Biology*, PhD thesis ed. University of Guelph, Ontario, Canada.
129. Wang, Y., B. Qiao, Y. Wang, X. Han, Y. Chu, and S. Xiong. 2006. Autoantibodies closely relate to the elevation level of in vivo hydrogen peroxide and tissue damage in systemic lupus erythematosus. *DNA and Cell Biology* 25:563-570.
130. Wentworth, P., A. D. Wentworth, X. Zhu, I. A. Wilson, K. D. Janda, A. Eschenmoser, and R. A. Lerner. 2003. Evidence for the production of trioxygen species during antibody-catalyzed chemical modification of antigens. *Proceedings of the National Academy of Sciences* 100:1490-1493.
131. Datta, D., N. Vaidehi, X. Xu, and W. A. Goddard. 2002. Mechanism for antibody catalysis of the oxidation of water by singlet dioxygen. *Proceedings of the National Academy of Sciences* 99:2636-2641.
132. Xu, X., R. P. Muller, and W. A. Goddard. 2002. The gas phase reaction of singlet dioxygen with water: a water-catalyzed mechanism. *Proceedings of the National Academy of Sciences* 99:3376-3381.
133. Saveliev, A. N., D. R. Ivanen, A. A. Kulminskaya, N. A. Ershova, G. K. Tat'yana, V. N. Buneva, A. S. Mogelnitskii, B. M. Doronin, O. O. Favorova, and G. A. Nevinsky. 2003. Amylolytic activity of IgM and IgG antibodies from patients with multiple sclerosis. *Immunology Letters* 86:291-297.
134. Ivanen, D. R., A. A. Kulminskaya, N. A. Ershova, E. V. Eneyskaya, K. A. Shabalin, A. N. Savel ev, T. G. Kanyshkova, V. N. Buneva, G. A. Nevinsky, and K. N. Neustroev. 2002. Human autoantibodies with amylolytic activity. *Biologia-Bratislava* 57:253-264.
135. Ivanen, D. R., A. A. Kulminskaya, K. A. Shabalin, L. V. Isaeva-Ivanova, N. A. Ershova, A. N. Saveliev, G. A. Nevinsky, and K. N. Neustroev. 2004. Catalytic properties of IgMs with amylolytic activity isolated from patients with multiple sclerosis. *Medical Science Monitor* 10:BR273-BR280.
136. Savel'ev, A. N., G. K. Tat'yana, A. A. Kulminskaya, V. N. Buneva, E. V. Eneyskaya, M. V. Filatov, G. A. Nevinsky, and K. N. Neustroev. 2001. Amylolytic activity of IgG and sIgA immunoglobulins from human milk. *Clinica Chimica Acta* 314:141-152.
137. Oren, Z., and Y. Shai. 1998. Mode of action of linear amphipathic α-helical antimicrobial peptides. *Peptide Science* 47:451-463.
138. Papo, N., and Y. Shai. 2005. A molecular mechanism for lipopolysaccharide protection of Gram-negative bacteria from antimicrobial peptides. *Journal of Biological Chemistry* 280:10378-10387.
139. Shai, Y. 1999. Mechanism of the binding, insertion and destabilization of phospholipid bilayer membranes by α-helical antimicrobial and cell non-selective membrane-lytic peptides. *Biochimica et Biophysica Acta (BBA)-Biomembranes* 1462:55-70.
140. Oleksiewicz, M. B., G. b. Nagy, and E. Nagy. 2012. Anti-bacterial monoclonal antibodies: back to the future? *Archives of Biochemistry and Biophysics* 526:124-131.
141. LaRocca, T. J., L. I. Katona, D. G. Thanassi, and J. L. Benach. 2008. Bactericidal action of a complement-independent antibody against relapsing fever *Borrelia* resides in its variable region. *The Journal of Immunology* 180:6222-6228.

142. Colombo, M. J., D. Abraham, A. Shibuya, and K. R. Alugupalli. 2011. B1b lymphocyte-derived antibodies control *Borrelia hermsii* independent of Fcα/μ receptor and in the absence of host cell contact. *Immunologic Research* 51:249-256.
143. Lam, J. S., L. A. MacDonald, M. Y. Lam, L. G. Duchesne, and G. G. Southam. 1987. Production and characterization of monoclonal antibodies against serotype strains of *Pseudomonas aeruginosa*. *Infection and Immunity* 55:1051-1057.
144. Deng, S. J., C. R. MacKenzie, J. Sadowska, J. Michniewicz, N. M. Young, D. R. Bundle, and S. A. Narang. 1994. Selection of antibody single-chain variable fragments with improved carbohydrate binding by phage display. *Journal of Biological Chemistry* 269:9533-9538.
145. Cygler, M., D. R. Rose, and D. R. Bundle. 1991. Recognition of a cell-surface oligosaccharide of pathogenic Salmonella by an antibody Fab fragment. *Science* 253:442-446.
146. Bundle, D. R., E. Eichler, M. A. J. Gidney, M. Meldal, A. Ragauskas, B. W. Sigurskjold, B. Sinnott, D. C. Watson, M. Yaguchi, and N. M. Young. 1994. Molecular recognition of a *Salmonella* trisaccharide epitope by monoclonal antibody Se155-4. *Biochemistry* 33:5172-5182.
147. Gidney, M. A. J., J. S. Plested, S. Lacelle, P. A. Coull, J. C. Wright, K. Makepeace, J.-R. Brisson, A. D. Cox, E. R. Moxon, and J. C. Richards. 2004. Development, characterization, and functional activity of a panel of specific monoclonal antibodies to inner core lipopolysaccharide epitopes in *Neisseria meningitidis*. *Infection and Immunity* 72:559-569.
148. Young, N. M., D. C. Watson, A. M. Cunningham, and C. R. MacKenzie. 2014. The intrinsic cysteine and histidine residues of the anti-*Salmonella* antibody Se155-4: a model for the introduction of new functions into antibody-binding sites. *Protein Engineering Design and Selection* 27:383-390.
149. Parker, M. J., K. Gomery, G. Richard, C. R. MacKenzie, A. D. Cox, J. C. Richards, and S. V. Evans. 2014. Structural basis for selective cross-reactivity in a bactericidal antibody against inner core lipooligosaccharide from Neisseria meningitidis. *Glycobiology* 24:442-449.
150. Woods, D. E., J. S. Lam, W. Paranchych, D. P. Speert, M. Campbell, and A. J. Godfrey. 1997. Correlation of *Pseudomonas aeruginosa* virulence factors from clinical and environmental isolates with pathogenicity in the neutropenic mouse. *Canadian Journal of Microbiology* 43:541-551.
151. Pasloske, B. L., B. B. Finlay, and W. Paranchych. 1985. Cloning and sequencing of the *Pseudomonas aeruginosa* PAK pilin gene. *FEBS Letters* 183:413-416.
152. Bélanger, M., L. L. Burrows, and J. S. Lam. 1999. Functional analysis of genes responsible for the synthesis of the B-band O antigen of *Pseudomonas aeruginosa* serotype O6 lipopolysaccharide. *Microbiology* 145:3505-3521.
153. Rahim, R., L. L. Burrows, M. A. Monteiro, M. B. Perry, and J. S. Lam. 2000. Involvement of the rml locus in core oligosaccharide and O polysaccharide assembly in *Pseudomonas aeruginosa*. *Microbiology* 146:2803-2814.
154. Coyne, M. J., K. S. Russell, C. L. Coyle, and J. B. Goldberg. 1994. The *Pseudomonas aeruginosa* algC gene encodes phosphoglucomutase, required for the synthesis of a complete lipopolysaccharide core. *Journal of Bacteriology* 176:3500-3507.

155. Jarrell, K. F., and A. M. Kropinski. 1981. Isolation and characterization of a bacteriophage specific for the lipopolysaccharide of rough derivatives of *Pseudomonas aeruginosa* strain PAO. *Journal of Virology* 38:529-538.
156. Berry, D., and A. M. Kropinski. 1986. Effect of lipopolysaccharide mutations and temperature on plasmid transformation efficiency in *Pseudomonas aeruginosa*. *Canadian Journal of Microbiology* 32:436-438.
157. Arsenault, T. L., D. W. Hughes, D. B. MacLean, W. A. Szarek, A. M. B. Kropinski, and J. S. Lam. 1991. Structural studies on the polysaccharide portion of "A-band" lipopolysaccharide from a mutant (AK1401) of *Pseudomonas aeruginosa* strain PAO1. *Canadian Journal of Chemistry* 69:1273-1280.
158. Hitchcock, P. J., and T. M. Brown. 1983. Morphological heterogeneity among *Salmonella* lipopolysaccharide chemotypes in silver-stained polyacrylamide gels. *Journal of Bacteriology* 154:269-277.
159. Westphal, O. 1965. Bacterial lipopolysaccharide-extraction with phenol water and further application of procedure. *Methods in Carbohydrate Chemistry* 1:83-91.
160. Masoud, H., E. R. Moxon, A. Martin, D. Krajcarski, and J. C. Richards. 1997. Structure of the variable and conserved lipopolysaccharide oligosaccharide epitopes expressed by *Haemophilus influenzae* serotype b strain Eagan. *Biochemistry* 36:2091-2103.
161. St Michael, F., T. J. Inzana, and A. D. Cox. 2006. Structural analysis of the lipooligosaccharide-derived oligosaccharide of *Histophilus somni* (*Haemophilus somnus*) strain 8025. *Carbohydrate Research* 341:281-284.
162. Lefranc, M.-P., C. Pommié, M. Ruiz, V. Giudicelli, E. Foulquier, L. Truong, V. Thouvenin-Contet, and G. Lefranc. 2003. IMGT unique numbering for immunoglobulin and T cell receptor variable domains and Ig superfamily V-like domains. *Developmental & Comparative Immunology* 27:55-77.
163. Pommié, C., S. Levadoux, R. Sabatier, G. Lefranc, and M.-P. Lefranc. 2004. IMGT standardized criteria for statistical analysis of immunoglobulin V-REGION amino acid properties. *Journal of Molecular Recognition* 17:17-32.
164. Wang, G., X. Li, and Z. Wang. 2009. APD2: the updated antimicrobial peptide database and its application in peptide design. *Nucleic Acids Research* 37:D933-D937.
165. Wang, Z., and G. Wang. 2004. APD: the antimicrobial peptide database. *Nucleic Acids Research* 32:D590-D592.
166. Wang, G., X. Li, and Z. Wang. 2016. APD3: the antimicrobial peptide database as a tool for research and education. *Nucleic Acids Research* 44:D1087-D1093.
167. Kyte, J., and R. F. Doolittle. 1982. A simple method for displaying the hydropathic character of a protein. *Journal of Molecular Biology* 157:105-132.
168. Arndt, K. M., K. M. Müller, and A. Plückthun. 1998. Factors influencing the dimer to monomer transition of an antibody single-chain Fv fragment. *Biochemistry* 37:12918-12926.
169. Kortt, A. A., M. Lah, G. W. Oddie, C. L. Gruen, J. E. Burns, L. A. Pearce, J. L. Atwell, A. J. McCoy, G. J. Howlett, and D. W. Metzger. 1997. Single-chain Fv fragments of anti-neuraminidase antibody NC10 containing five-and ten-residue linkers form dimers and with zero-residue linker a trimer. *Protein Engineering* 10:423-433.
170. Whitlow, M., B. A. Bell, S.-L. Feng, D. Filpula, K. D. Hardman, S. L. Hubert, M. L. Rollence, J. F. Wood, M. E. Schott, and D. E. Milenic. 1993. An improved linker for

single-chain Fv with reduced aggregation and enhanced proteolytic stability. *Protein Engineering* 6:989-995.
171. Wörn, A., and A. Plückthun. 2001. Stability engineering of antibody single-chain Fv fragments. *Journal of Molecular Biology* 305:989-1010.
172. Müller-Loennies, S., C. R. MacKenzie, S. I. Patenaude, S. V. Evans, P. Kosma, H. Brade, L. Brade, and S. Narang. 2000. Characterization of high affinity monoclonal antibodies specific for chlamydial lipopolysaccharide. *Glycobiology* 10:121-130.
173. Chua, J. E. H., P. A. Manning, and R. Morona. 1999. The *Shigella flexneri* bacteriophage Sf6 tailspike protein (TSP)/endorhamnosidase is related to the bacteriophage P22 TSP and has a motif common to exo-and endoglycanases, and C-5 epimerases. *Microbiology* 145:1649-1659.
174. Lindberg, A. A., R. Wollin, P. Gemski, and J. A. Wohlhieter. 1978. Interaction between bacteriophage Sf6 and Shigella flexneri. *Journal of Virology* 27:38-44.
175. Miyashita, H., T. Hara, R. Tanimura, F. Tanaka, M. Kikuchi, and I. Fujii. 1994. A common ancestry for multiple catalytic antibodies generated against a single transition-state analog. *Proceedings of the National Academy of Sciences* 91:6045-6049.
176. Andersen, P. S., M. Haahr-Hansen, V. W. Coljee, F. R. Hinnerfeldt, K. Varming, S. Bregenholt, and J. S. Haurum. 2007. Extensive restrictions in the VH sequence usage of the human antibody response against the Rhesus D antigen. *Molecular Immunology* 44:412-422.
177. Bye, J. M., C. Carter, Y. Cui, B. D. Gorick, S. Songsivilai, G. Winter, N. C. Hughes-Jones, and J. D. Marks. 1992. Germline variable region gene segment derivation of human monoclonal anti-Rh (D) antibodies. Evidence for affinity maturation by somatic hypermutation and repertoire shift. *Journal of Clinical Investigation* 90:2481.
178. Lucas, A. H., K. D. Moulton, V. R. Tang, and D. C. Reason. 2001. Combinatorial library cloning of human antibodies to *Streptococcus pneumoniae* capsular polysaccharides: variable region primary structures and evidence for somatic mutation of Fab fragments specific for capsular serotypes 6B, 14, and 23F. *Infection and Immunity* 69:853-864.
179. Zhou, J., K. R. Lottenbach, S. J. Barenkamp, A. H. Lucas, and D. C. Reason. 2002. Recurrent variable region gene usage and somatic mutation in the human antibody response to the capsular polysaccharide of *Streptococcus pneumoniae* type 23F. *Infection and Immunity* 70:4083-4091.
180. Russell, N. D., J. R. F. Corvalan, M. L. Gallo, C. G. Davis, and L.-a. Pirofski. 2000. Production of protective human antipneumococcal antibodies by transgenic mice with human immunoglobulin loci. *Infection and Immunity* 68:1820-1826.
181. Poon, K. K. H., E. L. Westman, E. Vinogradov, S. Jin, and J. S. Lam. 2008. Functional characterization of MigA and WapR: putative rhamnosyltransferases involved in outer core oligosaccharide biosynthesis of *Pseudomonas aeruginosa*. *Journal of Bacteriology* 190:1857-1865.
182. LaRocca, T. J., and J. L. Benach. 2008. The important and diverse roles of antibodies in the host response to *Borrelia* infections. In *Specialization and complementation of humoral immune responses to infection. Current Topics in Microbiology and Immunology*. T. Manser, ed. Springer. 63-103.

183. Connolly, S. E., and J. L. Benach. 2001. Cutting edge: the spirochetemia of murine relapsing fever is cleared by complement-independent bactericidal antibodies. *The Journal of Immunology* 167:3029-3032.
184. Šadžiene, A., P. A. Thompson, and A. G. Barbour. 1993. In vitro inhibition of *Borrelia burgdorferi* growth by antibodies. *Journal of Infectious Diseases* 167:165-172.
185. Becker, M., J. Bunikis, B. D. Lade, J. J. Dunn, A. G. Barbour, and C. L. Lawson. 2005. Structural investigation of *Borrelia burgdorferi* OspB, a bactericidal Fab target. *Journal of Biological Chemistry* 280:17363-17370.
186. Katona, L. I., S. Ayalew, J. L. Coleman, and J. L. Benach. 2000. A bactericidal monoclonal antibody elicits a change in its antigen, OspB of *Borrelia burgdorferi*, that can be detected by limited proteolysis. *The Journal of Immunology* 164:1425-1431.
187. Polonelli, L., J. Pontón, N. Elguezabal, M. D. Moragues, C. Casoli, E. Pilotti, P. Ronzi, A. S. Dobroff, E. G. Rodrigues, and M. A. Juliano. 2008. Antibody complementarity-determining regions (CDRs) can display differential antimicrobial, antiviral and antitumor activities. *PLoS One* 3:e2371.
188. Bechinger, B. 1999. The structure, dynamics and orientation of antimicrobial peptides in membranes by multidimensional solid-state NMR spectroscopy. *Biochimica et Biophysica Acta (BBA)-Biomembranes* 1462:157-183.
189. Braga, P. C., and D. Ricci. 1998. Atomic force microscopy: application to investigation of *Escherichia coli* morphology before and after exposure to cefodizime. *Antimicrobial Agents and Chemotherapy* 42:18-22.
190. Amro, N. A., L. P. Kotra, K. Wadu-Mesthrige, A. Bulychev, S. Mobashery, and G.-y. Liu. 2000. High-resolution atomic force microscopy studies of the *Escherichia coli* outer membrane: structural basis for permeability. *Langmuir* 16:2789-2796.
191. Rashid, M. H., and A. Kornberg. 2000. Inorganic polyphosphate is needed for swimming, swarming, and twitching motilities of *Pseudomonas aeruginosa*. *Proceedings of the National Academy of Sciences* 97:4885-4890.
192. McCarter, L., and M. Silverman. 1990. Surface-induced swarmer cell differentiation of *Vibrio parahaemoiyticus*. *Molecular Microbiology* 4:1057-1062.
193. Allison, C., and C. Hughes. 1991. Bacterial swarming: an example of prokaryotic differentiation and multicellular behaviour. *Science Progress* 75:403-422.
194. Harshey, R. M. 1994. Bees aren't the only ones: swarming in Gram-negative bacteria. *Molecular Microbiology* 13:389-394.
195. Beveridge, T. J., and J. L. Kadurugamuwa. 1996. Periplasm, periplasmic spaces, and their relation to bacterial wall structure: novel secretion of selected periplasmic proteins from *Pseudomonas aeruginosa*. *Microbial Drug Resistance* 2:1-8.
196. Kadurugamuwa, J. L., and T. J. Beveridge. 1997. Natural release of virulence factors in membrane vesicles by *Pseudomonas aeruginosa* and the effect of aminoglycoside antibiotics on their release. *Journal of Antimicrobial Chemotherapy* 40:615-621.
197. Mayrand, D., and D. Grenier. 1989. Biological activities of outer membrane vesicles. *Canadian Journal of Microbiology* 35:607-613.
198. Kadurugamuwa, J. L., and T. J. Beveridge. 1995. Virulence factors are released from *Pseudomonas aeruginosa* in association with membrane vesicles during normal growth and exposure to gentamicin: a novel mechanism of enzyme secretion. *Journal of Bacteriology* 177:3998-4008.

199. Meincken, M., D. L. Holroyd, and M. Rautenbach. 2005. Atomic force microscopy study of the effect of antimicrobial peptides on the cell envelope of *Escherichia coli*. *Antimicrobial Agents and Chemotherapy* 49:4085-4092.
200. Hyldgaard, M., T. Mygind, B. S. Vad, M. Stenvang, D. E. Otzen, and R. L. Meyer. 2014. The antimicrobial mechanism of action of epsilon-poly-L-lysine. *Applied and Environmental Microbiology* 80:7758-7770.
201. da Silva, A., and O. Teschke. 2003. Effects of the antimicrobial peptide PGLa on live *Escherichia coli*. *Biochimica et Biophysica Acta (BBA)-Molecular Cell Research* 1643:95-103.
202. Lau, P. C. Y., T. Lindhout, T. J. Beveridge, J. R. Dutcher, and J. S. Lam. 2009. Differential lipopolysaccharide core capping leads to quantitative and correlated modifications of mechanical and structural properties in *Pseudomonas aeruginosa* biofilms. *Journal of Bacteriology* 191:6618-6631.
203. Ivanov, I. E., E. N. Kintz, L. A. Porter, J. B. Goldberg, N. A. Burnham, and T. A. Camesano. 2011. Relating the physical properties of *Pseudomonas aeruginosa* lipopolysaccharides to virulence by atomic force microscopy. *Journal of Bacteriology* 193:1259-1266.
204. Kotra, L. P., N. A. Amro, G.-Y. Liu, and S. Mobashery. 2000. FEATURES - Visualizing bacteria at high resolution-atomic force microscopy combined with computational simulations provide insights about LPS, other surface features of bacterial cells. *ASM News-American Society for Microbiology* 66:675-681.
205. Alakomi, H. L., A. Paananen, M. L. Suihko, I. M. Helander, and M. Saarela. 2006. Weakening effect of cell permeabilizers on gram-negative bacteria causing biodeterioration. *Applied and Environmental Microbiology* 72:4695-4703.
206. Fu, Y., Y. Zu, L. Chen, T. Efferth, H. Liang, Z. Liu, and W. Liu. 2007. Investigation of antibacterial activity of rosemary essential oil against *Propionibacterium acnes* with atomic force microscopy. *Planta Medica* 73:1275.
207. Kintz, E., J. M. Scarff, A. DiGiandomenico, and J. B. Goldberg. 2008. Lipopolysaccharide O-antigen chain length regulation in *Pseudomonas aeruginosa* serogroup O11 strain PA103. *Journal of Bacteriology* 190:2709-2716.
208. Martínez-Morales, F., M. Schobert, I. M. Lopez-Lara, and O. Geiger. 2003. Pathways for phosphatidylcholine biosynthesis in bacteria. *Microbiology* 149:3461-3471.

APPENDIX

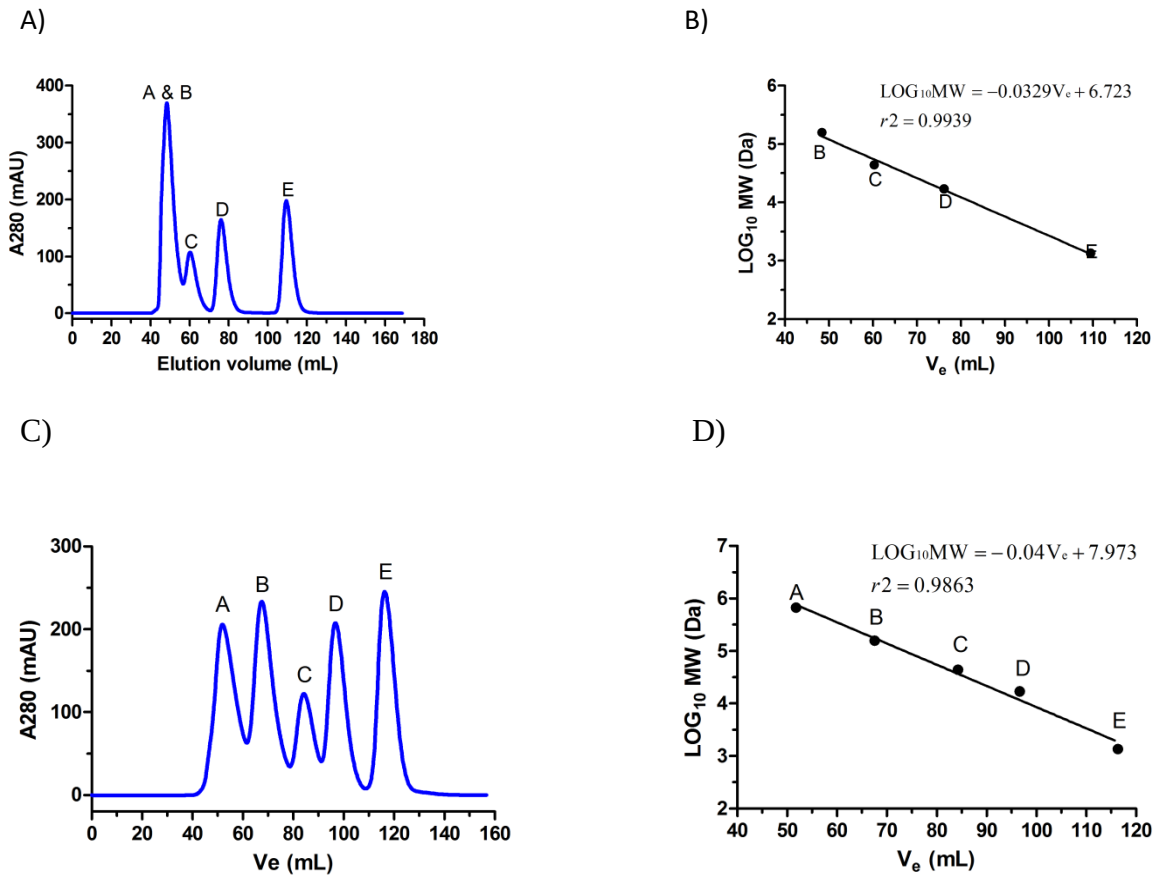

Figure 42. A) SEC Superdex™ S75 16/60 elution and its B) standard curve. C) SEC Superdex™ S200 16/60 elution and its D) standard curve.

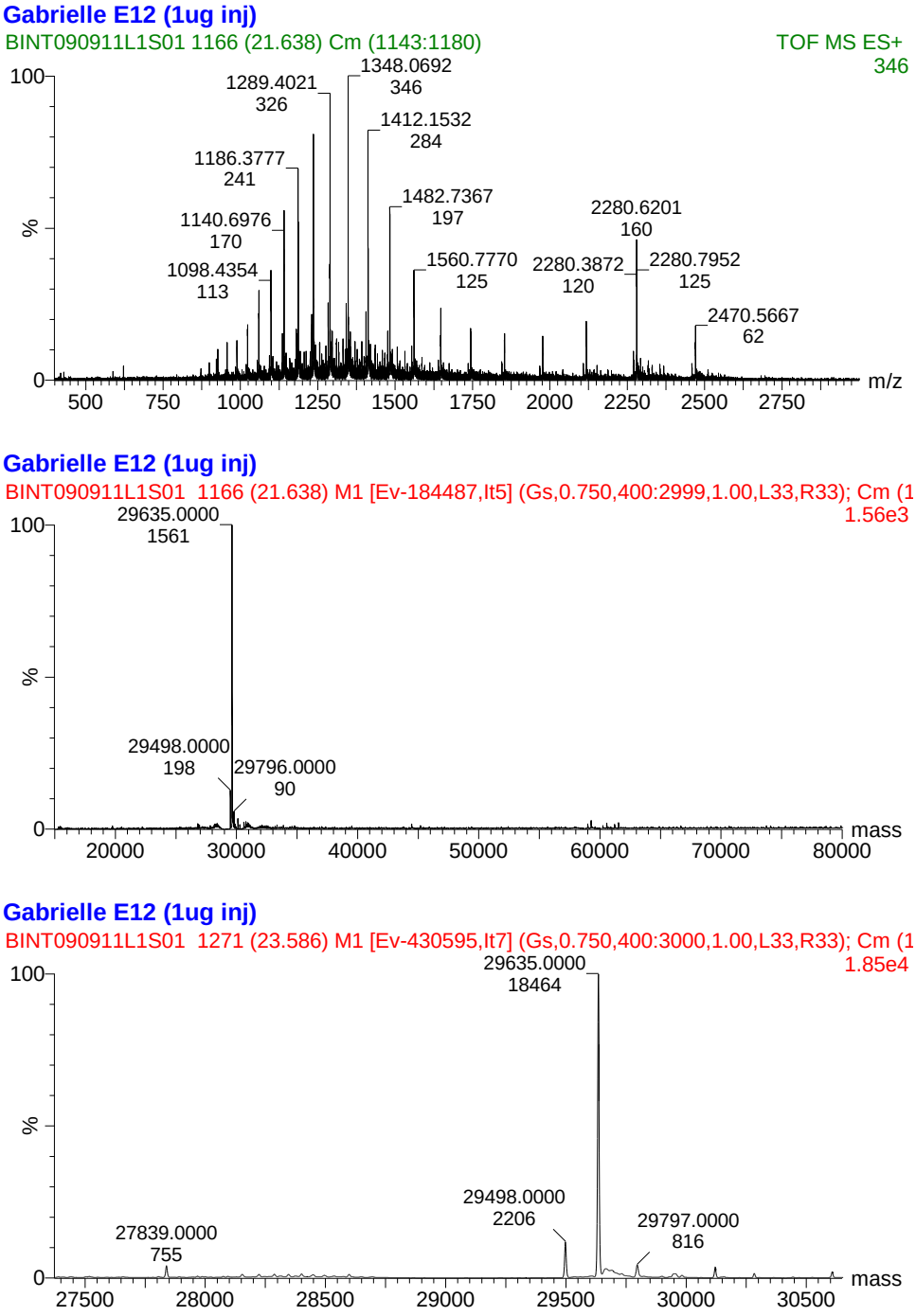

Figure 43. Mass spectroscopy analysis of S75 fraction E12, the S20 scFv monomer. Its MW was determined to be 29.6 kDa.

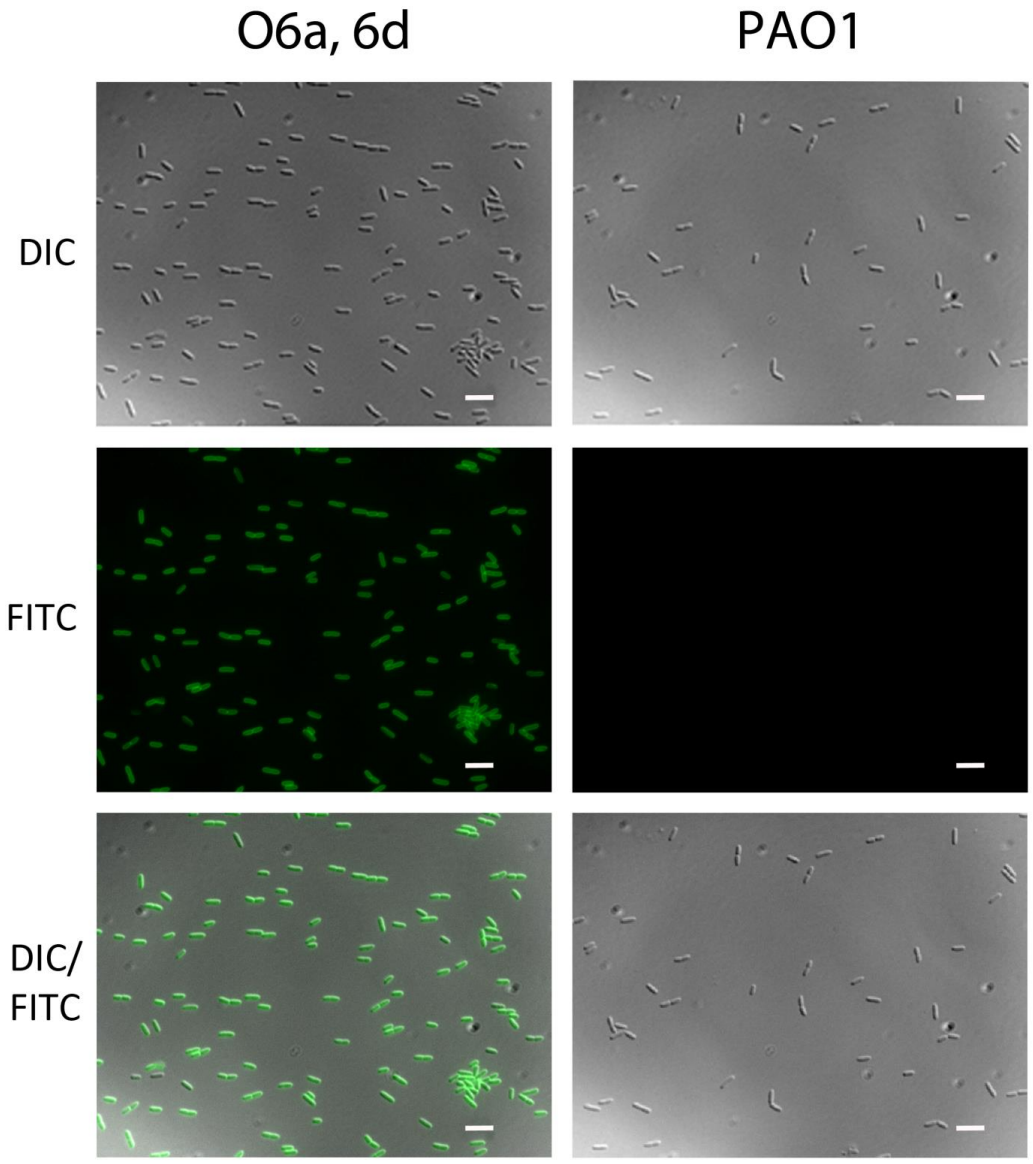

Figure 44. Fluorescence micrographs showing the binding of FITC-labelled S20 scFv towards *P. aeruginosa* strain O6a, 6d and its lack of binding towards PAO1 (O5). DIC, differential interference contrast. Magnification bars = 5µm.

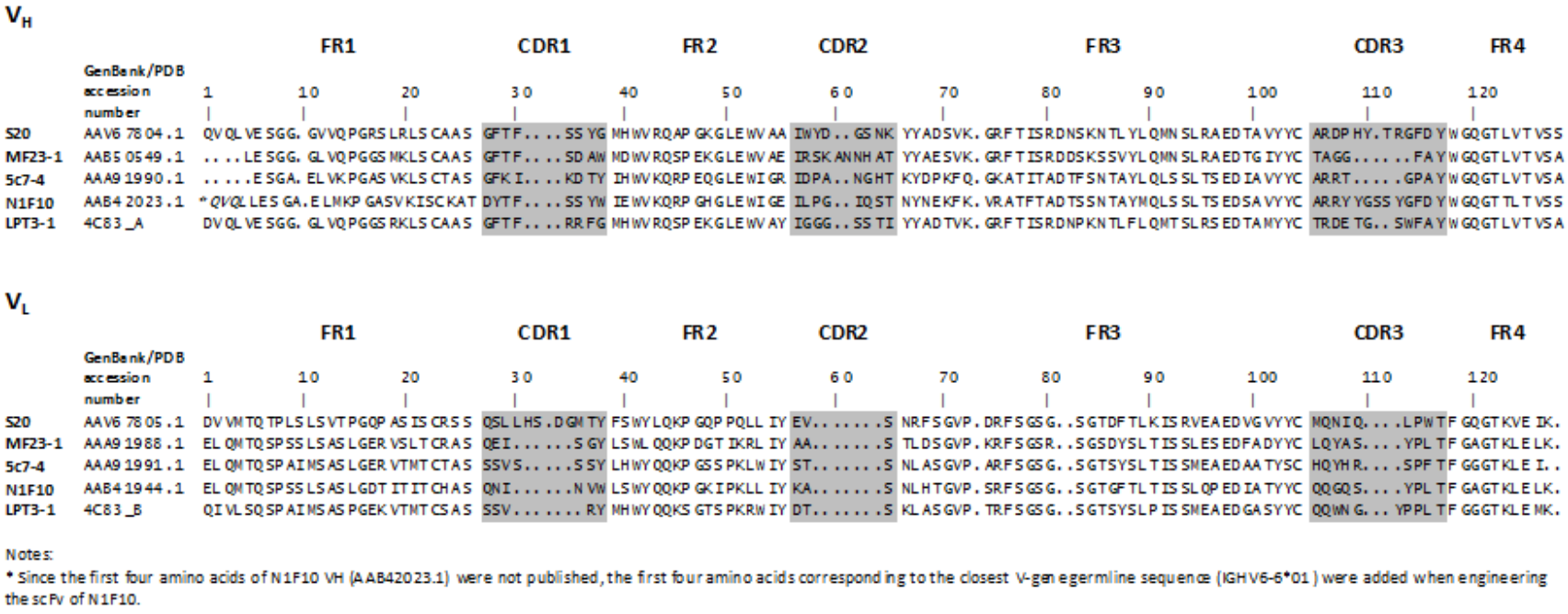

Notes:

* Since the first four amino acids of N1F10 VH (AAB42023.1) were not published, the first four amino acids corresponding to the closest V-gene germline sequence (IGHV6-6*01) were added when engineering the scFv of N1F10.

Figure 45. MSA of the VH and VL domains of the bactericidal S20 and MF23-1 and non-bactericidal mAbs 7-4, N1F10 and LPT3-1.

Table 4. The grand average of hydropathy (GRAVY) scores of all CDRs were calculated to determine if the bactericidal antibodies possess particularly hydrophobic CDRs that could integrate into and disrupt the membrane of *P. aeruginosa*. Scale: Hydrophilic: – 4.5 to – 3.5; Neutral: -3.5 to 0; Hydrophobic: 0 to 4.5 (167). Aside from CDR-H1, the CDRs of the S20 antibody are all neutral. That of the CDR-H1 is hydrophobic, but at the cusp of being neutral. Four of the CDRs from MF23-1 are considered hydrophobic; however, these values are mostly at the cusp of being neutral.

Antibody	CDR-H1	CDR-H2	CDR-H3	CDR-L1	CDR-L2	CDR-L3
S20	0.15	-1.225	-1.658	-0.427	-0.03	-0.389
MF23-1	0.138	-1.200	0.514	-0.833	0.93	0.022
7-4	-0.8	-0.825	-1.175	-0.157	-0.77	-1.778
N1F10	-0.812	0.725	-1.192	-0.450	-0.97	-1.278
LPT3-1	-0.263	0.688	-1.064	-0.640	-1.67	-1.320

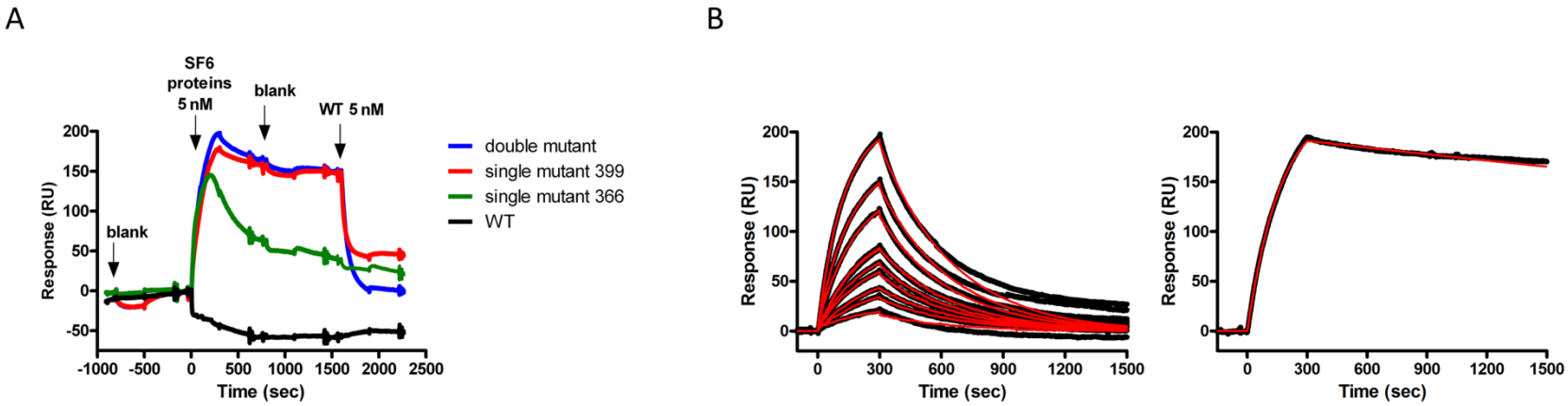

Figure 46. The SPR sensorgram of S20 scFv does not show evidence of enzymatic hydrolysis (glycanase activity) of the strain O6a, 6d *O*-polysaccharide. A) Hydrolysis of *Shigella* LPS was detected by the decrease in resonance units (RU) when wild-type Sf6 tailspike protein was injected over immobilized *Shigella* LPS, B) Hydrolysis of O6a, 6d LPS was not detected when S20 scFv was injected over the surface of immoblized LPS O6a,6d. Therefore, hydrolysis of O6a,6d LPS is likely not involved in the MOA of S20.

Model of O6ad scFv

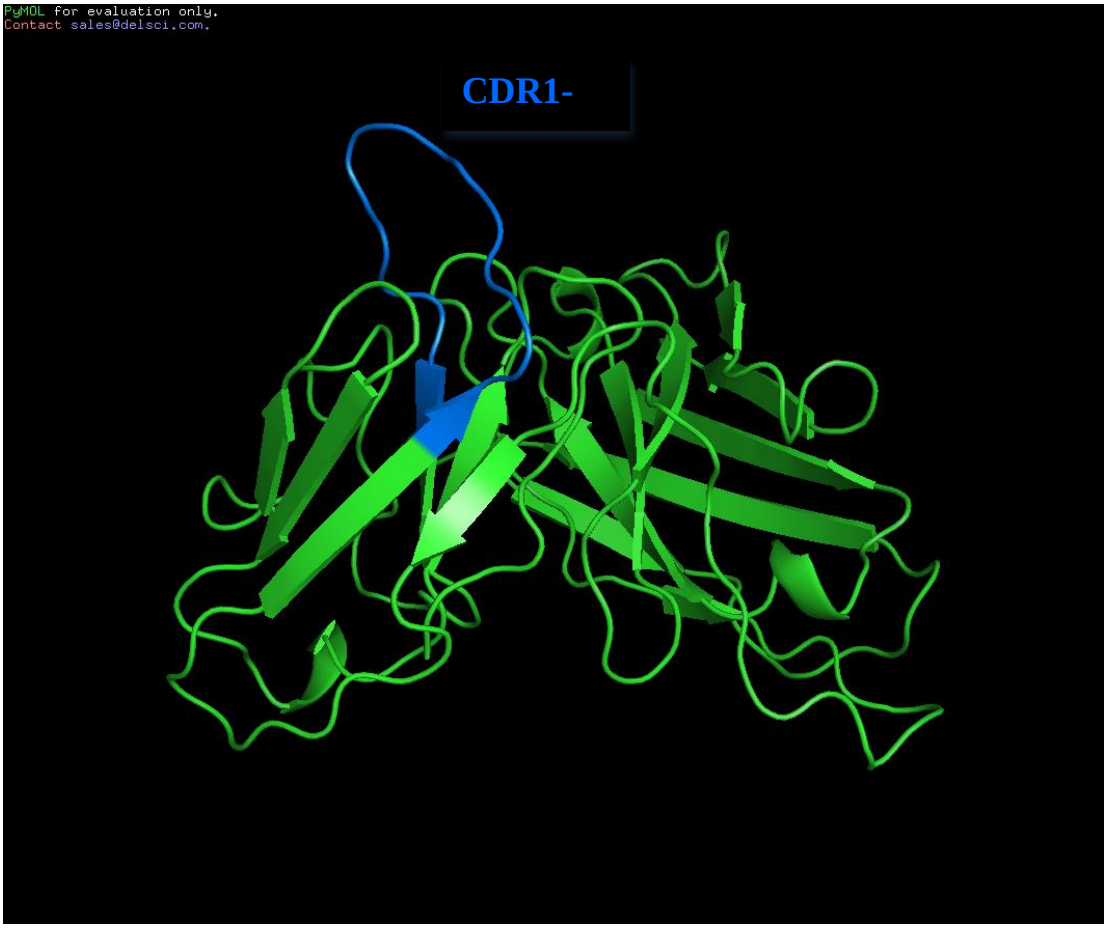

Figure 47. Crystal model of the S20 scFv, showing the long CDR1 of VL protruding from paratope.

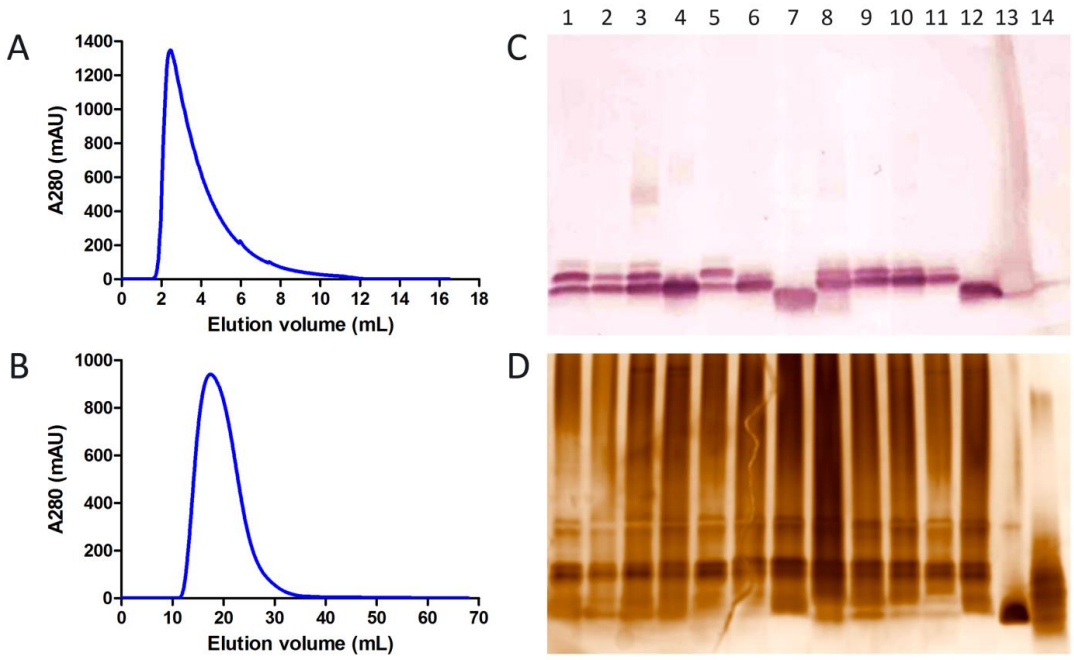

Figure 48. Purification and binding of mAb 7-4, an anti-inner core LPS binder. A. Elution profile of mAb 7-4 from MAb SelectSURE column. B. Chromatogram profile of the elution of mAb 7-4 from the HiPrep Desalting 26/10 column (GE Healthcare). C. Western immunoblot confirming the specificity of mAb 7-4 towards the inner core region of various smooth and rough strains of serotypes O6 and O5. D. Silver stain corresponding to the WB. Lane 1: O6 IATS; Lane 2: O6a, 6d; Lane 3: PAK; Lane 4: PAK *wbpO*; Lane 5: PAK *rmlC*; Lane 6: A28 (A+B-, O6-derived); Lane 7: H4 (A+B-, O6-derived, deep rough strain); Lane 8: O5 IATS; Lane 9: AK1401 (core +1, O5); Lane 10: AK1012 (A-B-, O5-derived); Lane 11: PAO1 (O5); Lane 12: PAO1 ΔalgC::tet; Lane 13: *S. enteritidis* purified LPS, 10 µg; Lane 14: *N. meningitidis*, purified LPS that LPT3-1 binds.

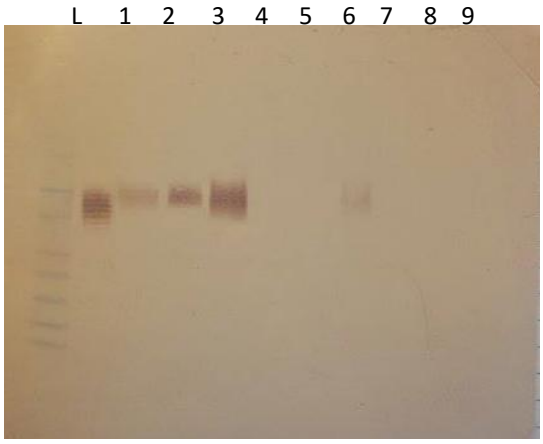

Figure 49. Western immunoblot showing the reactivity of purified N1F10 IgM towards various strains. Legend- Lane L: Protein ladder (used to direct the WB); Lane1: Purified O6a, 6d LPS, 10 µg; Lane 2: O6a, 6d LPS H-B; Lane 3: PAK LPS H-B; Lane 4: PAK *wbpO* LPS H-B; Lane 5: PAK *rmlC* H-B; Lane 6: O6 IATS LPS H-B; Lane 7: A28 LPS H-B; Lane 8: Fisher 1 LPS H-B; Lane 9: *Salmonella Typh*. B (ATCC 19585) LPS H-B. H-B: LPS purified by the Hitchcock and Brown method (158).

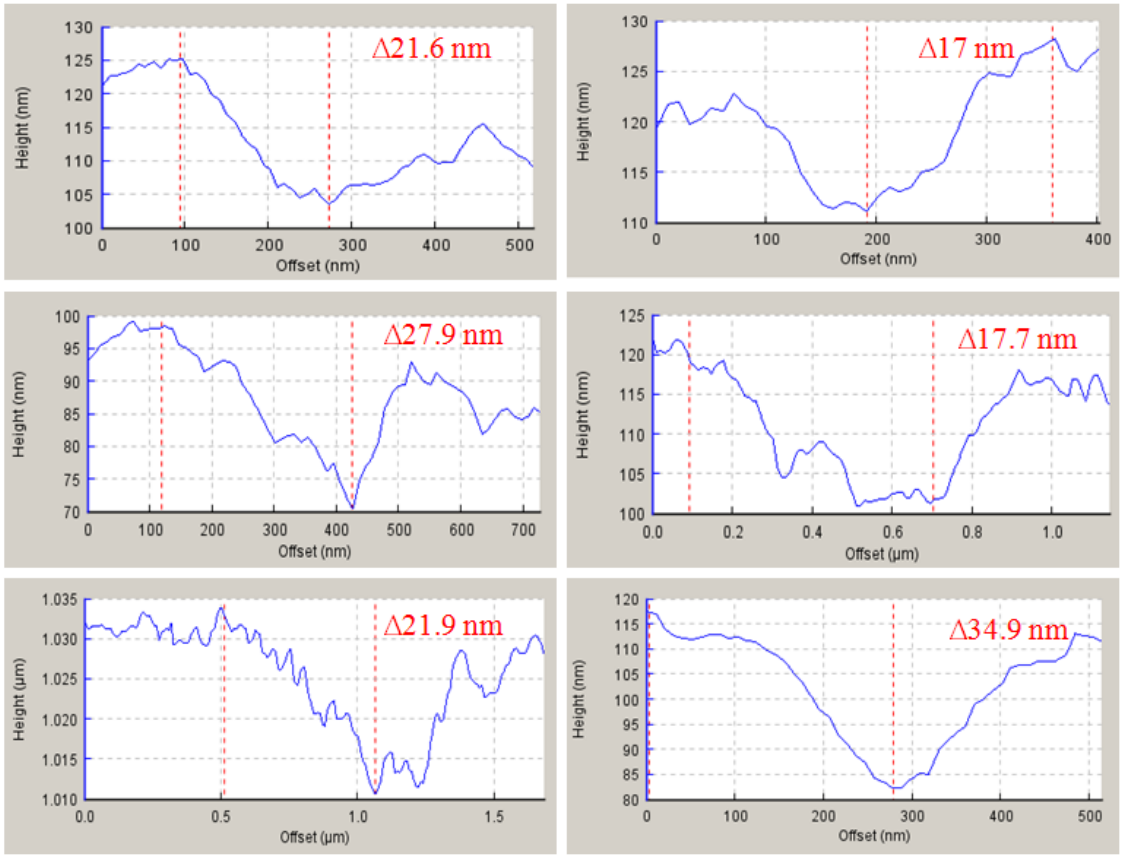

Figure 50. Membrane pits of 15-35 nm depth were measured on the surface of *P. aeuginosa* strain O6a, 6d cells treated with mAb MF23-1 at 0.4 × MIC_{50} (1 µM).

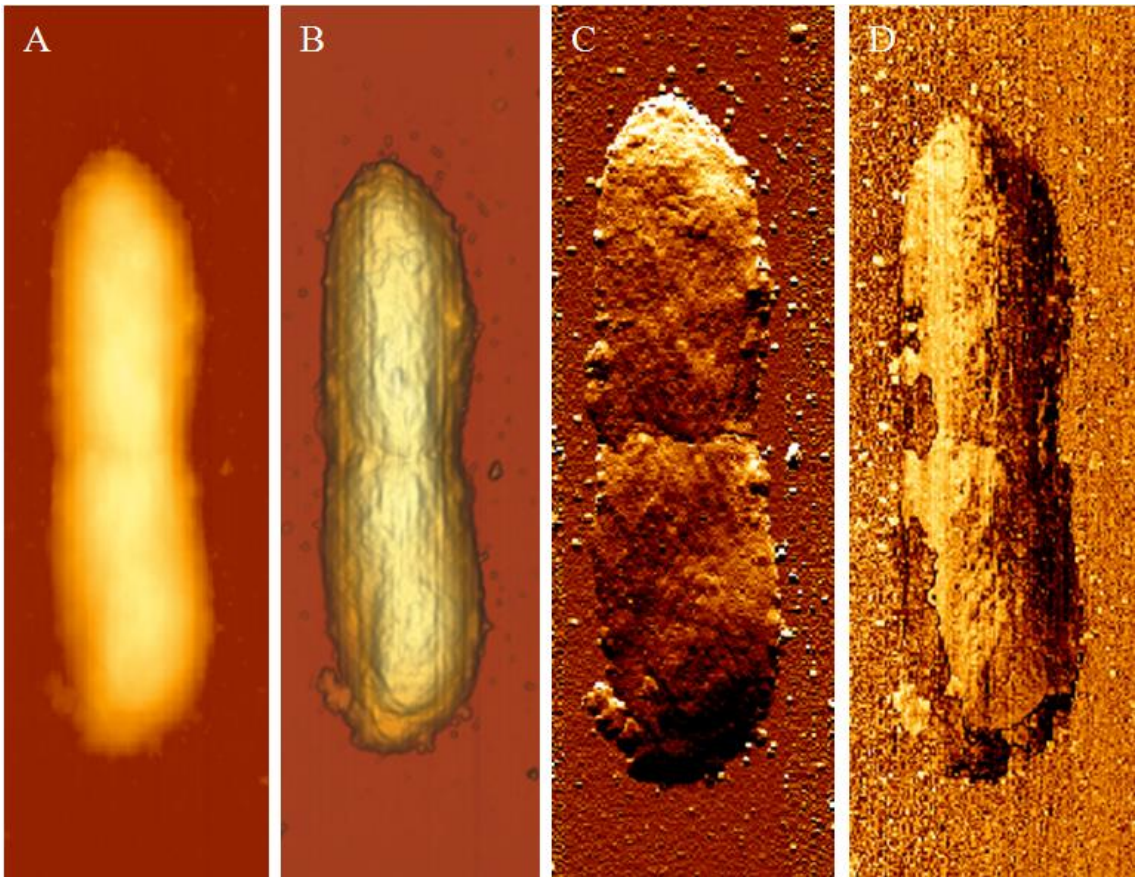

Figure 51. Height image, (B) topography (3D), (C) amplitude image and (D) phase image of a *P. aeuginosa* strain O6a, 6d cell treated with mAb MF23-1 at 4 × MIC_{50} (10 µM). Phase imaging use a softness / hardness scale where soft (adherent, elastic) surfaces are depicted as bright/white regions and hard (stiff, rigid) surfaces are depicted as darker regions. The phase image reveals that the OM (soft/adhesive material depicted in brighter colour) is in the process of sloughing from this cell, thereby exposing the underlaying peptidoglycan (rigid material depicted in darker colour) at the bottom and left side of this cell. Some micelle-like structures are found concentrated near the periphery of this cell; however, much less than the treatment at 1 µM. The cell was scanned in air using the intermittent contact mode (tapping mode; AC).

A)

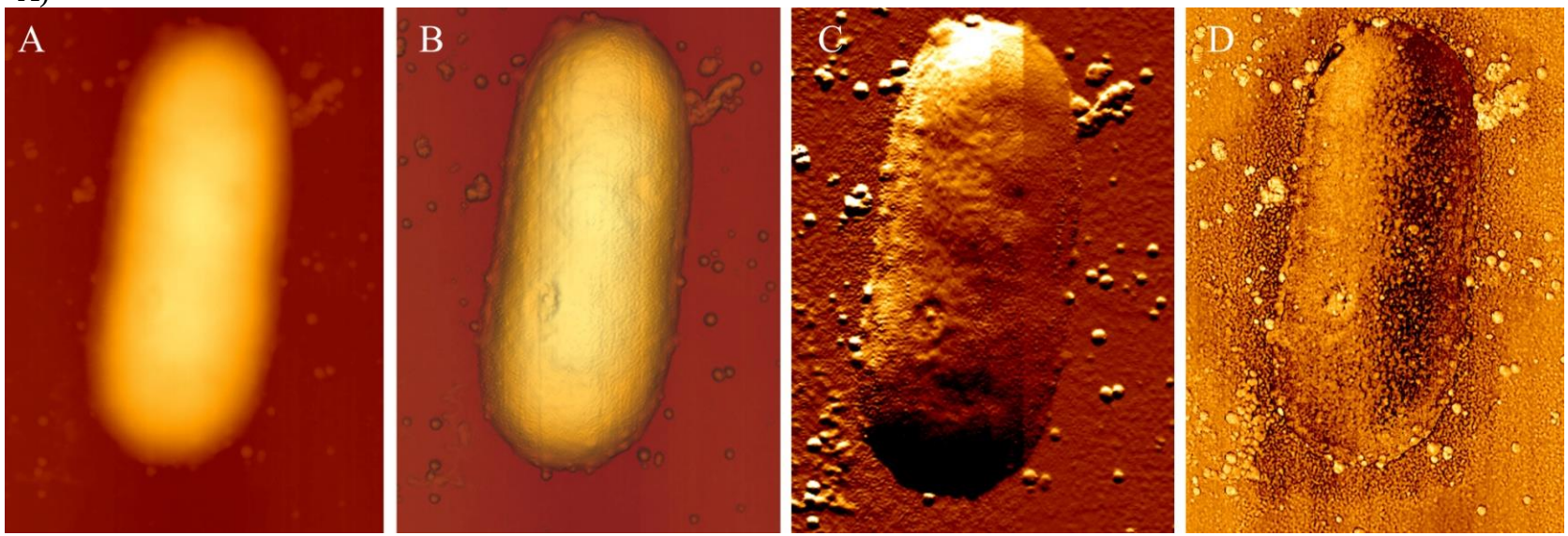

Figure 52. A) Height image, (B) topography (3D), (C) amplitude image and (D) phase image of a *P. aeuginosa* strain O6a, 6d cell treated with the S20 scFv monomer at 22 × MIC_{50} (10 µM). The 3D image revealed that the surface of this cell is much smoother than that of untreated cells (Figure 29). Since the varying lengths of the *O*-polyssacharide chains largely accounts for the roughness observed on untreated cells, this suggest that the LPS has largely been removed from this cell. The cell was scanned in air using the intermittent contact mode (tapping mode; AC).

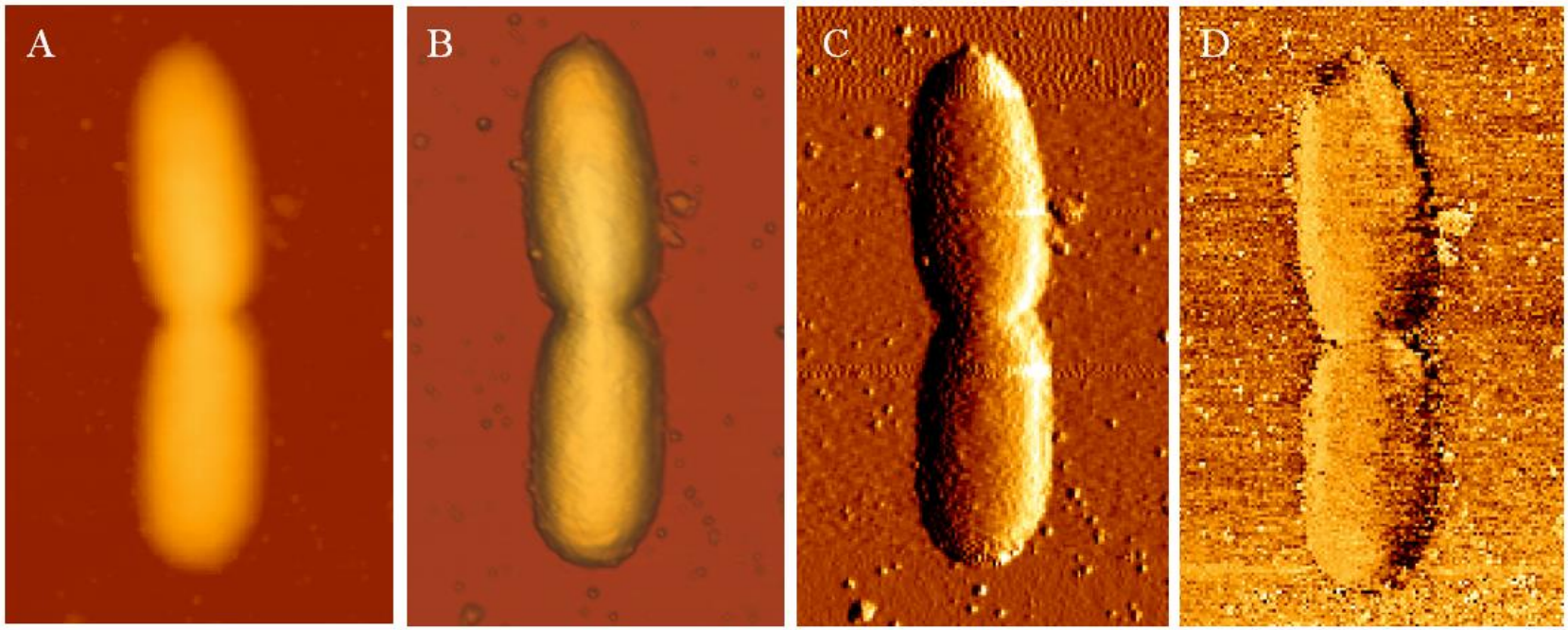

Figure 53. A) Height image, (B) topography (3D), (C) amplitude image and (D) phase image of a *P. aeuginosa* strain O6a, 6d cell treated with the S20 scFv monomer at 22 × MIC_{50} (10 µM). The 3D image revealed that the surface of this cell is much smoother than that of untreated cells (Figure 29). Since the varying lengths of the *O*-polyssacharide chains largely accounts for the roughness observed on untreated cells, this suggest that the LPS has largely been removed from this cell. The cell was scanned in air using the intermittent contact mode (tapping mode; AC).

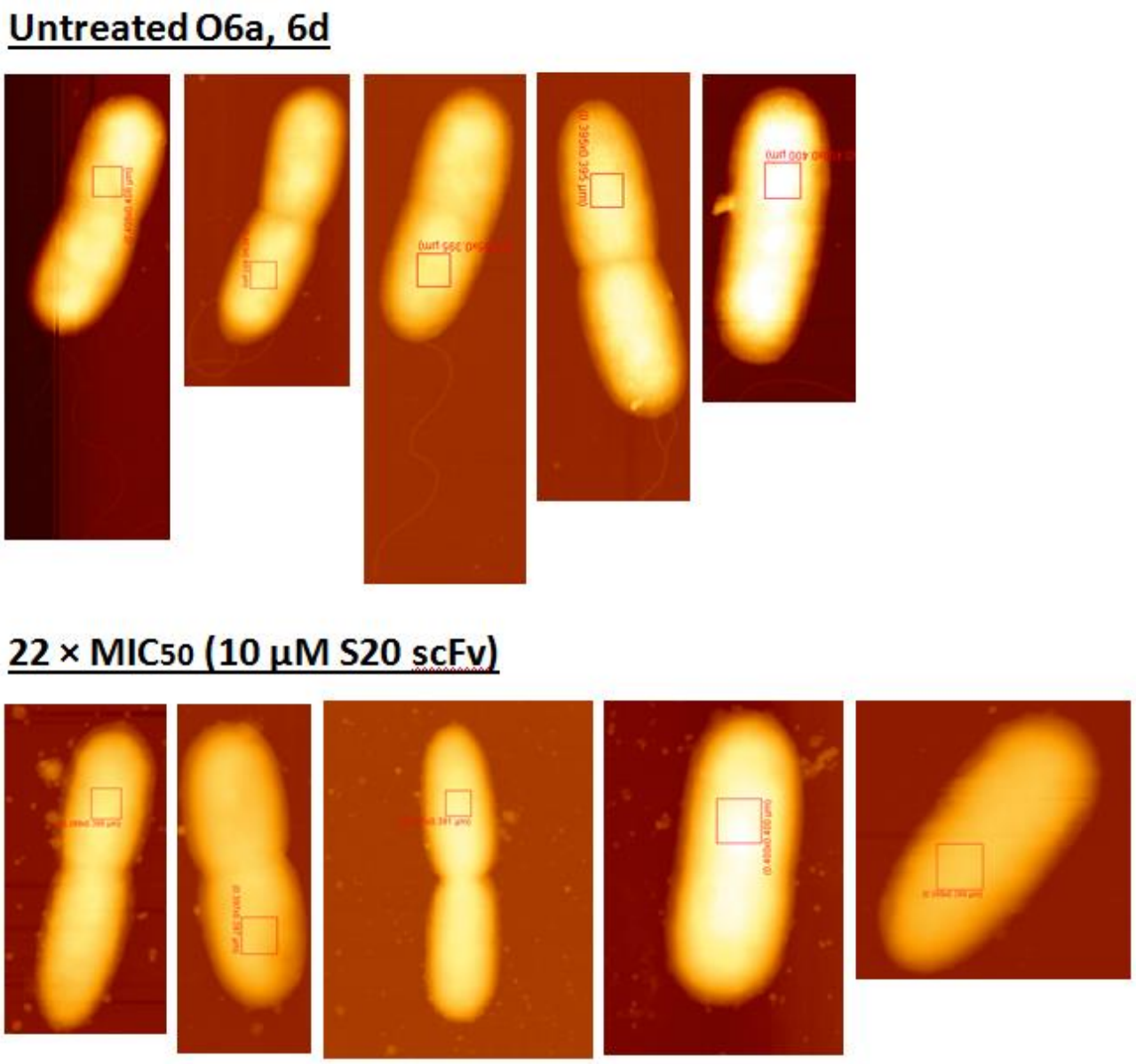

Figure 54. Surface area of 400 nm × 400 nm were randomly selected from five untreated and five S20 scFv-treated (10 µM) *P. aeruginosa* strain O6a, 6d. These were used to analyze the statistical differences in the surface roughness, as illustrated in Figure 39.